Investigating the Interplay Between Gibberellin Signaling and Cell Cycle Control

Camille Blakebrough-Fairbairn

School of Biosciences

Cardiff University

A thesis submitted in partial fulfilment of the requirements for the degree of

Doctor of Philosophy 2018

Preface

DECLARATION

This work has not been submitted in substance for any other degree or award at this or any other university or place of learning, nor is being submitted concurrently in candidature for any degree or other award.

Signed …… Date ……

STATEMENT 1

This thesis is being submitted in partial fulfillment of the requirements for the degree of PhD

Signed …… Date ……

STATEMENT 2

This thesis is the result of my own independent work/investigation, except where otherwise stated, and the thesis has not been edited by a third party beyond what is permitted by Cardiff University's Policy on the Use of Third Party Editors by Research Degree Students. Other sources are acknowledged by explicit references. The views expressed are my own.

Signed …… Date ……

STATEMENT 3

I hereby give consent for my thesis, if accepted, to be available online in the University's Open Access repository and for inter-library loan, and for the title and summary to be made available to outside organisations.

Signed …… Date ……

Acknowledgments

I would like to express my sincere gratitude to my supervisor, Prof. James Murray for providing me the opportunity to work on this project, and for all his help and guidance he has given me over the past four years. I would also like to thank Dr. Walter Dewitte for his expert scientific advice, guidance and support, and for generally being a kind-hearted human being who I see as an organised chaos with a brilliant scientific mind. I would also like to thank my second supervisor, Dr. Barend de Graaf, for his extremely useful and thorough technical advice, specifically in relation biochemical techniques and for helping to give me pep talks to continue the process.

For experimental advice, I would like to thank the members of the Murray lab who have all helped me out in many ways. Specifically, I would like to thank Dr. Emily Sornay for her expert scientific advice, for being a fantastic teacher who deserves recognition and more importantly, for being a caring and supportive friend. I would also like to acknowledge Dr. Simon Scofield for all the help and support in relation to qPCR's. Furthermore, I would like to thank Dr. Angaharad Jones for being so lovely and also putting up with my annoying questions. For technical advice, interesting conversations and a general enjoyment of their company, I thank Ms Jo Kilby and Ms Angela Marchebank. I have a lot of respect for Ms Jo Kilby for taking on a multitude of different roles and still managing to maintain a level head throughout all the comings and goings of the lab. She is a remarkable woman who deserves the upmost respect.

I thank Dr. Sonia Lopez de Quinto for her technical guidance on western blot analysis and allowing me to use some of her facilities in her lab (the 7-minute transfer system was a life saver!). My sincere gratitude goes to both Jez Smith and Dr. Rob Thomas for the endless hours they have spent to help me understand the dreaded statistical interphase of R. I have finally come to terms with it and realise it's an extremely powerful and useful tool that every biologist should learn to use. I never thought that statistics could be enjoyable, until I was introduced to the statistics clinic.

I would like to thank my collaborators who have helped contribute towards my research. In particular, I thank Dr. Francesco Masia for his expertise in analysing FLIM images for me. I thank Prof. Wolfgang Busch for allowing me to come to his lab at the Gregor Mendel Institute and use his facilities. Whilst I was there Ms Delayana Stoeva showed me all the facilities and guided me through all the procedures. My thanks also goes to Prof. Malcolm Bennett and Dr. Kristina Hill for their preliminary work and also allowing me to visit their lab twice in order to repeat their experiments.

I would especially like to thank my fantastic father for raising me in the best possible way and teaching me the most important values. I am also extremely grateful to have my stepmother (Janey-Mum) who has raised me as her own, without batting an eyelid. My sincere gratitude's also go out to the rest of my family and friends who have all been so supportive and I'm very lucky to have. I've appreciated the chance to form a closer bond with my mother and step-father as a result of living in Cardiff. Finally, I cannot put into words how much I value the support from my partner, James Hurst, who has been by my side throughout this process. He has dealt with all the crazy Camille times, the ups and downs, the emotional roller-coaster that I am.

Understanding the Interplay Between Gibberellin and Cell Cycle Control

Camille Blakebrough-Fairbairn

Due to the sessile nature of plants, cell expansion and proliferation are the key developmental processes that drive plant growth. Regulation of these mechanisms enables plants to alter their growth rates in response to environmental and developmental stimuli. This is integrated and co-ordinated by diverse hormonal pathways. Gibberellins (GAs) are plant-specific hormones that promote growth and regulate various developmental processes by signalling the destruction of a class of nuclear-localised growth repressors known as DELLA proteins. Little is known about the link between GA and cell proliferation. In *Arabidopsis thaliana*, there are five DELLA proteins that act as co-transcriptional regulators with overlapping but distinct functions. Two DELLA proteins associated with negative regulation of the GA signalling pathway are GAI (gibberellin insensitive) and RGA (repressor of ga1-3). Our evidence suggests that GAI and RGA regulate the G_1 to S phase of the plant cell cycle and are functionally different. GAI contains the LxCxE amino acid motif that putatively mediates binding to the RETINOBLASTOMA RELATED (RBR) protein, which prevents the G1-S transition. FRET-FLIM has revealed an *in situ* interaction between GAI and RBR, but not with RGA that contains a mutated motif. Furthermore, loss of *RGA* function reduces the effect of the cell cycle and CYCLIN DEPENDENT KINASE (CDK) inhibitor, KIP-RELATED PROTEIN2 on root growth whilst loss of *GAI* does not. Hence we suggest that the GAI-RBR complex represses cell proliferation and the GAI-RBR association might be under the control of CDK activity.

Table of Contents

Abbreviations

35S CaMV	35S Cauliflower mosaic virus
aa	Amino acid
ANOVA	Analysis of variance
At	*Arabidopsis thaliana*
bp	Base pair
CDK	Cyclin-dependent kinase
cDNA	Complementary DNA
CEI	Cortex endodermis initials
CFP	Cyan fluorescent protein
Chip-Seq	Chromatin-immunoprecipitation sequencing
CKI	CDK inhibitor
Co-IP	Co-immunoprecipitation
Col-0	*Colombia-0*
CYC	Cyclin
D8	*DWARF EIGHT*
DAS	Days after stratification
DELLA	Aspartic acid (D), Glutamic acid (E), Leucine (L), Leucine (L), Alanine (A)
DNA	Deoxyribonucleic acid
DNase	Deoxyribonuclease
dNTP	Deoxynucleotide
DP	Dimerisation partner

FLIM	Fluorescent lifetime imaging
FRET	Förster resonance energy transfer
E.coli	*Escherichia coli*
EDTA	Ethylenediaminetetraacetic acid
EDZ	Elongation/differentiation zone
E2F	*E2 TRANSCRIPTION FACTOR*
G_1/G_2/G_0	Gap 1/Gap 2/Gap 0
GA	Gibberellin
GA_3	Gibberellic acid 3
GAI	*GIBBERELLIN INSENSITIVE*
GAxOX	Gibberellin x-oxidase
GFP	Green fluorescent protein
GID	*GIBBERELLIN INSENSITIVE DWARF*
GLM	Generalised linear model
GLMM	Generalised linear mixed effects model
GM	Growth media
GRAS	GAI, RGA and SCARECROW
GST	Glutathione-s-transferase
ICK	INTERACTOR/INHIBITOR OF CYCLIN-DEPENDENT KINASE
IDD	*INDETERMINATE DOMAIN*
IPTG	Isopropyl-beta-D-thiogalactoside
kDa	Kilodaltons
KRP	*KIP RELATED PROTEIN*
LB	Luria-Bertani

Ler	*Landsberg erecta*
LM	Linear model
LMER	Linear mixed effects model
LxCxE	Leucine-X-Cystine-X- Glutamic acid
M	Mitosis
mRNA	Messenger RNA
MS	Murashige and Skoog medium
MYB	Myeloblastosis
MxCxE	Methionine-X-Cystine-X- Glutamic acid
OD	Optical density
oligoDT	oligo deoxythymine
PAC	Paclobutrazol
PBS	Phosphate buffer saline
PCR	Polymerase chain reaction
PI	Propidium iodide
PIF	*PHYTOCHROME INTERACTING FACTOR*
pRB	RETINOBLASTOMA protein
QC	Quiescent centre
RAM	Root apical meristem
RFP	Red fluorescent protein
RB	*RETINOBLASTOMA*
RBR	*RETINOBLASTOMA-RELATED*
RGA	*REPRESSOR OF GA1-3*
RHT	*REDUCED HEIGHT*

RNA	Ribonucleic acid
rpm	Revolutions per minute
qPCR	Quantitative PCR
S	Synthesis phase
SAM	Shoot apical meristem
SCR	*SCARECROW*
SDS	Sodium dodecyl sulfate
SDS-PAGE	Sodium dodecyl sulfate-polyacrylamide gel electrophoresis
SE	Standard error
SHR	*SHORTROOT*
SIM	*SIAMESE*
SMR	*SIAMESE-RELATED*
SLR	*SLENDER RICE*
SLY	*SLEEPY*
T-DNA	Transfer DNA
UV	Ultra violet
WT	Wild-type
YFP	Yellow fluorescent protein
Zm	*Zea Mays*

Introduction

Introduction

1.1 Root Development and Growth

Root growth is an important factor determining the overall development of a plant. This is particularly true for a germinating seedling, so it can acquire water, anchorage and nutrients necessary for further development. Plant growth is driven by cell expansion and proliferation, which is coordinated in the meristem, but the molecular mechanisms behind these processes are not yet fully understood. This study investigates novel roles of a family of transcriptional co-regulators that repress growth and their relation to a key cell-cycle regulator. Moreover, a putative protein interaction between these two factors is tested. Most experimental procedures in this study have been focused solely on the *Arabidopsis* root because its development can be easily monitored over time and it is an ideal system for imaging, due to its almost two-dimensional structure. Root development was examined by measuring root growth over time and root meristem size, cell number and cell production rate. Since the primary structure of root vascular tissue is laid down during embryogenesis, this topic will be covered first, followed by a general description of primary root growth and our current knowledge of the molecular mechanisms behind them.

1.1.1 Embryogenesis

The lifecycle of a plant alternates between haploid gametophytic and diploid sporophytic generations. Sporophytes produce megaspores and microspores that gives rise to female and male gametophytes, respectively (Harada *et al.*, 2010). These gametophytes produce the haploid egg and sperm cells that fuse to form a zygote; the first stage of the sporophytic generation. Embryogenesis is typically defined by the developmental period in which the zygote matures into an embryo by undergoing a series of differentiation events to form the main embryonic organs (Harada *et al.*, 2010).

In Arabidopsis and other higher plants, embryogenesis begins with the fertilisation of the egg cell by the sperm nucleus, resulting in a diploid zygote. Following from this, the zygote elongates to form the “proembryo” and divides asymmetrically and transversally to produce a small apical cell and a basal cell with distinct cell fates (Figure 1.1). The apical cell is referred to as the embryo proper and subsequently undergoes a series of cell divisions to determine overall structure of the embryo. The basal cell develops into the endosperm, which is the maternal tissue essential for the development of the zygotic embryo by acting as a nutritional source. During embryogenesis, organs and tissues are formed by partitioning events along the apical-basil axis, which constitutes the

shoot-root axis of the overall plant body (Harada *et al.*, 2010). In the case of eudicots, two cotyledons are formed in the apical region of the embryo, which eventually develop into two true-cotyledons containing a shoot apical meristem (SAM) between them. The procambium is laid down in the basal region of the embryo and is the meristematic tissue that gives rise to vascular tissue. The basal cell divides transversally to form a longitudinal file of cells known as the suspensor, which helps anchor the embryo to the endosperm. The uppermost cell of the suspensor is the hypophysis, which divides asymmetrically to give rise to the quiescent centre and stem cell niche of the root meristem. Hence, the root apical meristem (RAM) is formed from decedents of both the apical and basal cell. Both the SAM and RAM are essential regions of cell division that are responsible for maintaining initial plant growth (primary growth) and development post-embryonically. Formation of these organs and tissues are dependent on correct partitioning events along the apical-basal and radial axes during embryogenesis, and this is mainly controlled by polar transport of the plant hormone auxin (Liu *et al.*, 1993; Friml *et al.*, 2003). Development of the zygotic embryo and establishment of the basic body plan occurs during morphogenesis. During the maturation phase, the embryo develops into a mature seed where it is developmentally and metabolically arrested and is surrounded by the endosperm (Harada *et al.*, 2010). During this phase, the embryo becomes tolerant of desiccation and accumulates storage macromolecules such as starch, lipids and proteins (Harada *et al.*, 2010). Favourable environmental conditions, such as the uptake of water by imbibition, reactivates metabolic activity within the seed and encourages germination. Germination occurs when the radical penetrates through the epidermis and the seed coat (testa), which is driven by expansion of hypocotyl cells (Sliwinska *et al.*, 2009). The hypocotyl and the primary root is then formed from this radicle.

The plant model organism, *Arabidopsis thaliana*, has played an important role in furthering our understanding of the molecular mechanisms behind such developmental processes. This is because it has a short life cycle (approximately 6 weeks from seed to mature plant), a relatively small diploid genome (that has been fully sequenced) and simple growth conditions (Koornneef and Meinke, 2010). Furthermore, it can easily be genetically modified in a variety of different ways, such as *Agrobacterium*-mediated transformation by floral dipping.

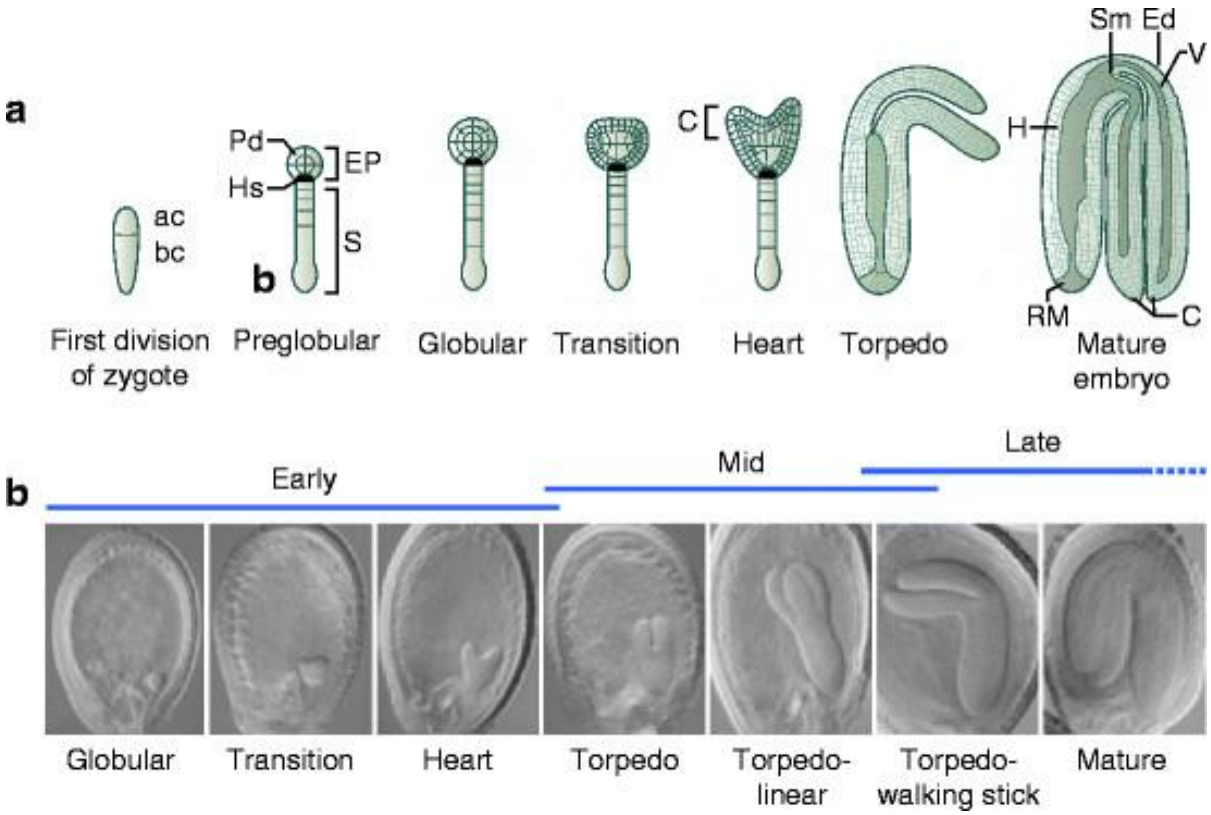

Figure 1.1 Overview of plant embryogenesis in *Arabidopsis*. Development of the embryo from post-fertilisation to the mature embryo is represented by (a) a diagram and (b) differential contrast interference micrographs of embryogenesis showing the overlapping early-, mid- and late- stages. Upon fertilization the zygote undergoes a transversal cell division to give rise to the terminal/apical cell (ac) and basal cell (bc). Formation of the preglobular stage involves the apical cell undergoing a series of divisions in different planes to form the main body of the embryo (embryo proper, EP), whilst the basal cell undergoes anticlinal divisions to give rise to a suspensor (S) that anchors the embryo to the seed and provides it with nutrients. At the top of the suspensor is the hypophysis (Hs), which eventually develops into the root mersitem (RM), whilst the protoderm (Pd) develops into the epidermis (Ed) of the mature embryo. From the globular to the transition stage, the embryo acquires a radial symmetry with the emergence of two cotyledons (C) connected by the shoot apical meristem (SAM). From the heart stage, the two cotyledons continue to develop. The root apical meristem (RAM) can be distinguished at the torpedo stage. From the walking-stick stage onwards, cell expansion becomes the main process that governs growth of embryo during the maturation phase. Adapted from Bewley *et al.* (2013).

1.1.2 Root growth

The increase in size of a plant (growth) and the rate at which it is altered over time (growth rate) depends on a variety of internal and external factors including endogenous and environmental signals. At the molecular level, a variety of signalling components confined to cellular and subcellular locations integrate these factors to regulate growth rate. In both the developing root and shoot, primary growth requires a pool of undifferentiated cells maintained in a stem cell niche, located in the apical meristems of the root and shoot tip. Since plant cells are unable to migrate around the plant, cell proliferation and expansion are the key processes that drive this growth to determine root length (Beemster, 1998). The orientation of these divisions and the polarity of cell growth is also a key factor in determining tissue patterning and organ shape. The root apical meristem (RAM) is a well-defined structure that consists of distinct cell patterning and cell types positioned along a longitudinal and radial axis (Figure 1.2) (Overvoorde *et al.*, 2010). The RAM is primarily composed of five tissue-types: the root cap, quiescent centre (QC), epidermis, ground tissue (cortex and endodermis) and stele (pericycle and vascular tissue). The radial pattern is established during embryogenesis and maintained by stem cell niche activity. Stem cells are able to remain in a continued state of self-renewal because of short-range signals administered by the QC (van den Berg *et al.*, 1997). Initials are produced as a result of stem cells dividing asymmetrically to produce one daughter cell that retains an indeterminate stem cell fate, and another daughter cell (the initial) that acquires a determinate cell identity and is incorporated into proximal meristem to eventually become part of differentiated tissues. In the proximal meristem root cells undergo repeated rounds of proliferative cell division. These cells are eventually pushed out and transition into the elongation/differentiation zone (EDZ) where they undergo elongation, enabling the root to push forward into its growth medium. Following cell expansion, cells enter the maturation zone where they mature and differentiate to form specific organs, such as lateral roots. To maintain these regions, the molecular components regulating these processes must be able to control the timing and extent of cell division, as well as coordinate cell expansion and differentiation, so that sufficient growth and development can occur (Heo *et al.*, 2011).

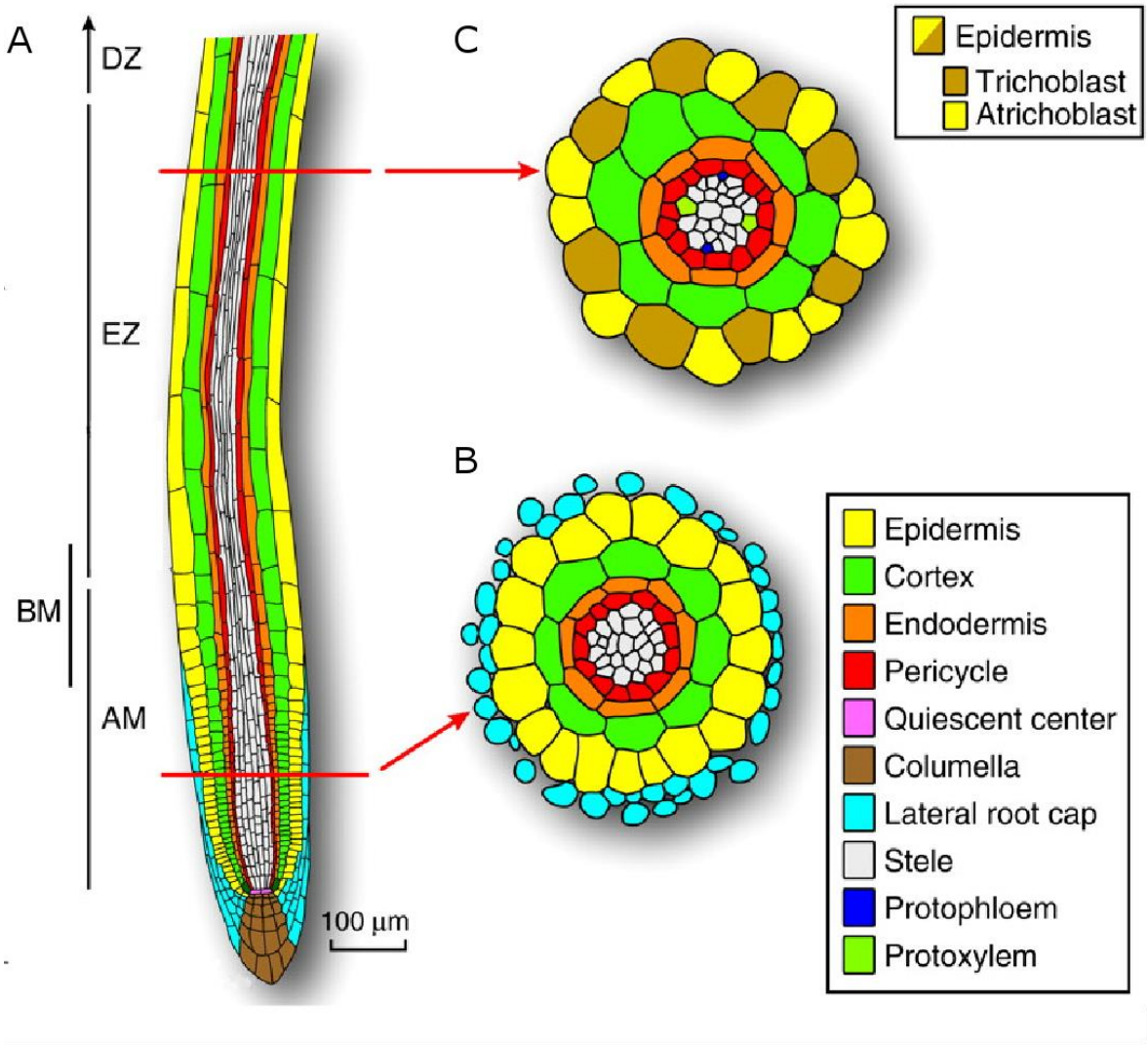

Figure 1.2 Longitudinal and radial patterning of the Arabidopsis root**.** (A) Longitudinal patterning of the root. The stem cell niche contains four sets of initials derived from stem cells: lateral root cap/epidermal, columella, cortical/endodermal and pericycle/vascular, surrounding a region of low mitotic activity known as the quiescent centre (QC). These initials give rise to the epidermis and lateral root cap, the columella (the central portion of the root cap), the ground tissue of the cortex and endodermis, and the vascular tissue and pericycle, respectively. The apical meristem (AP), basal membrane (BM), elongation zone (EZ) and differentiation zone (DZ) are indicated to the left of the root. Cell division occurs in the apical root meristem and cell elongation begins in the basal meristem and becomes established in the elongation zone (B) Radial patterning of cell files within the apical meristem (C) Radial patterning of cell files within the elongation zone. Differentiation at this stage begins to occur with the formation of the protophloem and protoxylem. Furthermore, endodermal cells with different identities are highlighted in this region. Trichoblasts give form root hair cells and atrichoblasts do not. Adapted from (Overvoorde *et al.*, 2010).

1.2 Regulation of the plant cell cycle

A new cell can only be made by duplicating an already existing one. The ability of an organism to make more cells is governed by the cell cycle. This is a fundamental process that is highly conserved amongst all living organisms; from unicellular protozoa to complex metazoans. The cell cycle consists of a series of controlled events that allows a cell to duplicate its DNA content and divide into two genetically identical daughter cells. In unicellular eukaryotes, it is essential for reproduction because each cell division produces a complete new organism. In multicellular organisms, a more complex cell cycle-mechanism is required (1) to produce an organism from a single zygote cell and (2) for the regeneration of tissues.

In all cases, the cell cycle is tightly regulated and consists of a series of biochemical switches leading to specific cell-cycle events. The molecular control mechanisms and components that regulate these processes are highly conserved amongst eukaryotes and have been studied in a variety of model organisms. As such, a brief overview of the cell-cycle in eukaryotes will be described here, before describing the plant cell cycle in more detail.

1.2.1 The eukaryotic cell cycle

At the most basic level, the mitotic cell cycle consists of two alternating phases of chromosome duplication (synthesis, also termed S phase) and chromosome segregation (Mitosis, also termed M phase). The M-phase is defined by two key events: (1) nuclear division (Mitosis) where replicated DNA is distributed into a pair of daughter nuclei and (2) cytoplasmic division (cytokinesis) where cells divide themselves into two daughter cells.

The mitotic cell cycle in eukaryotes usually consists of these two phases interspersed by two gap phases: G_1 (between M- and S- phase) and G_2 (between S- and M- phase). During G_1 phase, cells contain a single copy of their DNA and their progression to S phase is arrested. During G_2 phase, cells contain two copies of their DNA, since they have just undergone DNA replication in S phase, and progression to the M phase is arrested. Both phases allow time for a cell to grow and to monitor internal and external environmental conditions. It is important for a cell to continue to grow during the cell cycle, otherwise they will become smaller and smaller upon each division. Furthermore, a cell must be able to monitor its environment so it can respond accordingly by regulating cell cycle progression. The length of a cell cycle can vary considerably depending on the length of the gap phases. Thus, genetic regulation of cell cycle progression occurs mainly at the G_1-S and G_2-M checkpoints (Novak *et al.*, 1998; Jakoby and Schnittger, 2004).

Cell cycle progression begins at the G_1 phase, where cells either commit to entering the cell cycle or in some cases, particularly when extracellular conditions are poor, remain indefinitely in a specialized quiescent state, known as the G_0 (G zero) phase (Harashima *et al.*, 2013). Before making this commitment, the cell must first integrate developmental cues such as energy availability and hormone levels (Dewitte and Murray, 2003). Once a cell is committed to this process, it cannot return to its original state and must progress into the next stage of the cell cycle i.e. DNA replication.

1.2.2 Mechanisms of cell cycle control in eukaryotes

Cell-cycle control is governed by a family of serine-threonine protein kinases known as cyclin-dependent kinases (CDKs). As the name suggests, their activity is dependent on the function and availability of cyclins that act as regulatory subunits for the formation of cyclin/CDK complexes (Murray, 2004). The binding of different cyclins allows substrate specificity and therefore regulation at each cell-cycle transition (Menges *et al.*, 2007). Throughout cell-cycle progression, activities of these complexes lead to cyclical changes in the phosphorylation of target proteins that initiate or regulate the cell cycle (Alberts *et al.*, 2015). Indeed, it has been found in fission yeast (*Schizosaccharomyces pombe*) that a single cyclin is able to regulate both DNA replication and mitosis (Fisher and Nurse, 1996), thus supporting the idea that different levels of CDK activity promote cell-cycle progression at different stages (Stern and Nurse, 1996). Moreover, in lower eukaryotes, such as budding and fission yeast, a single CDK has been found to bind with and regulate different cyclins during the cell cycle (Morgan, 2006). In higher eukaryotes, the number of cyclins and CDKs in a species genome has generally increased over time as a result of evolution (Murray, 2004). CDKs in all eukaryotes have been found to contain a cyclin binding domain and have similar protein structure due to a conserved sequence of 300 amino acids.

Since the level of each cyclin type is one way of regulating CDK activity, it has been postulated that the diversity of cyclins in more complex organisms could be the result of their requirement for regulating different levels of cell-cycle activity (Murray, 2004). On the other hand, this diversity may reflect increasing complexity of tissue organization and specificity in these organisms. In eukaryotes, cyclins are classified by the stage of the cell cycle that they bind with CDKs and function. In general terms, G_1 to S phase is controlled by cyclin Ds, S phase progression by cyclin E and A, and mitosis by cyclin B's (Murray 2004, Menges et al. 2007). Homologs such as these types of cell-cycle regulator have been found in both higher and lower plants, although Cyclin E is absent in plants (Menges *et al.*, 2007).

1.2.3 The plant cell cycle

In plants, the cell cycle is responsible for controlling the timing and rate of cell division, as well as cell size. Since plants are sessile (immobile) organisms, it is important that they are able to respond to environmental stimuli physiologically by integrating internal and external cues. They can respond to a range of abiotic factors, such as light intensity, photoperiod, temperature, water availability and gravitational pull, and biotic factors such as bacteria, viruses and fungi. Most plant growth and development occurs post-embryonically due to the activity of meristems maintaining a pool of stem cells and an active zone of cell division (as described previously). The fact that they demonstrate such a high level of plasticity in their response to environmental variation, implies that they have developed unique aspects to their mechanisms of cell-cycle control. Plants also have the ability to produce whole new organs from non-dividing differentiated cells, thus demonstrating a high level of totipotency (De Veylder *et al.*, 2007). Such is the case in the formation of new lateral roots by the activation of new root primordia in the pericycle cell layer (De Veylder *et al.*, 2007).

Some plant and animal cells undergoing differentiation are able to go through a modified cell-cycle called the endocycle (Galbraith *et al.*, 1991). During endoreduplication, cells undergo successive rounds of DNA replication during the S-phase, without the occurrence of mitosis. This effectively doubles DNA content for each successive round (Joubes and Chevalier, 2000), thus increasing ploidy levels of individual cells. Although it is evident that all eukaryotes share similar cell-cycle control mechanisms, there are some key differences between plants and animals. The very nature of plant cells themselves, means that their biology is somewhat distinguished from other organisms. For example, during cytokinesis a new plant cell wall has to be built by specific plant genes that are not present in the mammalian cell cycle (Francis, 2009). A further key difference is that both the G_1 and G_2 are natural arrest points for the cell cycle, whereas in animals G_1 is the main arrest point (Francis, 2009).

Overall, it is likely that plants have developed a variety of complex mechanisms for regulating cell-cycle control and initiating different types of cell division. Furthermore, higher plants have evolved to contain various homologous subgroups of cell-cycle regulators and genes within them, which is reflective of the gene duplication and diversification events they have undergone (Menges *et al.*, 2007). These different subgroups, specifically in relation to Arabidopsis, will be discussed here.

1.2.4 Cyclin-Dependent Kinases (CDKs)

The modulation of CDK activity requires the binding of kinases/phosphatases and is regulated in a complex manner by phosphorylation/dephosphorylation and regulatory proteins (Vandepoele *et al.*, 2002). As mentioned earlier, cyclins are positive cofactors that activate and regulate CDK kinase activity by binding with them. Unlike yeast and similar to animals, plants have evolved to have many subclasses of CDKs, each with specific functions (Vandepoele *et al.*, 2002). The two main classes of CDKs that have been studied to date are: A-type (CDKAs) and B-type (CDKBs). CDKA is homologous to Cdk1 in animals and regulates both G_1 to S and G_2 to M checkpoints (De Veylder *et al.*, 2007). CDKA is the most numerous type of CDK found in plants (Joubès *et al.*, 2000) and unlike metazoans, is generally expressed throughout the cell cycle (Fobert *et al.*, 1996). CDKBs are plant specific and are associated with the regulation of mitosis (Vandepoele *et al.*, 2002; Endo *et al.*, 2012). Indeed, CDKBs have been shown to be primarily expressed during mitosis, as well as the G_2-to-M phase transition phase in *Arabidopsis* cell suspension cultures (Menges and Murray, 2002). They have been classified further into two sub-groups, based on the cell-cycle phase they regulate: CDKB1 and CDKB2 (Joubès *et al.*, 2000). Expression of these types appear to be under strict cell-cycle control; CDKB1 is expressed from late S to M phase and CDKB2 is expressed from G_2 to M phase (Endo *et al.*, 2012). The CDKB1 and CDKB2 subgroups in Arabidopsis each contain two members: CDKB1;1, CDK1;2 and CDKB2;1, CDKB2;2, respectively (Vandepoele *et al.*, 2002).

In Arabidopsis, twelve CDK-related genes have been identified based on sequence homology, which are divided into six groups (CDKA-F) (Vandepoele *et al.*, 2002). *Arabidopsis* contains a single gene for CDKA (CDKA;1) that is responsible for regulating various stages of the cell-cycle either on its own or in conjunction with other CDK types (Figure 1.3) (Vandepoele *et al.*, 2002). A more recent study examined *cdka;1* null mutants in *Arabidopsis* and found that they were viable, but had specific defects in S-phase entry, suggesting it predominantly regulates this phase of the cell cycle (Nowack *et al.*, 2012). These homozygous mutants were clearly compromised in their growth and development, such as distinctively small rosette leaves, small nuclei in trichomes, a reduction in root development, cotyledon expansion and hypocotyl elongation. However, although above ground organs had distinctively larger cells, they were still able to develop slowly, but continuously and correct organisation of the shoot apical meristem (SAM) was observed. Entry into S-phase is regulated by the RETINOBLASTOMA-RELATED (RBR) protein, which is a direct target of CDKA;1 phosphorylation (Figure 1.3). Furthermore, the authors found defects in root stem cell maintenance, which is also regulated by RBR. The authors went on to conclude that the main function of CDKA is to control RBR, since co-depletion of this protein and CDKA;1 rescued most of the observed phenotypic defects of *cdka;1* mutants alone (Nowack *et al.*, 2012).

1.2.5 CDK inhibitors

The activity of CDKs can be modulated by CDK inhibitors (CKIs), either by directly binding to CDK/CYC complexes, or by phosphorylating the CDK subunit (Vandepoele *et al.*, 2002). In Arabidopsis, there are two classes of CDK/CYC inhibitors: INTERACTOR/INHIBITOR OF CYCLIN-DEPENDENT KINASE (ICK) and SIAMESE (SIM)/SIM-RELATED (SMR) proteins (Dewitte and Murray, 2003, Churchman *et al.* 2006, Inze and De Veylder, 2006).

ICK proteins share a conserved C-terminal amino acid binding motif that is responsible for interacting with CDKs (Wang *et al.*, 1998; Joubès *et al.*, 2000; Torres Acosta *et al.*, 2011). More N-terminally, the CDK-interacting domain is an amino acid motif responsible for binding D-type cyclins (Wang *et al.*, 1998; Peres *et al.*, 2007). The first ICK to be described was the *Arabidopsis* ICK1 protein, which showed homology at its C-terminal to the metazoan Cip/Kip family (Wang *et al.*, 1997). Hence, they were renamed as KIP-RELATED PROTEINS (KRP). Deletion of the conserved C-terminal domain of ICK1/KRP1 disrupted its ability to inhibit CDK activity (Wang *et al.*, 1998; Zhou *et al.*, 2003). Since then, a total of seven *KRP* genes (*KRP1-7*) have been identified in the Arabidopsis genome (De Veylder *et al.*, 2001). Although all seven KRP proteins have been shown to be nuclear-localised, they demonstrate unique expression patterns (Bird *et al.*, 2007). The inhibitory action of KRPs on kinase activity had been demonstrated both *in vitro* and *in vivo* (Wang *et al.*, 1997, 1998; Zhou *et al.*, 2003). Arabidopsis lines overexpressing *KRP1* and *KRP2* under a constitutive promoter result in plants with a phenotype of small serrated leaves due to a reduction in cell number by mitotic inhibition (Zhou *et al.*, 2003). KRP2 has been demonstrated to modulate the onset of endoreduplication during leaf development and auxin-induced lateral root formation by inhibiting CDKA;1 and CYCD2;1 activity, respectively (Verkest *et al.*, 2005; Sanz *et al.*, 2011). Thus, KRP's have multiple and diverse roles in relation to inhibition of cell-cycle-regulated processes.

SIM/SMR proteins is a more recently described class of nuclear-localised CDK/CYC inhibitors, which consists of four members. They contain a putative cyclin binding motif and one shared motif with ICK/KRP proteins (EIEDFF). Protein interactions of SIM with both CDKA;1 and D-type cyclins have been demonstrated using FRET experiments (Churchman *et al.*, 2006). Similarly, the closely related *EL2* gene in rice has been shown to bind CDKA1;1 and D-type cyclins with Yeast-two-hybrid screening, *in vitro* pulldown assays and FRET analysis (Peres *et al.*, 2007). Similar to *Arabidopsis* plants overexpressing KRP proteins, plants overexpressing SIM are characterized by their slow growth rate and small serrated leaves consisting of enlarged epidermal cells with increased ploidy levels (Churchman *et al.*, 2006). Furthermore, recessive mutations in the *Arabidopsis* SIM gene results in plants with multicellular trichomes containing nuclei that have decreased ploidy levels

(Walker *et al.*, 2000). These results combined, suggest that SIM proteins are responsible for controlling the onset of endoreplication (Walker *et al.*, 2000; Churchman *et al.*, 2006).

1.2.6 Plant cyclins

Since monomeric CDKs do not have kinase activity, plant cyclins are regulatory proteins that are required to activate CDK activity. Cyclin levels can be modulated transcriptionally or post-translationally by targeted proteasome degradation. Fluctuations of cyclin levels during the cell-cycle therefore determine the timing and extent of CDK activity (Vandepoele *et al.*, 2002). Higher plants have evolved to have an increased number of cyclin genes in comparison to metazoans (Menges et al., 2007). For example, the relatively small genome of *Arabidopsis* contains 10 *CYCA*, 11 *CYCB* and 10 *CYCD* genes (Nieuwland *et al.*, 2007). Based on phylogenetic analysis revealing homology with animals and protists, the cyclins have been categorised into ten homologous classes in relation to these organisms. They are characterized by a conserved 250 amino acid region called the cyclin core that contains two domains: cyclin N and cyclin C (Nugent *et al.*, 1991). The N domain (approximately 100 amino acids long) is highly conserved and contains the defining CDK-binding site termed as a "cyclin box" (Wang *et al.*, 2004). The C domain is not as highly conserved and can vary between different cyclin subgroups (Nieuwland *et al.*, 2007).

In Arabidopsis, genome-wide analysis has revealed 49 putative cyclins isolated based on the C and N domains (Nugent *et al.*, 1991). Of these 49 putative cyclins, 31 contain both the C- and N-terminal, whilst 18 contain the N-terminus only (Vandepoele *et al.*, 2002; Wang *et al.*, 2004). Based on sequence analysis, plant cyclins have been classified into the following classes: A/B-, C-, D-, H-, T-, L-, T-, U-, SOLO DANCERS (SDS)- and CycJ18-type cyclins. Little is known about the C-, T-, L-, and U-type cyclins, apart from their expression patterns in different *Arabidopsis* tissues and the discovery of homologs in rice (*Oryza sativa*). The SDS and CycJ18 cyclins are quite divergent from others and are consequently treated as separate classes. CycJ18 is predominantly expressed in young seedlings and has been shown to complement the G_1 cyclin function in budding yeast (*Saccharomyces cerevisiae*), thereby activating the G_1 to S transition (Abrahams *et al.*, 2001). Mutational analysis of a homozygous *sds* null mutant had severe defects between homolog interactions during prophase 1 of meiosis (Azumi *et al.*, 2002). Furthermore, the fact that *SDS* expression has been shown to be localized specifically to male and female meiocytes suggests that the SDS cyclin has a novel, meiosis-specific function (Azumi *et al.*, 2002). In contrast to these putative cylclin classes, much more is known about A-, B-, D- and H-type cyclins and their relation to the cell cycle has begun to be elucidated (De Veylder *et al.*, 2007). Phylogenetically, the A- and B-type cyclins are more closely related to each other than other cyclin types (Wang *et al.*, 2004).

D-type cyclins are a particularly large group specific to and conserved between higher plants, and are divided into six subgroups, termed CYCD1-CYCD7 (Menges *et al.*, 2007). CDKA/cyclinD complexes are primarily responsible for regulating the G_1 to S phase of the cell cycle and have been shown to respond to mitogenic and other signals that promote the early stages of mitotic cell division (Dewitte and Murray, 2003). In *Arabidposis thaliana* there are 10 CYCD genes classified into seven subgroups (Menges *et al.*, 2007), each with functionally distinct roles (Oakenfull *et al.*, 2002). One of the major targets of CDKA/cyclinD complexes is RETINOBLASTOMA-RELATED, which is an important cell cycle regulator (Goodrich and Lee, 1993; Boniotti and Gutierrez, 2001). The most well characterized of these D-type cyclins in *Arabidopsis* is CYCLIN D3;1 (CYCD3;1) (Dewitte *et al.*, 2003). Constitutive overexpression of this protein resulted in increased CYCD3;1–associated kinase activity thereby reducing the amount of cells in G_1 phase. These plants had a distinct phenotype of hyperplasia in leaf cells. Furthermore, endoreduplication was strongly repressed causing defects in differentiation of leaf tissues (Dewitte *et al.*, 2003).

CYCA, CYCB and CYCD's are able to form active complexes with CDKA;1 and CDKBs to regulate different stages of the cell cycle (Figure 1.3). CYCH is unique as it only forms active complexes with CDKD, which is associated with regulation of the G_2 to M transition of the cell cycle. Broadly speaking, the G_1 to S transition is controlled by CYCD/CDKA;1 and CYCA/CDKA;1 complexes, whilst CDKB complexes are mitotic-specific, since the G_2 to M phase and the onset of mitosis is controlled by CYCA and CYCBs with CDKA and CDKB.

The diversity of cyclins and their binding to CDKs is a powerful strategy for plants because it allows multiple levels of cell-cycle control by regulating the synthesis, localisation and destruction of cyclins (Nieuwland *et al.*, 2007). This regulatory model of plant cell-cycle regulation is by no means exclusive for this purpose and a number of other examples of CDK-cyclin regulation involved in transcription and response to phosphate availability has been found (Nieuwland *et al.*, 2007).

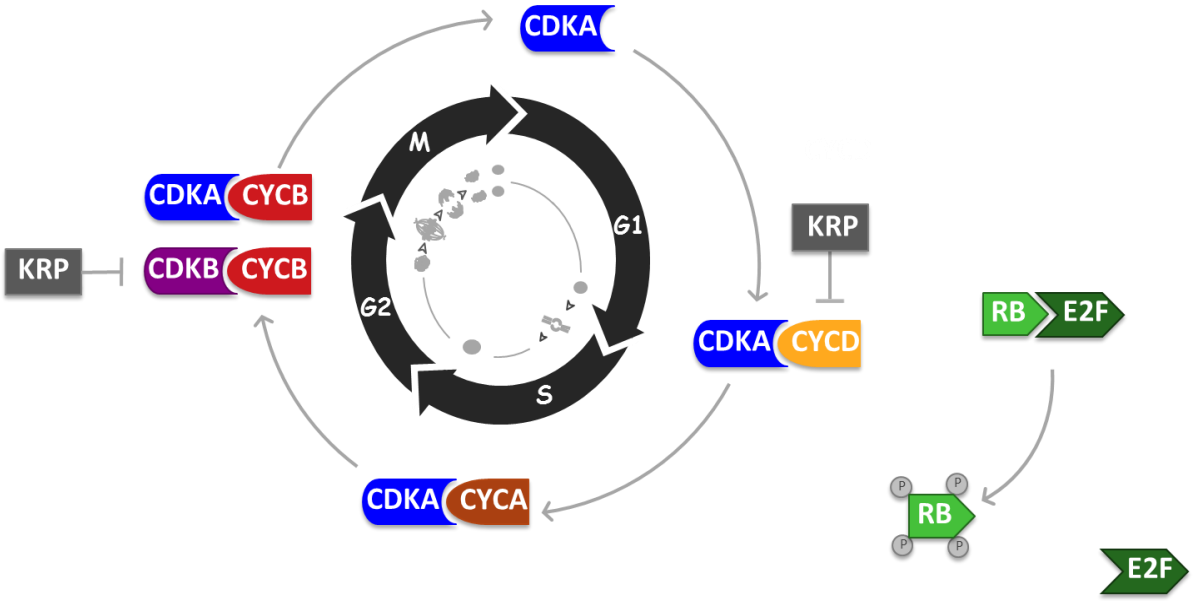

Figure 1.3 A simplified schematic of the plant cell cycle. When bound to plant cyclinDs, CDKA/cylinD complexes are primarily responsible for regulating the G_1 to S phase of the cell cycle by phosphorylating target proteins that control this transition (Zhao *et al.,* 2012). One of the main targets of this complex is the RETINOBLASTOMA-RELATED (RB) protein. CYCA interacts with CDKA during the S-phase. CDKBs (of two types: CDKB1 and CDKB2) are specific to regulation of the mitotic stage of the cell cycle by forming active complexes with CYCBs. Furthermore, CDKAs require the activity of CYCBs for regulating the transition from G_2 to M (Inze and De Veylder, 2006 Kawamura et al. 2006). KRP proteins can interact with both CYCD and CDKA subunits and inhibit kinase activity of these complexes. Adapted from (Scofield *et al.*, 2014).

1.3 The RETINOBLASTOMA protein

1.3.1 Structure and function of the RETINOBLASTOMA protein and its relation to plants

Most of the research on the RB protein (pRB) has been done on the human form since it was originally identified as the first tumor suppressor in animals (Friend et al., 1986). Indeed, the *RB* gene is usually inactivated or mutated in most forms of human cancer (Knudsen and Knudsen, 2006). It was later revealed that pRB plays an important role as a negative regulator of the cell cycle by controlling the transition from G1- to S-phase in a phosphorylation-dependent manner (Weinberg, 1995) (Figure 1.4). RB arrests cell cycle progression during the G1-phase whilst bound to heterodimeric E2F/Dimerisation partner (DP) transcription factor complexes, which is modulated by cyclin/CDK complexes (Weinberg, 1995; Dyson, 1996). Mitogenic signals activate the cyclin/CDK complexes to hyperphosphorylate RB, thereby releasing it from E2F/DP transcription factor complexes that facilitate the transition to S-phase (Weinberg, 1995). For some time, it was believed that retinoblastoma-related proteins (RBRs) were specific to animals alone (reviewed by Durfee et al. 2000), but orthologues have since been found in monocotyledons (Grafi *et al.*, 1996;

Xie *et al.*, 1996; Ach *et al.*, 1997), dicotyledons (Nakagami *et al.*, 1999; Kong *et al.*, 2000) and unicellular algae, such as *Chlamydomonas reinhardtii* (Umen and Goodenough, 2001). Therefore, RB has been evolutionarily conserved between a variety of different species, including plants.

The RETINOBLASTOMA-RELATED (RBR) protein in plants is similar to RB in terms of its structure and cell-cycle-specific function (Huntley *et al.*, 1998; Ramirez-Parra *et al.*, 2003, 2004; Gruissem, 2007). pRB is a member of the pocket family of proteins, meaning it contains specific domains that form a so called "pocket" for interactions with binding partners, such as transcription factors, so it can modulate the expression of specific genes. The overall structure of pRB is composed of an N-terminal region, a large central domain known as the A and B pocket, and a C-terminal region (Figure 1.4). In both plants and animals, pRB family members share high sequence homology across the AB binding domain (Murray, 1997). Furthermore, both RB and RBR proteins contain several other distinct domains conserved between them, particularly motifs related to E2F interactions and for binding a variety of cellular and viral proteins that contain the LxCxE motif, such as CYCD proteins. The LxCxE-binding domain is located within the B pocket domain and is indispensable for binding a diverse range of proteins containing this motif (Lee *et al.*, 1998).

As well as having this canonical function of regulating the cell cycle, it is well established that RBR has multiple roles in relation to plant growth and development. Similarly, the mammalian pRB also functions beyond cell cycle control and has been reported to interact with over one hundred different proteins to mediate pivotal processes such as cell differentiation, stem cell maintenance, apoptosis, DNA repair and genome stability (Morris & Dyson 2001; Chinnam & Goodrich 2011; Dick & Rubin 2013). In plants, RBR has similar roles, but only a few binding partners have been identified so its mechanisms for regulation of these processes are generally unknown.

In *Arabidopsis* there is a single *ATRBR1* gene that performs an essential role in gamete formation, stem cell maintenance, meiosis and plant development by controlling the fate between cell proliferation and differentiation (Magyar et al. 2012; Ebel et al. 2004; Park et al. 2005; Wildwater et al. 2006; Chen et al. 2009; Johnston & Gruissem 2009; Desvoyes et al. 2006; Borghi et al. 2010; Gutzat et al. 2011; Perilli et al. 2013; Harashima & Sugimoto 2016). Indeed, an *rbr* loss-of-function mutant demonstrates defects in meiosis and is gametophytic-lethal as a result of impaired female gametogenesis (Ebel *et al.*, 2004; Johnston and Gruissem, 2009; Johnston *et al.*, 2009). This is because the *rbr* mutant fails to restrict mitosis during development of the megaspore and therefore prevents its differentiation into a functional female gamete (Ebel *et al.*, 2004; Johnston and Gruissem, 2009). Development of the male gametophyte is also affected by the loss of RBR function, thus implying that it is required for determining cell fates, as well as proper gamete

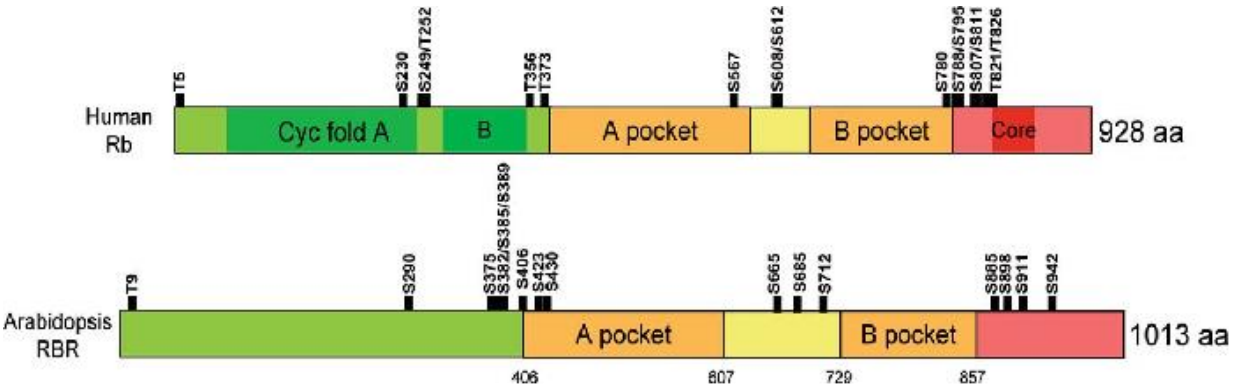

Figure 1.4: Comparative domains of the human pRB and Arabidopsis RBR proteins defined by amino acid positioning. The protein consists of three protease resistant domains (the N-terminal, A & B domain) and a C-terminal region. The majority of pRB binding partners bind to the highly conserved A-B "pocket region", which also contains the LxCxE binding domain. The overall molecular weight of pRB and RBR is 100kDa and 125kDa, respectively. Putative CDK phosphorylation sites for Arabidopsis RBR are also indicated. From (Desvoyes *et al.*, 2014).

formation (Johnston *et al.*, 2008). The role of AtRBR1 in a developmental context is best understood in the stem cell niche of root meristem. Within this region, the QC maintains a slowly dividing pool of undifferentiated cells that maintains the more frequently dividing surrounding stem cell initials. Due to the low rate of cell division in the QC, these cells are more protected from DNA damage, whilst the surrounding cells are more vulnerable (Fulcher and Sablowski, 2009; Furukawa *et al.*, 2010). It has been shown that RBR binds to the transcription factor, SCARECROW (SCR), to impose this quiescent state, as well as repressing asymmetric cell divisions in the QC (Cruz-Ramírez et al. 2012, 2013). More recent publications have also revealed that ATRBR1 also plays a pivotal role in maintaining genome integrity by directly regulating the DNA damage response (Biedermann *et al.*, 2017; Horvath *et al.*, 2017).

In *Arabidopsis* RBR1 is able to interact with three isoforms of E2F transcription factors, E2FA, E2FB and E2FC, which is dependent on their association with either DPA or DPB (Magyar *et al.*, 2000). RBR modulates the E2F-DP complex by either inhibiting or activating their transcriptional activity (Magyar, 2008). The aforementioned E2F proteins have differential roles in relation to mitosis and the endocycle. Overexpression of E2FA and DPA resulted in an increase in mitotic activity and endoreduplication (De Veylder *et al.*, 2002), whilst overexpression of E2FB induced mitosis, but decreased endoreduplication (Magyar *et al.*, 2005; Sozzani *et al.*, 2006). Recent advances within this field demonstrated that E2FA stimulates proliferation and endoreduplication through RBR alone and RBR complexes (Magyar *et al.*, 2012). Conversely, silencing of E2FC leads to an increase

in cell proliferation and a compromised endocycle, thus suggesting that E2FC and E2FB have antagonistic roles, whilst E2FA has dual functions (Magyar, 2008).

A paper by Kobayashi *et al.* (2015) indicated that AtRBR1 may also be associated with the G_2-to-M phase of the cell cycle by interacting with a particular subset of MYB transcription factors that regulate the expression of G_2/M genes. They demonstrated that amongst five MYB proteins containing three repeats in the MYB domain, MYB3R, some of them acted as transcriptional activators, whilst others acted as potential repressors by associating with different E2F isoforms. Interestingly, ATRBR1 was found to bind to both an activator, MYB3R4, and a repressor, MYB3R3, which associate with a particular E2F isoform depending on the developmental stage of leaf development and the transcriptional activity of the MYB protein itself (Kobayashi *et al.*, 2015). Therefore, RBR may have transcriptional activation roles as well as repression in relation to regulation of such developmental processes. Overall, it is evident that RBR is a very promiscuous protein that acts as a central hub between cell division and differentiation by responding to endogenous and environmental cues.

1.4 Gibberellic acid

1.4.1 Hormonal signaling in the root

Phytohormones (plant hormones) acting on different cell types play a pivotal role in determining plant architecture due to their ability to control various developmental processes. Phytohormones are small signaling molecules that respond to internal and environmental stimuli with multiple regulatory pathways. Many of these compounds have been identified in the model organism *Arabidopsis thaliana* and their functions have been well-defined by analysing biosynthetic and signaling mutants, in conjunction with experiments involving exogenous hormonal application. These studies demonstrate that different phytohormones have dynamic and distinct roles, acting on discrete cell types to drive plant growth and development. Plant hormone biology is a complex field, but our understanding of it over the past few years has significantly increased our knowledge of hormone signaling, transport, perception, metabolism, biosynthesis and response (Santner and Estelle, 2009; Takatsuka and Umeda, 2014).

In the primary root, the major hormones that regulate growth and development are auxin, cytokinins and gibberellins, as well as other hormones such as brassinosteroids, ethylene, abscisic acid (ABA) and strigolactones (Takatsuka and Umeda, 2014) (Figure 1.5). In particular, the formation and maintenance of the root meristem is largely controlled by the antagonistic interaction of auxin and cytokinin (Su et al. 2011). Together they regulate the balance between cell

division and differentiation by determining the region of mitotic activity and the transition zone where cells begin to differentiate (Su et al. 2011). The signal transduction pathways of these hormones are confined to the receptors that they bind to and their cellular/subcellular location (Jaillais and Chory, 2010).

Understanding the cross-talk between these signaling pathways, as in specific interactions of components shared between more than one pathway (Mundy *et al.*, 2006), and how they integrate internal and external cues to coordinate growth can help us to grasp their individual roles and subcellular localisation. For a more detailed insight into the role of these phytohormones and how they are integrated into distinct zones to control root cell division and elongation, see the reviews by Takatsuka & Umeda, 2014 and Benková & Hejátko, 2008.

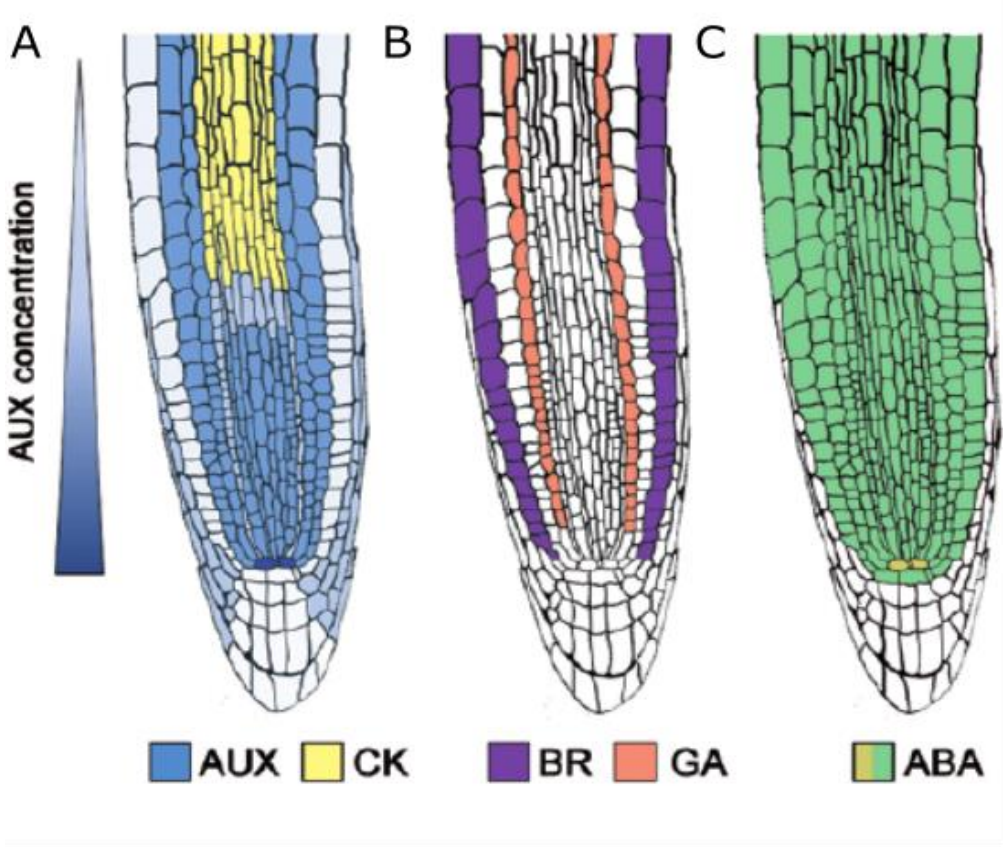

Figure 1.5 (A) Auxin (AUX-blue) and Cytokinin (CK-yellow) distribution in the root meristem. Auxin is the main regulator of root meristem function and patterning. Demonstrated here is the general basipetal gradient across the root tip. CK is localised to the transition zone and is responsible for regulating cell division and size within this region. (B) Brassinosteroid (BR-purple) distribution in the RAM regulates cell division and size in the epidermis. Gibberellic acid (GA-orange) controls cell proliferation and meristem development in the endodermis. In the RAM, abscisic acid (ABA) inhibits cell division. Maintenance of the QC (beige) positively affects root growth, but cell division in the remaining meristem (green) negatively influences inhibition of it. Adapted from (Reitz *et al.*, 2015).

Hormone	Function and localisation
Auxin	The major plant growth regulator of root meristem function and patterning (Blilou *et al.*, 2005; Kieffer *et al.*, 2010). This depends upon local accumulation of auxin and the developmental context in which it is perceived (Kieffer *et al.*, 2010). Polar auxin distribution is maintained by PIN efflux channels that regulate cell division and expansion during root development (Blilou *et al.*, 2005). Auxin also mediates lateral root (LR) formation and has multiple roles during LR development (Fukaki *et al.*, 2007; Du and Scheres, 2018).
Cytokinin	Regulates cell division and cell size in the transition zone. Cytokinin works antagonistically with auxin to determine root meristem size by controlling the rate of cell differentiation (Dello Ioio *et al.*, 2007).
Gibberellin	Controls cellular expansion, cell proliferation and meristem development in the endodermis during root development (Ubeda-Tomás *et al.*, 2009).
Brassinosteroids	Regulates cell division and cell size in the epidermis of the root meristem (Hacham *et al.*, 2011; Fridman *et al.*, 2014).
Abscisic acid (ABA)	Inhibits cell division in the RAM (Zhang *et al.*, 2010). Regulates hydrotropism via the elongation zone and in cortical cells (Dietrich *et al.* 2017). Accumulates throughout all tissue layers of the RAM, apart from the lateral root cap (LRC) and columella cells.
Ethylene	Functions synergistically with auxin to regulate root growth by localised inhibition of cellular expansion (Růžička *et al.*, 2007; Strader *et al.*, 2010), root gravitropism (Buer *et al.*, 2006), inhibit lateral root development (Lewis *et al.*, 2011) and promote root hair growth and differentiation (Pitts *et al.*, 1998). A recent study has revealed that ethylene also inhibits cell proliferation in the root meristem (Street *et al.*, 2015).
Strigolactones	Promotes elongation of seminal/primary and adventitious roots and inhibit lateral root formation (Kapulnik, Delaux, *et al.*, 2011; Ruyter-Spira *et al.*, 2011; Rasmussen *et al.*, 2012; Kumar *et al.*, 2015). They have also been shown to interact with ethylene and auxin to regulate root hair elongation (Kapulnik, Resnick, *et al.*, 2011).

Table 1.1 A summary of the main hormones and their function in the developing root of *Arabidopsis*

Gibberellin signaling plays a pivotal role in regulating a variety of developmental and growth processes and demonstrates cross-talk with multiple other signaling pathways (Lor and Olszewski, 2015). GA levels are strongly affected by environmental stimuli such as light, temperature, osmotic potential and water availability (Hedden and Thomas, 2012; Colebrook *et al.*, 2014). As a result, plants are able to respond to abiotic stress through the GA signaling pathway to alter their physiology and biochemistry (Colebrook *et al.*, 2014). Here, I will discuss our current knowledge of gibberellin structure, biosynthesis, hormonal perception and the GA signal transduction pathways for modulating plant growth.

1.4.2 On the origins of GA

The effects of gibberellins were first recognized and published during the end of the 19th century when plant pathologists in Japan were investigating a devastating disease of rice, known as 'bakanae' (foolish seedling). Symptoms of this disease included elongated seedling growth with pale yellow, slender leaves and stunted roots. In 1938, this phenotype was attributed to a compound derived from *G. fujikuroi,* from which the researchers Yabuta and his associate Yusuke Sumiki isolated this substance and named after (gibberellin) (Yabuta T., 1938). It was not until the mid-1950's that GAs were found to be naturally occurring substances in plants and since then, over a hundred different types have been identified from all sources (http://www.plant-hormones.info/gibberellin_nomenclature.htm) (Yamaguchi, 2008).

1.4.3 Gibberellin biosynthesis and structure

Gibberellins (GAs) comprise a class of carboxylic acids that have a tetracyclic diterpenoid structure (Lor and Olszwski, 2015, Hedden and Thomas, 2012) (Figure 1.6). Terpenes are a large and diverse class of organic hydrocarbons produced in a wide variety of plants and formed by the combination of several isoprene (CH_2=C(CH_3)-CH=CH_2) units. They are classified by the number of isoprene units in the molecule and a prefix is used to denote the amount of terpene units required to assemble it. Terpenoids are terpenes that have been chemically modified by either demethylation (removal of methyl groups) or oxidation (addition of oxygen atoms). Based on these classifications, diterpenoids are composed of two modified terpene and four isoprene units. Tetracylcic indicates that the molecule contains four rings in its molecular structure (Figure 1.6).

All GAs are synthesised in plastids by the terpenoid pathway and then modified in the endoplasmic reticulum and cytosol to become biologically active forms. In higher plants, they are produced primarily from the methylerythritol phosphate (MEP) pathway. This pathway initially involves trans-geranylgeranyl diphosphate (GGDP) synthesising a hydrocarbon intermediate *ent*-kaurene,

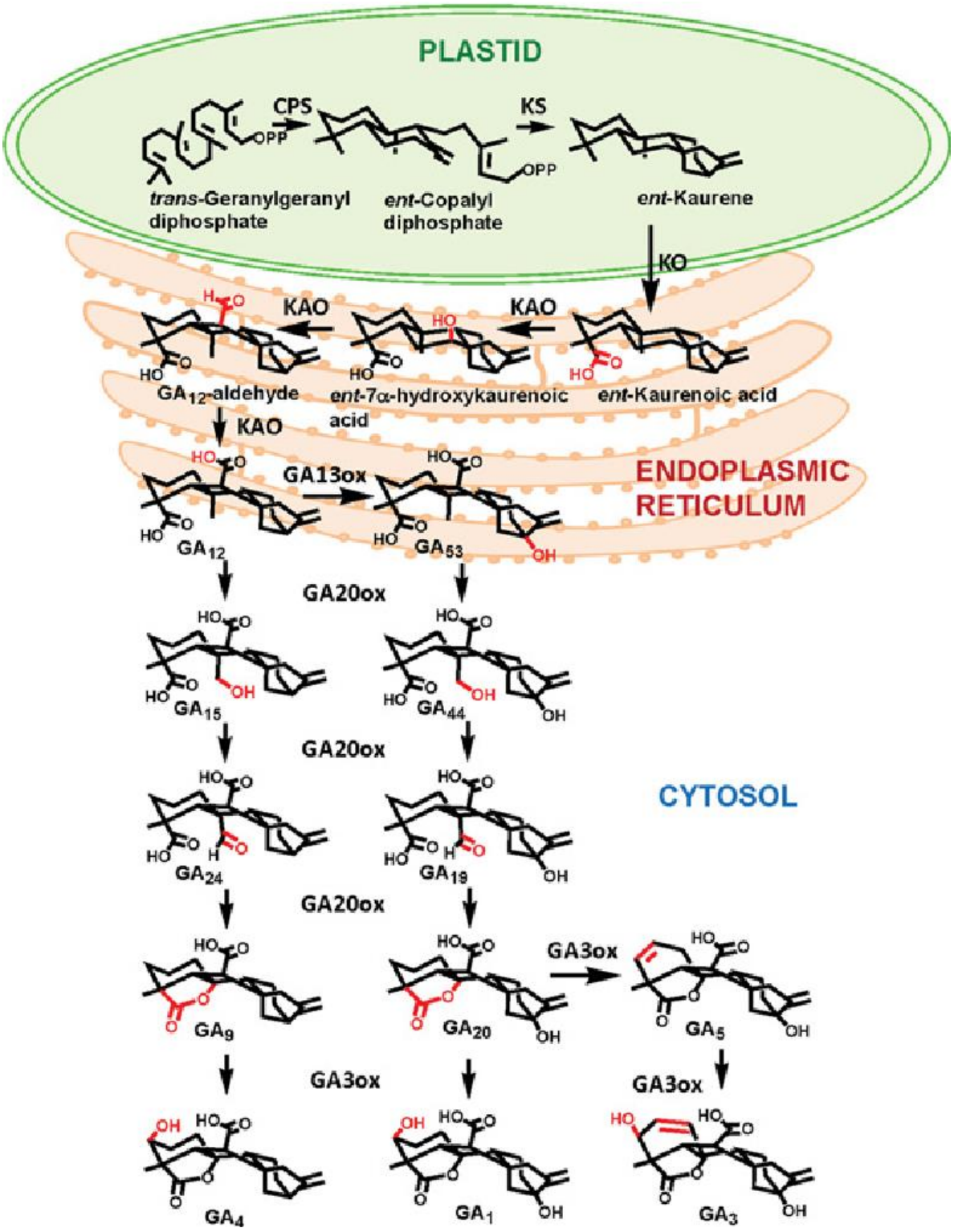

Figure 1.6 A simplified schematic of the GA-biosynthetic pathway from trans-geranylgeranyl diphosphate in the plastid to the production of bioactive gibberellins GA_1, GA_3 and GA_4 in the cytosol. Active GAs are produced by conversion of GA precursors, which is catalysed by GA20ox and GA3ox and inactivated by GA2ox. From (Hedden and Thomas, 2012).

which is subjected to a series of chemical modifications (Hedden and Thomas, 2012). Three classes of enzymes are used to synthesis GA from GGDP: 1) terpene synthases (TPSs) in the plastid 2) cytochrome P450 monooxygenases (P450s) in the endomembrane system, and 3) 2-oxoglutarate–dependent dioxygenases (2ODDs) in the cytosol (Yamaguchi, 2008). For a detailed overview of this biosynthetic pathway see the review by Heddon and Thomas, 2012.

GAs are ubiquitous in higher plants and have also been found in some lower plants, as well as several fungal species and certain species of endophytic bacteria (Hedden and Thomas 2012). The majority of GAs in plants are inactive and either exist as biosynthetic precursors, or catabolites (or precursors) of the active hormones. GA levels are therefore regulated at both biosynthesis of its precursors, through hydroxylation by GA 20-oxidases (GA20OX) and GA 3-oxidases (GA3OX) and degradation, which is mainly catalysed by GA–oxidases (GA2OX). GAs come in two forms, based on the number of carbon atoms in their *ent*-gibberellin structure, *ent*-gibberellane (C_{20}) or 20-nor-*ent*-gibberellane (C_{19}). They are termed GA_1 through to GA_n, based on the order of their discovery. The C_{19} structure has lost its carbon 20 and in place is a five-member lactone bridge linking carbon 4 and 10 (Figure 1.6). Most biologically active forms of gibberellins are generally of this structure.

The most common forms of bioactive GAs in plants are: gibberellin A_1 (GA_1) gibberellic acid (GA_3) and gibberellin A_4 (GA_4). Both GA_1 and GA_4 are likely to be functionally active (hormone) forms because they are found universally in plants and co-occur with their biosynthetic precursor and metabolites, often at much higher concentrations than the hormones themselves (Heddon and Thomas 2012). GA_3 is well-known for its discovery as the first gibberellic acid to be isolated and characterised from the fungal pathogen, *Gibberella fujikuroi,* (now reclassified as *Fusarium fujikuroi)* and its subsequent use in commercial applications.

1.4.4 The Green Revolution

The Green Revolution (most prominent from 1960-1970) was a major agricultural breakthrough that dramatically increased global crop productivity (Evans, 1998). This was largely down to a combination of high-yielding crop varieties with modern cultivation techniques, such as the application of synthetic fertilizers and pesticides (Gale, M. D. & Youssefian, 1985; Dyson, 1996; Conway, 1997; Evans, 1998). Unknown to the time, Gibberellin (GA) was the key phytohormone associated with semi-dwarf varieties of rice (*Oryza sativa*) and wheat (*Triticum aestivum*) that were selectively bred to produce higher yields during the green revolution (Pearce *et al.*, 2011). These cultivars displayed alterations in growth, resulting in shorter and stronger stems, which was mediated by mutations affecting either GA response or biosynthesis (Pearce *et al.*, 2011). This semi-dwarfed phenotype was advantageous to the agricultural industry because crops were less

sussceptible to lodging (falling over) and have an increased grain yield to straw mass ratio (Gale, M. D. & Youssefian, 1985; Evans, 1993). Semi-dwarfing genes responsible for this phenotype are termed as either GA-insensative or GA-sensistive and will be discussed in detail later.

Research into GA signaling has revealed that bioactive GAs play a key role in controlling the developmental processes of cell division and expansion (reviewed by Claeys et al. 2014), which are crucial for plant growth. However, the molecular components that integrate GA signaling and how they regulate growth at the cellular level is still not entirely understood (Heo *et al.*, 2011). If we can enhance our understanding of the GA pathway, then we can potentially use this information to further increase crop yields and reliability in a much more specific and controlled way than has been done before.

1.4.5 How GA promotes growth and development

GAs promote organ growth by enhancing cell elongation and in some cases, cell division. It can also promote various developmental processes such as seed dormancy and germination, vegetative growth and flowering, pollen maturation and seed development (Davière and Achard, 2013; Lor and Olszewski, 2015). This essential role is reinforced when examining the phenotype of biosynthetic mutants for gibberellic acid (GA-deficient mutants) of *Arabidopsis thaliana*, which demonstrate defects in all of these processes. For example, the *ga1-3* mutant contains a large deletion in the *GA1* gene, which encodes the catalytic enzyme, *ent*-copalyl diphosphate synthase, responsible for the first step of GA biosynthesis (Sun and Kamiya, 1994; Tyler *et al.*, 2004). A large reduction in bioactive GAs in this mutant results in plants being severely dwarfed, dark green in colour, male-sterile and unable to germinate (Koornneef and van der Veen, 1980; Silverstone *et al.*, 2001). All of these defects can be rescued by exogenous application of GA (Koornneef and van der Veen, 1980). For some time, it had been recognized that GA is a regulator of shoot growth, but it has also been demonstrated to be an important regulator of root growth (Fu and Harberd, 2003; Griffiths *et al.*, 2006; Ueguchi-Tanaka *et al.*, 2007; Willige *et al.*, 2007). Indeed, the aforementioned *ga1-3* mutant (Sun and Kamiya, 1994) exhibits shorter roots. Furthermore, it has recently been reported that GA regulates root cell elongation (Ubeda-Tomás *et al.*, 2009), which will be discussed in more detail later.

1.4.6 The GA-GID1-DELLA mechanism for mediating plant growth

The growth control mechanisms behind GA action have not yet been fully characterized, but recent progress in the understanding of its synthesis and biochemical pathway in relation to cell expansion has dramatically improved our knowledge of such processes (Yamaguchi, 2008). The discovery that

GA functions by binding with a soluble receptor known as GIBBERELLIN INSENSITIVE DWARF1 (GID1) (Ueguchi-Tanaka *et al.*, 2005; Griffiths *et al.*, 2006) was an important factor in defining the GA signaling pathway. Using a mutant based approach, GID1 was first identified in rice (Ueguchi-Tanaka *et al.*, 2005), followed by three functionally redundant orthologues in *Arabidopsis thaliana* – *GID1a*, *GID1b* and *GID1c* (Nakajima *et al.*, 2006). The fact that the *gid1a-c* triple mutant is severelly dwarfed and insensitive to GA implies it is essential as a functional receptor for the gibberellin response (Griffiths *et al.*, 2006; Iuchi *et al.*, 2007; Willige *et al.*, 2007).

A regulatory pathway has emerged in which DELLA proteins act as repressors of GA signalling (Peng *et al.*, 1997; Silverstone *et al.*, 1998; Ikeda *et al.*, 2001; Chandler *et al.*, 2002; Itoh *et al.*, 2002). Repression of GA responses is controlled by DELLA proteins through their regulation of transcription and this has recently been covered in several reviews (Davière and Achard, 2013; Claeys *et al.*, 2014). This repression is relieved by the production of bioactive GAs in response to environmental and developmental stimuli, which promotes the rapid degradation of DELLA proteins via the ubiquitin-proteasome pathway - an important mechanism used in hormone signalling for the regulation of transcriptional repressor abundance (Santner and Estelle, 2009).

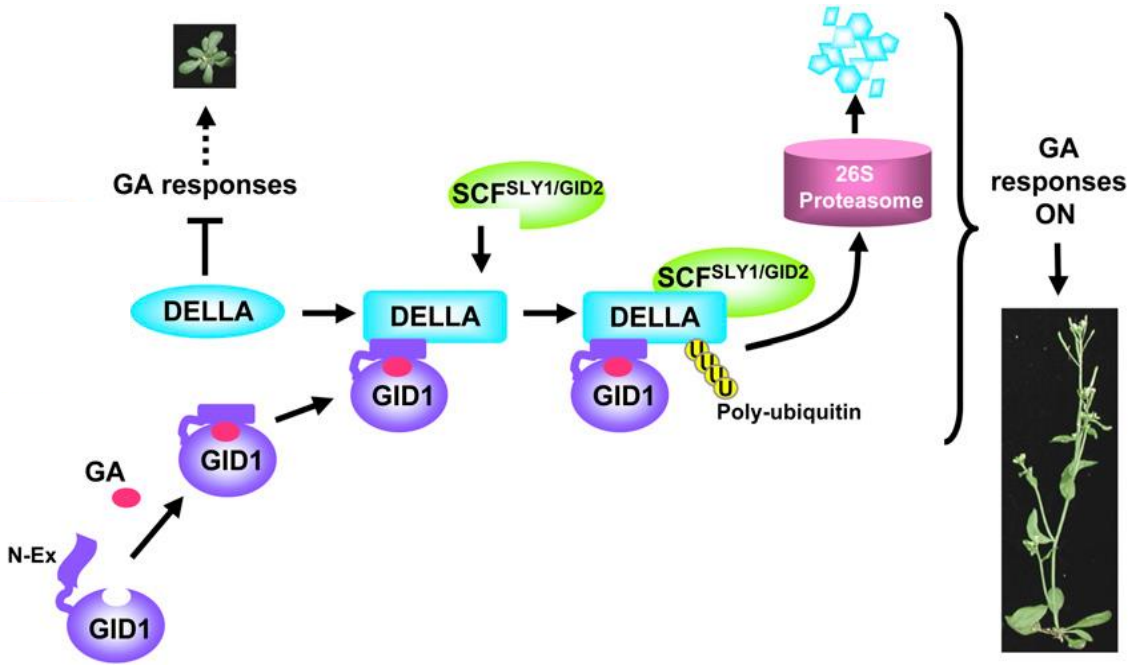

Figure 1.7 Model of GA signalling in plants. Bioactive GA binds to GID1. The GA-GID1 complex then binds to DELLA proteins incorporating $SCF^{SLY1/GID2}$ which initiates polyubiquitination and degradation via the ubiquitin-proteasome pathway. This promotes activation of GA responses. When DELLAs are unbound to the GA-GID1 complex, they negatively regulate GA responses by co-transcriptional activation of GA repressive genes. Adapted from (Sun, 2010).

This pathway is initiated by the presence of bioactive GAs binding to the C-terminal end of the GID1 receptor, resulting in a conformational change of a flexible region at the N-terminal end of GID1 (Griffiths *et al.*, 2006; Nakajima *et al.*, 2006) and causing it to fold across the GA-binding pocket and exposing a DELLA domain-binding site (Murase *et al.*, 2008; Shimada *et al.*, 2008). Increased levels of GA and the subsequent binding of this hormone to its receptor, promotes formation of the GA-GID1-DELLA complex (Ueguchi-Tanaka et al. 2005; Shimada et al. 2008; Ueguchi-Tanaka et al. 2007). Assembly of DELLAs into this complex leads to a conformational change within the GRAS domain of the DELLA protein that facilitates binding of an F-box protein, known as GIBBERELLIN INSENSITIVE 2 (GID2) in rice and SLEEPY (SLY) in *Arabidopsis* (McGinnis *et al.*, 2003; Sasaki *et al.*, 2003; Hirano *et al.*, 2010; Ariizumi *et al.*, 2011). These proteins act as substrate receptor subunits for the E3 ubiquitin ligase SCF (Skp-Culin-F-box) protein complex, which tags DELLA proteins by polyubiquitination and targets its degradation by the 26S proteasome (McGinnis *et al.*, 2003; Sasaki *et al.*, 2003; Dill *et al.*, 2004) (Figure 1.7).

1.5 DELLA proteins

1.5.1 The structure and function of DELLA proteins

DELLA proteins are class of nuclear-localised transcriptional regulators that are a subfamily of the GRAS (named after the first three proteins to be discovered - GAI, RGA and SCARECROW) superfamily (Pysh et al. 1997, 1999). GRAS proteins function as transcriptional regulators and have diverse functions (Peng *et al.*, 1999; Ikeda *et al.*, 2001; Chandler *et al.*, 2002). Members of this superfamily all have a conserved C-terminal GRAS domain, which is attributed to its regulatory function, and contain various leucine heptad repeats (LHR) together with nuclear localisation signals. The DELLAs have been named after a highly conserved binding motif consisting of the amino acids aspartic acid (D), glutamic acid (E), leucine (L), leucine (L) and alanine (A) that is located at the N-terminal portion and is necessary for GID1 binding (Dill, Jung, & Sun, 2001; Griffiths et al., 2006; Willige et al., 2007). Another defining feature of the DELLA family is the precence of a second motif, TVHYNP (also named after the most commonly occuring amino acids in the sequence), positioned close to the DELLA motif. The DELLA/TVHYNP motif is collectively termed as the DELLA domain (Figure 1.8). Mutations within this region, such as the *Arabidopsis* semi-dominant *gai-1* mutant alelle (containing a 17 aa deletion) (Koorneef *et al.*, 1985), leads to a semi-dwarfed phenotype as GAI protein is rendered insensitive to GA-targeted degradation (Dill et al., 2004; Koorneef et al., 1985; Peng et al., 1997). Semi-dwarf plants therefore have a reduced GA response and demonstrate stunted growth and reduced elongation (Koorneef *et al.*, 1985; Peng and Harberd,

1993). This phenotype closely resembles that of a GA-biosynthetic mutant, but cannot be rescued by exogenous GA.

Figure 1.8 The general structure of DELLA proteins. Here, the N-terminal DELLA binding domain including the DELLA/TVHYNP motifs is highlighted. The C-terminal GRAS domain is also highlighted. The red line indicates the proposed protein modification responsible for semi-dwarfing alleles of wheat. From (Lor and Olszewski, 2015).

In *Arabidopsis* there are five *DELLA* genes (*GA-INSENSITIVE [GAI], Repressor of ga1-3 [RGA], RGA-LIKE1 [RGL1], RGL2,* and *RGL3*) which have distinct, but overlapping functions in relation to plant growth and development (Dill and Sun, 2001; S. Lee *et al.*, 2002; Wen and Chang, 2002; Tyler *et al.*, 2004). Orthologous genes have also been identified in various agricultural plant species, such as *SLENDER RICE1 (SLR1)* in rice (*Oryza sativa*) (Ikeda *et al.*, 2001), *DWARF-8 (D8)* in maize (Winkler and Freeling, 1994) and most notably, *REDUCED HEIGHT1* (*RHT1)* in wheat (*Triticum aestivum*) (Peng *et al.*, 1999). Mutant alleles of the *rht1* gene in common bread wheat are responsible for the semi-dwarf cultivars of the green revolution. Bread wheat has a hexaploid genome, consisting of three homoeologous chromosome sets (A, B and D genome). Peng *et al.* (1999) identified semi dominant mutant dwarfing alleles at two loci, *Rht-B1* and *Rht-D1,* which have a reduced response to GA due to deletions within their DELLA region.

GAI and *RGA* are primarily associated with negative regulation of GA-signalling and this function is highly conserved among monocots and dicots (Dill & Sun, 2001). Both of these proteins demonstrate partial redundancy in relation to repression of the GA-signalling pathway and are 82% identical in amino acid sequence (Dill and Sun, 2001). Consequently, RGA and GAI are the main repressors controlling vegetative growth, such as stem and hypocotyl elongation, and floral induction (Peng *et al.*, 1997; Dill *et al.*, 2001; Fleck and Nicholas P. Harberd, 2002). In relation to root growth, loss of function of both GAI and RGA in the *ga1-3* mutant background is able to supress the *ga1-t* phenotype, thus demonstrating that the GA-GID1-DELLA pathway acts to regulate this process (Fu and Harberd, 2003).

GAI was first identified in the semi-dwarfed recessive *gai-1* mutant described earlier (Koorneef *et al.*, 1985). RGA was originally identified in the GA biosynthetic mutant, *ga1-3*, where a recessive mutation was able to confer a partial suppression of the dwarf phenotype (Silverstone *et al.*, 1997).

Since then, a mutant form of RGA-GFP containing the same 17 aa deletion as the *gai-1* mutant line, was constructed and demonstrated a similar phenotype as described for *gai-1* (Dill *et al.*, 2001).

1.5.2 How GA relates to cell division control in a DELLA-dependent manner

We currently have very little knowledge as to how GA relates to cell division control, but two papers in 2009 published in conjunction with each other have shed light on this matter. These studies revealed that GA signaling is able to positively regulate cell division and negatively regulate the duration of the mitotic window (Achard *et al.*, 2009; Ubeda-Tomás *et al.*, 2009).

Using genetic and pharmacological approaches, Ubeda-Tomás et al. 2009 examined the role of GA-signaling in the endodermis and how it regulates root meristem size. Targeted expression of a GA-insensitive mutant form of GAI in dividing endodermal cells disrupted cell proliferation and blocked an increase in meristem size (Ubeda-Tomás *et al.*, 2009). This revealed a novel function of GA controlling root cell proliferation by signaling the destruction of DELLAs in endodermal cells (Ubeda-Tomás *et al.*, 2009). To further understand the function of DELLAs in restricting cell proliferation, an accompanying paper used a kinematic approach to analyse leaf, shoot and root meristem growth of the GA-biosynthetic mutant line *ga1-3*, which they compared with WT and a quadruple DELLA null mutant (*gai-t6, rga-t2, rgl1-1, rgl1-2*) (Achard *et al.*, 2009). Their results implied that accumulation of DELLAs in the *ga1-3* line is sufficient to reduce early leaf growth and decrease shoot and root meristem size by reducing the rate of cell proliferation. Moreover, the authors transformed a Cyclin B1-GUS translational reporter construct into the *ga1-3* mutant line and a double mutant DELLA line, *gai-t6 rga-t2* (lacking both RGA and GAI) in order to visualize cells at the G_2-M phase. This allowed them to monitor mitotic activity in the root meristem. They found that the number of dividing cells in the proximal meristem of the *ga1-3* line was significantly reduced in comparison to the *gai-t6 rga-t2* and that GA treatment was sufficient to increase the amount of dividing cells in the *ga1-3* mutant. Interestingly, they revealed that transcript levels of CDK inhibitors (CKIs), specifically KRP2, were increased in *ga1-3* when compared to WT. Therefore, it is likely that DELLAs restrict cell proliferation by modulating the cell cycle, specifically by enhancing the levels of CDK inhibitors (Achard *et al.*, 2009). In support of these findings, a recent paper published by Serrano-Mislata *et al.* in 2017, discovered that DELLAs limit meristem size by directly upregulating *KRP2* transcript levels in the inflorescence tip. This was discovered using Chip-Seq analysis of dwarf transgenic plants expressing a GA-resistant form of RGA in inflorescence apices and is the first example demonstrating a direct link between the DELLA pathway and the cell cycle (Serrano-Mislata *et al.*, 2017).

These papers combined are an important step in understanding the GA-signaling pathway associated with growth control and the rate of cell proliferation. It is likely that GA plays an important role in modulating the cell cycle because it is a regulator of growth, which depends on the rate of cell proliferation and cellular elongation. Exactly how these mechanisms are integrated remains unknown and further research into the molecular components that control them is required. Research into how DELLAs control gene expression by acting as transcriptional regulators has helped elucidate how these mechanisms might work. A paper published in 2014, revealed that DELLA proteins directly regulate the activity of a plant-specific class I TCP transcription factor family, which are key regulators of cell proliferation (Martín-Trillo and Cubas, 2010; Daviere *et al.*, 2014). In the inflorescence shoot apices of *Arabidopsis* seedlings, DELLAs were shown to bind directly to the DNA-recognition domain of class I TCP factors, thereby inhibiting their transcriptional activity (Daviere *et al.*, 2014). GA antagonizes this repression by signaling the targeted destruction of DELLA proteins, which leads to an enrichment of TCP factors to promotors of core cell-cycle genes. The authors went on to conclude that this GA-regulated interaction in the shoot is a novel mechanism for controlling plant height (Daviere *et al.*, 2014).

1.5.3 The role of DELLAs as transcriptional co-activators and inhibitors

DELLAs have diverse and multiple roles during plant development and in response to abiotic and biotic stresses. There is mounting evidence to suggest that this is due their promiscuous ability to interact with various transcription factors or regulatory proteins from different families (Davière & Achard 2013; Davière & Achard 2016; Locascio et al. 2013; Serrano-Mislata et al. 2017). Indeed, the main outcome of hormonal signalling pathways is alterations in gene expression levels (Locascio *et al.*, 2013). Moreover, since DELLA proteins are nuclear localised and are structurally similar to the mammalian Signal Transducers and Activation of Transcription (STAT) family of proteins (Richards *et al.*, 2000), it is likely that they are involved in transcriptional regulation.

Although DELLA proteins do not contain any identifiable DNA binding domains, they have been shown to associate with promoters of GA-responsive, cytokinin-responsive and *KRP2* genes by chromatin immunoprecipitation (Zentella *et al.*, 2007; Park *et al.*, 2013; Marín-de la Rosa *et al.*, 2015; Serrano-Mislata *et al.*, 2017). Furthermore, several experiments have demonstrated that DELLA proteins are able to induce the transcription of genes (Zentella *et al.*, 2007; Gallego-Bartolomé, Kami, *et al.*, 2011) and that the DELLA domain itself is responsible for this type of transactivation (Hirano *et al.*, 2012). This emerging evidence suggests that DELLAs act as transcriptional co-activators by binding with transcription factors (TFs), and thereby induce the expression of genes that are associated with the suppression of GA responses (Lor and Olszewski,

2015). In support of this theory, modified DELLA proteins with enhanced transcriptional activity and reduced transcriptional activity demonstrated an increase and decrease in growth repression activity, respectively (Hirano *et al.*, 2012). Moreover, increasing reports have revealed that DELLAs are able to bind with over 100TFs and regulate their association with target promoters (de Lucas *et al.*, 2008; Feng *et al.*, 2008; Hou *et al.*, 2010; Lim *et al.*, 2013; Daviere *et al.*, 2014; Fukazawa *et al.*, 2014; Yamaguchi *et al.*, 2014; Yoshida *et al.*, 2014; Resentini *et al.*, 2015). Recently it has been shown that, although the GRAS domain does not activate transcription alone, it facilitates the interaction of DELLAs to intermediate DNA-binding proteins (Hirano *et al.*, 2012), such as GAI-ASSOCIATED FACTOR (GAIF1) and members of the indeterminate domain (IDDs) protein family (Fukazawa *et al.*, 2014; Yoshida *et al.*, 2014). Another interesting study (Marín-de la Rosa *et al.*, 2015) found that RGA is enriched to promotors of 12 different transcription families. Moreover, they demonstrated that RGA and GAI act as transcriptional co-activators by binding with type-B ARABIDOPSIS RESPONSE REGULATORS (ARR) at the promoters of cytokinin-regulated genes. Cytokinin and GA have been shown to antagonistically regulate multiple plant developmental processes (Weiss and Ori, 2007), including root growth (Ubeda-Tomás *et al.*, 2008; Achard *et al.*, 2009; Marín-de la Rosa *et al.*, 2015).

Independent of transactivation activity, DELLAs have also been shown to physically bind with and inhibit the activation of transcription factors. The first studies to demonstrate this resulted from research into the integration of gibberellin signalling and light during cell elongation (de Lucas *et al.*, 2008; Feng *et al.*, 2008; Santner and Estelle, 2009). Both papers support the idea that DELLAs are transcriptional regulators by demonstrating a direct interaction of RGA and GAI with two nuclear transcription factors, PHYTOCHROME INTERACTING FACTOR 3 (PIF3) and PIF4 (de Lucas *et al.*, 2008; Feng *et al.*, 2008). These basic helix-loop-helix transcription factors are members of a larger subfamily, bHLH, that share similar DNA-binding domains (de Lucas *et al.*, 2008; Feng *et al.*, 2008). When DELLAs interact with the binding domains of PIF3 and PIF4, their transcriptional activity is sequestered to inhibit hypocotyl elongation during photomorphogenesis (de Lucas *et al.*, 2008; Feng *et al.*, 2008; Plackett *et al.*, 2014). Since then, DELLAs have been found to competitively bind with and inhibit the activity of a variety of other proteins, including transcription factors, transcriptional regulators and co-chaperones that impinge on a range of developmental and hormonal pathways (Lor & Olszewski 2015; Davière & Achard 2016). For example, DELLAs have been shown to mediate the activity of: the class I TCP family of transcription factors associated with the regulation of cell proliferation (Daviere *et al.*, 2014), the BRASSINAZOLE RESISTANT1 (BZR1) transcription factor associated with regulation of gene expression in response to brassinosteroid signalling (Gallego-Bartolomé *et al.*, 2012) and the JA ZIM-domain 1 (JAZ1)

transcription factor, a key repressor of jasmonate (JA) signalling (Hou *et al.*, 2010). Thus, DELLA proteins not only repress the GA-response, but also influence the activity of other signalling pathways. This would explain why GA signalling demonstrates such a high level of cross-talk with other hormonal signalling pathways and these molecular mechanisms have been studied extensively for a variety of developmental processes (Gallego-Bartolomé, Arana, *et al.*, 2011; An *et al.*, 2012; Bai *et al.*, 2012; Gallego-Bartolomé *et al.*, 2012; Hou *et al.*, 2016). Cross talk between GA signalling pathways in relation to plant growth has been covered in detail in the reviews by Lor & Olszewski (2015) and Davière & Achard (2016). Furthermore, a recent paper has revealed that these DELLA-associated transcriptional networks have been evolutionary conserved over time, playing increasing roles in coordinating multiple regulatory pathways and reinforcing the fact that DELLAs are likely to act as regulatory 'hubs' in higher plants (Briones-Moreno *et al.*, 2017).

1.5.4 SCARECROW and the missing link

SCARECROW (SCR) and SHORTROOT (SHR) are important members of the GRAS superfamily. In the *Arabidopsis* root, SCR and SHR function as a heterodimer complex to control specification and maintenance of the stem cell niche and ground tissue formation (Di Laurenzio *et al.*, 1996; Helariutta *et al.*, 2000; Sabatini *et al.*, 2003; Paquette and Benfey, 2005; Cui and Benfey, 2009). Radial patterning within the stem cell niche is determined as a result of tightly controlled mechanisms that regulate cell specification and cell division. Asymmetric cell divisions and the spatial context in which they are confined, play an important role in establishing this type of cell patterning (Cruz-Ramírez *et al.*, 2012). A recent paper investigating the spatial restriction of asymmetric cell divisions within the stem cell niche of the *Arabidopsis* root has discovered that this process relies on the physical binding of SCR to the RETINOBLASTOMA-RELATED (RBR) protein (Cruz-Ramírez *et al.*, 2012). Biochemical analysis revealed that the SCR-RBR interaction is mediated by the binding of RBR to a highly conserved Leu-x-Cys-x-Glu (LxCxE) amino acid motif contained within the SCR protein (Cruz-Ramírez *et al.*, 2012). This was achieved by generating a variant of the SCR protein where the LxCxE motif was mutated to AxCxA and its capacity to bind RBR was tested using a yeast two hybrid assay (Cruz-Ramírez *et al.*, 2012). The authors found that the SCR^{AxCxA} variant maintained its interaction with SHR with the same efficiency as WT SCR, but lost its capacity to bind RBR, thus confirming that this motif is essential for the SCR-RBR interaction (Cruz-Ramírez *et al.*, 2012).

The *Arabidopsis* GAI gene is closely related in sequence to SCR (Peng *et al.*, 1997) and contains the LxCxE motif, thus suggesting a potential interaction with the RBR pathway. Interestingly, GAI homologues are found in some early land plants, all monocotyledons and some dicotyledons, with

the LxCxE motif being highly conserved between them. Conversely RGA homologues are found only in dicots and do not contain this motif, but instead have a highly conserved equivalent of MxCxE. The fact that these motifs have been so highly conserved throughout history (since the divergence of monocots and dicots approximately 130 million years ago) strongly suggests that there must be some sort of functional relevance for these differences between RGA and GAI.

Further evidence to support a potential interaction between RBR and DELLA proteins is that there is a significant overlap (70%) between the expression profiles of their target genes (Figure 1.9). Moreover, emerging research into how GA controls cell proliferation (Achard *et al.*, 2009; Ubeda-Tomás *et al.*, 2009) provides an indication of how DELLA proteins regulate the cell cycle, but there is currently no published evidence to suggest a direct binding between DELLA proteins and RBR. Here, I report on my findings from investigating a putative interaction for both RGA and GAI with RBR, to determine whether there is a functional difference between these DELLA proteins, specifically in relation to their molecular mechanisms of regulating cell cycle control.

AGI Locus		RBR target
At2g45900	Expressed protein (Exp-PT1)	
At1g15550	GA3ox1	y
At5g51810	GA20ox2	
At1g50420	SCL3	y
At4g19700	RING-E3 HCa type (RING)	y
At3g63010	GID1b	y
At3g05120	GID1a	y
At4g36410	UBC17	
At2g04240	XERICO	y
At1g54120	Expressed protein	y
At1g56650	MYB75	
At5g19340	Expressed protein	y
At4g23060	IQD22	y
At1g17830	Expressed protein	y
At5g18840	Sugar transporter, putative similar to ERD6	
At5g03670	Expressed protein	y
At1g29270	Expressed protein	
At3g30180	BR6ox2	y
At1g68570	H+-dependent oligopeptide transport family protein	y
At5g67480	BT4 (BTB/TAZ domain protein 4)	y
At5g47550	Cys protease inhibitor, putative/cystatin	y
At1g21250	WAK1 (Wall-Associated Kinase1)	y
At5g05180	Expressed protein	y

Figure 1.9 There is a 78% overlap between the top highest DELLA induced genes and RBR targets and 70% in total. These observations were made by comparing microarray data sets for DELLA and RBR targets. From (Zentella *et al.*, 2007; Borghi *et al.*, 2010).

Aims and objectives:

Using the *Arabidopsis thaliana* as a model system for investigating DELLA proteins in the developing root, I will attempt to address the following aims:

1. Investigate a putative interaction between RBR and GAI (and possibly RGA). The GAI protein contains an LxCxE motif and the RBR protein contains a corresponding LxCxE binding pocket domain. The recent finding that a closely related GRAS protein, SCR binds RBR through its LxCxE motif suggests a putative interaction between GAI and RBR. The fact that RGA contains an MxCxE motif, would suggest it does not bind with RBR and that there is a functional difference between GAI and RGA in relation to cell cycle regulation. A biochemical approach and the use of Förster resonance energy transfer (FRET) will be used to investigate these interactions *in vitro* and *in vivo*, respectively.

2. Determine whether or not there is a functional difference between GAI and RGA in relation to plant growth and development. Although GAI and RGA are highly similar in amino acid sequence and have overlapping functions, they still may have developed unique aspects to their molecular mechanisms of control. In order to investigate putative differences, the expression patterns of RGA and GAI in the primary root will be investigated using translational reporter lines with a GFP tag. Furthermore, null mutants for *rga* and *gai* will be individually crossed to a *ga1* biosynthetic mutant to generate homozygous lines in order to investigate differences between these mutant phenotypes. This will be done by performing kinematic analysis of primary root growth, root meristem size and cell number and cell production rate.

3. Understand the molecular mechanism as to how GA relates to cell division control. If a direct binding between GAI and RBR is found, it will be important to understand the molecular basis for this interaction and what it leads to. Whether RBR modulates the activity of GAI or vice versa, would be a key question to address. In order to understand how GA relates to cell division control, null mutant lines for *rga* and *gai*, and the *ga1* biosynthetic mutant will be crossed with cell cycle mutant lines either overexpressing cyclinD's or KRPs. The resulting phenotypes of these lines will be examined. Furthermore, transcript levels of key cell cycle regulator genes will be quantified in these mutant lines.

Chapter 2

Materials and Methods

Chapter 2: Materials and Methods

2.1 Plant Lines and Growth Conditions:

2.1.1 Seed sterilisation

Seeds grown *in vitro* were surface sterilised by submerging them in a bleach solution [20 % bleach in ultrapure deionised water, 0.1% Tween] for 6 minutes and rinsing five times in autoclaved deionised water. Seeds were then re-suspended in sterile 0.2% agarose. The sterilisation procedure was conducted under a laminar flow hood to ensure sterile conditions were maintained throughout.

For surface sterilisation of seeds at the Gregor Mendel Institute (GMI), Vienna, in the laboratory of Prof. Wolfgang Busch, the protocol for use of their high-throughput root phenotyping pipeline was followed (Slovak et al, 2015). For this purpose, seeds were sterilised in an airtight box with chlorine gas in a chemical fume hood. This involved placing seeds in 1.5 ml microcentrifuge tubes on a rack (approximately 100 seeds for each tube), which was placed in the airtight box along with a beaker containing 130 ml of 10% sodium hypochlorite and a magnetic stirrer bar. The box was then placed with the beaker lined-up to a magnetic stirrer and 3.5 ml of 37% hydrochloric acid was rapidly added to it to generate chlorine gas. The lid of the container was quickly sealed shut with clamps to make it airtight and the chemical reaction was left to sterilise the seed for 1 hour. The lid was then removed and left to vent in the chemical hood for a further half an hour. Tubes were sealed shut prior to removal from the hood to ensure they remained sterile.

2.1.2 *In vitro* growth conditions

Surface sterilised seeds were grown on plates containing germination (GM) root media consisting of 2.3 g/L Murashige and Skoog medium (MS), 1.5% agar and 0.75% sucrose. GM root media is specifically used to allow vertical growth of seedlings over the surface of the medium. Prior to growth, seeds on plates were subjected to a stratification treatment by imbibing in the dark at 4°C for 2-3 days, to help synchronise germination. Plates were then transferred to a Percival growth cabinet (Percival Scientific Inc, USA) with 16 h-light/8 h-dark at a constant temperature of 21°C and 70% humidity. For screening of transgenic plants with resistance genes, GM root media was supplemented with the appropriate selective reagent.

For experiments involving exogenous GA application, or for seeds unable to synthesise GA to germinate, GM root media was supplemented with 10 and 2.5 µM GA_3 (Sigma-Aldrich, USA), respectively. For experiments involving GA inhibition, seedlings were first grown on GM root and then

transferred to fresh plates containing GM root media supplemented with 10 µM of the GA-biosynthetic inhibitor, paclobutrazol (PAC – Simga-Aldrich).

2.1.3 Plants in soil

Either seedlings grown *in vitro* or seeds were directly transferred to a 3:1 mixture of soil to sand. Plants were grown under controlled conditions in one of two plant growth rooms with a 16-hour photoperiod at 21°C. Watering was performed regularly every 2-3 days.

2.1.4 WT plants and loss of function mutants

All *Arabidopsis thaliana* plant lines used were either in the *Columbia-0 (Col-0)* or *Landsberg erecta (Ler)* ecotype backgrounds. Loss-of-function *rga* mutants had previously been described as having a similar phenotype to wild type (WT) plants. The *rga-28* allele contains a T-DNA insertion 718 nucleotides after the translation start site (TSS) of the *RGA* gene, which does not contain any introns (Tyler *et al.*, 2004). This allele had been transformed into the *Col-0* ecotype null mutant to generate an *rga-28* null mutant. The loss-of-function *gai-td1* mutant allele is from the SAIL collection (SAIL_82_F06) and contains a T-DNA insertion 192 nucleotides after the TSS of the *GAI* gene (Sessions *et al.*, 2002). The *GA1* biosynthetic mutant has also been described previously (Tyler *et al.*, 2004). The *ga1-t* allele (SALK_023192) contains a T-DNA insertion that has been isolated in the *Col-0* ecotype and has the same insertion point as the *ga1-3* allele in Ler. Transcript levels of *RGA* for *rga-28*, *GAI* for *gai-td1* and *GA1* for *ga1-t* were checked by qPCR on cDNA extracted from 10-day-old seedling using primers designed to flank the T-DNA insertion points (Table 2.3). Furthermore, these lines were genotyped using allele specific-primers (Table 2.3).

Gene	Locus	Mutant Allele	Mutant Type	Ecotype	Source
GAI	At1g14920	*gai-td1*	T-DNA (SAIL)	Col-0	Sessions *et al*., 2002
RGA	At2g01570	*rga-28*	T-DNA (SALK)	Col-0	Tyler et al., 2004
GA1	At4g02780	*ga1-t*	Deletion	Col-0	Shu et al., 2013

Table 2.1: loss of function mutant lines used for experiments

2.1.5 Transgenic plants

Transgenic *Arabidopsis* lines that either act as translational reporters or confer constitutive expression of a particular gene, were obtained from various sources.

The pRGA::GFP-RGA transgenic *Arabidopsis* line in the *Landsberg erecta (Ler)* background was generated to investigate the function and localisation of RGA under the control of its native promoter

(Silverstone *et al.*, 2001). This line contains a translational reporter of the *GFP-RGA* fusion gene (GFP fused to the N-terminal), which is flanked 8-Kb upstream of the 5' and 5.8-Kb downstream of the 3'end of the RGA locus (Silverstone *et al.*, 2001). The 35S::GFP-RGA line is also in the Ler ecotype and contains the GFP-RGA fusion protein, but is driven by the 35S Cauliflower Mosaic Virus (CaMV) promoter for ectopic expression. The type of GFP protein used in pRGA::GFP-RGA is the S65T GFP variant, which contains a single-point mutation resulting in enhanced fluorescence, photostability and a shifted excitation peak of 488 nm (Heim *et al.*, 1995). The pGAI::GAI-GFP transgenic line is also in the *Ler* ecotype and has been described previously (Fleck and Nicholas P. Harberd, 2002). This line contains a translational reporter of the *GAI-GFP* fusion gene driven by its native promoter. The exact region of this promoter is unknown as the paper that published the line did not specify. A summary of the different transgenic plants used is provided in Table 2.2.

Transgenic line	**Promoter**	**Antibiotic selection**	**Ecotype**	**GFP variant**	**Source**
pGAI::GAI-GFP	Native	Kan	Ler	Unknown	Fleck & Harberd 2002
35S::GAI-GFP	35S CaMV	Kan	Ler	Unknown	Fleck & Harberd 2002
pRGA::GFP-RGA	Native	Kan	Ler	S65T	Silverstone et al., 2001
35S::GFP-RGA	35S CaMV	Kan	Ler	S65T	Silverstone et al., 2001
35S::KRP2-GFP	35S CaMV	Kan	Col-0	smGFP	Bird et al., 2007
35S::KRP2	35S CaMV	Kan	Col-0	n/a	Bird et al., 2007
35S::CYCD3;1	35S CaMV	Kan	Ler	n/a	Dewitte et al., 2003
pE2FA::E2FA-GFP	Native		Col-0	Unknown	Magyer et al., 2012
pRBR::RBR-GFP	Native	Kan	Col-0	Unknown	Magyer et al., 2012
pRBR::RBR-RFP	Native	Hygro	Col-0	n/a	Ben Scheres (unpublished)

Table 2.2: List of transgenic lines used for experiments

2.1.6 Crossing procedures of *Arabidopsis* plants

Crosses were performed by selecting 3 – 4 of the eldest unopened flowers of the primary inflorescence stem and removing their petals, sepals and stamens for emasculation with fine (Type 5) forceps. Stigmas with observed pollen contamination and with unwanted flowers were removed. The pistols of these emasculated flowers were left to mature for between 1 - 2 days before cross pollination with

pollen from ripe stamens of the donor plant. To avoid contamination of unwanted pollen, forceps were cleaned regularly with 70 % ethanol and water between crosses. Successful pollination was observed by the development and gradual elongation of siliques. Once siliques of these F1 crosses had matured and dried, they were subsequently collected in an eppendorf tube and incubated at 37°C overnight to dry.

2.1.7 Selection of homozygous lines from F1 crosses

The seeds of F1 siliques were grown in soil and allowed to self-fertilise. Once mature, F2 siliques of these plants were collected and dried. Seeds of these siliques were taken to the next generation by planting 20-30 of them on soil. The genotypes of the F2 progeny were established with allele-specific primers to select for homozygous lines. Once homozygous plants had been identified, they were allowed to self-fertilise until they had developed F3 siliques. Seedlings from this generation were also genotyped and/or grown on an appropriate antibiotic selection medium to double-check that the plant is homozygous for all target alleles. Plants containing the *ga1-t* mutant allele are unable to germinate and have a distinctive phenotype of dark green leaves and severely stunted growth. Therefore, selection of homozygous lines containing this mutation were identified firstly, by plating seeds out onto GM root media (section 2.1.2) and transferring the ones that don't germinate to growth media supplemented with 10 µM GA_3 and secondly, by their distinctive phenotype. For selection of homozygous lines expressing GFP- or RFP-tagged protein, seedlings from F3 progeny were observed under a fluorescent microscope. Multiple F3 progeny were analysed until a line consistently expressing GFP/RFP in all of the observed seedlings (at least 30) was identified.

2.2 Molecular Techniques

2.2.1 Isolation of *Arabidopsis* genomic DNA

Genomic DNA used for genotyping and cloning was isolated from Arabidopsis plants using one technique. Fresh leaf plant material was harvested (usually cuttings of leaves at an earlier stage of growth development, or from whole seedlings) and ground in 1.5ml microcentrifuge tubes with a small clean pestle. 400µl of DNA extraction buffer (200 mM Tris, 250 mM NaCl, 25 mM EDTA and 0.5% w/v sodium dodecyl sulfate (SDS)) was added to the tube and briefly vortexed. Samples were then spun at maximum speed (14,000 rpm) in a benchtop microcentrifuge for one minute and 300 µl of the resulting supernatant was decanted into a new tube. An equal volume of isopropanol was added to precipitate the DNA. The tubes were inverted and incubated at room temperature for at least two minutes. Samples were then spun at 14,000 rpm for 15 minutes to pellet the DNA. The supernatant was discarded and the remaining pellet was washed in 1ml of 70% ethanol, followed by centrifugation

at 14,000 rpm for five minutes. The supernatant was removed and pellets were air-dried under a laminar flow hood for at least ten minutes to remove any residual ethanol. Dried pellets were then re-suspended in 50 – 100 µl of nuclease-free ultrapure MilliQ water (Merck Millipore, USA).

2.2.2 Isolation of plasmid DNA

Plasmids were isolated from minipreps of bacterial *E.coli* cultures using the commercially available QIAprep® Spin Miniprep Kit (QIAGEN GmbH, Germany). Minipreps were generated by incubating bacteria in 3 ml of LB broth containing a working concentration of the appropriate selection antibiotic (see 2.3.4 for concentrations) and incubating overnight at 37°C with gentle agitation (225 rpm). Cells were pelleted by centrifugation at 13,000 rpm for 2 minutes and resuspended in the resuspension solution according to the manufacturer's protocol. Cells were lysed by the addition of an alkaline solution containing proteases for removal of proteins and after 5 minutes, addition of a neutralization buffer. Samples were then subjected to centrifugation at 13,000 rpm for ten minutes at room temperature. The resulting supernatant was then added to a column containing a silica membrane to capture the DNA. Columns were washed several times with an ethanol-containing solution and centrifuged for a further minute at maximum speed to remove residual wash buffer. To elute the bound DNA, 50 µl of ultrapure deionised MilliQ water was added to the columns and spun at 13,000 for one minute. Samples were stored at -20°C.

2.2.3 Determination of nucleic acid concentration

For rough estimates of DNA/RNA concentrations, samples were run on an agarose gel to visualise DNA/RNA fragments alongside a DNA fragment size marker. The intensity of the band was compared to the intensity of other DNA fragments with known concentrations e.g. a DNA ladder.

More precise estimations of DNA/RNA concentrations were obtained using a NanoDrop-1000 Spectrophotometer (ThermoFisher Scientific, USA). This instrument allows the user not only to measure the DNA content, but also the purity of the sample by measuring the ratio of absorbance between 260 and 280 nm. Typical ratios of pure DNA samples are between 1.8 and 2.0. The measurement taken at absorbance 260 nm is used to determine DNA concentration. Even more accurate DNA/RNA quantifications were determined using a Qubit® 2.0 Fluorometer (ThermoFisher Scientific, USA) following their protocol and using the reagents provided in the DNA/RNA Qubit® Assay Kit.

2.2.4 Polymerase chain reaction (PCR)

Amplification of DNA was performed by PCR in a thermal cycler (Mastercylcer Pro, Eppendorf, Germany). Parameters were set based on the type of DNA polymerase used, the annealing temperatures of the primers and the length of the target fragment to be amplified. Primers were designed to be between 20-30 bps long, with a GC content between 40-45% and a minimal melting temperature (Tm) of 55°C, using Primer3 software (Koressaar and Remm, 2007). The software optimized primer selection based on minimal probability of formation of hairpin structures and primer dimers when primers were designed in pairs. Primer sequences and their purpose are provided in Table 2.3. For general diagnostic procedures, such as genotyping, the Qiagen Taq PCR Master Mix Kit (Qiagen, Netherlands) was used. For cloning purposes, DNA fragments of high accuracy were amplified using the Phusion High-Fidelity DNA Polymerase (Finnzymes, ThermoScientific, USA). All PCR products were analysed by gel electrophoresis. The protocols for use of these enzymes is described below.

Phusion High-Fidelity DNA polymerase

Since cloning requires high accuracy of DNA synthesis, amplification was performed with the Phusion High Fidelity DNA polymerase (New England Biolabs, USA) because it is reported to have a low error rate. Typical PCR reactions were performed in a total volume of 50 µl consisting of 5X Phusion HF buffer (making a final concentration of 1X), 200 µM of each dNTP, 0.5 µM of each forward and reverse primer, one unit of DNA polymerase and 1-5 µl of DNA template (depending on the concentration) and ultrapure MilliQ water to make up the final volume. Typical cycling conditions involved an initial denaturation step at 98°C for 30 seconds, followed by 30 cycles of: denaturation at 98°C for 30 seconds, annealing at or below the primer Tm for 30 seconds and extension at 72°C for 30 seconds/1kb of template length. A final extension was performed at 72°C for ten minutes and cooled at 4°C.

Qiagen Taq polymerase

Taq Polymerase comes as a 2X PCR Master Mix from Qiagen (1.5 mM $MgCl_2$, 200 µM of each dNTP, 5 units/ul Taq DNA polymerase). Typical PCR reactions were performed in a total volume of 10 µl containing 5 µl of 2X PCR Master Mix (to make a final concentration of 1X), 0.2 µM of each forward and reverse primer, 1 µl of DNA template and ultrapure MilliQ water to make up the final volume. Typical cycling conditions involved an initial denaturation step at 94°C for 3 minutes, followed by 30-35 cycles of: denaturation at 94°C for 30 seconds, annealing at or below the primer Tm for 30 seconds and extension at 72°C for one min/kb of template length. A final extension was performed at 72°C for ten minutes and cooled at 4°C.

2.2.5 Agarose gel electrophoresis

Agarose gels were made by adding 1% high-grade agarose powder (BIOLINE) to 1 x TAE (Tris-acetate-EDTA) buffer (40 mM Tris pH 8.0, 20 mM acetic acid, and 1 mM EDTA), which was heated until the agarose powder had melted and dissolved into the TAE buffer. This solution was then cooled slightly before the addition of SafeView (NBS Biologicals, UK) at the specified amount of 5 µl per 100 ml and poured into a casting mould with a sample well comb. Once set, the gel tank was filled with 1 x TAE buffer until the gel was fully submerged. DNA/RNA samples were combined with an appropriate amount of 6 x loading dye (30% glycerol and 0.25% Bromophenol Blue) and briefly vortexed or pipetted up-and-down to mix. 5-20 µl of each sample was then loaded into individual wells of the gel alongside 5 µl of a DNA fragment size marker: a 1 kb SmartLadder (Eurogentec, Belgium). DNA/RNA was electrophoresed at a constant voltage of 90V for approximately 30 minutes using a Bio-Rad Power Pack 300 (BioRad). Bands were visualised and captured with a UV transilluminator (Syngene).

2.2.6 Recovery of DNA from agarose gels and PCR reactions

DNA was isolated from agarose gels and PCR reactions using the Macherey-Nagel Nucleospin® Gel and PCR Clean-up kit (Macherey and Nagel, Germany) following the manufactures protocol. DNA fragments were excised from the gel by placing on a blue-light illuminator and using a semi-transparent orange filter. This method minimises the occurrence of DNA mutations instead of using UV for visualisation. Fragments were excised with a clean scalpel blade, placed in a 1.5 ml eppendorf tube and weighed. For each 100mg of gel weight, 200 µl of NTI binding buffer was added. Samples were then incubated at 50°C until the gel had completely dissolved. The resulting solutions were added to columns containing a silica gel for to bind the DNA and spun at 11,000 g for 30 seconds. The flow through was removed and columns were washed twice with the appropriate buffer containing an ethanol solution. The columns were centrifuged for a further minute to remove residual wash buffer and DNA was eluted with 50 µl of ultrapure deionised MilliQ water.

2.2.7 Digestion of DNA with restriction endonucleases

All digestion reactions of DNA were performed with restriction endonucleases from New England Biolabs (NEB, USA). Typical reactions were made up to a final volume of 20 µl containing 0.5 – 1 µg of DNA, 1X buffer, 1 - 5 units of enzyme/ug DNA and ultrapure deionised MilliQ water. Reactions were incubated at 37°C for a minimum of two hours. Resulting fragments were analysed by gel electrophoresis (see 2.2.4).

2.2.8 Ligation

Digested DNA fragments were ligated into vectors with corresponding restriction sites using the T4 DNA ligase enzyme (NEB, USA). Typical ligation reactions were made up to a final volume of 10 µl with a vector:insert ratio of 1:3, 1X reaction buffer and 1 µl of T4 DNA ligase. Reactions were incubated either at room temperature for 1 hour or at 4°C overnight. For transformation procedures, ligations were used immediately and otherwise were stored at -20°C.

2.2.9 Sequence analysis

All DNA sequences were analysed on an AB13730XL sequencing analyser provided by an external service (Eurofins, MWG, UK). Samples were prepared according to the manufactures protocol. Typically, a total volume of 15 µl containing a concentration of 50 ng/µl for plasmid DNA was sent. Analyses of sequences was performed using MaCVector 15.3.3 software (MacVector, Inc, USA).

2.2.10 Isolation of *Arabidopsis* RNA

RNA was isolated from *Arabidopsis* plant tissue using TriPure Isolation Reagent (Roche Diagnostics Ltd., UK). Approximately 50-200 mg dry weight of seedlings grown *in vitro* 7-10 days after stratification (DAS) were flash-frozen and ground in liquid nitrogen to a fine powder using a pestle and mortar. The powder was transferred to 2 ml eppendorf tubes, whilst maintaining frozen conditions throughout. 1.5 ml of Tripure isolation reagent (or 1 ml for less plant material) was added to each tube, mixed and then incubated for at least 5 minutes at room temperature. 350 µl (or 200 µl for less material) of chloroform was added to the solution and mixed. This was incubated at room temperature for 2-15 minutes with occasional mixing and was subsequently centrifuged at 12,000 g for 15 minutes at 4°C to separate the different phases. The colourless upper phase was then transferred to a fresh 1.5 ml eppendorf tube and an equal volume of isopropanol was added to precipitate the RNA. After mixing and incubating at room temperature for 10 minutes, the solution was centrifuged at maximum speed (14,000 rpm) for 10 minutes at 4°C. The supernatant was discarded and the resulting RNA pellet was rinsed twice with 1 ml of freshly prepared 70% ethanol, by vortexing and centrifuging at maximum speed for 1 minute each time. The supernatant was removed and the pellet was allowed to air-dry under a laminar flow hood for approximately 5 minutes, ensuring that the pellet doesn't completely dry out. The pellet was then resuspended in 50-100 µl of nuclease-free water heated to 80°C and mixed thoroughly. The sample was then split in half where one half was stored at -20°C and the other was treated with 1 µl of DNase and incubated at 37°C for 15-30 minutes. 11 µl of DNase inactivation reagent was then added to the tube, mixed and incubated at room temperature for 5 minutes prior to centrifugation at maximum speed for 2 minutes. The supernatant was transferred to a fresh tube

and the RNA concentration was measured either on the ND-1000, or the Qubit (see 2.2.3 for details). RNA samples were also normalised and run on a 1% agarose gel for visualisation and the quality was determined by comparing the ratio of 28S to 18S ribosomal RNA species after separation by gel electrophoresis. Only high-quality samples were used for subsequent experiments.

2.2.11 Reverse transcription (RT) for cDNA synthesis:

Synthesis of cDNA was performed using the RETROscript RT-PCR kit (Ambion Inc, USA). 1 ug of DNase-treated total RNA was combined with 2 µl of Oligo d(T) primer and nuclease-free water to make a total volume of 12 µl. The reaction was briefly mixed and incubated at 85°C for 5 minutes, before being placed directly onto ice for 2 minutes to enable the oligo d(T) primer to anneal to the mRNA. For the extension, 4 µl of dNTP, 2 µl of 10x RT buffer, 1 µl RNAse inhibitor and 1 µl RTase (MuMV) reverse transcriptase was added to the reaction to make a final volume of 20 µl. For more than one reaction, a master mix was made and an aliquot of 8 µl was added to each tube. Samples were then incubated at 42°C for 1 hour to induce reverse transcription and the reaction was heat-inactivated at 95°C for 2 minutes. The resulting cDNA was then diluted 1/20 with the addition of 380 µl of nuclease-free water to prepare a working stock for real-time PCR (RT-PCR). Samples were stored at -20°C until required.

2.2.12 Real-Time Polymerase Chain Reaction (RT-PCR):

Synthesised cDNA was used for RT-PCR using the qPCRBIO SyGreen Mix (PCR Biosystems Ltd, UK). Primer combinations were designed to target 5' and 3' ends of specific genes to produce PCR products of approximately 200 bp (Table 2.3). For each primer pair a working stock solution was made by adding 12.5 µl of each 100 µM primer stock to 975 µl of nuclease-free water (Milli Q) to make a final concentration of 1.25 µM per primer and 2.5 µM combined. RT-PCR reactions were set-up to contain 5 µl of 2x PCRBIO SyGreen Mix with 2.5 µl of the primer stock and 2.5 µl of cDNA to make a final volume of 10 µl per reaction. For each cDNA sample and primer combination, RT-PCR reactions were performed in triplicate to account for any outlier values. *Actin 2* (*ACT2* – AT3G18780) was used as a housekeeping gene and transcript levels were measured for each cDNA sample. The raw data of target genes was analysed by referencing to this gene.

2.3 General *Escherichia coli* Techniques

2.3.1 *E.coli* strains and growth conditions

All standard cloning procedures were performed with *E.coli* DG1 chemically competent cells (Eurogentec, Belgium). For protein expression, BL21 (DE3) chemically competent cells (ThermoFisher

Scientific, USA) were used because they contain the T7 RNA polymerase gene linked to IPTG induction for expression vectors containing a T7 promoter.

2.3.2 Transformations of chemically competent cells

E.coli stains were transformed using the heat-shock method. Chemically competent cells were provided in 50 µl aliquots and stored at -80°C. Prior to transformation, an aliquot was taken and placed on ice to thaw thoroughly. Once thawed, 1-5 µl of plasmid DNA was added to the cells and incubated on ice for 30 minutes. They were then heat-shocked by incubating at 42°C for 40 seconds and placed on ice for a further 5 minutes. Cells were recovered by adding 250 µl of LB broth and incubating for 1 hour at 37°C with gentle agitation (225 rpm). From here, 50-200 µl of cells were spread onto agar plates containing the appropriate antibiotic for selection. Plates were air-dried under a laminar flow hood prior to incubation overnight at 37°C.

2.3.3 Selection of transformants

Transformed cells were selected by growing them on LB media containing the appropriate antibiotic. In theory, only cells that have taken up the plasmid DNA of interest should grow in the presence of the selection antibiotic because they contain a resistance gene for it. Different concentrations were used depending on the antibiotic: 50 µg/mL for kanamycin, 50 µg/mL for ampicillin and 100 µg/mL for carbenicillin. Selected colonies were analysed by PCR to confirm that they were carrying the correct DNA of interest. Primers specific to the insertion were used for this purpose. Restriction digests were also carried out for plasmids yielding correctly-sized amplicons to confirm the presence of the DNA insert and distinguish between PCR false positives. Finally, plasmids were sent off for sequencing to ensure the correct sequence was present.

2.4 Biochemical techniques

2.4.1 Protein extraction from whole seedlings

Seedlings were grown on MS root media from 7 – 12 days after stratification (DAS). After this growth period, they were flash-frozen in liquid nitrogen. Frozen seedlings were then ground in liquid nitrogen using a pestle and mortar and the resulting powder was homogenised in one volume (700 µl) of ice-cold extraction buffer consisting of 50 Mm Tris-HCL Ph7.5, 100 Mm NaCl, 1 % (v/v) Nonidet P-40, 1 mM PMSF, and 1 x cOmplete™ protease inhibitor cocktail (Roche, Germany). Extracts were vortexed and spun twice at 14,000 rpm for 15 minutes in a benchtop microcentrifuge, decanting the supernatant each time. Total protein concentrations were calculated using the Bradford Assay.

2.4.2 Extraction of nuclear proteins (nuclei preps)

Nuclei were isolated from Arabidopsis whole seedlings (WS) or root cultures using a sucrose gradient and following a protocol adapted from Bowler et al (2004). Plant material was weighed, flash frozen in liquid nitrogen and ground into a fine powder using a pestle and mortar. The powder was then re-suspended in 30 ml of buffer EB1 (0.4 M sucrose, 10 mM Tris-HCL, pH 8.0, 5 mM βm-ME. 0.1 mM PMSF, 1x cOmplete™ Protease Inhibitor Cocktail, Roche, Germany) per 2-5g of wet weight plant matter. The solution was then thawed and poured over 4 layers of miracloth (Millipore, USA) into a 50 ml falcon tube on ice, which was then centrifuged at 2800 g for 20 minutes at 4°C. The supernatant was then discarded and the resulting pellet was re-suspended in 1 ml of EB2 buffer (0.25 M sucrose, 10 mM Tris-HCL, pH 8.0, 10 mM $MgCl_2$, 1% Triton X-100, 5 mM βm-ME. 0.1 mM PMSF, 1x cOmplete™ Protease Inhibitor Cocktail, Roche). The solution was transferred to a 1.5 ml eppendorf tube and spun at 12,000 g for 10 minutes at 4°C. The supernatant was discarded and the pellet was re-suspended in 500 µl buffer EB3 (1.7 M sucrose, 10 mM Tris-HCL, pH 8.0, 2 mM $MgCl_2$, 0.15% Triton X-100, 5 mM βm-ME. 0.1 mM PMSF, 1x cOmplete™ Protease Inhibitor Cocktail). The solution was then overlaid on top of 500 µl of EB3 in a fresh eppendorf tube and spun at 16,000 g for 30 minutes at 4°C. The supernatant was removed and the pellet was re-suspended in sonication buffer (10 mM potassium phosphate, pH7, 0.1 M NaCl, 0.3% sarkosyl, 10 mM EDTA, 0.1 mM PMSF, 1X cOmplete™ Protease Inhibitor Cocktail). Sonication was performed using a Soniprep 150 (MSE Ltd, UK) with an exponential microprobe (3 mm diameter). The machine was set to a low power and 10% amplitude microns. Samples were sonicated for a few seconds to help burst open nuclei and release proteins.

2.4.3 Protein quantification using the Bradford Assay

To quantify protein extracts, the Bovine Serum Albumin (BSA) standard set (BIO-RAD, California, USA) was used. BSA protein standards ranging from 0.125 mg to 2 mg in concentration were used to compute a standard curve as a reference for calculating unknown protein concentrations. For the case of 0mg of protein, ultrapure nuclease-free water was used. For each BSA standard, 5 µl was aliquoted into a 96-well plate, which was performed in triplicate to account for any error. Experimental protein extracts of unknown concentration were diluted 1 in 5 before aliquoting in the same way as the BSA standards. Once all the samples had been aliquoted, 200 µl of QuickStart™ Bradford 1x Dye Reagent (BIO-RAD) was then added with a multichannel pipette to decrease the timing between samples. The absorbance was then read in a microplate reader (Tecan Trading AG, Switzerland) at a wavelength of 595nm. From here, a BSA standard curve was computed and the concentration of each experimental sample was calculated using the equation of this curve.

2.4.4 Analysis and size-separation of protein fractions

All protein samples were combined with either 1x, 2x or or 6x SDS-PAGE (Laemmli) buffer (depending on the final concentration of the extract) and denatured by heating to 95°C for 5 mins, before loading onto a polyacrylamide gel. The concentration of acrylamide in the gel ranged from between 8-10%, depending on the size of the expected fragments. Polyacrylamide gels were hand-cast according to the recipes described by Harlow and Lane (1998) and using the Mini PROTEAN Tetra Cell kit (BIO-RAD, USA). Protein samples were fractionated by running at a constant rate of 100-150 volts until the loading dye had run off from the bottom of the gel. The resulting gel was either coomassie stained or blotted to a membrane depending on the experimental purpose.

2.4.5 Coomassie staining of polyacrylamide gels

Coomassie staining was performed using recipes provided by Syrovy and Hodny (1991). SDS gels were incubated on an orbital shaker (Amished, China) for at least half an hour in coomassie blue stain (45% methanol, 10% glacial acetic acid, 45% H_2O and 3g/L coomassie brilliant blue R250). Once the gel was sufficiently stained, residual stain was removed and placed in a container for further use. The gel was then submerged it in de-stain solution (same recipe as the stain, but without coomassie blue added) and incubated on an orbital shaker for half an hour, or until the solution turned blue. This was then removed and fresh de-stain solution was added to the gel, which was incubated for a further half an hour. The process was repeated until the gel had reached satisfactory clarity and bands could be easily visualised.

2.4.6 Antibodies used for pull-downs and western blot analysis

For detection of RBR protein, a commercially available polyclonal antibody (AS11 1627, Agrisera, Sweden) was obtained. This antibody was produced against the *Arabidopsis thaliana* RBR1 (ATRBR1) protein 236 amino acids from the C-terminal. It was not affinity purified, but was deemed suitable by the suppliers for use in Co-IPs and western blot analysis. For detection of GFP-tagged protein a commercially available polyclonal antibody was used (TP401, Torrey Pines, USA). This antibody was produced against the full length GFP and can detect GFP variants, as well as the WT version, but has only been deemed suitable for western blot analysis. For pull-down experiments, either GFP-Trap agarose coated magnetic beads (Chromotek) were used or a commercially available polyclonal GFP antibody (ab290, Abcam, UK). For detection of GAI/RGA protein an anti-GAI antibody produced by Nottingham University (courtesy of Prof. Malcolm Bennett) that cross reacts with RGA.

2.4.7 Western blot analysis

Proteins fractionated on a polyacrylamide gel were transferred either to a PVDF or nitrocellulose membrane using a semi-dry transfer machine (Bio-rad, California, USA). For this purpose, the transfer membrane and 3MM whatman chromatography paper was cut into rectangles measuring 5.5 x 8.8 cm. For use of PVDF membranes, it was first necessary to soak them in 100% methanol for a minimum of 10 seconds in order to activate the membrane to allow sufficient transfer. The 3MM rectangles were soaked in transfer buffer (25 mM Tris-HCl - pH 7.6, 192 mM glycine, 20% methanol, 0.03% SDS) and then three were stacked on top of each other onto the semi-dry apparatus. The transfer membrane was then placed on top, followed by the gel and three more pre-soaked 3MM rectangles. Air bubbles were removed by rolling a pipette tip over the transfer membrane/gel sandwich with slight pressure. The transfer was run for 1.2 hours at 60mA/gel (~1.24mA/cm^2). The membrane was then incubated with blocking buffer consisting of 5% milk powder (< 2% fat) dissolved in phosphate buffer saline containing 0.1% Tween (PBS-T). Primary and secondary antibody concentrations were used following the manufacturer's instructions, unless otherwise stated.

For detection of GFP protein, membranes were incubated with the Torey Pines anti-GFP antibody with a 1:3000 dilution in PBS-0.05% Tween 20 (PBS-T) containing 5% milk powder for 2 hours at RT, followed by a HRP-conjugated goat anti-rabbit IgG (Santa Cruz) secondary antibody (1: 20000) for 1 hour at RT. After each antibody incubation step, filters were washed with PBS-T for 3 x 10 mins. For detection of RBR protein, membranes were probed with the Agrisera anti-RBR1 antibody (1:6000, 2 hours at RT), followed by a HRP-conjugated rabbit anti-chicken IgY (PIERCE) secondary antibody (1: 20000, 1 hour at RT) in PBS-T containing 5% milk powder. After each antibody incubation step, filters were washed with PBS-T, PBS-T containing 2% milk powder and PBS-T for 10 mins each. Membranes were developed with ECL detection reagent (Amersham). For detection of GAI and GAI-GFP protein, membranes were incubated with the Nottingham University anti-GAI antibody (1:2000, 2 hours at RT) and HRP-conjugated rabbit anti-sheep IgG (Santa Cruz) secondary antibody (1: 25,000, 1 hour at RT) in PBS-T containing 5% milk powder. After each antibody incubation steps filters were washed with PBS-T 3 times for 10 mins.

2.4.8 Co-Immunoprecipitation (Co-IP) experiments

Co-IP experiments were performed on total protein extracts of whole seedlings or on sonicated nuclei preps. For extracts expressing GFP-tagged protein, one of the following methods was used.

Method 1: The pull-down was performed using magnetic-coated agarose beads conjugated to an anti-GFP antibody - GFP-Trap_MA beads (ChromoTek GmbH, Germany). The beads were vortexed and 25

µl was aliquoted into 1.5 ml eppendof tubes per reaction. 500 µl of ice-cold dilution/wash buffer (10 mM Tris/Cl pH 7.5, 150 mM NaCl, 0.5mM EDTA) was added to the tube and the beads were separated from the solution with a powerful magnet (Invitrogen Dynal, Norway). The supernatant was then removed and the wash was repeated twice. For whole seedling proteins extracts, 500-1000 µg of total protein was combined with dilution/wash buffer to make a total volume of 500 µl. For nuclear extracts, 200 µl of sonicated sample was combined with 300 µl of dilution/wash buffer. At least 50 µl of each sample was saved for immunoblot analysis. Either of these solutions were then combined with the equilibrated beads and tumbled end-over-end for 1 hour at 4°C. The beads were magnetically separated until the supernatant was clear. 50 µl of the supernatant was saved for immunoblot analysis and the rest was discarded. 500 µl of ice-cold dilution/wash buffer was added to the tube and magnetically separated. The supernatant was discarded and the wash was repeated twice. The beads were re-suspended in 50 µl of 2x Laemmli SDS-PAGE buffer (0.125 M Tris/Cl pH 6.8, 4% SDS, 20% glycerol, 60 mM DTT and 0.02% bromophenol blue). Immunocomplexes were disassociated by boiling the samples at 95°C for ten minutes. Again, the beads were magnetically separated and the supernatant was loaded onto an SDS-PAGE gel for size separation and subsequent immunoblot analysis.

Method 2: Either 200 µl sonicated nuclei, or 500-1000 µg of whole seedling extract was combined with 1 ml of IP buffer (50 mM Tris pH 7.5, 150 mM NaCl, 20, 0.2% Triton X-100, 1.25 mM EDTA, 1x cOmplete™ Protease Inhibitor Cocktail, Roche) and 1-5 µg of anti-GFP antibody (Abcam PLC, UK). The reaction was then tumbled end-over-end for 3-8 hours or overnight at 4°C. 50 µl of protein A conjugated magnetic beads, Dynabeads (ThermoFisher Scientific, USA) was added to the reaction and tumbled end-over-end for 4 hours or overnight at 4°C. The beads were magnetically separated and the supernatant was decanted and saved for immunoblot analysis. The beads were then washed 3 times with 1 ml IP buffer for 5 minutes each time. A further 2-3 rinses were performed using IP buffer without proteinase inhibitors. The beads were re-suspended in 50 µl of 2x Laemmli SDS-PAGE buffer. Immunocomplexes were disassociated by boiling the samples at 95°C for ten minutes. Again, the beads were magnetically separated and the supernatant was loaded onto an SDS-PAGE gel for size separation and subsequent immunoblot analysis.

For the pull-down of extracts expressing RBR protein, the AtRBR1 antibody (Agrisera, Sweden) was used. 1 µl of RBR1 antibody was pre-incubated with 40 µl of IgY resin (Genscript, China) in 1 ml of buffer (50 mM Tris pH7.5, 100 nM Nacl, 10mM EDTA, 0.2% NP40) at 4°C for 5 hours. The solution was then spun at 5000 g for 1 minute and the supernatant was removed. The pellet was resuspended in 1 ml wash buffer as described in the manufacturers protocol (8.5 g NaCl, 1.4 g Na_2HPO_4, 0.2 g NaH_2PO_4 in 1000 ml Distilled water, pH 7.4) and spun again at 5000 g for 1 minute. The wash step was repeated

twice. The resin pellet was re-suspended in 400 µl of IP buffer (50 mM Tris pH 7.5, 100 mM NaCl, 0.1% NP40, 1 mM EDTA and 1x cOmplete™ Protease Inhibitor Cocktail) and 500 ug of protein extract was added to the solution, which was incubated on an end-to-end rotator overnight at 4°C.

2.4.9 Glutathione S-transferase (GST) Assay

For the GST Assay, the pGEX2TK-P vector described by Huntley et al (1998) was used. This either contained the ZmRB-1 (Maize RB) as described by the authors, or *Arabidopsis* RBR. The AtRBR coding sequence was amplified from cDNA with primers designed to incorporate a *BamH*I and *Xho*I restriction site at the 5' and 3' end, respectively (Table 2.3). This amplicon and the pGEX2TK-P vector were then digested (see 2.2.7) with the *BamH*I and *Xho*I restriction enzymes so that the insert could be ligated into the vector (see 2.2.8). Following transformation into *E.coli* cells (see 2.3), the vector was sent off for sequencing before subsequent use in these experiments.

Transformation of competent cells and bulking-up of single colonies

50µl of competent cells (DG1 or BL21 (DE3)) were transformed with 1 µl of plasmid DNA and incubated on ice for 15 mins. The cells were then heat shocked for 35 seconds at 42 °C and incubated on ice for a further 5 min. 250µl of LB media was added and the resulting culture was incubated in a 37°C shaker at 225 rpm for 40 min to an hour. After incubation, the culture was spread onto agar plates containing the appropriate amount of selective antibiotic (100 µg/ml for Carbenicillin, 50 µg/ml for Kanamycin) and left for 20 min under a laminar flow hood to dry. For this purpose, two different amounts were spread across plates to optimize chances of single colonies e.g. 50 – 100 µl onto one plate and 150 – 200 µl onto another. Once dry, the plates were incubated overnight at 37°C. The next day, individual colonies were selected and inoculated into 5ml LB broth with appropriate amount of antibiotic (100µg/ml for Carbenicillin) and incubated overnight at 37°C in a shaking incubator (225rpm).

Protein induction

From the overnight liquid culture, 4ml of was inoculated into 200ml LB broth containing the appropriate amount of antibiotic and incubated at 37 °C in a shaking incubator until the OD_{600} reached between 0.6 - 1 (ideally 0.8). Once an appropriate OD_{600} had been reached, 0.1mM IPTG was added for induction. The liquid culture was incubated for 4 hours at 30°C. To monitor protein expression, 1 ml samples were taken and spun in a benchtop microcentrifuge at allocated time intervals of 1, 2, 3 and 4 hours after induction. After incubation, the 200 ml liquid culture was decanted into a centrifuge flask and spun at 4000 *g* for 20 min. The resulting pellet was weighed and frozen at -80 °C.

Extraction of soluble proteins

The bacterial pellet was re-suspended in 9.5ml of Plant Buffer (50mM Tris, pH 7.5; 100mM Nacl; 1 mM PMSF and 1 x cOmplete™ protease inhibitor cocktail) per gram. Either DTT or beta-mercaptopethanol was added to make a final concentration of 5mM, followed by 100ug/ml of Lysozyme (1 µL of a 100mg/ml stock) and 1 µL Benzonase Nuclease per 5 mL of Plant Buffer. Bacteria were then lysed by the addition of Triton X-100 from a 20% (w/v) stock to make a final concentration of 1%. The solution was then incubated on ice with gentle agitation for 30 mins and subsequently spun for 10 mins 16,000 x g at 4 °C. The resulting supernatant was removed and combined with an appropriate amount of GST resin (Pierce Glutathione Agarose) that had been pre-washed according to the manufacturer's protocol (Thermo Scientific).

GST assay

The same protocol as described by Huntley et al (1999) was followed. This involved pre-incubating approximately 1 µg of fusion protein on beads (GST alone as a control) for ten minutes at room temperature in Z' buffer (25 mM Hepes pH7.5, 12.5 mM $MgCl_2$, 20% glycerol, 0.1% NP-40, 150 mM KCL) containing 150 µg bovine serum albumin and 5% heat-inactivated foetal calf serum and 1 mM dithiothreitol (DTT). 1 mg of total protein extract was then combined with the solutions containing GST resin and incubated for 3 h at 4 °C. Following incubation, the beads were washed four times in 1 ml of NETN buffer (20 mM Tris pH8.0, 100mM NaCl, 1mM EDTA, 0.5% NP-40) and pelleted each time by spinning at 10,000 *g* for 1 min in a benchtop microcentrifuge. The beads were then boiled in SDS-PAGE buffer (2x) at 95 °C for 5 minutes and directly loaded onto an SDS gel.

2.3 Kinematic analysis of the root growth and cell division

Root growth was captured by scanning plates daily with an Epson scanner and a resolution set to 600 dpi. Primary root lengths of individual seedlings were then measured using either Fiji (Schindelin *et al.*, 2012) or Rootnav software (Pound *et al.*, 2013). Average daily root growth rate was calculated by obtaining the difference in root length between each day and dividing the summation of these values by the total number of days. Confocal laser scanning microscopy was performed using a Ziess LSM 710 confocal microscope with a 20x objective to image root tips stained with 0.1 mg/mL propidium iodide (PI). The resulting image data was converted into individual quantitative cell measurements using semi-automatic image analysis software, Cell-O-Tape (French *et al.*, 2012), in Fiji. Primary root apical meristems were analysed to measure cortical growth, cell length, meristem size and cell division according to Nieuwland *et al.* (2009). Cell production rate was calculated by diving average hourly root

growth rate of individual seedlings by the average size of their elongated cells (Rymen *et al.*, 2010; Baskin, 2013).

For root growth analysis at the GMI, Vienna, the protocol described by Slovak et al (2015) was followed using the facilities provided for high-throughput root phenotyping. Here, they have the ability to scan up to 16 plates at a time. The BRAT software plugin (Slovak *et al.*, 2014) for Fiji was used to automatically detect scanned roots of seedlings grown vertically on plates. Each root was subject to quality control to check the accuracy of its detection and segmentation.

2.4 Bioinformatics

2.4.1 BLAST search for GAI and RGA homologues

The amino acid sequences for GAI (AT1G14920.1) and RGA (AT2G01570.1) protein was obtained from the Arabidopsis Information Resource (TAIR) database online (https://www.arabidopsis.org/, 02/08/17). To search for GAI and RGA homologues, a tBLASTn search was performed on the NCBI website (https://blast.ncbi.nlm.nih.gov/Blast.cgi, 02/08/17). This was done by inputting the amino acid sequence for each individual protein and specifying the refseq_genomic database. For GAI, the taxa for *Viridiplantae* (taxid:33090) was also specified as an additional search parameter. Since RGA is only present in dicots, the *Dicotyledoneae* taxa (taxid:71240) was specified. The top matching sequences with the highest percentage identity were obtained as a result of these searches and aligned with the original reference sequence in MacVector.

2.4.2 Protein homology modelling

Protein homology modelling was performed by Dr. Salvatore Ferla from the School of Pharmacy and Pharmaceutical Science, Cardiff University. The preparation of a homology model is characterised by three main steps: (1) Finding the primary amino acids sequence of the protein that needs to be built (target protein), choosing the correct 3D crystal structure of a homologues protein (template protein) and aligning them using alignment software, such as Clustal Omega (Sievers et al, 2011). This software is able to place the amino acid sequences so that the matched stretches of amino acids correspond to common amino acids pattern that form structural or functional features, like secondary structure or catalytic residues. The most suitable template protein is chosen running a similarity search on the target protein amino acids primary sequence using the online Protein Blast search tool that identifies proteins which shares a primary amino acid sequence identity with the target protein and for which a crystal structure (3D structure) is available on the Protein Data Bank (PDB, Berman et al, 2000). (2) The homology model is automatically generated by building the 3D structure of the target protein using the atom spatial coordinates of the amino acids of the template. The program MOE2015.10 was

used for this purpose (Molecular Operating Environment, 2015). (3) Final step is the energy minimization in order to obtain a conformation of the model that can represent the nearest local minimum of potential energy.

For the RBR model, the crystal structure of RB tumour suppressor protein (PDB ID: 1N4M), was used (Lee et al. 2002). The primary amino acidic sequence of RBR (downloaded from UniProt) was loaded in MOE together with the 3D structure of template to be used (crystal structure 1N4M), aligned (following the alignment published by Oh-Lee et al, 1998) and the final 3D model was obtained. Moreover, an induced fit option was used, selecting the peptide from HPV E7 presenting the motif LxCxE (PDB ID: 1GUX) bound to the RB pocket. In this way, the model was forced to maintain the shape of the binding site. The final model was refined by energy minimization with RMSD of 0.1.

For the GAI model, the crystal structure for the first 113 amino acids of GAI was available on the PDB data bank (PDB ID: 2ZSH), but it did not include the LxCxE motif which starts at amino acid 174. Therefore, this area is missing in the crystal structure. A Protein Blast search revealed a 34% identity between the GAI and the crystal structure of the GRAS domain of SCL7 in Oryza sativa (PDB ID: 5HYZ). The GRAS domain contains the LxCxE motif. For this reason, two templates were used for the preparation of GAI homology model. Following the previous reported procedure, the primary amino acidic sequence of GAI (downloaded from UniProt) was loaded in MOE together with the two 3D structure of templates to be used (crystal structure 2ZSH and 5HYZ), aligned (following the alignment published by Li et al, 2016 for the GRAS domain area) and the final 3D model was obtained. The final model was refined by energy minimization with RMSD of 0.1.

2.5 FLIM/FRET analysis

2.5.1 Generation of FLIM images

Vertically grown primary roots of seedlings from 3-4 DAS were mounted in water for imaging. FLIM was performed in the time-domain using a confocal laser scanning microscope (Zeiss LSM 880) additionally equipped with a pulsed laser and a single-photon counting devise within the picosecond time resolution (PicoQuant Hydra Harp 400). A 40X water immersion objective was used for FLIM images of the root meristem of seedlings expressing either GFP-tagged protein as the donor only or in the presence of RFP-tagged protein as the acceptor. Photon counting was performed using SymphTime 64 software (PicoQuant). GFP fluorescence was excited with a 485 nm linearly polarized diode laser (LDH-D-C-485) operated at a repetition rate of 40 MHz. Each image was obtained using the same confocal settings, including a scan speed of 2, a frame size of 512 x 512, a pinhole diameter of 2 µm and 12 cycles per image.

2.5.2 Analysis of FLIM images to determine FRET

FLIM images were analysed using the "Factorization into Spectra and Concentrations of Chemical Components" (FCS^3) method as described by Masia et al, 2013. This is a method that was recently developed to extract quantitative chemical information from hyperspectral coherent anti-Stokes scattering microscopy images (Masia et al, 2013). It uses a non-negative matrix factorization which decomposes the data into a linear combination of few components of given spectra. FSC^3 is versatile and can be readily adapted to most hyperspectral multidimensional data. For more detailed information on these algorithms please read the aforementioned article.

2.6 Statistical analysis

Raw data was converted into a format that is compatible for statistical analysis in R (Version 3.3.3, R Development Core Team, 2017). For analysis using generalised linear mixed effects (GLMM) or linear mixed-effects regression (LMER) models, the lme4 package was used in R (Bates, Maechler, Bolker, and Walker 2015). For each dataset, the initial distribution was assessed by plotting all the values of the dependent variable as a density plot. An appropriate statistical model was selected depending on the distribution of the dependent variable and whether it was categorical or continuous, the number of independent variables and whether they should be defined as fixed or random terms. Potential interacting factors were also incorporated into the model and tested for significance to determine whether they should be included. Where the effect of one categorical independent variable on one continuous dependent variable was being assessed, a one-way ANOVA (a specific type of generalised linear model) was used to compare the means of two or more (unrelated) groups.

For model validation, graphical residual analysis was performed by producing residual plots and assessing their distribution for normality. This included a normal probability plot (Q-Q plot), where the residual values were plotted against theoretical values from the normal distribution, a residual vs. fitted plot and a histogram of the residuals. All outputs from each model and the residual plots have been included in the appendices as specified in the text.

Chapter 3

GAI, RGA and RBR are differentially expressed in *Arabidopsis* Roots

Chapter 3: GAI, RGA and RBR are differentially expressed in *Arabidopsis* Roots

Introduction:

Investigating the expression pattern of a gene and production of the corresponding protein over time can reveal important information about its cellular/subcellular localisation. Furthermore, the presence of two or more proteins in the same region can be compared to determine whether or not they are differentially produced. One of the most commonly used techniques to visualise a protein is to genetically modify it to contain a molecular tag that allows it to be observed using microscopy. This molecular tag, or reporter gene, usually codes for a fluorophore that emits light when excited with a specific wavelength. Different types of reporter genes can be utilised depending on the objective of the experiment, which can either be fused to the N- or C- terminal of the target gene. Green fluorescent protein (GFP) is the most common type of reporter of expression used in cellular and molecular biology (Phillips, 2001) because it was the first fluorescent protein isolated from the jellyfish, *Aequoria victoria* (Shimomura *et al.*, 1962). Many derivatives of GFP have since been engineered by genetic modification to produce enhanced, brighter versions of GFP and different colour variants such as YFP (Yellow) and CFP (blue). The expression pattern of a gene and cellular localisation of the synthesised protein can be investigated using translational reporters that have been transformed into the genome of an organism of interest. Translational reporters are a specific type of construct designed to incorporate a gene of interest, driven by its own promoter and fused in frame to a reporter gene. Since these types of reporter lines are driven by their own promoters and are usually subjected to signals and stability determinants of the native protein, they can reveal information on the native localisation of a protein. They can be particularly useful to complement experiments where ectopic expression of a gene (constitutive expression of a gene in all tissues) is used to gain further understanding of a gene's function.

As well as at the protein level, it is also important to understand the expression of a gene at the transcriptional level. One way to examine the expression levels of genes is to generate transcriptomic data. Transcript levels of large set of genes can be measured using microarrays and more recently, RNA-sequencing. In *Arabidopsis*, a variety of microarray datasets have been developed as a result of the AtGenExpress initiative (http://atpbsmd.yokohama-cu.ac.jp/AtGenExpressJPN/). After sequencing the Arabidopsis genome (Arabidopsis Genome Initiative, 2000), the AtGenExpress initiative was established to further our understanding of genome function. This is a multinational collaborative movement that was set up to establish transcriptome patterns for a variety of tissues, developmental stages, hormonal treatments and adaptive responses to biotic and abiotic stress.

Collaborative partners agreed to use the same *Col-0* seed stock for each type of experiment. Most microarray datasets were obtained using the Affymetrix®, ATH1 chip (Redman *et al.*, 2004). This chip contains 22,746 oligonucleotide probes for detecting 23,000 different genes; almost the entire genome of Arabidopsis (Redman *et al.*, 2004).

A useful tool for integrating these types of expression profiles in a visual and tissue-specific manner is the electronic Fluorescent Pictograph (eFP) Browser (http://www.bar.utoronto.ca/). This web-based tool integrates various microarray or other large-scale data sets and portrays them in a visual format, based on the experimental samples used to generate these data sets (Winter *et al.*, 2007). Thus, the eFP browser can help facilitate the interpretation and analysis of these types of data sets (Winter *et al.*, 2007). The Arabidopsis eFP browser explores microarray datasets obtained primarily from the AtGenExpress initiative to visualise gene expression profiles for *Arabidopsis thaliana* (Winter *et al.*, 2007). Many of these datasets have been generated for specific tissues and in response to hormonal and chemical treatments at various developmental stages.

Here, the hypothesis that the DELLA protein GAI binds with RBR (and RGA does not) is investigated in order to further our understanding of how GA regulates cell division control. If a putative interaction between these proteins is to be investigated, it is first important to establish that (1) both proteins are expressed at the same time and (2) both proteins are localised to the same subcellular compartments. Clearly an interaction can only physically take place if there exists a moment of time where both proteins are present and are within close proximity of each other. Here, the expression profiles of *GAI*, *RGA* and *RBR* in the developing root of *Arabidopsis* are determined to establish whether or not they are co-expressed and co-localised and to investigate differences between their expression patterns. This was done by imaging plants expressing translational reporters for *RGA*, *GAI* and *RBR* and combining this with *in silico* transcriptional data obtained from the eFP browser. Since the active region of cell division is situated within the apical root meristem, most of my confocal analysis was specific to this region. Overall, it was found that all three genes were expressed in the root and were nuclear localised, but their expression patterns varied between different regions of the root. When comparing these differential expression patterns, I found that *GAI* and *RBR* were more similar than *RGA* in terms of their spatio-temporal expression at both the protein and transcript level. Furthermore, I report my findings from treatment experiments of the translational reporter lines for *GAI* and *RGA* to alter their levels of gibberellins (GAs). This was done alongside plant lines that ectopically express these genes and are driven by the 35S Cauliflower Mosaic Virus (CaMV) promoter, in order to further our understanding of their function and determine how they respond to these altered levels of GA. As described in more detail in Chapter 1, the current working model for the signalling activity of GA in plants has been well defined (Sun, 2010). It states that in the presence of

bioactive GA, it binds to its receptor GID1 that binds to and targets DELLA proteins by incorporating a ubiquitin ligase complex, leading to polyubiquitination and subsequent degradation by the 26S proteasome. When GA levels are low, DELLA levels are high and repress GA signalling (and thus plant growth) by inhibiting the transcription of GA responsive genes (Sun, 2010). Therefore, altering GA levels in lines expressing GAI-GFP and RGA-GFP should have a direct effect on the accumulation of these proteins.

3.1 Results:

3.1.1 GAI-GFP, GFP-RGA and RBR-GFP can be detected by immunoblot analysis

To report on the expression of GAI, RGA and RBR in the *Arabidopsis* root the previously described translational reporter lines pGAI::GAI-GFP (Fleck & Harberd 2002), pRGA::GFP-RGA (Silverstone et al. 2001) and pRBR::gRBR-GFP (Magyar *et al.*, 2012) were used. Before visualising these lines with confocal microscopy, immunoblot analysis was first performed in order to determine that the full-length protein was being produced. For the pGAI::GAI-GFP line, immunoblot analysis had been attempted using an anti-GAI antibody, but without successful detection of the GAI or GAI-GFP transgene (Fleck & Harberd 2002). Although the protein was reported to be undetectable, ectopic expression of the GAI-GFP fusion protein by the 35S promoter conferred a dwarf phenotype similar to that of a GA-deficient mutant, thus suggesting it is functional (Fleck & Harberd 2002). In the case of the pRGA::GFP-RGA, immunoblot analysis had previously been used to successfully detect the GFP-RGA fusion protein (Silverstone et al. 2001). Furthermore, the fusion protein had been shown to be functional since it was able to rescue the phenotype caused by the *rga* null mutation in a GA-deficient mutant background (Silverstone et al. 2001). To investigate this further, immunoblot analysis was performed on total protein extracts of the described translational reporter lines to see if GAI-GFP and GFP-RGA could be detected with an anti-GFP and anti-GAI antibody (that also cross reacts to RGA). Furthermore, both lines were treated with the GA biosynthetic inhibitor, paclobutrazol (PAC), to see if the overall expression levels of GAI-GFP and GFP-RGA from whole seedlings could be increased. Total protein extracts were performed on 10-day-old seedlings expressing either the pGAI::GAI-GFP or the pRGA::GFP-RGA construct that had been transferred to plates in the absence (mock) and presence of 10µM PAC 18 hours prior. Immunoblot analysis using an anti-GFP and anti-GAI antibody confirmed that the full-length fusion proteins GAI-GFP and GFP-RGA could be detected, since a band was visualised that corresponded to their predicted size (GFP is approximately 27 kDa, RGA is 64 kDa and GAI 58 kDa) in both experimental conditions (Figure 3.1A, B). Endogenous GAI and RGA levels were undetectable on the western blot that was probed with anti-GAI (Figure 3.2 B). Perhaps this was due endogenous levels of these proteins being generally low in comparison to the rest of the total

protein content of these seedlings (Figure 3.1B). The 18 hour PAC treatment also did not appear to increase endogenous levels enough to be visualised. Furthermore, it was difficult to determine whether this PAC treatment effectively increased GFP-RGA protein levels (Figure 3.1 A, B). This is because the level between PAC treated and –untreated samples appeared to be approximately the same. However, although protein levels were normalised to 10 µg, the concentrations of other proteins detected by unspecific binding of the GFP antibody appeared to be lower in the PAC-treated sample when compared to the untreated sample (Figure 3.1A). In the case of 18 hour PAC treatment of pGAI::GAI-GFP, levels of GAI-GFP appeared to be slightly increased in comparison to the untreated control sample, although this was not quantified (Figure 3.1 A). When a similar blot was probed with anti-GAI, it was difficult to infer whether there was an increase in GAI-GFP or GFP-RGA levels because the blot had been overloaded with 20 ug of total protein content instead of 10 ug and had an increased amount of unspecific binding.

The pRBR::RBR-GFP construct had previously been reported to be functional, since it was able to rescue the *rbr1* null mutant phenotype (Magyar et al. 2012). To confirm that both RBR and RBR-GFP could be detected in this line and to test the ability of a commercially available *Arabidopsis thaliana* RBR1 antibody (AtRBR1, Agrisera) to detect RBR protein, immunoblot analysis was performed. This was done on total protein extracts of Ler, pRBR::RBR-GFP and G54 seedlings grown for 7 days after completion of stratification (DAS). The G54 line is in the *Ler* ecotype and is a constitutive overexpresser of the *CYCLIN D3;1* (*CYCD3;1*) gene, which codes for a protein that forms a complex with CDK complexes to phosphorylate RBR (Dewitte et al., 2003). Overexpression of CYCD3;1 leads to an increased phosphorylation of RBR, thus increasing the turnover of RBR (Dewitte et al., 2003). Immunoblot analysis revealed that both proteins could be detected and corresponded to their predicted size (RBR is approximately 125 kDa) (Figure 3.1B). Furthermore, there was an increased concentration of endogenous RBR in the G54 line, as expected (Figure 3.1B).

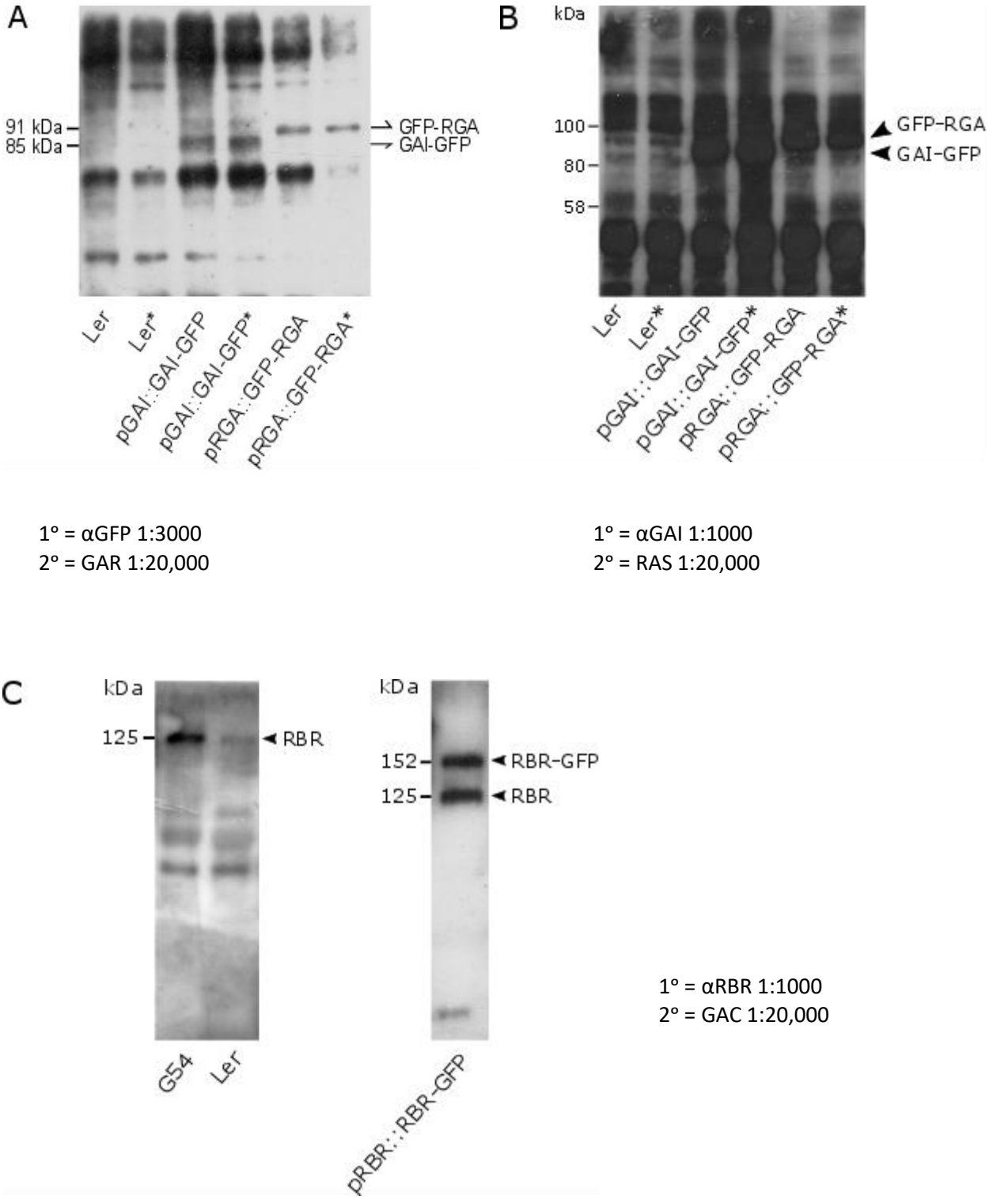

Figure 3.1: Western blot analysis on total protein extracts of *Arabidopsis* whole seedlings using anti-GFP, anti-GAI and anti-RBR antibodies. Protein extracts (10-20 µg) from Wild Type (WT), pGAI::GAI-GFP and pRGA::GFP-RGA 10-day-old seedlings in the *Ler* ecotype were separated on an 8% SDS gel and probed with (A) an anti-GFP (Torrey Pines) antibody and (B) an anti-GAI (Nottingham University) antibody. The * indicates seedlings treated with PAC for 18 hours (C) Protein extracts (20 µg) of G54 and WT 10-day-old seedlings in the *Ler* ecotype and pRBR::RBR-GFP seedlings in the *Col-0* ecotype. Membranes were probed with an anti-RBR1 antibody (Agrisera).

3.2.2 GAI, RGA and RBR accumulate in the root and are nuclear-localised

After establishing that the fusion proteins in the pRGA::GFP-RGA, pGAI::GAI-GFP and pRBR::RBR-GFP lines could be detected using immunoblot assays, I investigated their expression levels *in vivo* by visualising primary roots 7 DAS with confocal microscopy (Figure 3.3). Analysis of the GFP levels for each reporter line demonstrated that GAI-GFP, GFP-RGA and RBR-GFP could be detected in the root and that all three proteins were nuclear-localised (Figure 3.3). Previous studies demonstrated that expression of GFP-RGA fusion protein was localised to the nucleus of onion epidermal cells and Arabidopsis root cells (Silverstone et al. 1998, Silverstone et al. 2001). Furthermore, the subcellular localisation of GAI-GFP and RBR-GFP has also been reported to be in the nucleus (Fleck & Nicholas P. Harberd 2002; Magyar et al. 2012). Images captured with confocal microscopy at a high magnification (40x) confirmed these observations and demonstrated that the subcellular localisation is more specific than that of the nucleus as a whole (Figure 3.2). GFP intensities were detected in the outer nuclear compartment, but not to the nucleolus, suggesting that the subcellular localisation of these fusion proteins is specific to the nucleoplasm.

Although GAI-GFP, GFP-RGA and RBR-GFP were all expressed in the root, their expression patterns varied in a tissue-specific manner and within different regions of the root. Most of the confocal images obtained were of the root tip where the meristematic region is located, but in this case cells within the elongation zone were also visualised, as well as lateral roots and lateral root primordia (Figure 3.3). In order to compare expression patterns in the meristematic region, the targeted focal plane was within the middle of the root where the QC can be visualised. For pGAI::GAI-GFP seedlings, GAI-GFP was much more difficult to detect either because the overall level of accumulation was lower or because the type of GFP used in this construct produces a weaker signal than that of GFP-RGA and RBR-GFP. Therefore, confocal settings were altered to increase the digital gain of the laser in order to effectively capture GAI-GFP intensity. At the root apex, GAI-GFP intensity was localised predominantly to the cortical cell layer of the proximal root meristem (the region of active cell division), as well as some cells within the epidermis, endodermis, vasculature tissue of the central stele and the root cap (Figure 3.3.Ai). No GAI-GFP signal was detected in the stem cell niche (QC and initials). Further away from the proximal meristem, signal intensity of GAI-GFP decreased and was barely detectable in cells entering the transition and elongation zone. However, further along the root in some elongating cells GAI-GFP signal was visible in the cortical cell layer (Figure 3.3Bi). Roots of seedlings were also visualised in the maturation zone where lateral roots and lateral root primordia are situated. GFP accumulation was observed mostly [in some cells of] the cortical layer and the vasculature of the proximal meristem of more mature lateral roots (Figure 3.3Di). In younger lateral roots and lateral root primordia (LRP), GFP intensity was observed in some cells of the cortical cell layer, but generally at lower levels (Figure

Figure 3.2: Nuclear localisation of GAI-GFP, GFP-RGA and RBR-GFP

Representative confocal images of GAI-GFP, RGA-GFP and RBR-GFP intensity in the root meristem of *Arabidopsis* seedlings 5 days after stratification (DAS) for the translational reporter lines, pGAI::GAI-GFP, pRGA::GFP-RGA and pRBR::RBR-GFP, respectively. Images were obtained at a high magnification using a 40x objective with water immersion. The microscope was focused to the left or right outer edge of the RAM where cell division takes place to mainly image the epidermal (Ep), cortical (C) and endodermal (En) cell layers within this region. Propidium Iodide (PI) was used for staining of cell walls and as a counterstain. Both GFP and PI was excited with a 488 laser. For each confocal image, the combined channel image for GFP (green) and PI (magenta) is shown (top left). The single channel images for GFP (top right) and PI (bottom left) are portrayed in grayscale, alongside the transmitted light image (bottom right).

Scale bars represent 5 µm

pGAI::GAI-GFP

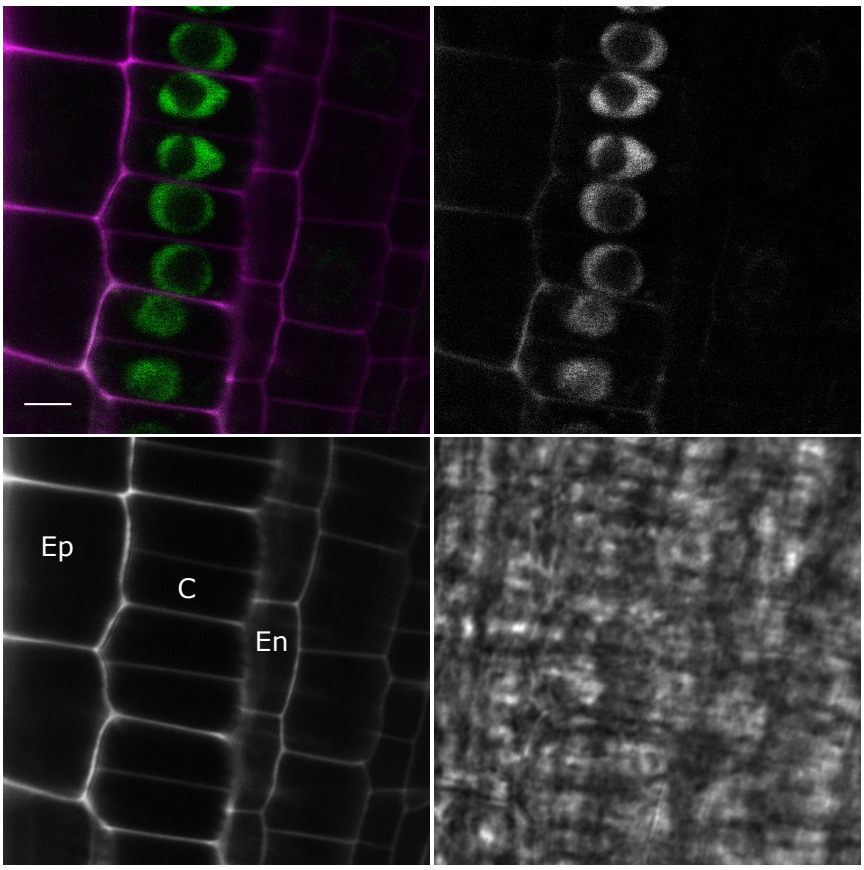

pRGA::GFP-RGA

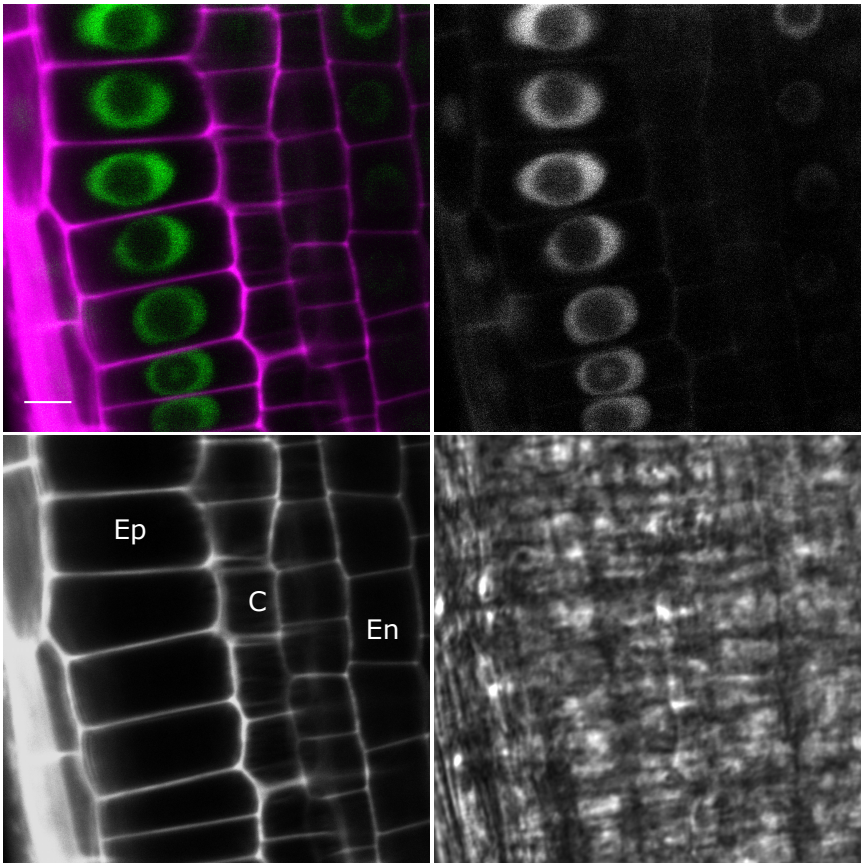

pRBR::RBR-GFP

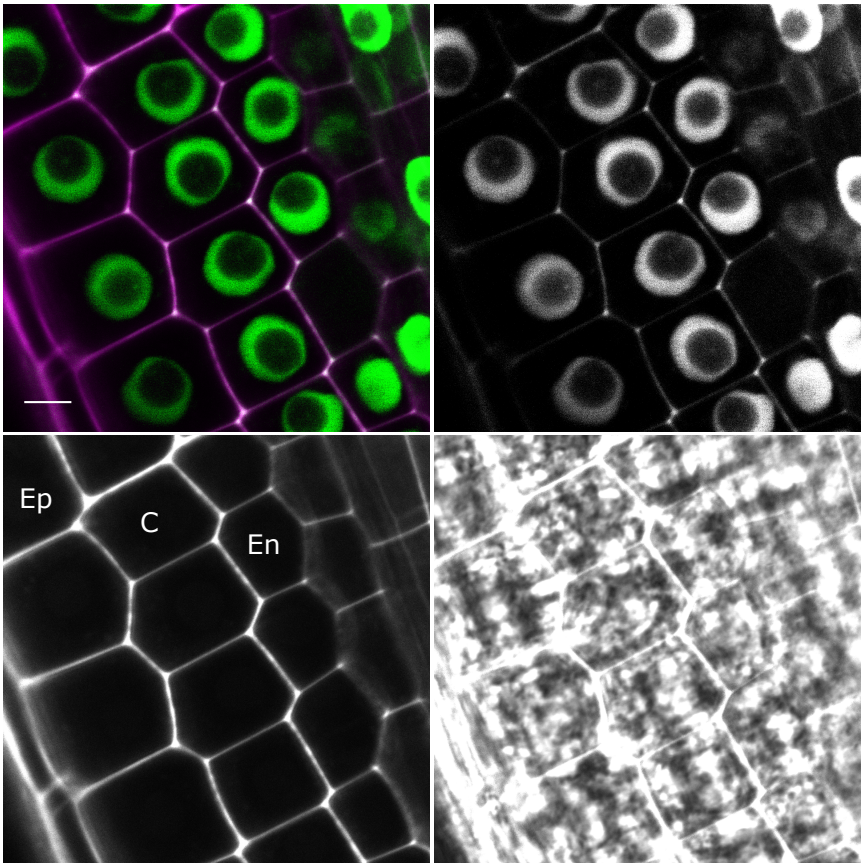

3.3Ci). Within this region, no GFP signal was detected in elongating cells of any of the tissue layers that comprise the primary root. Interestingly, whenever GFP signal was detected in lateral roots/lateral root primordia, it was in two adjacent cells of the proximal root. Since this expression pattern was specific only to some of the cells, perhaps it is the case that GAI-GFP within this region is activated in a time dependent manner.

When visualising the pRGA::GFP-RGA line, GFP-RGA intensity was higher and more consistently produced throughout all tissues of the proximal root (epidermis, cortex, endodermis, pericycle and the central stele/vasculature) in comparison to the accumulation of GAI-GFP (Figure 3.3Aii). Furthermore, GFP-RGA intensity was also detected in the transition/elongation zone and did not appear to decrease between these regions. Similar to GAI-GFP, no GFP-RGA signal was detected in the stem cell niche, but was detected in the root cap (Figure 3.3Aii). Further along the root in elongating cells of the epidermis, cortex, endodermis, pericycle and vasculature, RGA-GFP accumulation was also present (Figure 3.3Bii), but eventually decreased and was no longer detectable in the maturation zone of the primary root and closer to the hypocotyl (Appendix – Figure 3.4.2). This was observed for all pRGA::GFP-RGA roots over all roots visualised as part of this experiment (n=9). GFP-RGA accumulation was also detected in lateral roots and lateral root primordia of these seedlings throughout all tissue layers (Figure 3.3C,Dii). In relation to analysis of the pRBR::RBR-GFP line, RBR-GFP intensity was higher and therefore easier to detect than both GAI-GFP and GFP-RGA in the root. Similar to GFP-RGA, RBR-GFP intensity was consistently accumulated in all tissue layers of the apical root including the epidermis, cortex, endodermis, pericycle and the central stele/vasculature and the root cap (Figure 3.3Aiii). However, the intensity in the central stele/vasculature appeared to be higher in the proximal meristem than in elongating cells. In contrast to both GAI-GFP and GFP-RGA, RBR-GFP was also detected in the stem cell niche, including QC cells and stem cell initials (Figure 3.3A).

3.2.3 GAI, RGA and RBR proteins differentially accumulate in the root during seedling establishment

Since establishing that GFP-RGA, GAI-GFP and RBR-GFP are nuclear-localised and differentially accumulate in the root, I wanted to investigate further to determine dynamic changes in their patterns during early seedling development. Therefore, a time-course analysis was performed of pRGA::GFP-RGA, pGAI::GAI-GFP and pRBR::RBR-GFP seedlings from 2-7 DAS. GFP intensity in the root was visualised and captured with confocal microscopy every 24 hours during this time-period. For the expression of GAI-GFP, 2 days old seedlings (2 DAS, n=3) had a lower intensity when compared seedlings aged between 3-7 DAS. Previous observations of GAI-GFP intensity being predominantly localised to the nuclei of cortical cells within the proximal root meristem remained consistent throughout all days of the time course experiment (Figure 3.4i). An attempt to capture GAI-GFP in the

Figure 3.3: Accumulation of GAI-GFP, GFP-RGA and RBR-GFP in the root

Representative confocal images of GAI-GFP, RGA-GFP and RBR-GFP intensity in the root of *Arabidopsis* seedlings 7 days after stratification (DAS) for the translational reporter lines, (i) pGAI::GAI-GFP, (ii) pRGA::GFP-RGA and (iii) pRBR::RBR-GFP, respectively. Different regions of the root have been captured including:

(A) The root apical meristem
(B) The maturation zone for pGAI::GAI-GFP and pRGA::GFP-RGA and the elongation zone for pRBR::RBR-GFP.
(C) Emerging lateral roots
(D) Mature lateral roots

Propidium Iodide (PI) was used for staining of cell walls and as a counterstain. Both GFP and PI was excited with a 488 laser. For each confocal image, the combined channel image for GFP (green) and PI (magenta) is shown (top left). The single channel images for GFP (top right) and PI (bottom left) are portrayed in grayscale. The transmitted light image is also shown (bottom right).

Scale bars represent 50 µm for images A, B and C of the translational reporter line (i) pGAI::GAI-GFP and 20 µm for image D. Scale bars represent 50 µm for images A, B and D of the translational reporter line (ii) pRGA::GFP-RGA and 20 µm for image C. Scale bars represent 50 µm for images A, B and C of the translational reporter line (iii) pRBR::RBR-GFP and 30 µm for C.

A (i)

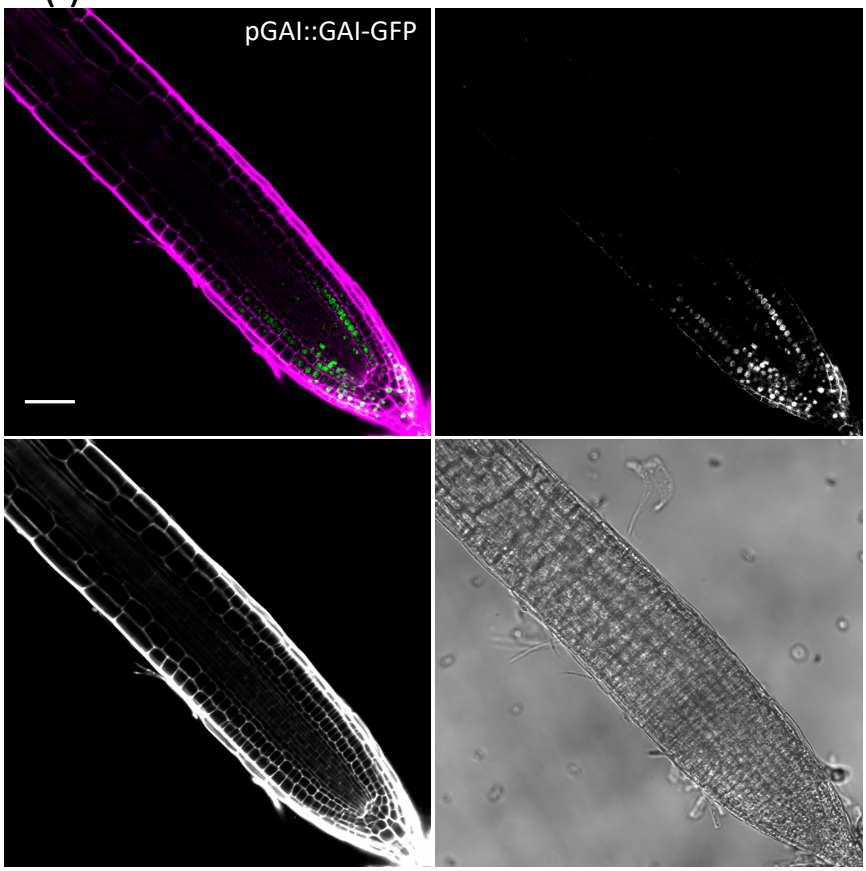

B (i)

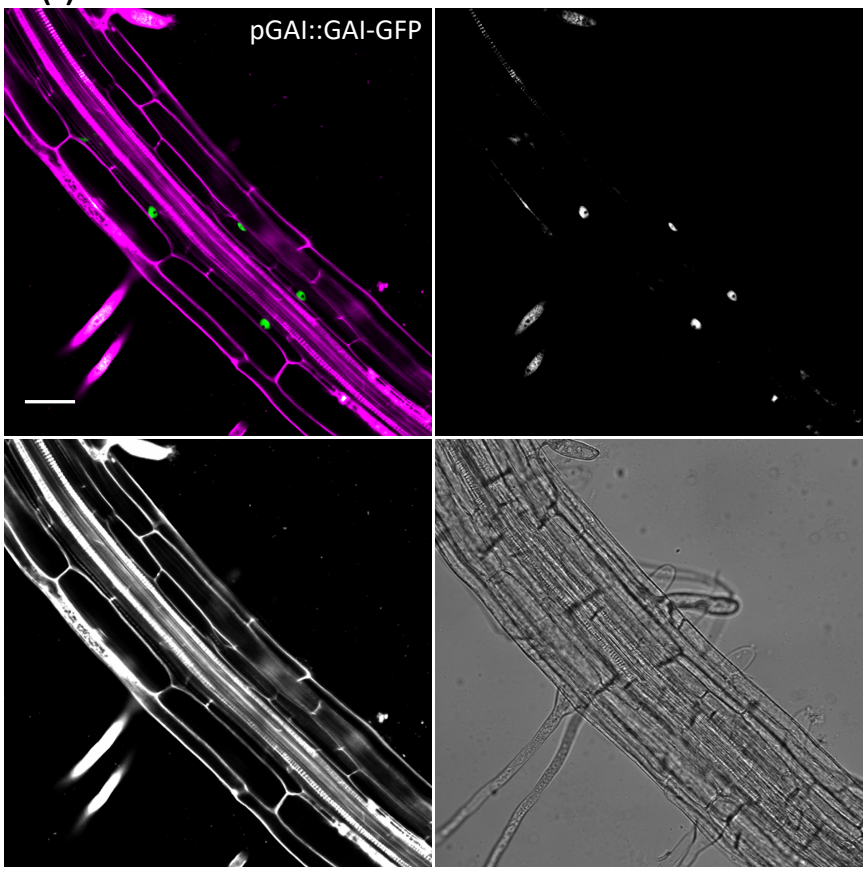

C (i)

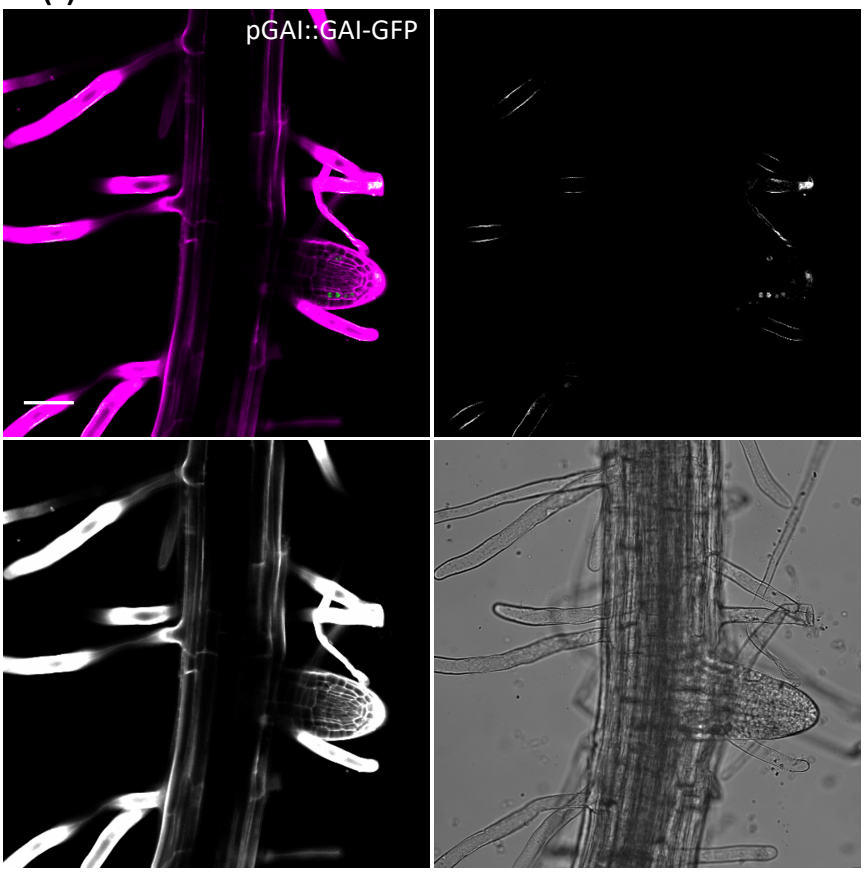

D (i)

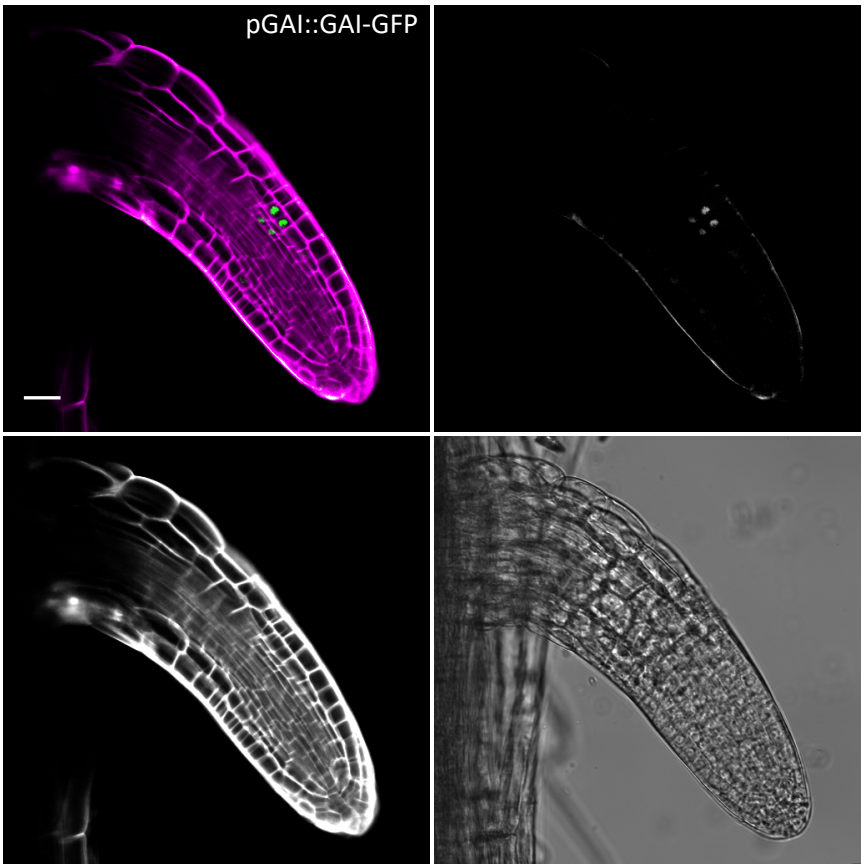

A (ii)

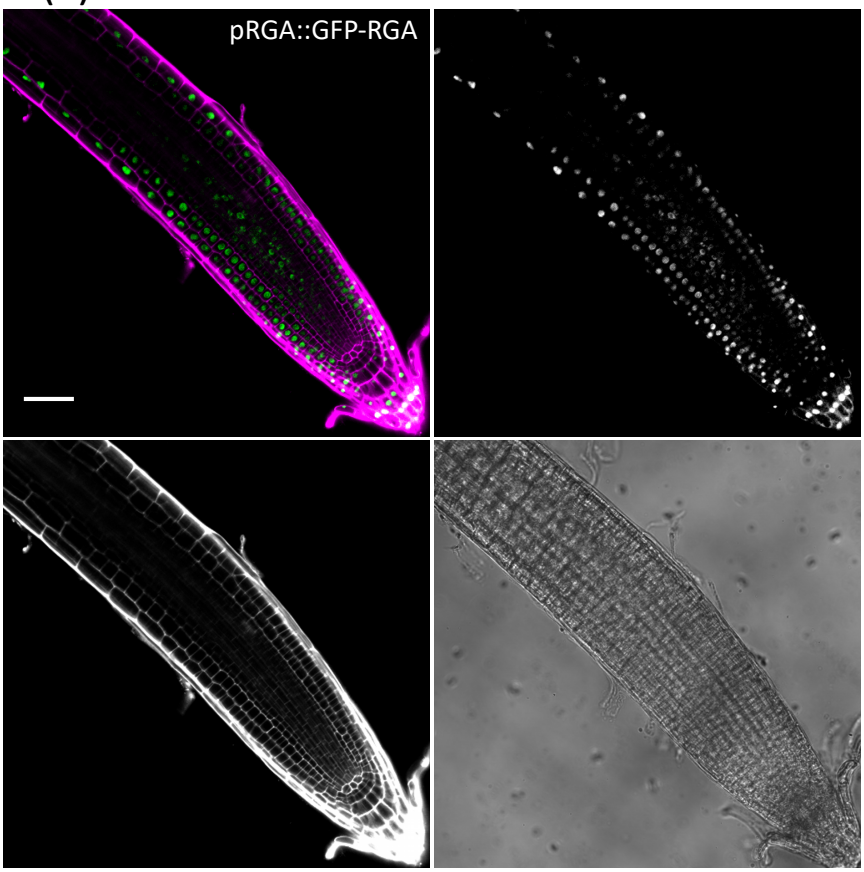

B (ii)

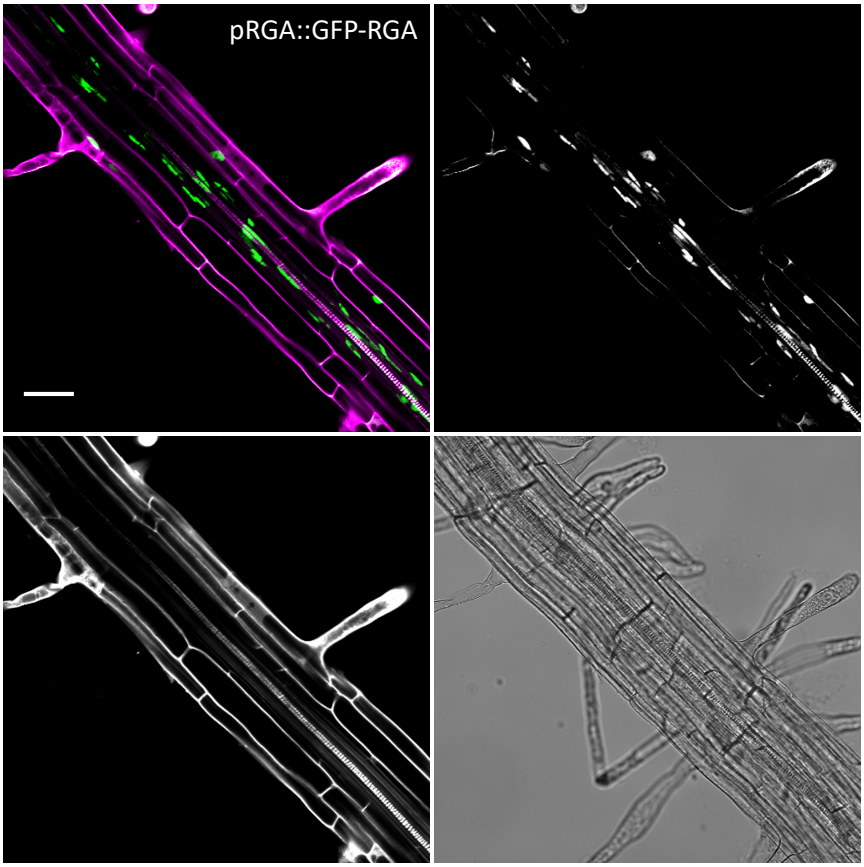

C (ii)

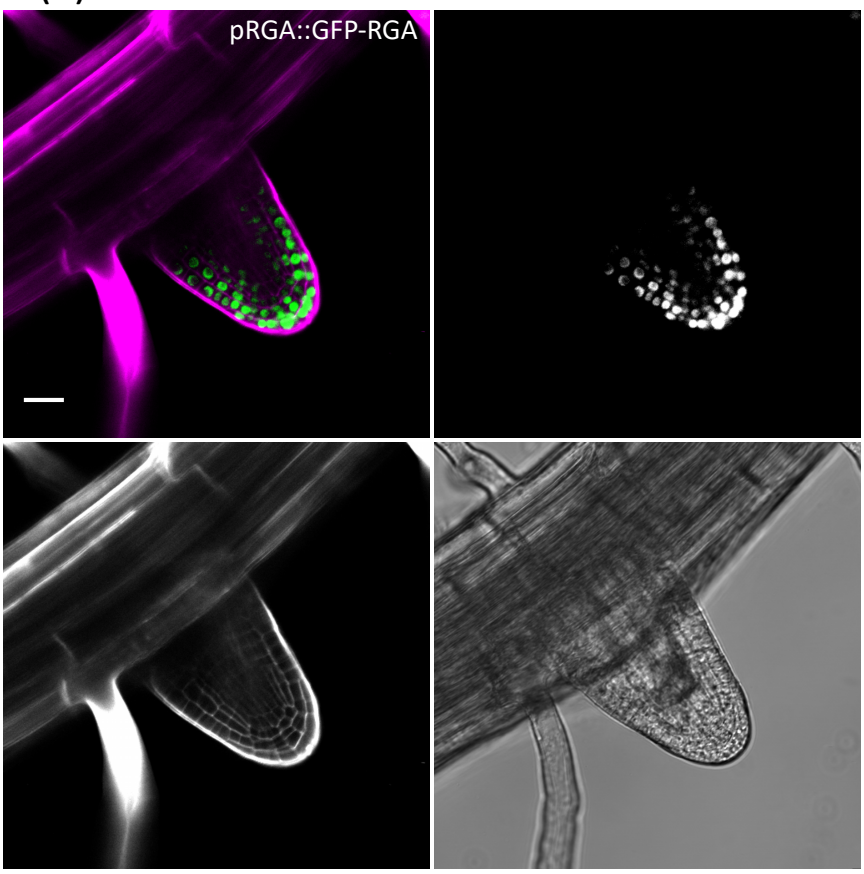

D (ii)

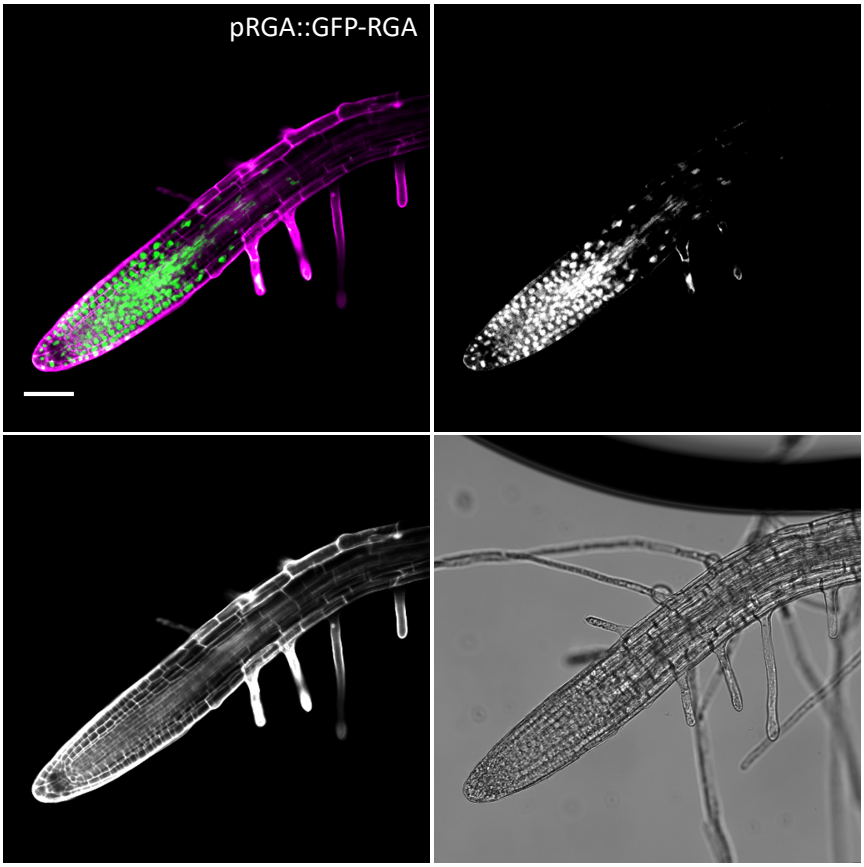

A (iii)

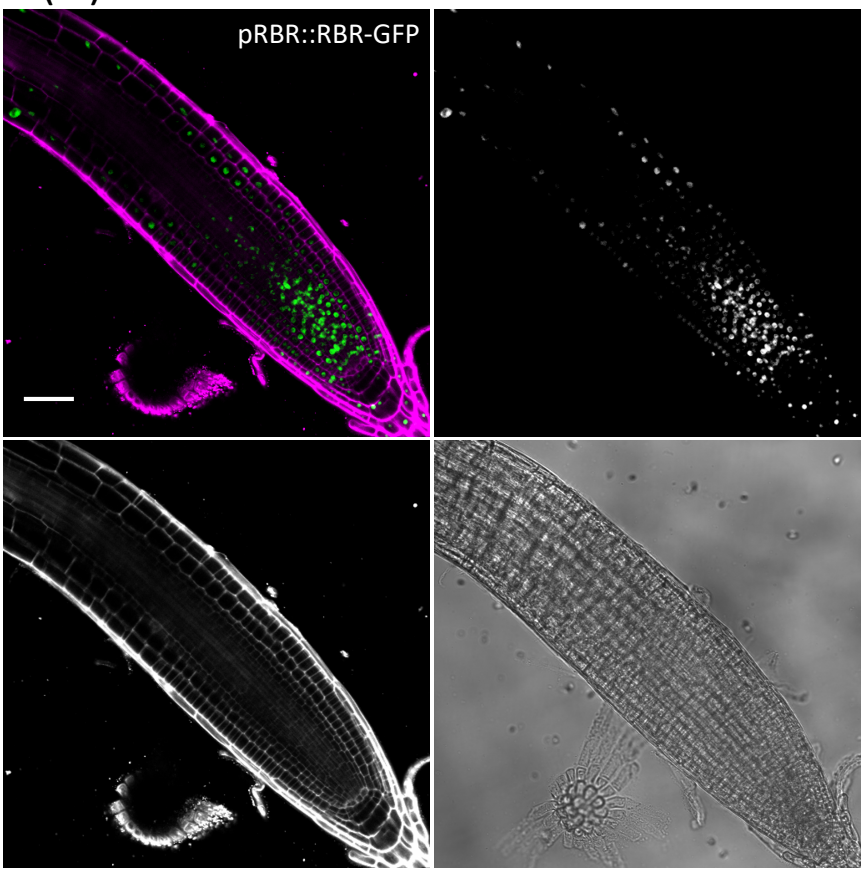

B (iii)

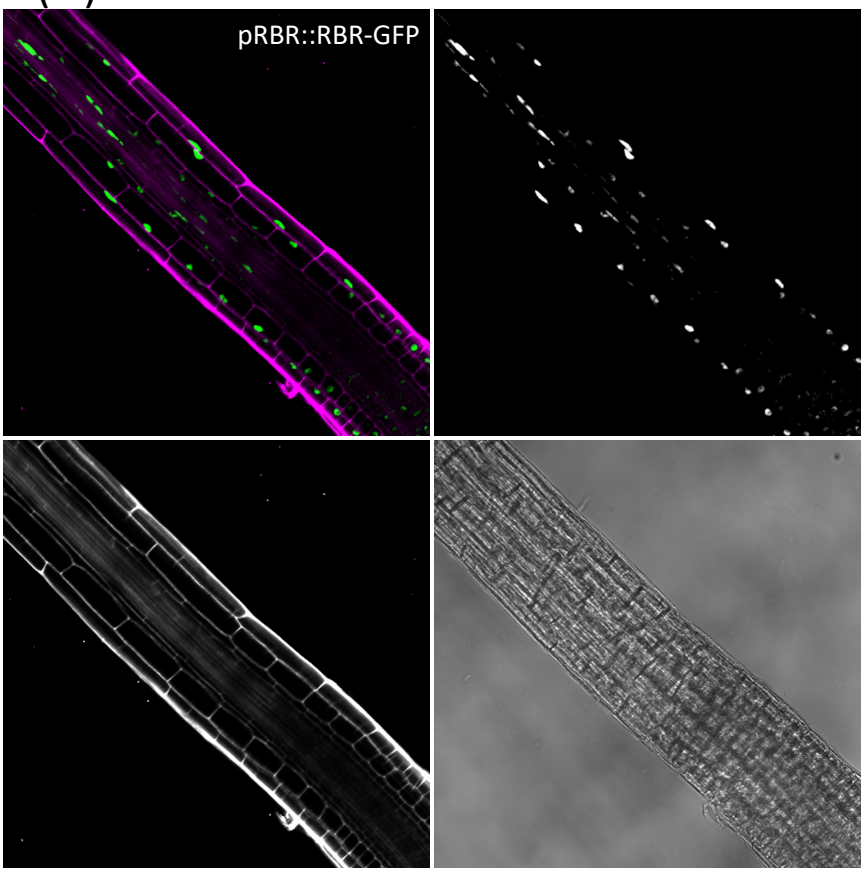

C (iii)

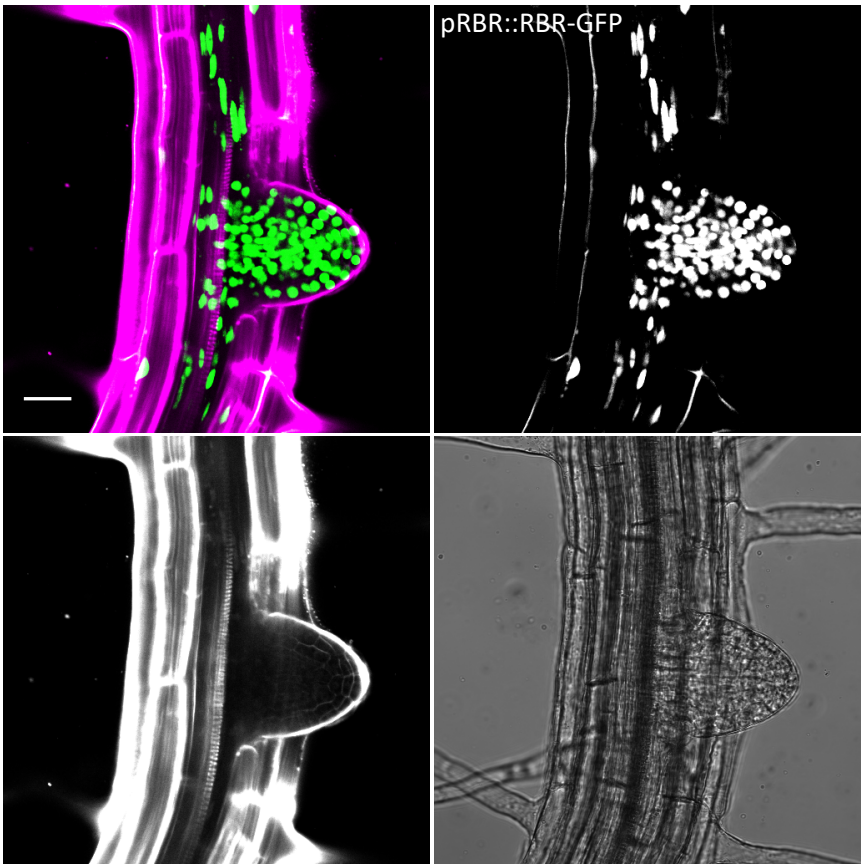

D (iii)

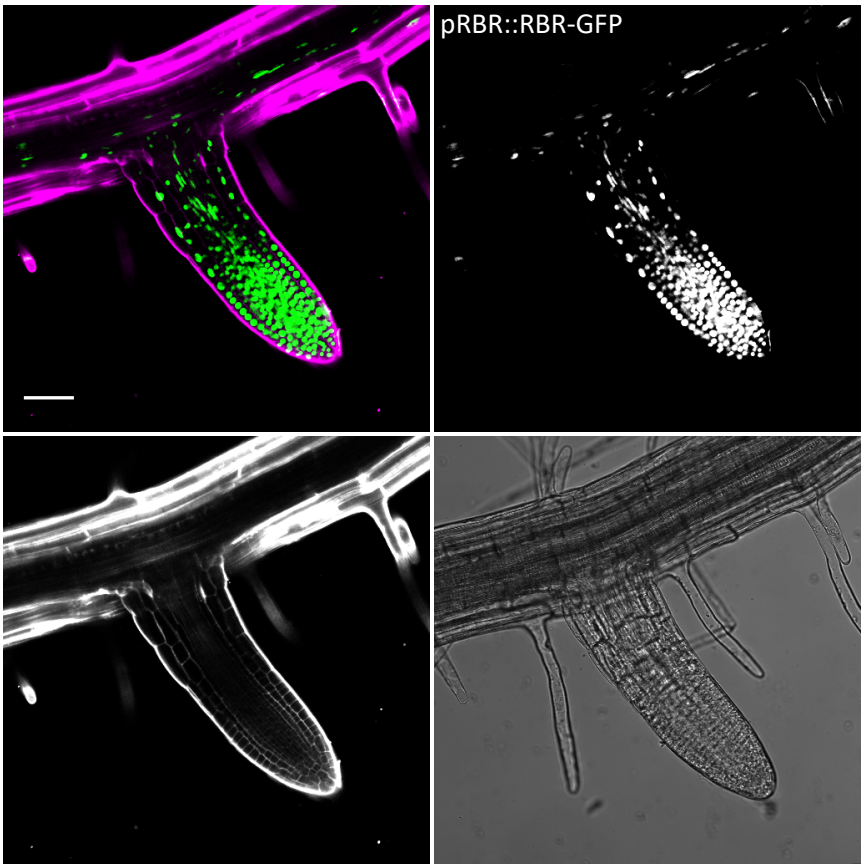

RAM at 1 DAS, but it was difficult to obtain a clear image even after removing the seed coat so the time-course for all of the described lines was from 2 DAS. One observation was that sometimes an image of a pGAI::GAI-GFP root was captured whereby the GFP intensity was highest in smaller cells at the root apex. As mentioned earlier from previous observations of lateral root/lateral root primordia of pGAI::GAI-GFP roots at 7 DAS, this pattern of accumulation occurred in two adjacent cells of the proximal meristem. Cells within this region are undergoing the developmental process of cell division. Once a cell has completed the mitosis (M) phase, the resulting daughter cells are smaller than their parent. Therefore, GAI-GFP intensity appeared to be brightest in cells that had just undergone mitosis. Conversely, this type of expression pattern for either GFP-RGA or RBR-GFP was no observed.

The expression pattern of GFP-RGA remained constant and did not vary throughout all days of the experiment (2-7 DAS) and was observed in the nuclei of cells within all tissue layers of the apical root, apart from the QC and stem cells initials (Figure 3.4ii). Unlike GAI-GFP and as mentioned previously, GFP-RGA intensity did not appear to vary between the proximal meristem and the transition/elongation zone. However, similar to GAI-GFP, GFP-RGA levels did appear to be highest in the cortical cell layer of the root meristem and lower in the endodermis.

The time-course analysis performed on pRBR::RBR-GFP seedlings revealed that RBR-GFP accumulation was localised to the nuclei of all tissue types that comprise the apical root, and this was consistent across all days (2-7 DAS). Although RBR-GFP was also detected in cells within the transition/elongation zone of the root, expression was higher at the basal end and throughout all tissues of the RAM, including the proximal root (epidermis, cortex, endodermis, pericycle and the central stele/vasculature), the stem cell niche (QC and initials) and the columella root cap. This pattern was consistent across all days of the experiment and is similar to that of the accumulation pattern of GAI-GFP, but contrasts with the pattern of GFP-RGA, which did not differentially accumulate between these regions. However, unlike GAI-GFP, where intensity is highest in the cortical cell layer of the proximal root, RBR-GFP intensity was present in all tissue layers and did not appear to vary between them (Figure 3.4i). GAI, RGA and RBR transcript levels in the root meristem were also analysed using the eFP browser. Since the microarray dataset for this purpose was based on transcriptional expression from a single seedling, only qualitative analysis could be inferred from these results and are described in the appendices (Appendix 3.1.1 and 3.1.2).

3.2.4 GAI and RGA accumulation are under the control of GA in the root meristem

To further our understanding of how GAI and RGA respond to altered levels of GA, experiments were performed where the translational reporter lines, pGAI::GAI-GFP and pRGA::GFP-RGA, were treated with exogenous GA and PAC (Figure 3.5i,ii). Furthermore, PAC treatment experiments were performed

Figure 3.4: Accumulation of GAI-GFP, GFP-RGA and RBR-GFP in the root during seedling establishment

Representative confocal images of GAI-GFP, RGA-GFP and RBR-GFP intensity in the root of *Arabidopsis* seedlings over time from 2-7 days after stratification (DAS) for the translational reporter lines, (i) pGAI::GAI-GFP, (ii) pRGA::GFP-RGA and (iii) pRBR::RBR-GFP, respectively.

Propidium Iodide (PI) was used for staining of cell walls and as a counterstain. Both GFP and PI was excited with a 488 laser. For each confocal image, the combined channel image for GFP (green) and PI (magenta) is shown (top left). The single channel images for GFP (top right) and PI (bottom left) are portrayed in grayscale. The transmitted light image is also shown (bottom right).

Scale bars represent 50 μm

Day 2 (i)

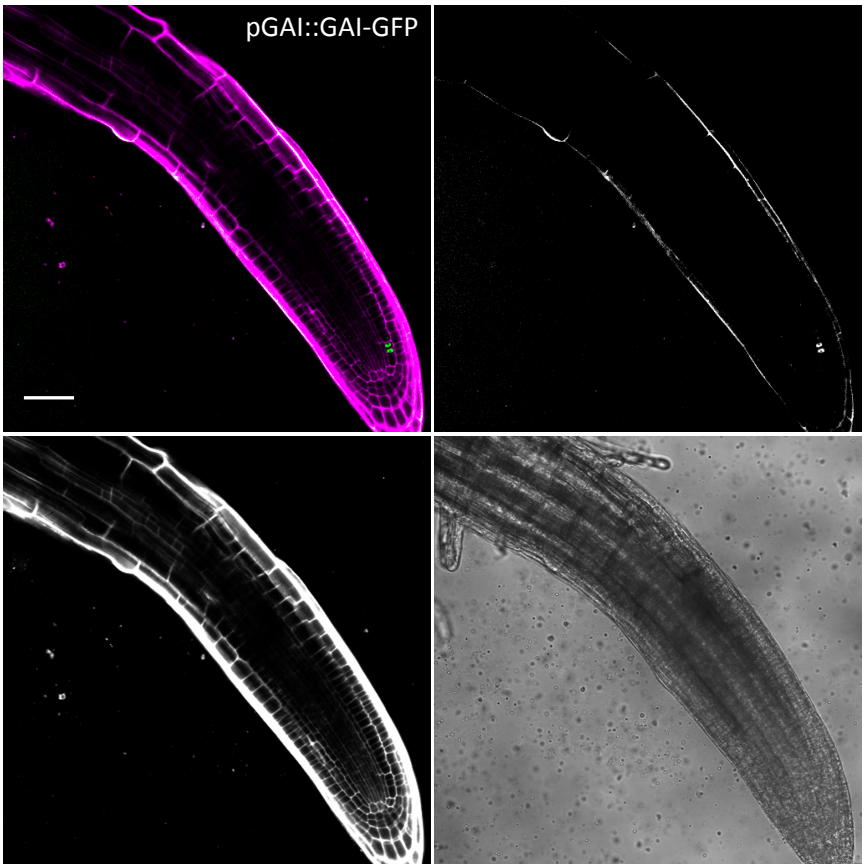

Day 3 (i)

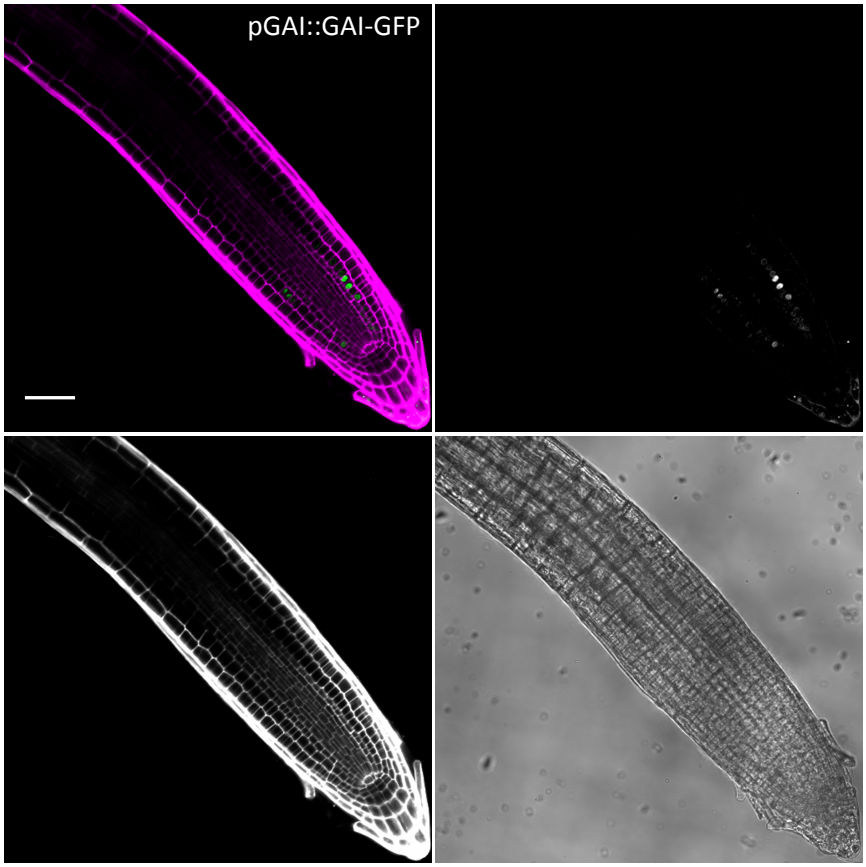

Day 4 (i)

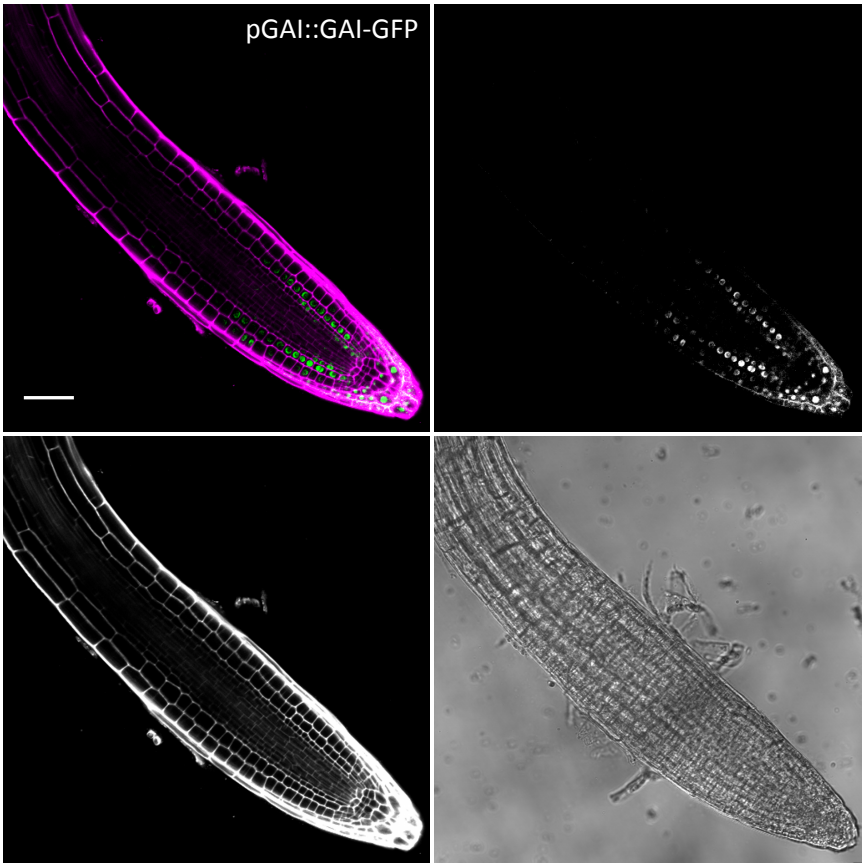

Day 5 (i)

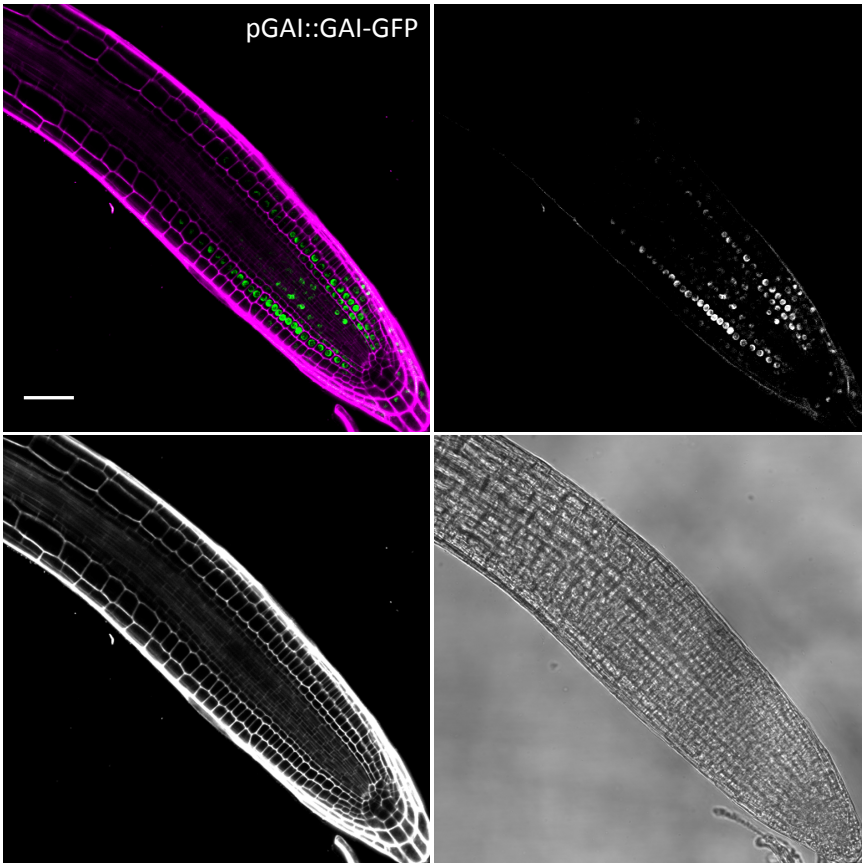

Day 6 (i)

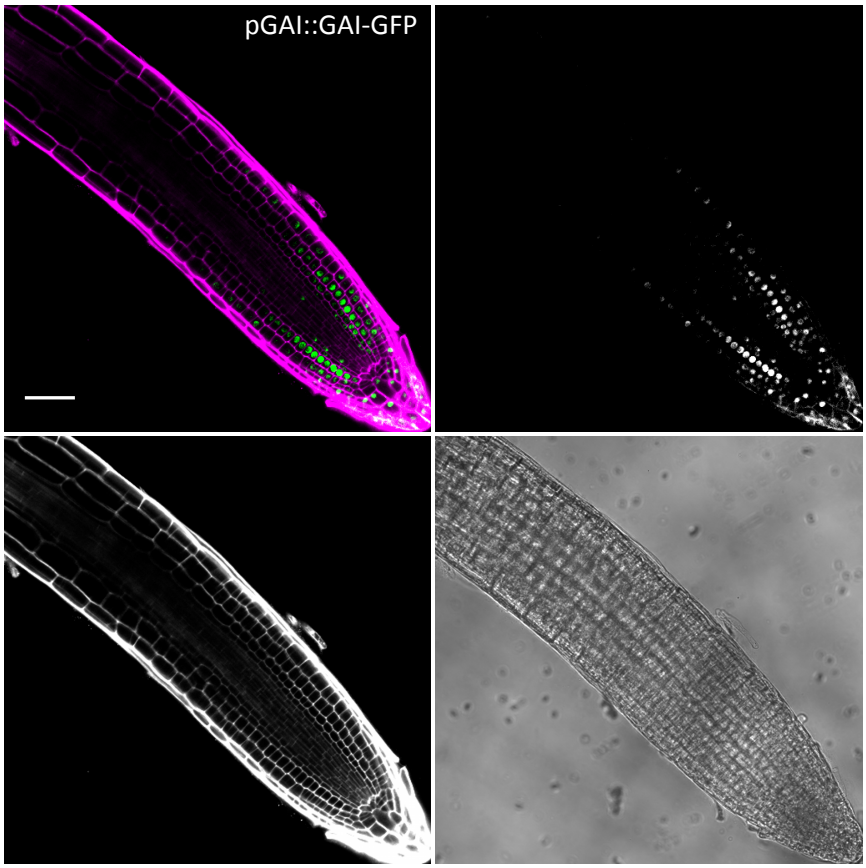

Day 7 (i)

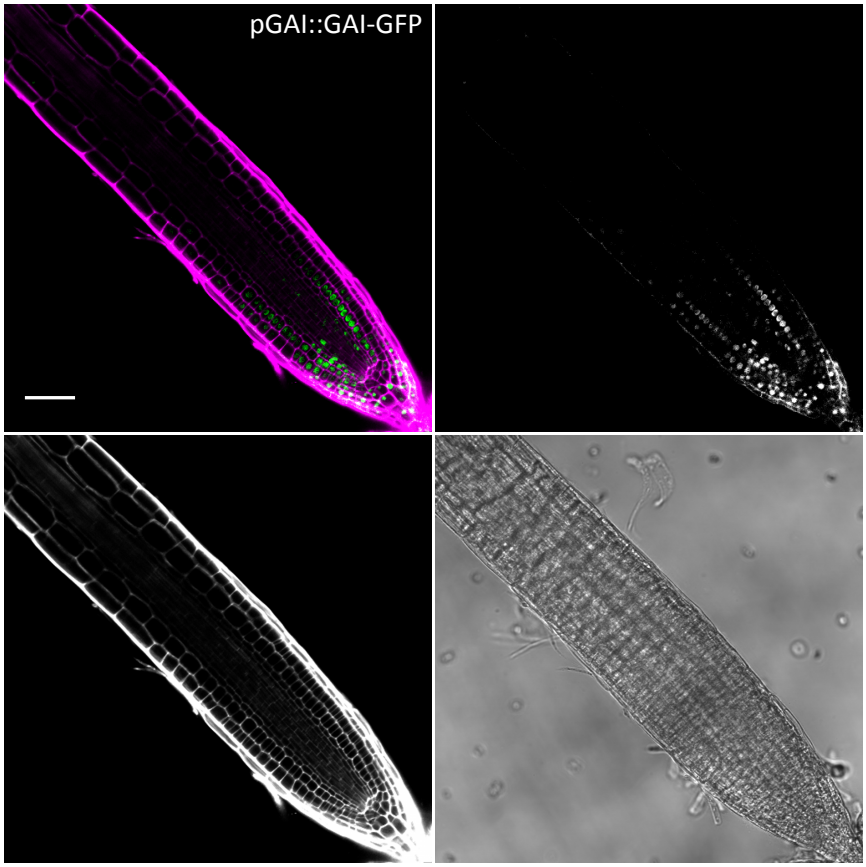

Day 2 (ii)

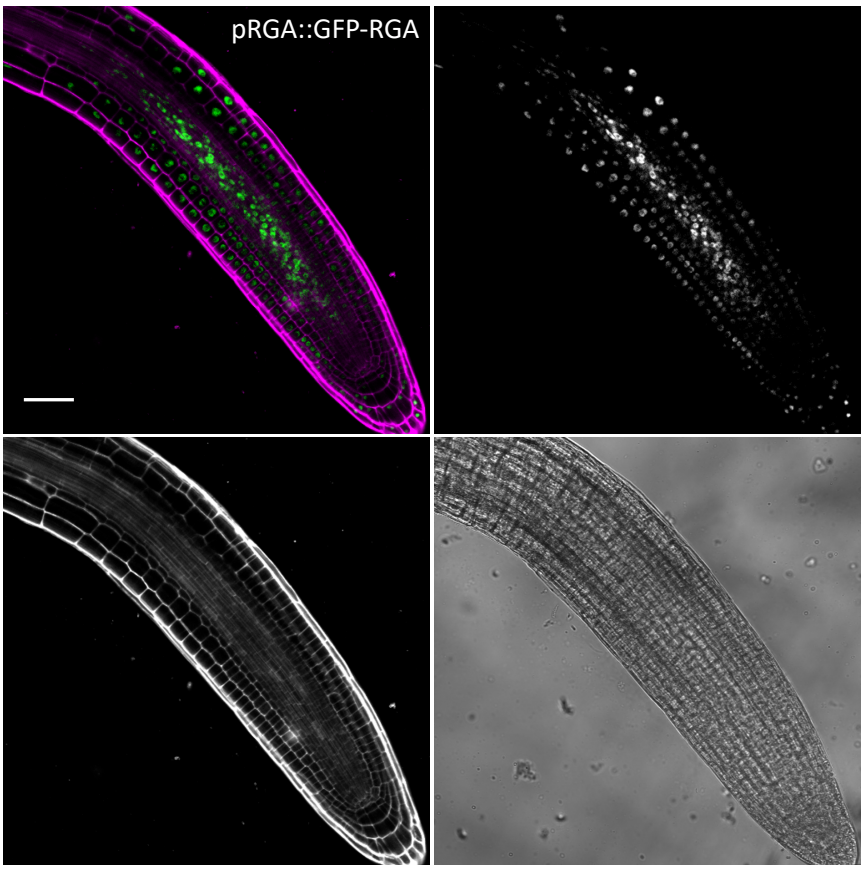

Day 3 (ii)

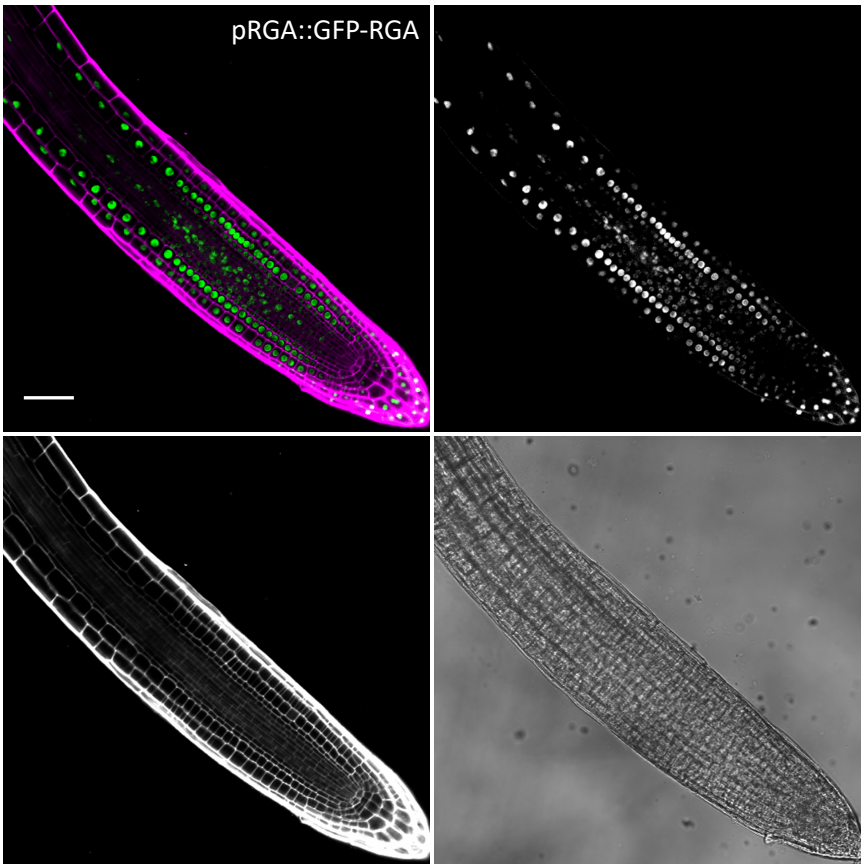

Day 4 (ii)

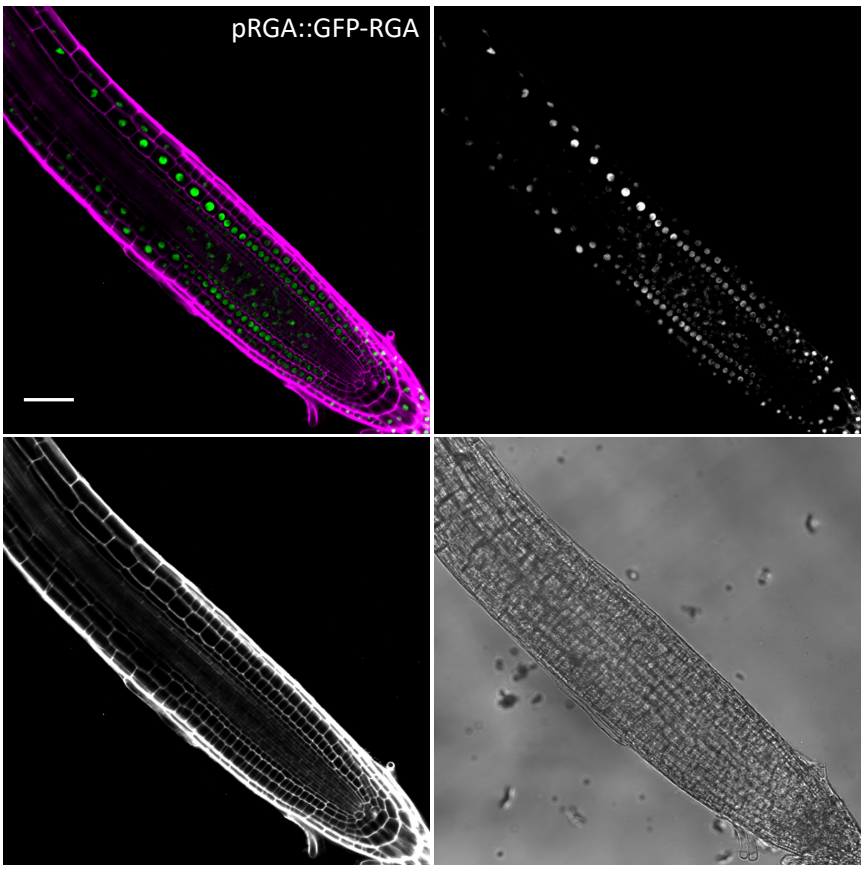

Day 5 (ii)

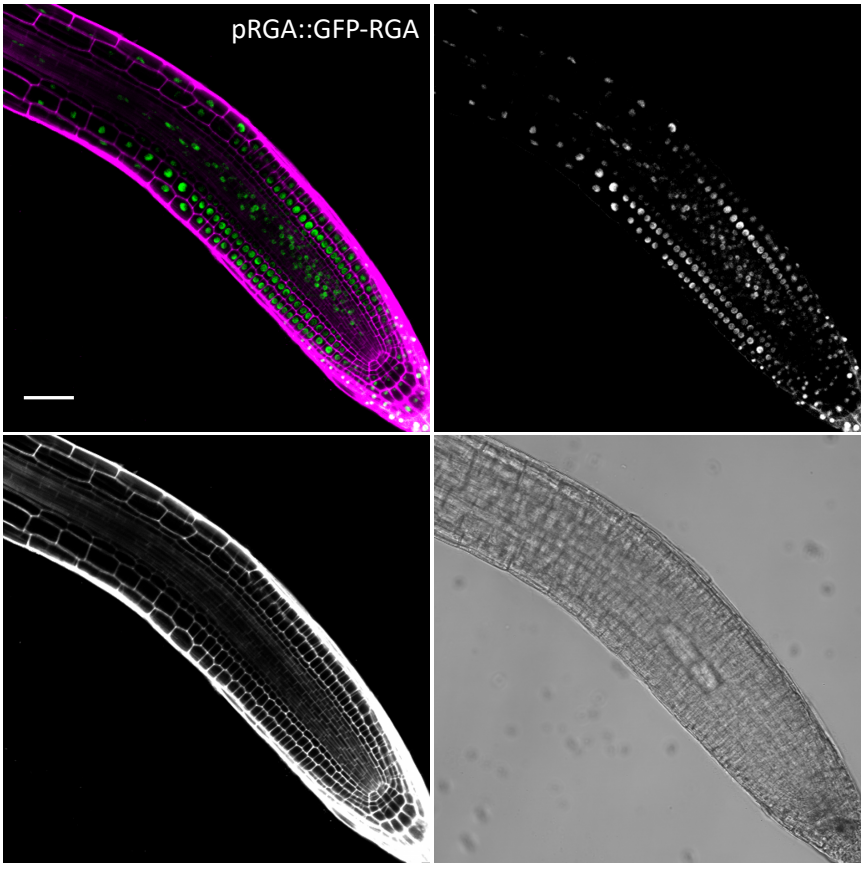

Day 6 (ii)

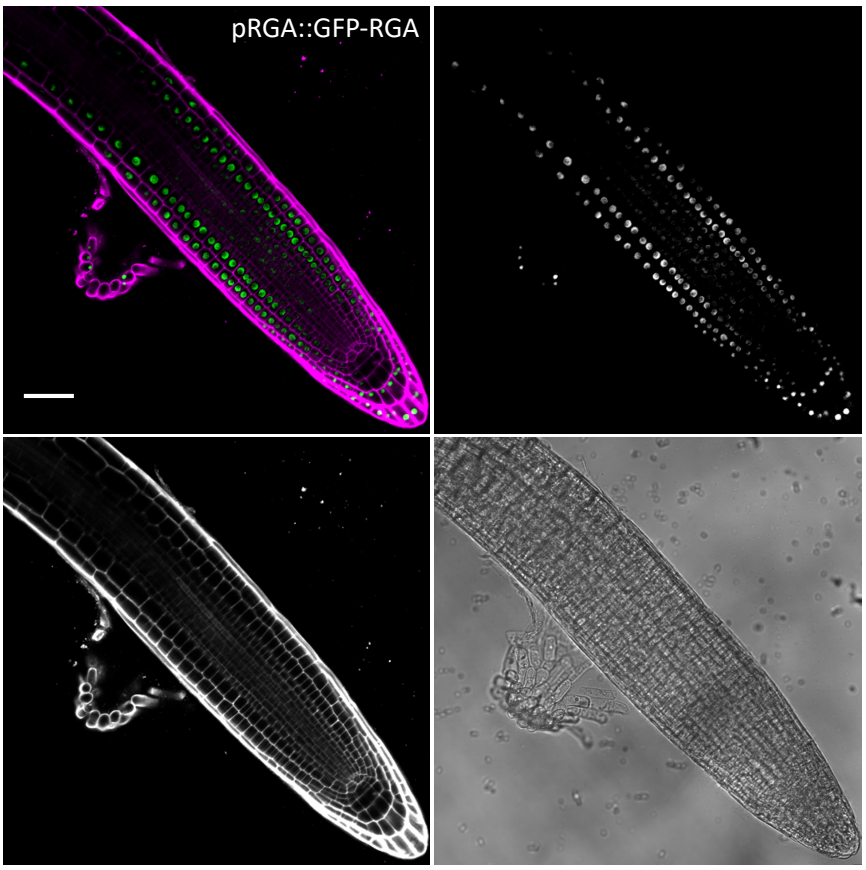

Day 7 (ii)

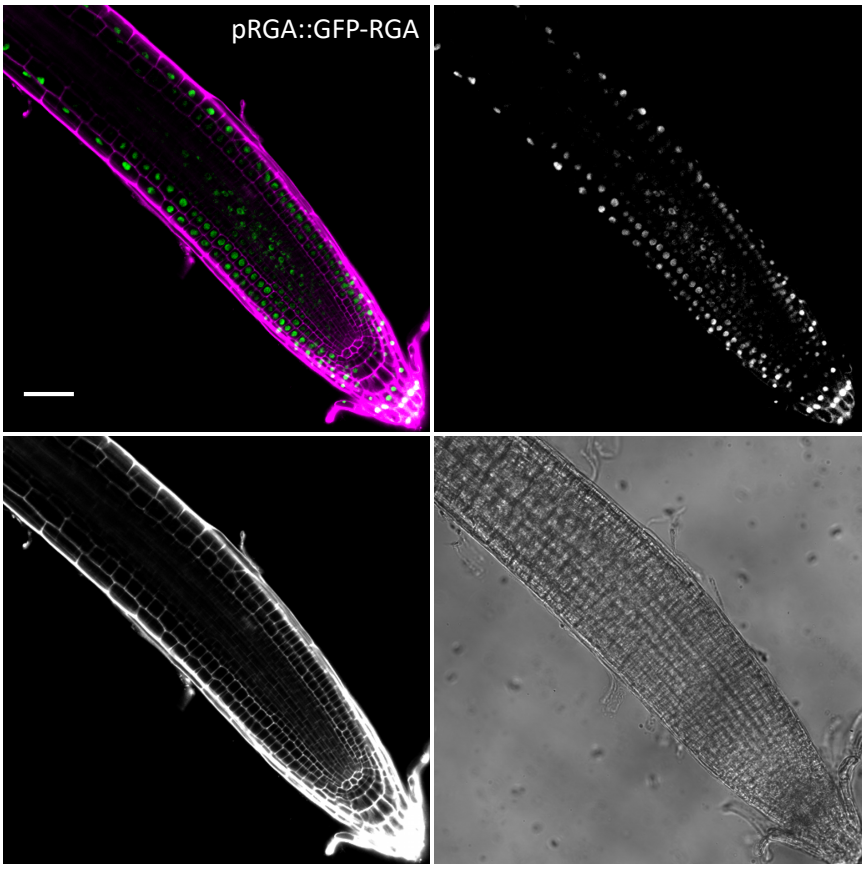

Day 2 (iii)

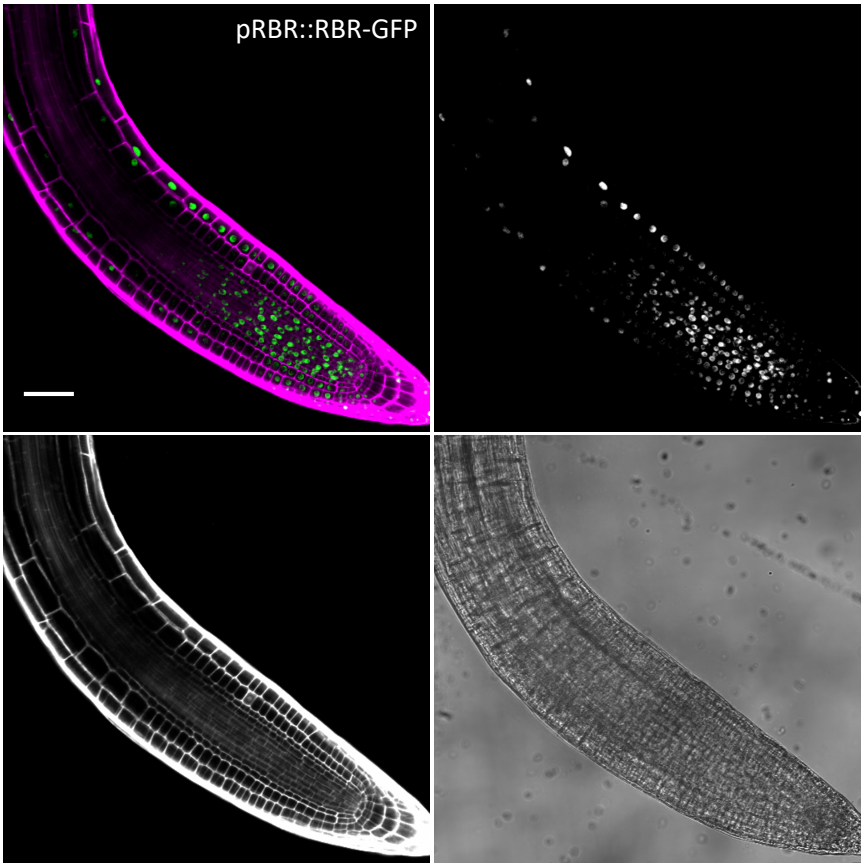

Day 3 (iii)

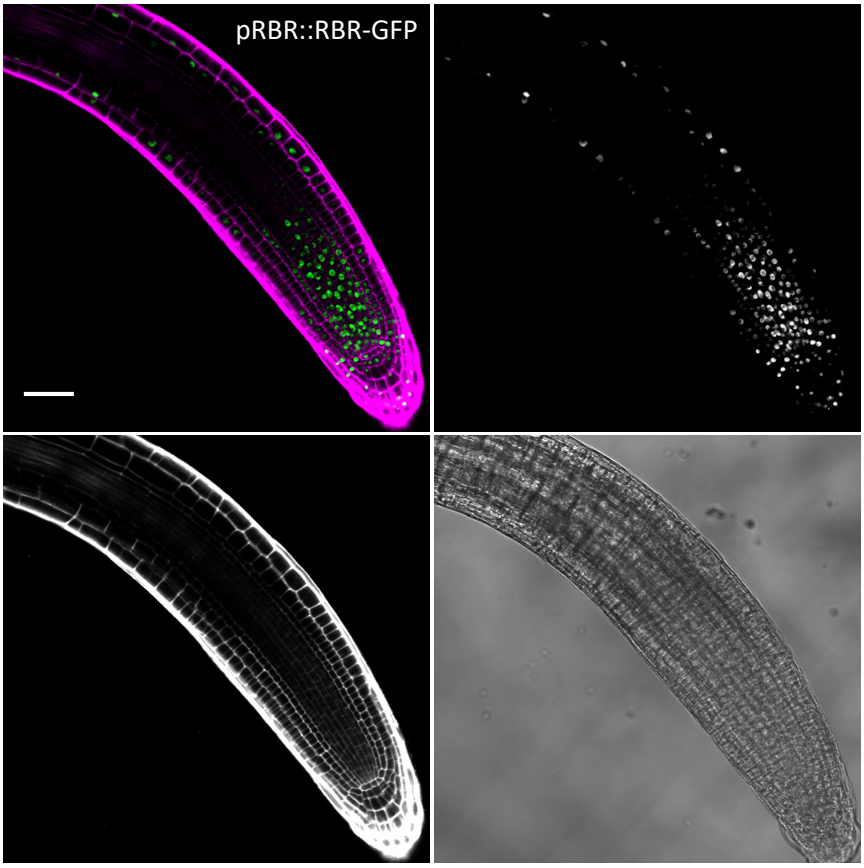

Day 4 (iii)

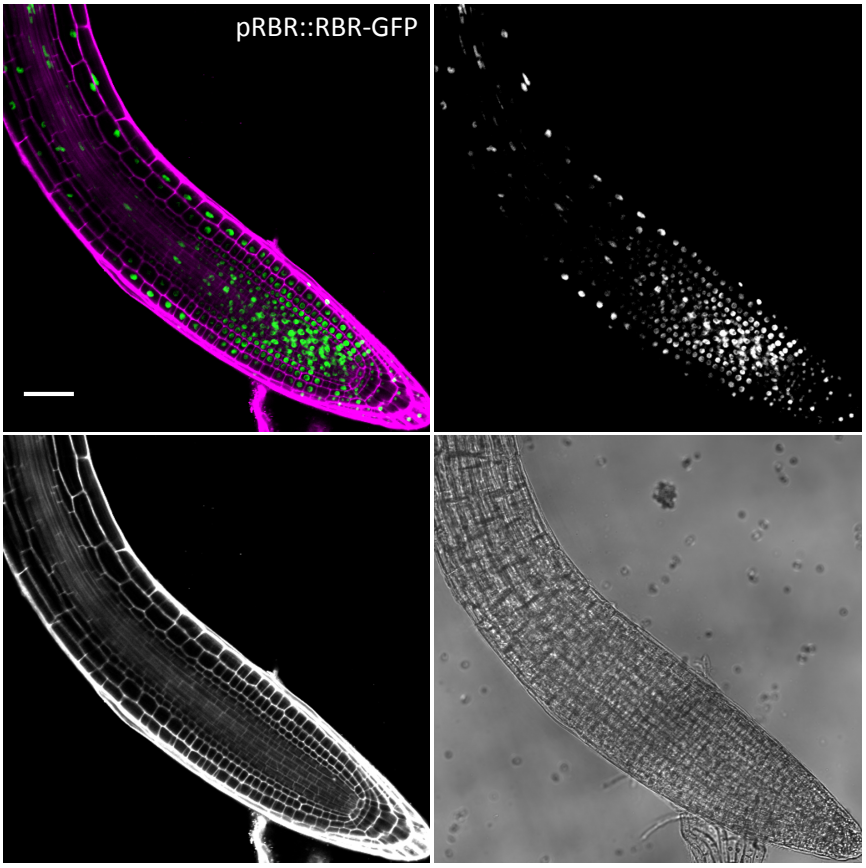

Day 5 (iii)

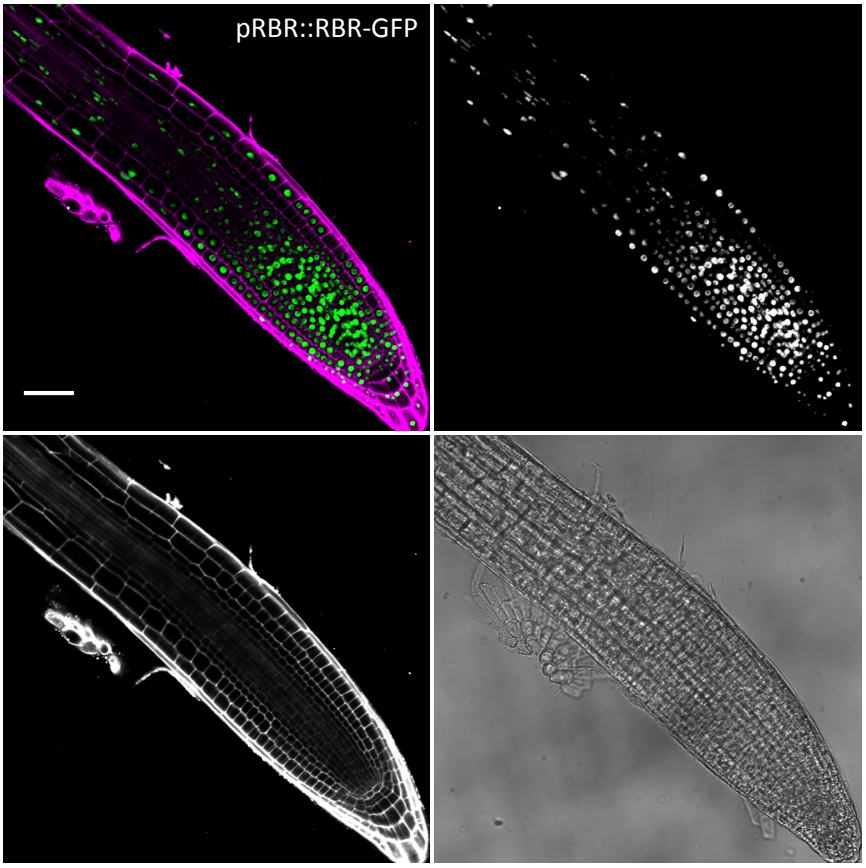

Day 6 (iii)

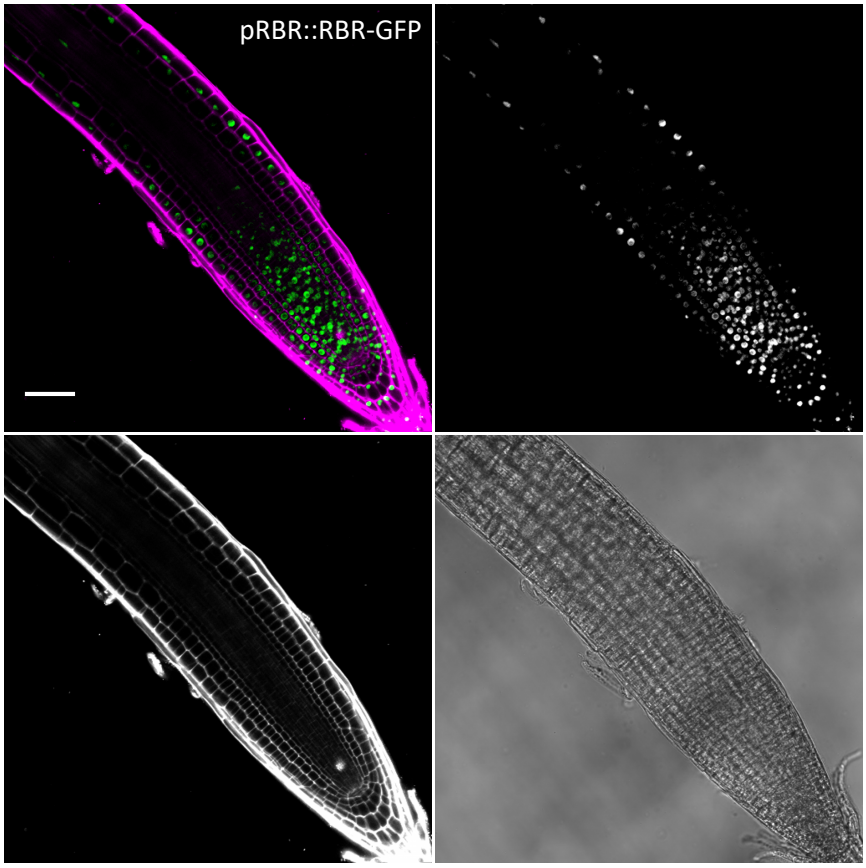

Day 7 (iii)

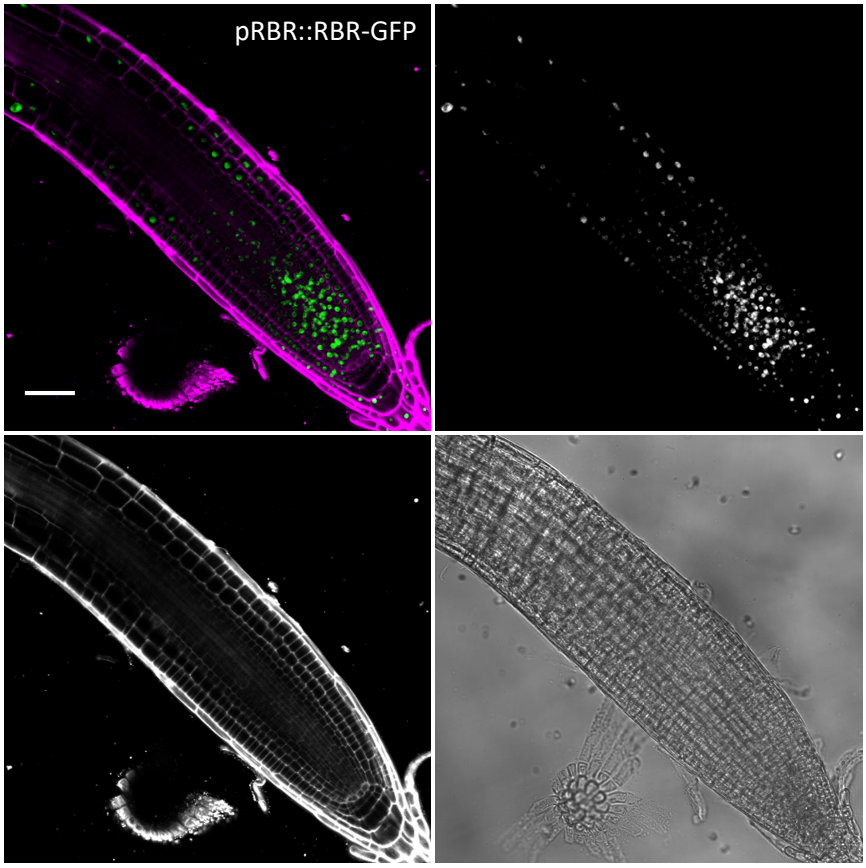

on plant lines that constitutively express GAI-GFP and RGA-GFP from the 35S CaMV promoter (Figure 3.5iii,iv). Previous studies had reported on these types of experiments, but demonstrated conflicting results in relation to the treatment of GAI-GFP (Fleck and Harberd 2002, Dill et al. 2004, Tyler et al., 2004). Fleck and Harberd (2002) performed experiments where they treated the pGAI::GAI-GFP and 35S::GAI-GFP lines with 100µM GA_3 over a time-course and found that GFP levels were unchanged when compared to the control treatment. In contrast to this finding, more recent papers by Dill et al (2004) and Tyler et al (2004) found that GA treatment did indeed lead to the degradation of GAI.

To clarify these conflicting results, I therefore performed my own treatment experiments to determine whether or not both GAI and RGA are under the control of GA. It is also useful to determine whether or not these treatments are effective especially in the case of the PAC treatment because I wanted to be able to increase the levels of my target proteins for further experimental work. If the working model is correct, treating GAI-GFP and RGA-GFP with GA should effectively decrease their protein levels, whilst treatment with PAC, as an inhibitor of the GA biosynthetic pathway should increase their levels. To test this hypothesis I grew pGAI::GAI-GFP and pRGA::GFP-RGA seedlings for 8 DAS before transferring to either control growth media (GM root) or supplemented with either 10µM PAC or 10µM GA_3 for 18 hours. Roots of these seedlings were then imaged with confocal microscopy to see how GFP levels changed in relation to the control (Figure 3.5i,ii). In the case of GA treatment, both GAI-GFP and RGA-GFP levels were decreased in the root meristem (Figure 3.5i,ii). This observation was consistent for all seedlings that had undergone the treatment (pGAI::GAI-GFP, n=10 and pRGA::GFP-RGA, n=11). However, although overall GAI-GFP expression was decreased, I noticed that there were some cells that still expressed GAI-GFP in the root after treatment (Figure 3.5i). This observation was always found in two adjacent cells within the same file of the proximal meristem.

In the case of the PAC treatment experiment, GAI-GFP and RGA-GFP intensity in the root meristem was increased in relation to the control. PAC treatment also affected the overall size of the root, which closely resembled that of a GA-biosynthetic mutant. GAI-GFP expression after this treatment was increased mainly in the proximal meristem and decreased at the transition/elongation zone (Figure 3.5i), whereas GFP-RGA expression was increased consistently throughout all regions of the root meristem (Figure3.5ii).

When investigating the 35S::GAI-GFP and 35S::GFP-RGA lines, it was noticed that overexpression of these proteins lead to decreased GFP expression in the root meristem (Figure 3.5iii,iv). This was particularly true for the 35S::GFP-RGA line where no GFP-RGA signal was detected in the root meristem and this was consistent across all seedlings observed as part of this experiment (n=13). For 35S::GAI-GFP seedlings, there was some nuclear-localised GAI-GFP signal detected in cortical cells of

Figure 3.5: Accumulation of GAI-GFP and RGA-GFP after PAC and GA treatment

Representative confocal images of GAI-GFP and RGA-GFP intensity in the root of *Arabidopsis* seedlings for the translational reporter lines, (i) pGAI::GAI-GFP and (ii) pRGA::GFP-RGA treated with GA and PAC. Seedlings were grown for 8 days before being transferred to plates containing growth media supplemented with either 10 μM PAC or 10 μM GA_3 or nothing in the case of the control (mock treatment) for a further 18 hours. A representative *Ler* control image using the same confocal settings for detection of the corresponding GFP-tagged protein and also transferred to PAC to show the effect it has on a WT root meristem. Seedlings of (iii) 35S::GAI-GFP and (iv) 35S::GFP-RGA at 5 DAS were also treated with PAC and representative confocal images are shown.

Propidium Iodide (PI) was used for staining of cell walls and as a counterstain. Both GFP and PI was excited with a 488 laser. For each confocal image, the combined channel image for GFP (green) and PI (magenta) is shown (top left). The single channel images for GFP (top right) and PI (bottom left) are portrayed in grayscale, alongside the transmitted light image (bottom right).

Scale bars represent 50 μm

Mock (i)

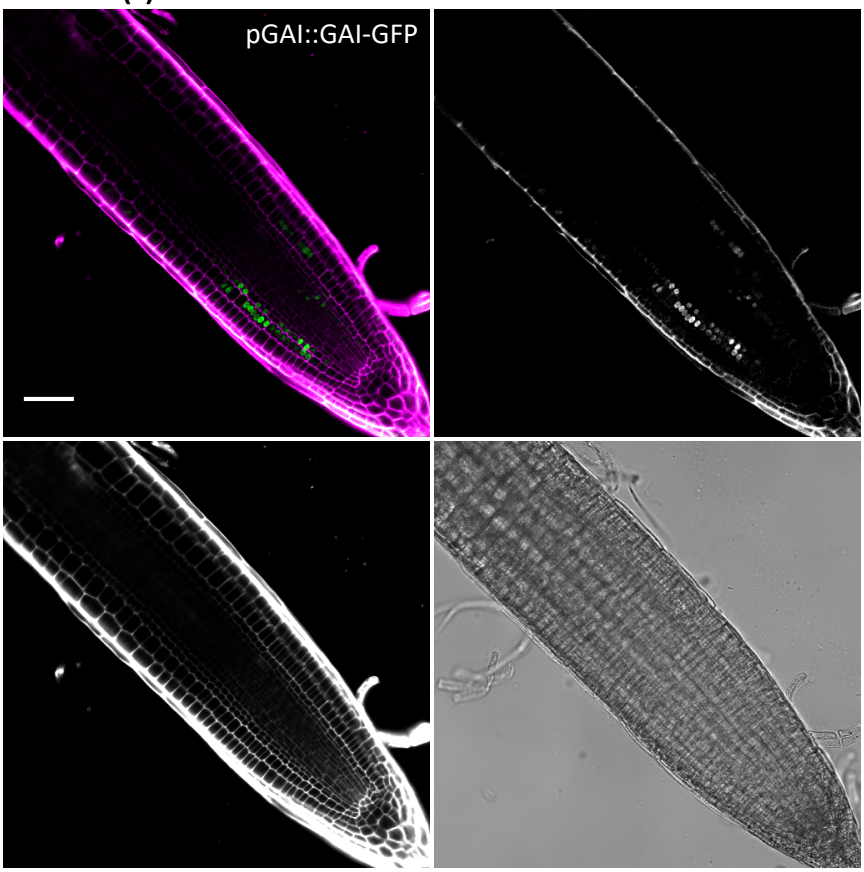

GA (i)

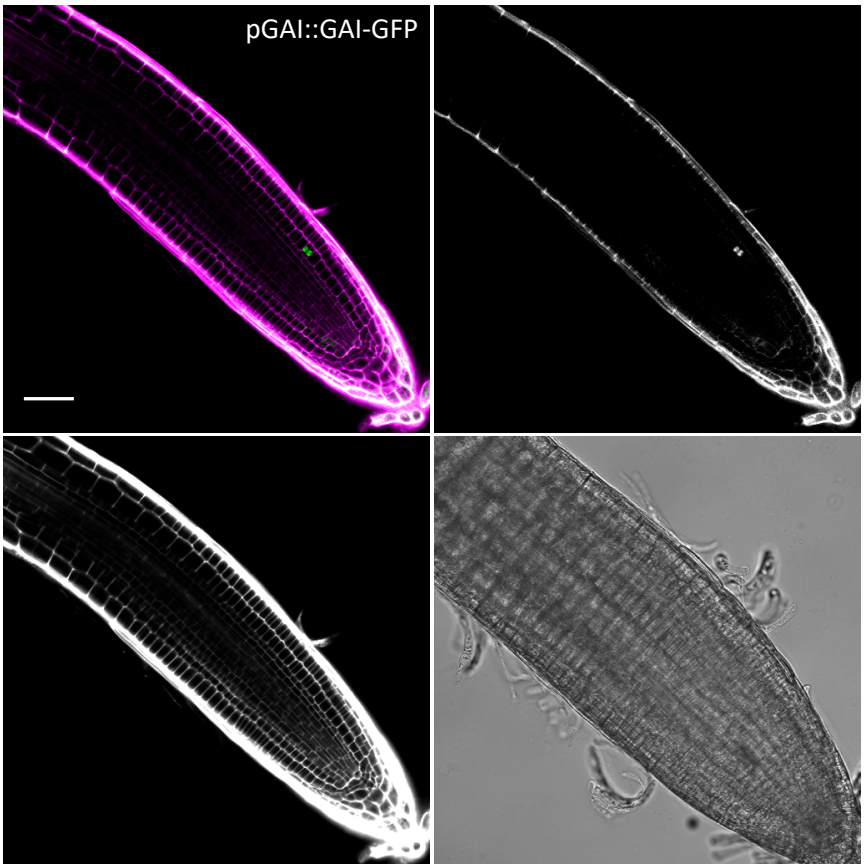

PAC (i)

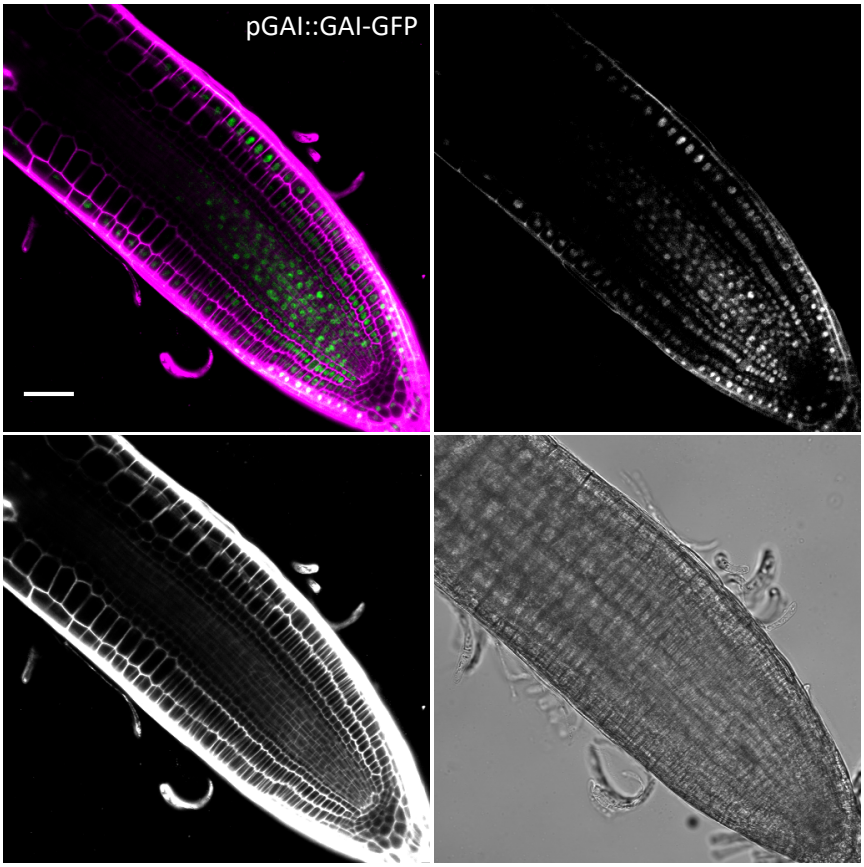

PAC (i) - Ler

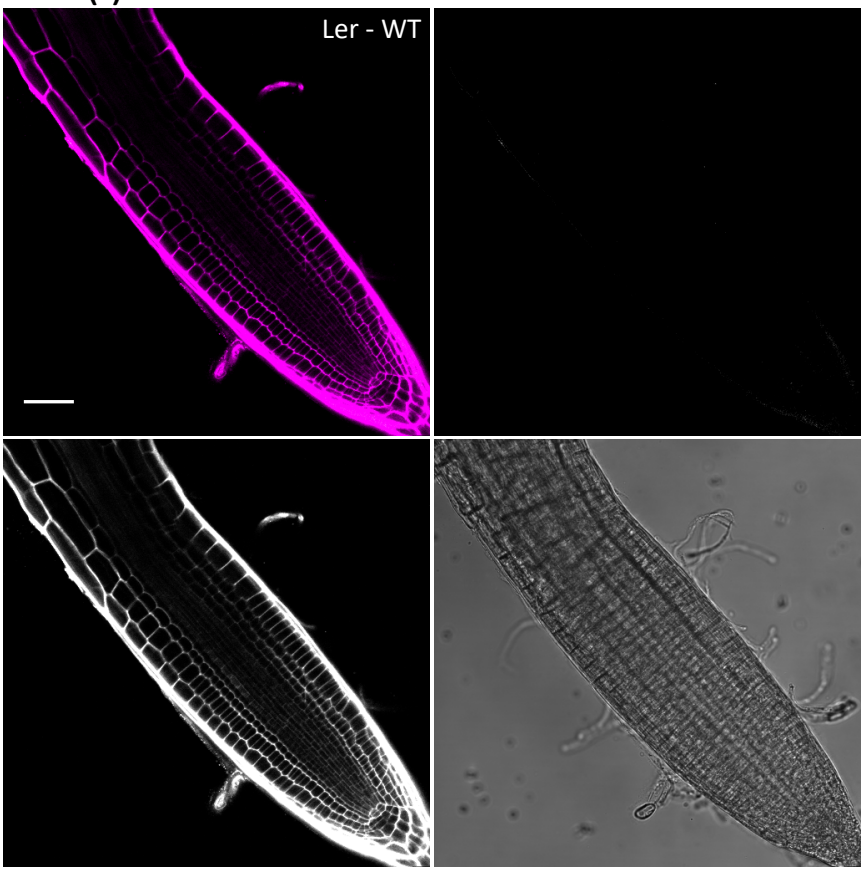

Mock (ii)

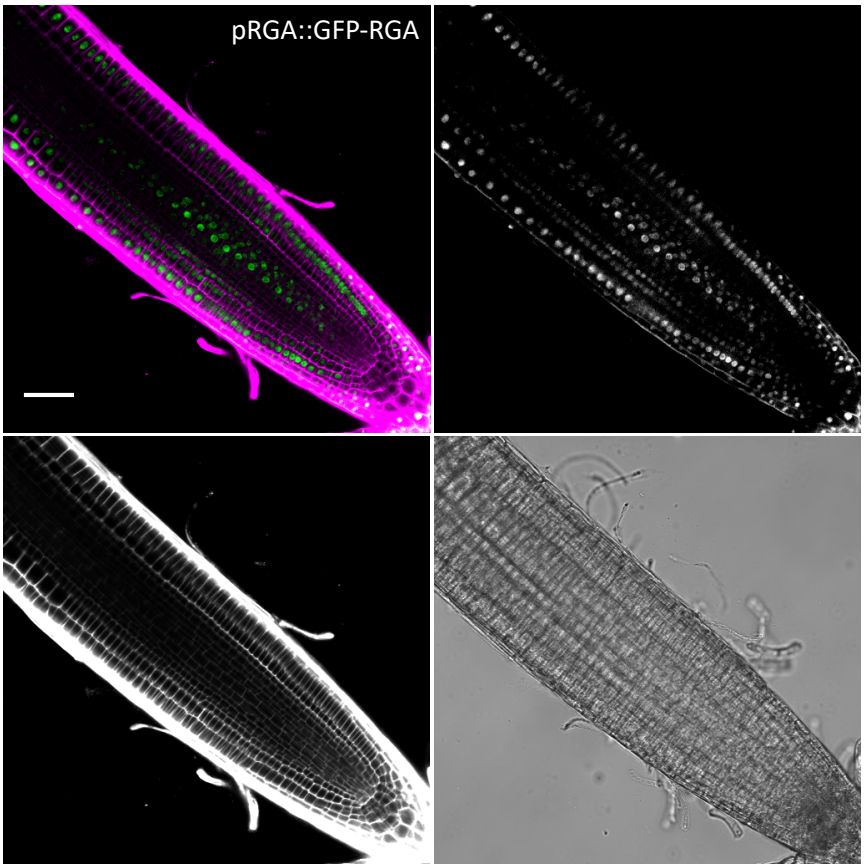

GA (ii)

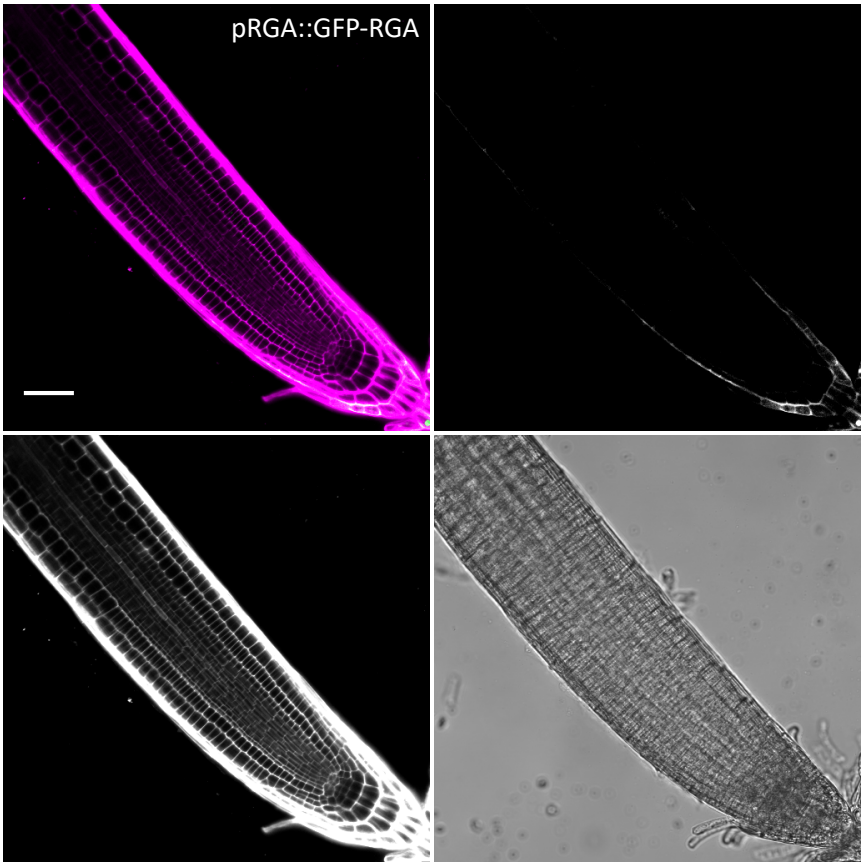

PAC (ii)

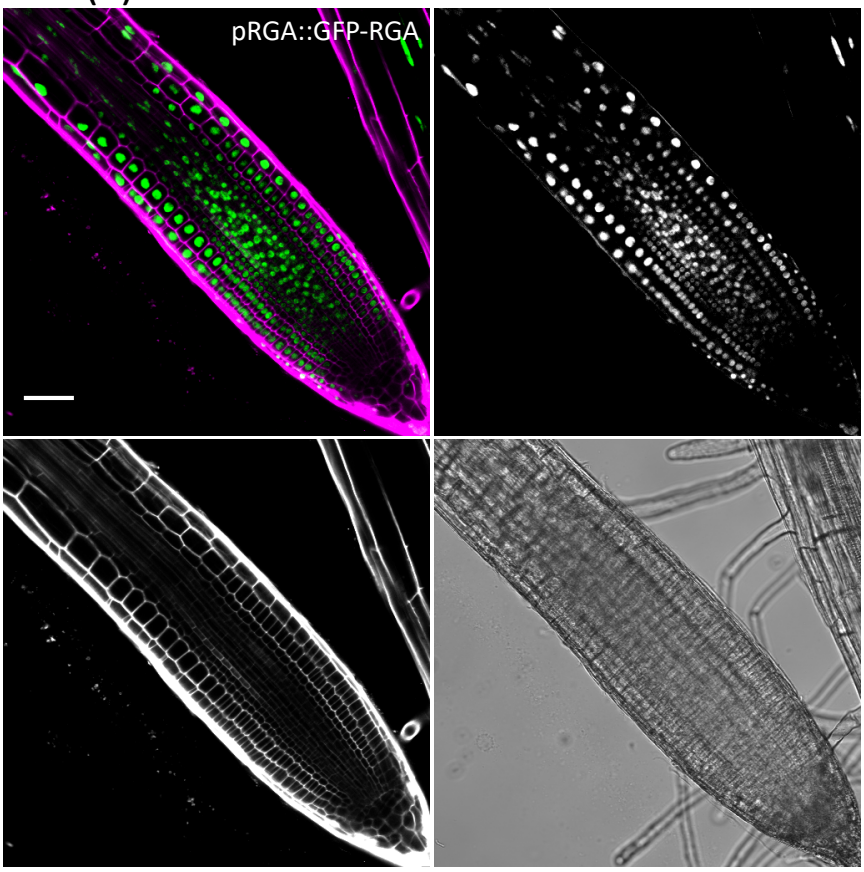

PAC (ii) - Ler

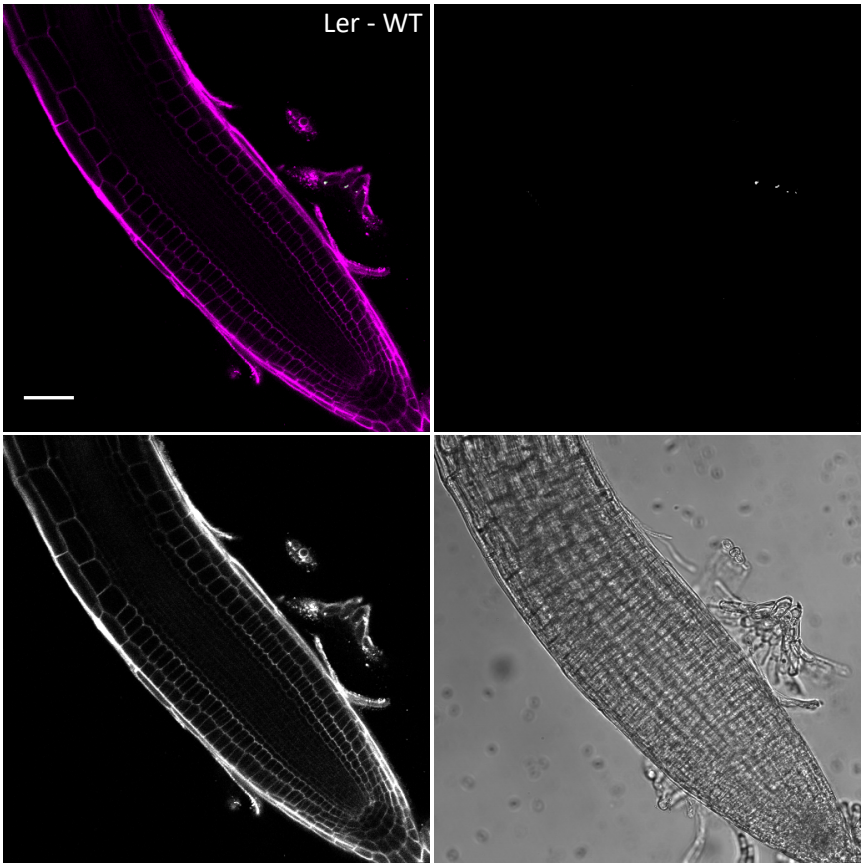

Mock (iii)

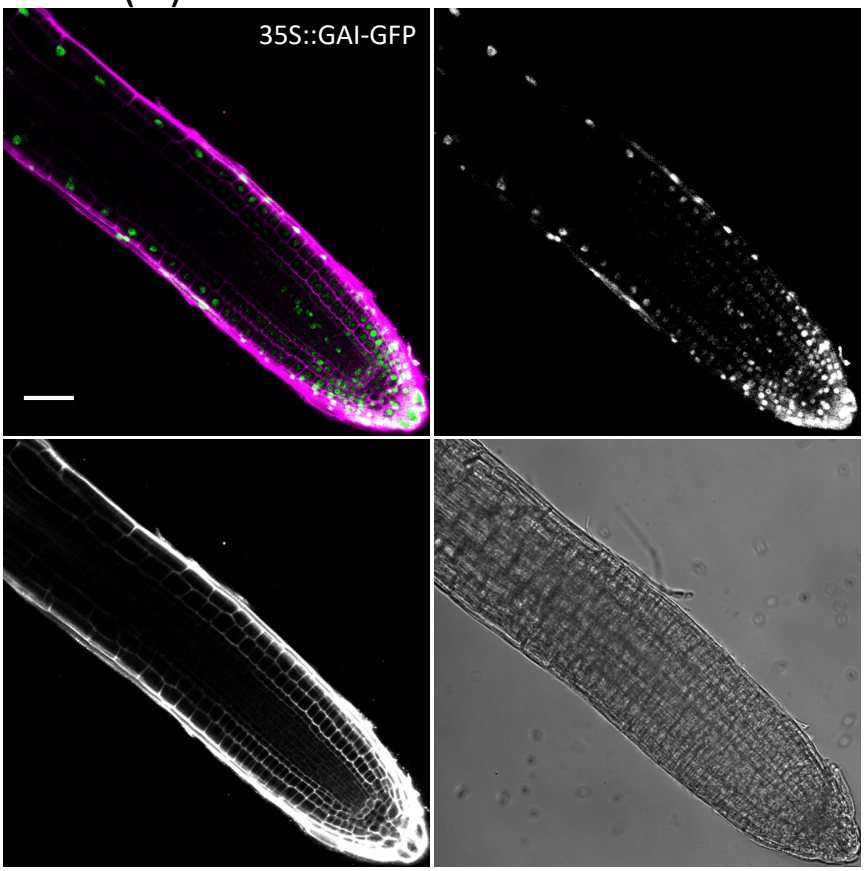

PAC (iii)

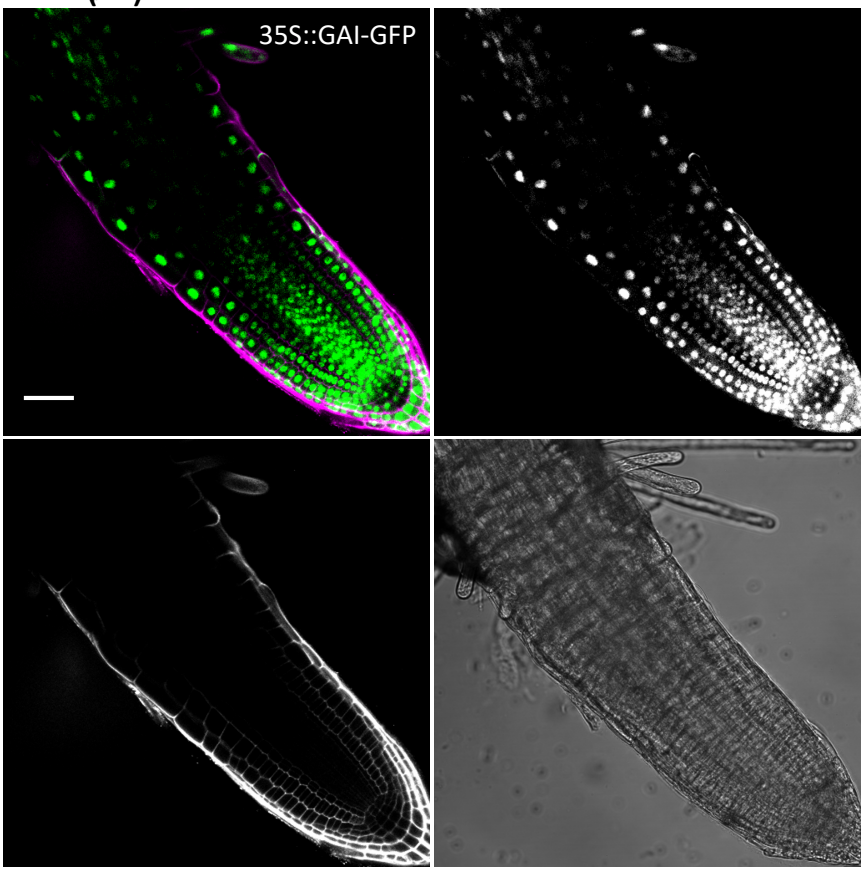

Mock (iv)

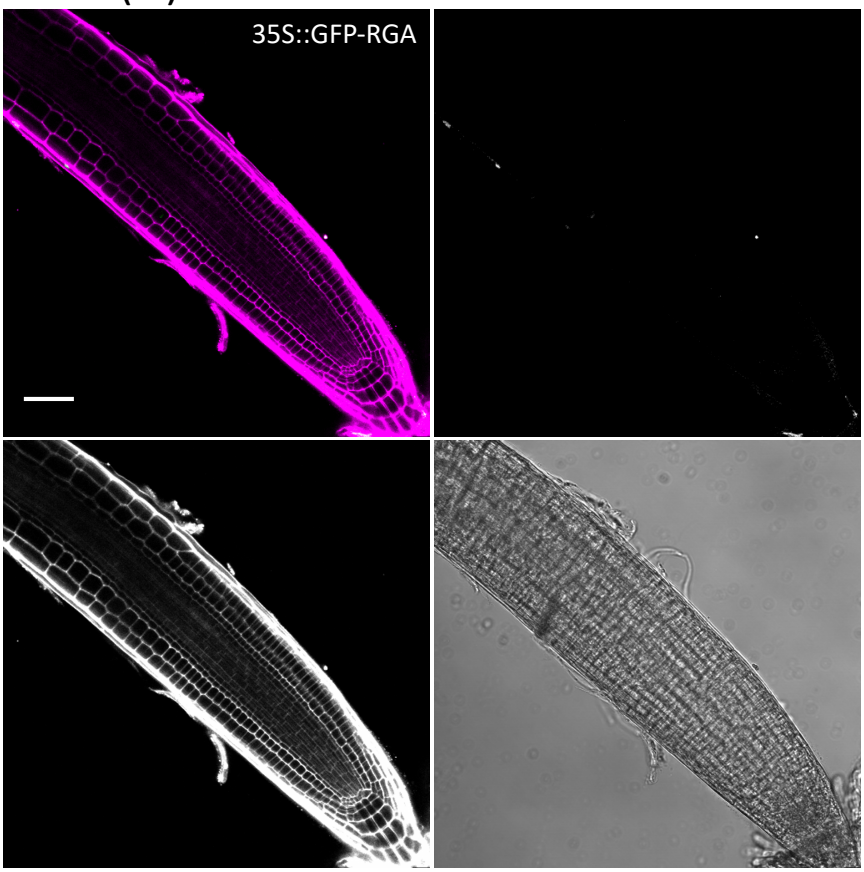

PAC (iv)

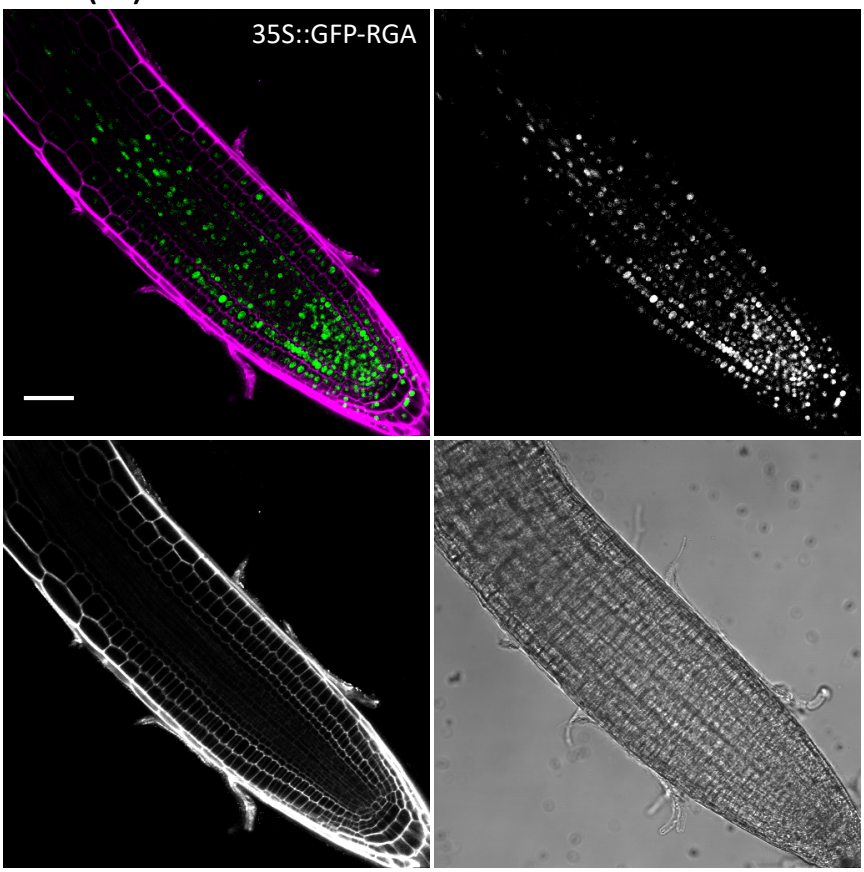

the proximal meristem, at the root tip and in elongating cells (Figure 3.5iii). The root phenotype of this line also appeared to differ from that of 35S::GFP-RGA. For example, the root meristem size was smaller in 35S::GAI-GFP seedlings when compared to 35S::GFP-RGA seedlings that had a similar phenotype to WT. The observation made before that GAI-GFP intensity was higher in smaller cells of the root meristem was not seen for this line. Since both 35S::GAI-GFP and 35S::GFP-RGA seedlings demonstrated low GFP expression in the root meristem, GA treatment experiments were not carried out in this case. Besides, GA treatment experiments of pGAI::GAI-GFP and pRGA::GFP-RGA seedlings had already shown a reduction in GFP levels, which demonstrates that both GAI-GFP and GFP-RGA do respond to increased levels of GA. However, the PAC treatment experiment was conducted on these overexpresser lines to determine whether the lack of GFP expression in the root meristem was a result of targeted protein degradation by the GA pathway. Therefore, 35S::GAI-GFP and 35S::GFP-RGA seedlings were grown for 5 DAS and then transferred to GM root supplemented with 10µM PAC or no PAC as a control for at least 18 hours. Roots were imaged with confocal microscopy after the duration of the treatment at 6 DAS. For the 35S::GAI-GFP line, PAC treatment resulted in an increase of GAI-GFP expression in all tissue layers of the root meristem, particularly at the basal end of the root tip (Figure 3.5iii). Overall, GFP intensity appeared to be more concentrated and highest in this region, which was consistent for all 35S::GAI-GFP seedlings observed in this experiment (n=9). PAC treatment also affected the overall size of these roots by increasing the thickness at the root tip and even more so in the elongation zone. For the 35S::GFP-RGA line, PAC treatment was also effective at increasing GFP-RGA levels (Figure 3.5iv), which was consistently expressed throughout all tissue layers of the root meristem for all the seedlings observed (n=13). Unlike 35S::GAI-GFP seedlings, there did not appear to be a concentration gradient of GFP-RGA expression as the intensity remained constant throughout the root meristem (Figure 3.5iv). PAC treatment also increased the thickness of the root, but the effect was less severe in the elongation zone when compared to that of the 35S::GAI-GFP seedlings treated under the same conditions.

3.2.5 GAI-GFP accumulates during the G_1 transition of the cell cycle

The observation from my time-course experiment that GAI-GFP intensity tended to be brighter in smaller cells was unreported until now. As described previously, this finding is indicative that GAI-GFP levels are higher after the process of cell division. However, this has not been experimentally confirmed. One way to demonstrate this is to cross the pGAI::GAI-GFP line to a cell cycle reporter that is able to indicate when cells have entered the G_1 phase of the cell cycle. Confocal microscopy can then be used to image these crosses at the F1 stage to determine whether or not GAI-GFP intensity is brighter in the G_1 phase. For this purpose, I obtained an S-G_2-M cell cycle reporter line that is functional in *Arabidposis* roots (unpublished, developed by Angarahad Jones at Cardiff University). This line

contains a region of the AtCyclinB1;1 gene that codes for a Destruction Box (DB), tagged with 3 copies of mCherry and driven by a ribosomal promoter to allow high production in dividing cells (pRPS5a::DB-mCherry(3x)). After obtaining crosses between these lines, I grew the F1 seeds on plates until 4 DAS. Confocal microscopy was then used to obtain images of both GFP and mCherry accumulation in the RAM. Cells undergoing the G_1 phase of the cell cycle were indicated by the absence of mCherry signal, whilst cells in the S-G_2-M phase were indicated by the presence of mCherry. Consistent across all the images captured of the RAM for these crosses, GFP intensity tended to be highest where mCherry signal was lowest or undetectable. To complement this observation, low or no GFP signal was generally observed in cells that had a high level of mCherry intensity (Figure 3.6a). To quantify this, GFP and mCherry intensity of the nucleus and the cell as a whole was measured for individual cells (n=33) across different images (n=4) and normalised to compare between them (Figure 3.6b). Overall, these results support the hypothesis that GAI-GFP accumulates in cells that are in the G_1 transition of the cell cycle.

Figure 3.6: Accumulation of GAI-GFP in the root meristem in the presence of a cell cycle reporter

(A) Representative confocal image of GAI-GFP and mCherry intensity in the RAM of F1 crosses between pGAI::GAI-GFP and a S-G_2-M cell cycle reporter. Seedlings were grown for 4 DAS before being visualised. GFP was excited with a 488 laser and mCherry was excited with a 543 laser. The combined channel image for GFP (green) and mCherry (magenta) is shown (top left). The single channel image for GFP (top right) and mCherry (bottom left) are portrayed in grayscale, alongside the transmitted light image (bottom right).

(B) Normalised GFP intensity for the nucleus and mCherry intensity for the whole cell, measured for 33 individual cells from four different images.

A

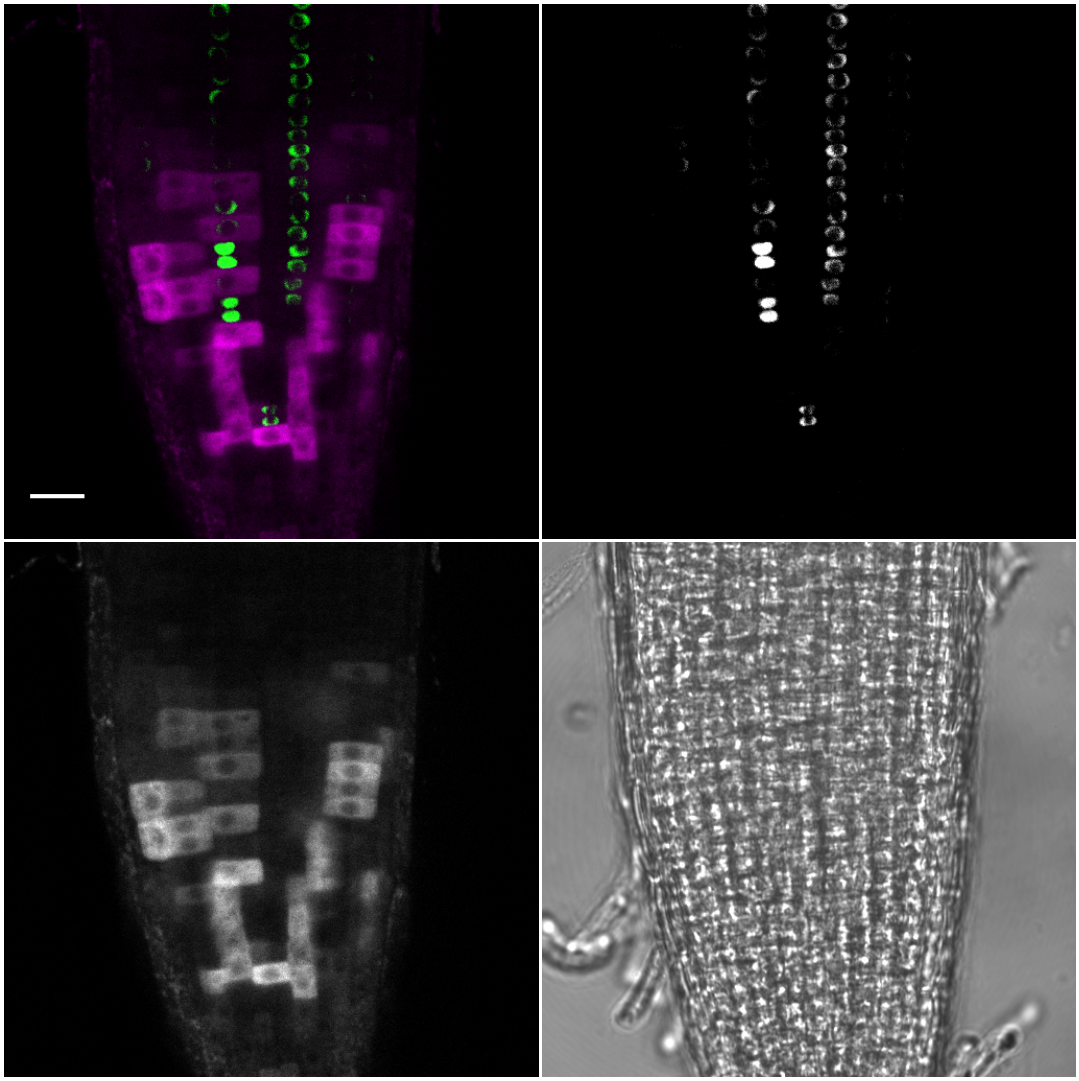

B

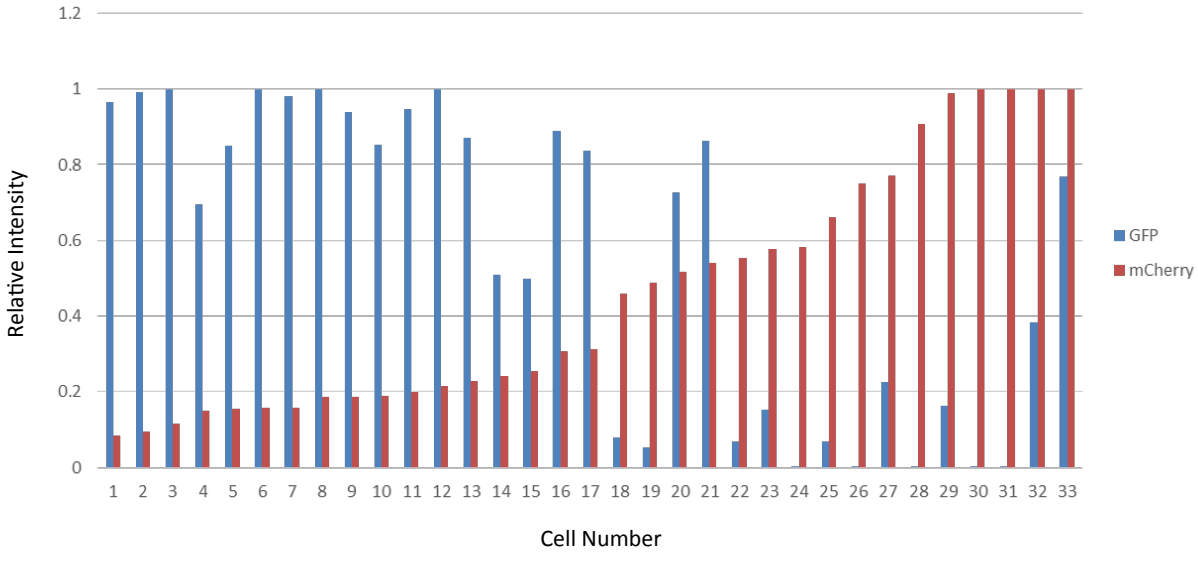
1.2
1
0.8
0.6
0.4
0.2
0
Relative Intensity
1 2 3 4 5 6 7 8 9 10 11 12 13 14 15 16 17 18 19 20 21 22 23 24 25 26 27 28 29 30 31 32 33
Cell Number
GFP
mCherry

3.3 Discussion

The accumulation and localisation of RGA, GAI and RBR in Arabidopsis was investigated using translational reporter lines containing GFP-tagged versions of these proteins and monitoring their expression levels in the root overtime. Furthermore, integration of transcriptomic data into a visual format to demonstrate root-specific expression of *RGA*, *GAI* and *RBR* was performed in order to compare with the observed proteomic patterns. Indeed, it can be the case that proteomic and transcript levels vary for each individual gene, but it is still interesting to compare between them to further our understanding of how a gene is expressed at the post -transcriptional and accumulates at the -translational level. It should also be noted that being able to express a GFP-tagged protein in a target organism does not necessarily confirm its functionality. It is therefore important to test the functionality of the translational reporter lines before using them in future experiments, especially if protein interactions are to be investigated. Immunoblot analysis of pGAI::GAI-GFP, pRGA::GFP-RGA and pRBR::gRBR-GFP demonstrated that the full-length fusion proteins GAI-GFP, RGA-GFP and RBR-GFP could be detected. These proteins had previously been reported to be functional by the authors who generated them for their analysis (Silverstone *et al.*, 2001; Fleck and Nicholas P Harberd, 2002; Magyar *et al.*, 2012).

Accumulation of RGA, GAI and RBR had previously been shown to be nuclear localised for all three proteins (Silverstone *et al.*, 2001; Fleck and Nicholas P Harberd, 2002; Magyar *et al.*, 2012). My analysis confirmed that GAI-GFP, GFP-RGA and RBR-GFP are co-localised to the nucleoplasm of the nucleus and co-accumulate in some tissue layers of the root, particularly the cortical cell layer. However, there are some key differences in their expression and accumulation patterns at the transcriptional and protein level, respectively. For example, whilst *RGA* is expressed consistently throughout the proximal meristem and continues into the elongation zone, *RBR* and *GAI* demonstrate a concentration gradient of expression where their levels are highest at the root tip. This observation in relation to RBR is consistent with those described in the paper by Magyar *et al.*, 2012. In this study, the authors found that RBR-GFP accumulation was mainly localised to cells undergoing mitosis, and to a lesser extent, cells undergoing differentiation and endoreduplication (Magyar *et al.*, 2012). They also describe a phenotype for the pRBR::RBR-GFP line as having a smaller sized meristem in comparison to WT plants, which is likely to be the result of increased RBR levels decreasing mitotic activity in the proximal meristem. This further supports the idea that RBR-GFP is functional in *Arabidopsis* plants. RBR has also been shown to be involved in regulating asymmetric cell divisions in the stem cell niche of the root meristem (Cruz-Ramírez *et al.*, 2012), so it is consistent that expression levels within this region is high and this is what was found from my analysis at both the protein and transcriptional level.

In the case of *GAI*, and similar to *RGA*, expression was predominantly localised to the cortical cell layer of the root meristem and the tissue with the lowest expression levels tended to be the endodermis. This is an interesting finding because a more recent study investigating cell proliferation in the *Arabidopsis* root, found that GA-signalling in endodermal cells controls root meristem size (Ubeda-Tomás *et al.*, 2009). In support of this, a more recent study examined the accumulation of fluorescein (Fl)-labelled GA_3 and found that it is mainly localised to the endodermal layer of elongating cells (Shani et al., 2013). Therefore, the low expression levels of GAI-GFP and GFP-RGA observed in the endodermis could be the result of GA-targeted inhibition, even though GA expression is mainly localised to elongating cells. Although findings from the time-course experiment found that the primary region of GAI-GFP expression was in cortical cells, the eFP browser indicated that there were also other tissues within the central stele that had high levels of GAI expression, such as cells within the central stele/vasculature. As mentioned previously, the functionality of the GAI-GFP protein had been previously reported because overexpression of this protein resulted in a dwarf and floral phenotype (Fleck and Nicholas P. Harberd, 2002). Interestingly, overexpression of RGA-GFP did not confer this type of phenotype and grows very similar to that of a wild type (WT) plants (Silverstone et al., 2001), suggesting that GAI and RGA may have different functions.

The observation and experimental confirmation that GAI-GFP accumulates in dividing cells of the RAM supports the hypothesis of a putative binding between GAI and RBR. This is because RBR is responsible for regulating the transition between G_1 and S phase of the cell cycle and therefore is being produced at the same time as GAI. The fact that this observation was not made in the case of GFP-RGA supports the idea that GAI and RGA are functionally different in the context of the cell cycle. Furthermore, from my GA treatment experiments of pGAI::GAI-GFP seedlings, it was found that although overall GAI-GFP levels were reduced throughout the root meristem, the accumulation of this protein between adjacent cells of the proximal meristem was not affected. If an interaction between RBR and GAI exists, then this observation would imply that RBR is stabilising the levels of GAI whilst bound to it and thus preventing its targeted degradation in the presence of bioactive GA. To investigate this further, the putative interaction should be tested both *in vitro* and *in vivo*. To test this *in vivo* crosses between pGAI::GAI-GFP and RBR::RBR-RFP can be made and FRET analysis performed on the regions of the root meristem where the interaction is likely to take place i.e. in cells that have high GAI-GFP intensity and supposedly just after cell division. There is currently little evidence to describe the molecular mechanisms of how GA relates to cell division control. However, previous studies have demonstrated that GA is able to control cell proliferation in *Arabidopsis* in a DELLA-dependent manner (Achard et al. 2009, Ubeda-Tomás et al. 2009). For example, Achard et al. (2009) demonstrated that expressing a non-degradible form of *gai* in endodermal cells of the root mersitem was sufficient to disrupt cell

proliferation and reduce mersitem size. Being able to prove an interaction between RBR and GAI would provide us with a better insight into the mechanisms behind such processes.

Another observation made for the expression of GAI-GFP, was that GFP levels were low in seedlings that had just germinated (2 DAS) and then increased to more constant levels thereafter, which occurred within a 24 hour period between 2-3 DAS. Consistent with this observation, GAI-GFP intensity was lower in lateral root primordia in roots of pGAI::GAI-GFP seedlings, when compared to more mature lateral roots. This may be indicative of a critical time-point where the expression of GAI is lower in younger primary roots and lateral root primordia i.e. just after germination and at the beginning of lateral root formation, respectively. It had previously been demonstrated that transcript levels for GAI were highest in 12-h and 24-h-imbibed seeds, prior to germination and then decrease from 2-5 days after germination (Tyler *et al.*, 2004). Perhaps it is the case that GAI-GFP is expressed at higher levels before germination and then decrease, before a subsequent increase to more consistent levels thereafter. However, it should be noted that the practicality of obtaining images of seedlings at 2 DAS was difficult to acquire a substantial sample size to confirm this. In contrast to these findings for GAI-GFP, there was no time-dependent expression pattern observed in pRGA::GFP-RGA and pRBR::RBR-GFP seedlings i.e. both GFP-RGA and RBR-GFP expression levels remained consistent throughout all days of the time-course and only varied in specific regions of the root as described previously.

When examining lines that ectopically express GAI-GFP and GFP-RGA in *Arabidopsis* roots, GFP intensity in the root meristem was very low, particularly in the case of 35S::GFP-RGA. Previous experiments that report on the treatment of 35S::GFP-RGA with GA showed images of the root tip where GFP-RGA signal can clearly be visualised (Silverstone et al. 2001). However, they only show images of the outer layer of the root i.e. at the surface and not the middle of the root where my images were captured. It may be the case that GFP-RGA is expressed in the root, but only on the outer surface as I was unable to detect GFP-RGA in the root mersitem for this line. My observation implies that there GFP-RGA accumulation in the root meristem may be tightly controlled despite it is being overexpressed. For the overexpression of GAI-GFP, a simliar observation was made, but not as severe as in the cae of GFP-RGA. In fact, there was still some GFP intensity detected in the root meristem, particularly at the basal end. This supports the idea that GAI and RGA function varies in the root apical meristem. Treatment of 35S::GAI-GFP and 35S::GFP-RGA lines with PAC resulted in accumulation of both GAI-GFP and GFP-RGA protein levels in most cells within the root tip. This was particularly notable for GAI-GFP, resulting in a pattern expected for a gene expressed under 35S promoter control. This confirms the tight protein level regulation in the meristematic region and suggests that GA is

controlling the accumulation of these proteins, leading to targeted degradation as a mechanism to counteract the fact that they are being overexpressed.

In relation to my treatment experiments with GA and PAC, the results generally support the theory that RGA and GAI are under the control of GA because they respond to the treatments as the model for GA signalling predicts. For the expression of GAI-GFP, previous experiments had reported conflicting results in relation to treatment with GA (Fleck and Harberd 2002, Dill et al. 2004, Tyler et al., 2004). My experiments demonstrated that GA treatment clearly decreased overall GAI-GFP intensity as expected, apart from in a specific subset of cells in the proximal meristem as described previously. Perhaps this is why different papers reported on GA having different effects on the expression of this fusion protein. In relation to RGA-GFP, GA treatment decreased GFP intensity in all cells of the proximal meristem as expected. Previous studies had reported on this, as well as the treatment of endogenous RGA with GA and showed that RGA protein levels were also downregulated in response to GA treatment (Silverstone et al. 2001). PAC treatment of both lines increased GAI-GFP and GFP-RGA levels as expected, but for GAI-GFP the expression was concentrated to the root tip, whilst GFP-RGA expression was throughout the whole of the root meristem, which further supports the theory that GAI and RGA may have different functions in this region.

To conclude, it has been demonstrated that GAI, RGA and RBR are co-localised to nucleus of cells within the root meristem and there is a period of time where these proteins are all co-expressed, but there is differential expression between them depending on tissue-type and the regions that comprise the meristem. The fact that *GAI* and *RBR* have more similar expression patterns at the protein and transcriptional level would suggest that they are more likely to form a putative interaction than RGA with RBR. Since *GAI* and *RBR* expression was particularly high in the cortical cell layer within the proximal meristem of the root where cell division takes place, it seems likely that the putative interaction may take place here. The observation of high levels of GAI-GFP in pairs of smaller cells that are in G_1 phase, having recently completed division is strongly suggestive of a cell cycle link.

Chapter 4

The effect of the putative GAI/RBR interaction on root growth

Chapter 4 – The effect of the putative GAI/RBR interaction on root growth

Introduction

One way to examine the role of a particular gene/protein is to generate genetically modified (GM) plant lines that mutate or knock-out a targeted allele that renders the gene to be un-functional and termed as a 'null' mutant. Kinematic analysis can then be performed on these lines by comparing their rates of elongation and division to WT controls in order to examine phenotypic differences and thus determine whether a particular mutation has an effect on the growth and architecture of the plant. Analysing root growth is a relatively easy way of assessing how a mutation of a particular gene (the genotype) affects the phenotype of the plant itself. Individual seedlings can be grown on plates containing growth media and scanned on a daily basis over time. Root growth can then be analysed by measuring individual roots for each day and assessing their growth rates during this time period. Upon germination, rapid root growth must occur so a seedling can acquire all the necessary nutrients from its surrounding environment and develop further. It is therefore an extremely important process for a plant to undergo and this is altered by endogenous, as well as exogenous factors. Since GA signalling is associated with promoting growth, mutated genes associated with this pathway can lead to different phenotypes thereby altering root growth rates and architecture. Confocal microscopy can also be used at the end of the experiment to understand how the root apical meristem (RAM) is affected by these particular mutations at the cellular level.

GA has been shown to be a regulator of root growth in *Arabidopsis* (Fu and Harberd 2003). Indeed, a GA biosynthetic mutant, *ga1-3*, has much shorter primary root growth when compared to WT (Fu and Harberd, 2003). As mentioned previously, the GA signalling pathway in elongating cells has been well defined (Chapter 1), but there is little evidence to suggest how GA regulates growth in actively dividing cells. GA has been shown to regulate root growth in elongating endodermal cells by signalling the destruction of the two main DELLA growth repressor proteins, GAI and RGA (Ubeda-Tomás *et al.*, 2009). Moreover, a paper by Fu and Harberd (2003) showed that introduction of an *rga* null mutation into the *ga1-3* mutant background, was sufficient to partially rescue the reduced growth phenotype of the *ga1-3* line alone. This was also the case for a *gai* mutant, but was less severe in its ability to rescue the reduced growth phenotype of the *ga1-3* mutant. Introducing both *gai* and *rga* null mutations was able to substantially supress the *ga1-3* phenotype, suggesting that GAI and RGA have overlapping roles in relation to inhibition of root growth (Fu and Harberd 2003). A more recent study by Achard *et al.* (2009), reported the effect of the *ga1-3* mutation on primary root growth and at the cellular level in the RAM. They found that primary root growth, root meristem size, cell number and

cell production rate was significantly reduced in this mutant line when compared to WT seedlings (Achard *et al.*, 2009). To develop our current understanding of how GAI and RGA inhibit root growth at the cellular level, methods from the both experiments by Fu and Harberd (2003) and Achard *et al.* (2009) were integrated and repeated. The mutant lines described in these papers were in the Ler ecotype. In order to repeat this in a different ecotype, crosses were performed using *gai* and *rga* null mutants in the *Col-0* ecotype. These mutant lines were crossed to a GA biosynthetic mutant, *ga1*, from the same ecotype to generate plants homozygous for both mutations. Here, I report on the analysis of primary root growth and the cellular phenotype in the RAM of the aforementioned crosses to investigate potential differences between RGA and GAI function, specifically in relation to cell division.

As mentioned previously in Chapter 1, there is reason to believe that a putative interaction between GAI and RBR exists in *Arabidopsis*. RBR regulates the G_1 – S transition of the cell cycle and is modulated by the kinase activity of CDK/Cyclin complexes by phosphorylation. Results from Chapter 3 implied that there were key differences between the overall expression and protein accumulation patterns of *GAI* and *RGA* in the root, with GAI-GFP protein accumulation occurring in a cell-cycle dependent manner with highest intensity levels at the beginning of G_1 phase. To further our understanding of how GAI and RGA are associated with the cell cycle, crosses between *gai* and *rga* null mutants to specific cell cycle reporter/overexpresser lines were made to determine whether they have an effect on their root growth phenotypes, such as root growth rates over time.

For this purpose the previously described RBR translational reporter line, pRBR::gRBR-GFP (Magyar *et al.*, 2012) in the Col-0 ecotype was used (described in Chapter 2). Furthermore, we possess various cell cycle overexpresser lines associated with the G_1 transition of the mitotic cell cycle that alters the phosphorylation of RBR by either increasing or reducing kinase activity. Ectopic expression is conferred since they have been transformed with a construct driven by the 35S CaMV promoter. The 35S::KRP2-GFP line is in the *Col-0* ecotype and overexpresses the *KIP-RELATED PROTEIN2* (*KRP2*) gene, which encodes a protein that inhibits the activity of CDK complexes during the cell cycle and therefore decreases RBR phosphorylation (De Veylder *et al.*, 2002; Inzé and De Veylder, 2006). These plants have a distinctive phenotype of severely impaired growth, a reduction in the rate of cell division and cell elongation, small serrated leaves and in some cases, infertility. Once these crosses had been established, primary root growth was assessed and compared to relevant controls in order to determine whether removal of GAI or RGA function affected the growth rate of this line. Furthermore, endogenous GA levels were altered by the addition of exogenous PAC and GA and to assess how root growth rates of these mutants were affected.

4.1 Results

4.1.1 GAI and RGA are functionally redundant in the presence of GA

To investigate how root growth is affected by GAI and RGA, the null mutant lines, *gai-td1* and *rga-28* in the Col-0 ecotype (see Chapter 2 for details) were used. These lines had been previously been published as loss-of-function mutants by T-DNA insertion (Tyler et al 2004). Firstly, root growth of these single null mutants was assessed to see whether removal of GAI or RGA function alone was sufficient to produce a difference in root growth phenotypes. Previous studies had reported that single null mutants for *gai* and *rga* had no obvious phenotypic effects and closely resembled that of WT plants, suggesting that GAI and RGA are functionally redundant (Peng *et al.*, 1997; Dill and Sun, 2001; Tyler *et al.*, 2004). To investigate this further, a preliminary experiment was performed to assess root growth from 3-8 DAS consecutively, for the single null mutants, *gai-td1* and *rga-28*, alongside WT (Col-0). For each mutant line, a total of 30 seedlings were grown alongside WT seedlings, distributed across 6 plates (i.e. 5 mutant seedlings grown against 5 WT per plate).

Overall, primary root growth from 3-8 DAS for all lines was found to be linear (Figure4.1A). At 3 DAS, there did not appear to be any substantial difference in root length when comparing between genotypes, with mean values of WT = 4.64 mm (SE = 0.130), *gai-td1* = 4.46 mm (SE = 0.224) and *rga-28* = 4.52 mm (SE = 0.212). This was also the case at the end of the experiment at 8 DAS (Figure 4.1A), with mean root lengths of 35.1 mm for WT (SE = 0.540), 34.3 mm for *gai-td1* (SE = 0.901) and 34.5 mm *rga-28* (SE = 0.874). Furthermore, the median vales for root length appeared to be similar between these genotypes (Figure 4.1C). The fact that there was little variation between these values suggests that there was no difference in the growth rates of WT, *gai-td1* and *rga-28* seedlings for the duration of the experiment. Indeed, when comparing the mean root lengths for each genotype over time, the slopes of the fitted lines did not appear to vary between them (Figure 4.1A).

To test these findings statistically, the data was incorporated into an appropriate statistical model and accounting for the fact that repeated measurements of individual seedlings were recorded over time. In contrast to a more traditional approach of using a repeated measures ANOVA for these types of datasets, a generalised linear mixed effects model (GLMM) was used to analyse this data. This type of mixed effects model was used because it provides a better fit for the data, especially when it is not normally distributed. Furthermore, they allow random terms to be incorporated into the model to account for their variability. Therefore, the variability in root growth across different plates i.e. plate variability, could be controlled for by factoring it into the model as a random term. For this model, the association between genotype and root length over time was assessed with a Gamma family and identity link, which included the main effects of day and genotype, their interaction and a random

Figure 4.1 Analysis of root growth for WT, *gai-td1* and *rga-28* seedlings from 3-8 days after stratification (DAS) represented by:

(A) Average root length for each genotype plotted over time fitted with a linear trendline

(B) The predicted lines for root length over time per genotype as determined by the statistical model used to analyse the data and plotted over the raw data values

(C) Boxplots for each genotype over time, with the final day enlarged for better visualisation of the distribution of root lengths. The boxplots show the median value as represented by the dividing line, as well as the lower and upper interquartile ranges, with whiskers extending 1.5 times the interquartile range.

A

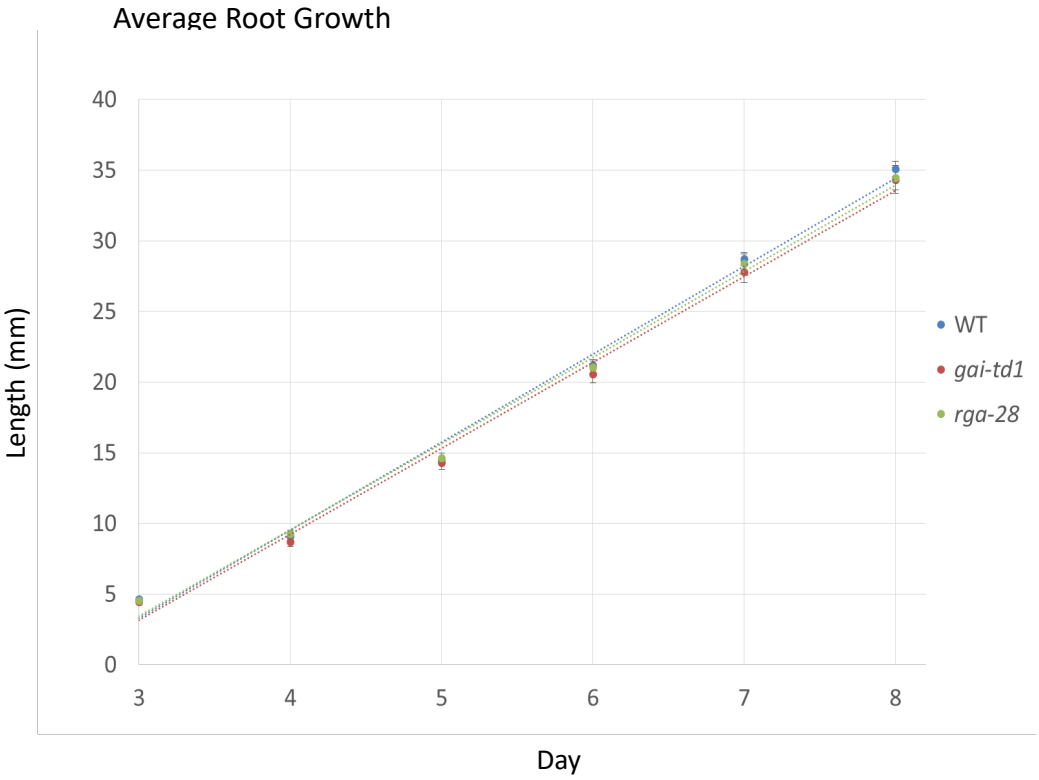
Average Root Growth
Length (mm)
40
35
30
25
20
15
10
5
0
3
4
5
6
7
8
Day
WT
gai-td1
rga-28

B

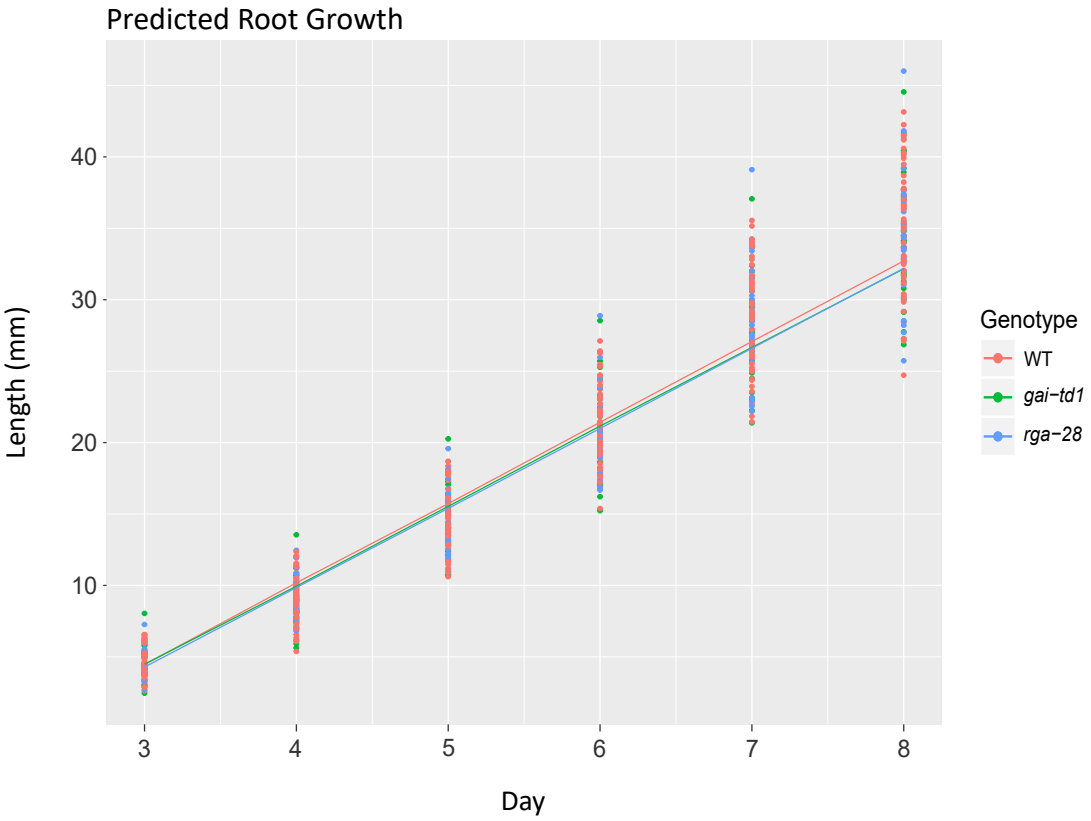
Predicted Root Growth
Length (mm)
40
30
20
10
3
4
5
6
7
8
Day
Genotype
WT
gai−td1
rga−28

C

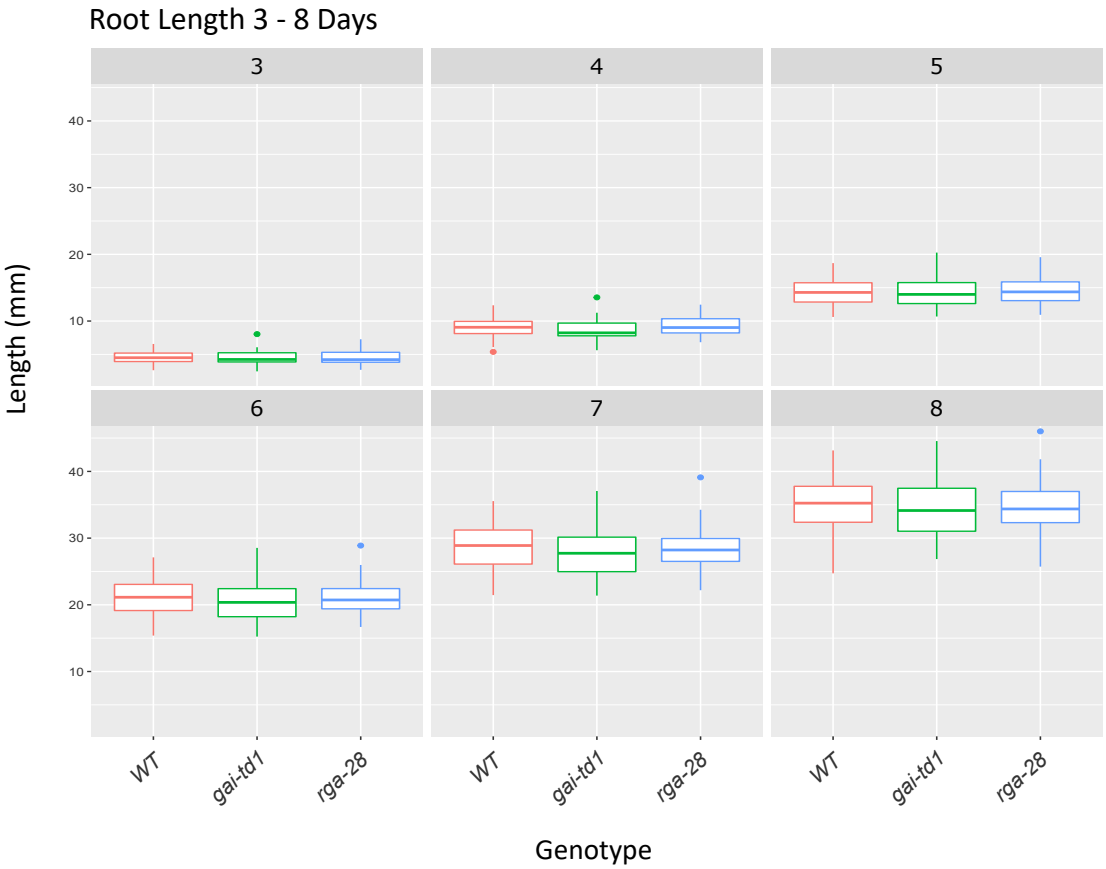
Root Length 3 - 8 Days
3
4
5
6
7
8
Length (mm)
40
30
20
10
WT
gai-td1
rga-28
Genotype

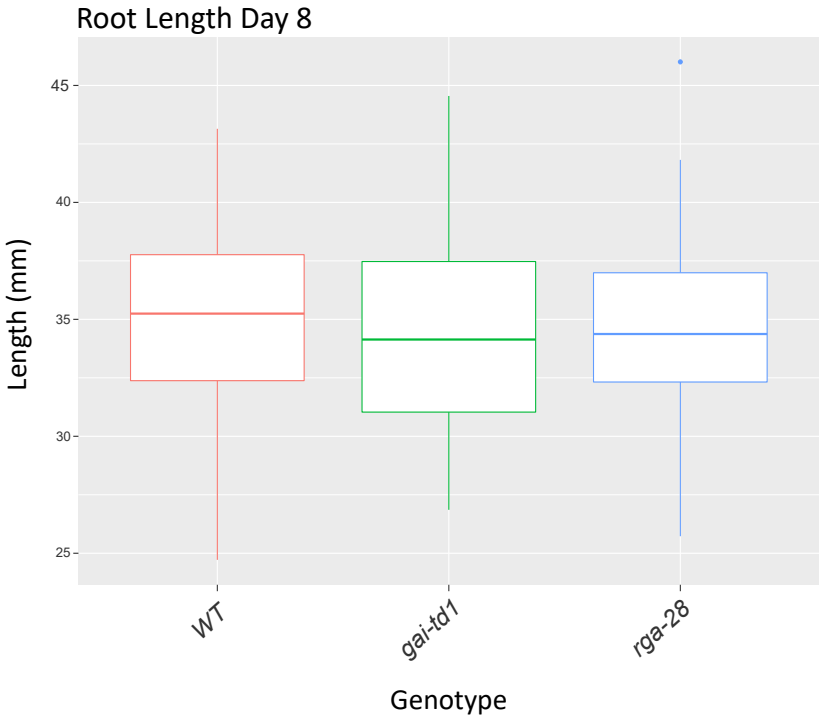
Root Length Day 8
Length (mm)
45
40
35
30
25
WT
gai-td1
rga-28
Genotype

effect of plate variability (Appendix 4.1A). The model output demonstrated that root length was significantly different between days for each genotype, but there was little variation in the predicted root growth rates between these genotypes (Table 4.1). This was evident from plotting the fitted lines of the model for root length over time, which showed little variation in the slopes of WT, *gai-td1* and *rga-28* (Figure 4.1B). Indeed, there was no significant difference in the daily root growth rate of WT seedlings when compared to *gai-td1* (t_2= -0.66, p=0.507) and *rga-28* (t_2= -0.39, p=0.696). Furthermore, there was no significant difference between the daily root growth rate of *gai-td1* seedlings when compared to *rga-28* (t_2= 0.22, p=0.825). These results therefore support previously reported evidence that GAI and RGA are functionally redundant in the presence of endogenous GA, because the single null mutants closely resemble that of WT in relation to their root growth phenotypes.

Genotype	Root growth rate (mm/day)	Standard Error	t-value	p-value
WT	5.65	0.106	53.21	<0.001
gai-td1	5.56	0.133	41.75	<0.001
rga-28	5.60	0.135	41.44	<0.001

Table 4.1: Daily root growth rates for each genotype as predicted by the statistical model (GLMM). For each calculation, there was always one degree of freedom. Levels of significance are represented by: * p<0.05, ** P<0.01 and *** p<0.001. The p-value refers to the difference in growth rate between days.

To investigate these findings further an additional control, the GA deficient mutant line, *ga1-t*, was introduced into these experiments. GA-deficient mutants of *Arabidopsis thaliana* stabilise DELLAs and thus demonstrate defects in growth processes associated with its function. For example, *ga1-3* biosynthetic mutants are severely dwarfed, dark green in colour, male-sterile, unable to germinate and all of these defects can be rescued by exogenous application of GA (Koornneef and van der Veen, 1980). The *ga1-t* line contains the same mutant allele as the *ga1-3* line, but was generated in the Col-0 ecotype instead of Ler. Since GA regulates germination, this meant that all lines had to be pre-treated with exogenous GA to allow the *ga1-t* mutant to germinate and to ensure that the same conditions were applied to all. This was done by germinating seeds on root media supplemented with 10 µM GA_3 and then transferring seedlings 1 DAS to control root media for the rest of the experiment. Root growth was then measured from 4-8 DAS. Unfortunately, measurements for 6 DAS were not obtained during this particular experiment, but it was still possible to assess relative growth rates for these lines by plotting the data and with an appropriate statistical model.

Figure 4.2 Analysis of root growth for *Col-0* WT, *ga1-t*, *gai-td1* and *rga-28* seedlings from 4-8 days after stratification (DAS) represented by:

(A) Average root length for each genotype plotted over time fitted with a linear trendline

(B) The predicted lines for root length over time per genotype as determined by the statistical model used to analyse the data and plotted over the raw data values

(C) Boxplots for each genotype over time, with the final day enlarged for better visualisation of the distribution of root lengths. The boxplots show the median value as represented by the dividing line, as well as the lower and upper interquartile ranges, with whiskers extending 1.5 times the interquartile range.

A

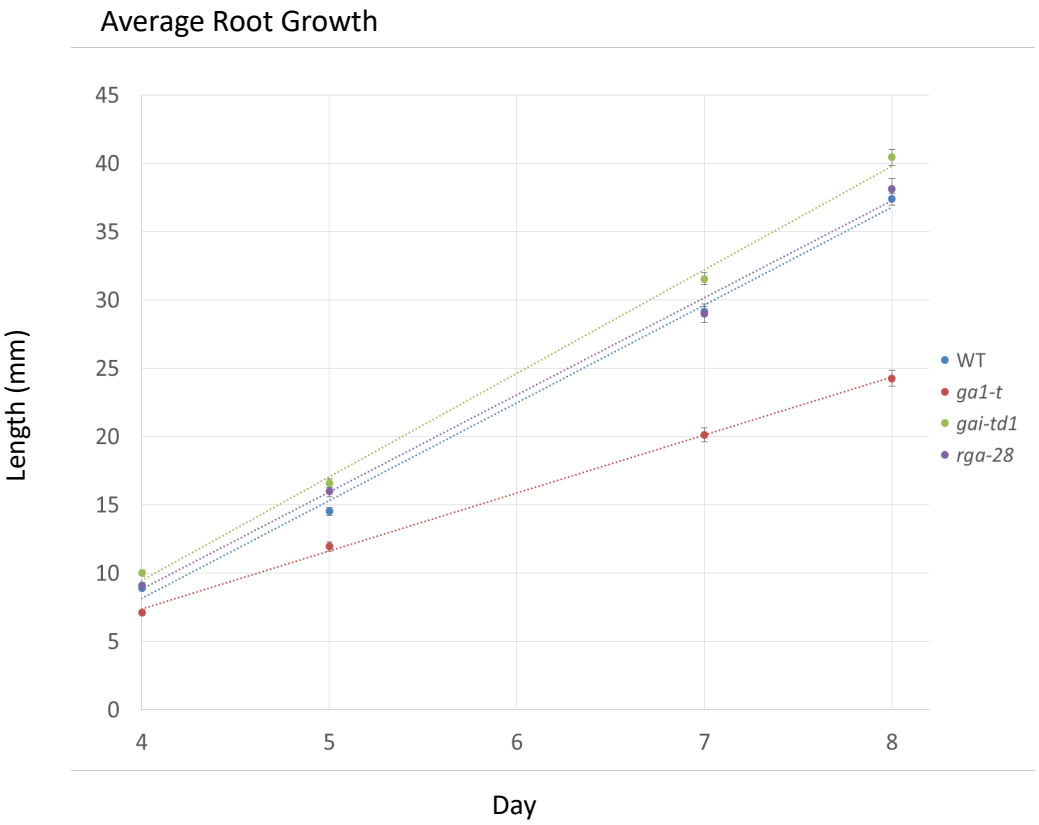
Average Root Growth
Length (mm)
45
40
35
30
25
20
15
10
5
0
4
5
6
7
8
Day
WT
ga1-t
gai-td1
rga-28

B

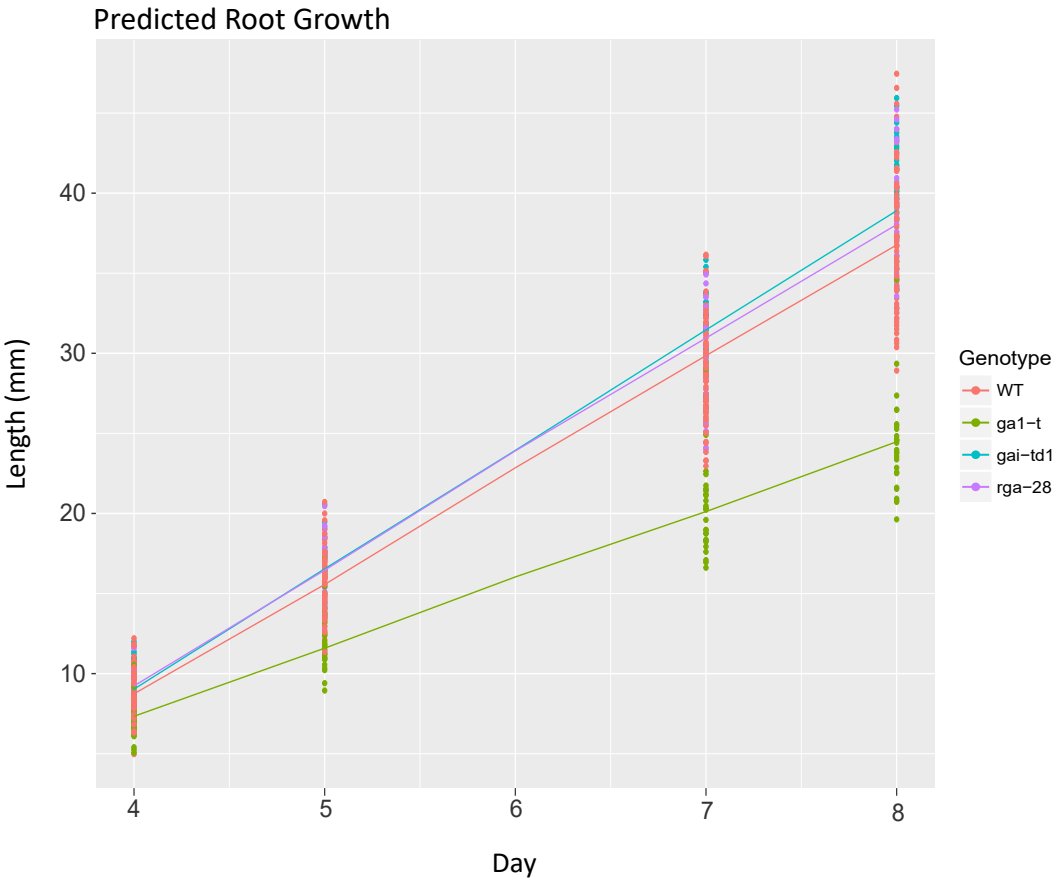
Predicted Root Growth
Length (mm)
40
30
20
10
4
5
6
7
8
Day
Genotype
WT
ga1−t
gai−td1
rga−28

C

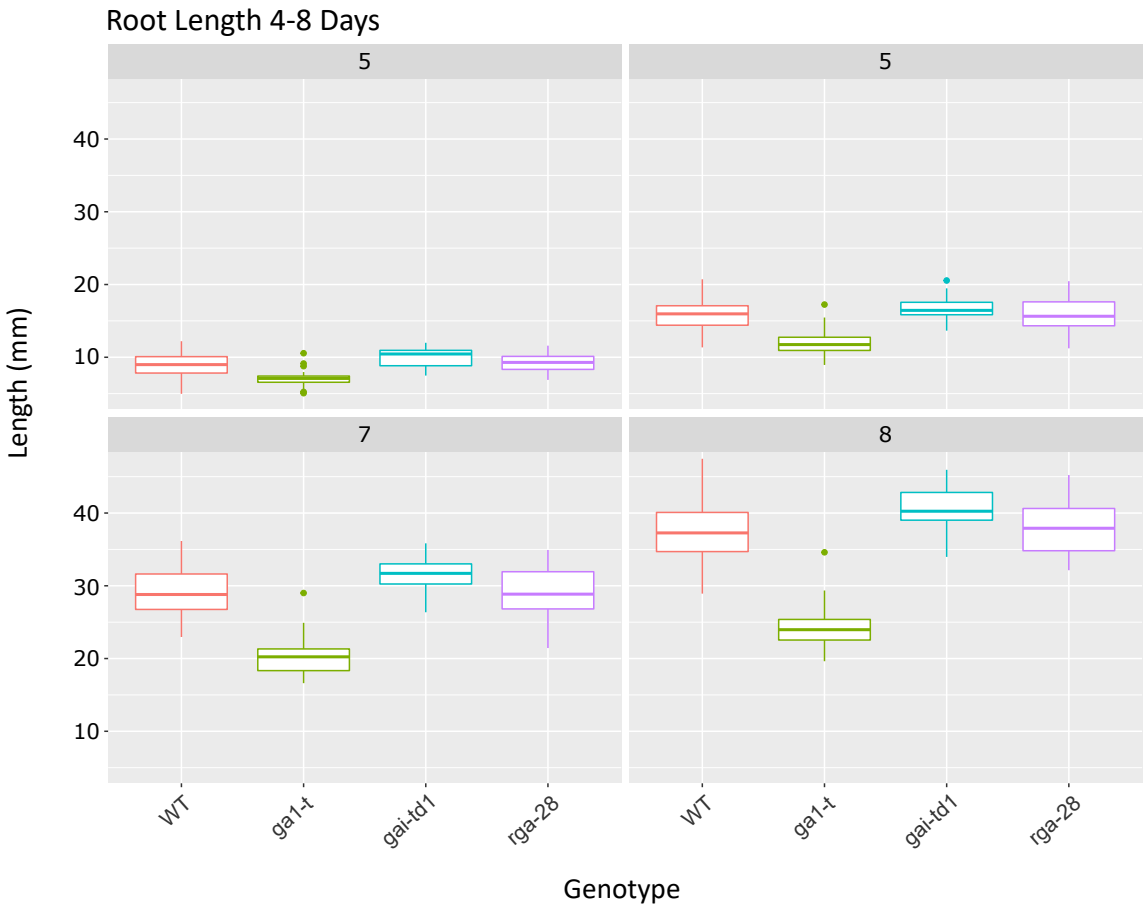
Root Length 4-8 Days
5
5
7
8
40
30
20
10
Length (mm)
WT
ga1-t
gai-td1
rga-28
Genotype

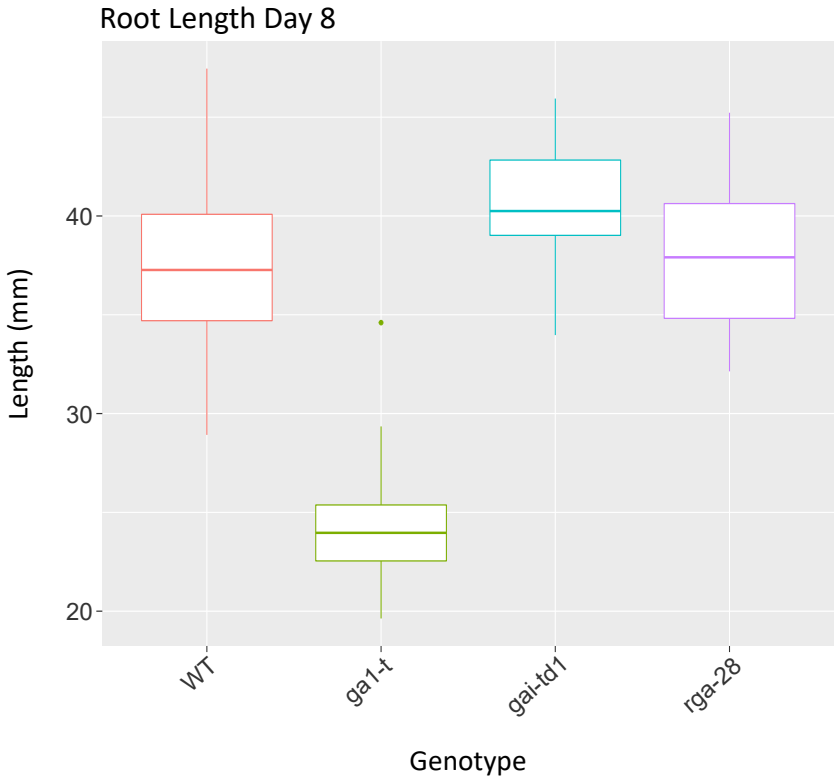
Root Length Day 8
40
30
20
Length (mm)
WT
ga1-t
gai-td1
rga-28
Genotype

Overall, primary root growth from 4-8 DAS across all lines was found to be linear (Figure 4.2A). At 4 DAS, there appeared to be a difference in root length between genotypes (Figure 4.2A,B), with mean values of: WT = 8.93 mm (SE = 0.167), *ga1-t* = 7.11 mm (0.222), *gai-td1* = 10.02 mm (SE = 0.232) and *rga-28* = 9.10 mm (0.237). By the end of the experiment at 8 DAS, there also appeared to be a difference between the mean root lengths for these genotypes with WT = 37.40 mm (SE = 0.450), *ga1-t* = 24.27 mm (SE = 0.583), *gai-td1* = 40.47 mm (SE = 0.583) and *rga-28* = 38.15 mm (SE = 0.759). When plotting the average values for each genotype over time, the slope of the fitted lines for WT and *rga-28* did not appear to vary substantially, suggesting there was little variation between overall growth rates of these seedlings (Figure 4.2A). The fitted line for *gai-td1* had a slightly higher slope than that of WT and *rga-28*, which remained consistent between days. The initial root growth experiment showed no difference between these genotypes, so the increased slope for *gai-td1* could be the result of them germinating slightly earlier than the other lines, especially since they already had a higher average root length when comparing between genotypes at 4 DAS. For *ga1-t*, the slope of the fitted line for average root growth appeared to be substantially lower than that of WT, *rga-28* and *gai-td1*, suggesting the growth rates of these seedlings were reduced.

To test this statistically, the association between genotype and root length over time was assessed using a GLMM model with a *Gamma* family and *identity* link, which included the main effects of day and genotype, their interaction and a random effect of plate variability (Appendix 4.1B). The model outcome demonstrated that root length over time was significantly different between days with WT seedlings having daily root growth rate of 6.9 mm per day (Table 4.2). When comparing the growth rate of WT to *gai-td1* seedlings, there was a slight decrease of 0.33 mm per day, but this was not significant (t_3= -1.73, p= 0.083). There was also no significant difference in root growth rates when comparing WT to *rga-28* (t_3= 0.75, p=0.454) seedlings. However, there was a significant difference between *ga1-t* seedlings when compared to WT with a reduction of 2.54 mm per day (t_3= -17.4, p<0.001). Furthermore, there was a significant difference between the root growth rate of *ga1-t* seedlings when compared to both *gai-td1* and *rga-28*, with a daily reduction of 2.87 mm (t_3= -14.1, p<0.001) and 2.67 (t_3= -13.4, p<0.001), respectively. There was no significant difference between the daily root growth rate of *gai-td1* seedlings when compared to *rga-28* (t_3=0.81, p=0.421), even though *gai-td1* seedlings grew at an increased rate of 0.19 mm per day. These results support findings from the previous root growth experiment that there is no phenotypic difference between WT, *gai-td1* and *rga-28* seedlings. However, the root growth rate of the *ga1-t* line was significantly reduced in comparison to the aforementioned lines, thus supporting previously reported evidence that GA is a regulator root growth (Fu and Harberd, 2003).

Genotype	Root growth rate (mm/day)	Standard Error	t-value	p-value
WT	6.92	0.105	65.75	<0.001
ga1-t	4.38	0.127	34.60	<0.001
gai-td1	7.25	0.174	41.63	<0.001
rga-28	7.06	0.170	41.52	<0.001

Table 4.2: Daily root growth rates for each genotype as predicted by the statistical model (GLMM). For each calculation, there was always one degree of freedom. Levels of significance are represented by: * p<0.05, ** P<0.01 and *** p<0.001. The p-value refers to the difference in growth rate between days.

4.1.2 Removal of GAI or RGA function confers different root phenotypes in a GA deficient mutant background

To investigate a potential difference between RGA and GAI in the developing root, the same approach as described by Fu and Harberd (2003) was used. Here, the authors used a mutant based approach using a GA-deficient mutant background (*ga1-3*) for GAI and RGA in order to modulate GA response. Hence, a double mutant loss-of-function approach was adopted in the Col-0 ecotype by crossing *ga1-t* to *gai-td1* and *rga-28* and selecting for homozygous lines (described in Chapter 2). By comparing the root growth rates between these lines with respect to that of *ga1-t* seedlings, differences between their ability to rescue this reduced growth phenotype could be determined. For this purpose, primary root growth, meristem size, cortical cell number and cell production rate was measured for *ga1-t rga-28* and *ga1-t gai-td1* seedlings grown alongside Col-0 wild-type (WT) and *ga1-t* seedlings treated under the same conditions (Figure 4.3). All lines were pre-treated on root growth media supplemented with 2.5 µM of GA_3 to allow germination. The amount of GA_3 was reduced from 10 µM used in the previous experiment in order to minimise the effect it might have on root growth. A pilot experiment was performed by germinating *ga1-t* seedlings on either 1, 2.5, 5, 7.5 and 10 µM of GA_3 and assessing their germination rates. The lowest concentration where all of the seedlings germinated was 2.5 µM so this amount was used in subsequent experiments (data not shown). For each mutant line, a total of 40 seedlings were grown alongside WT seedlings, distributed across 8 plates (i.e. 5 mutant seedlings grown against 5 WT per plate). Primary root growth was measured consecutively from days 3-9 DAS and confocal microscopy was used to image the RAM of these crosses on the final day of the root growth experiment.

Overall, primary root growth from 3-9 DAS across all genotypes was found to be linear (Figure 4.1A). On the first day of the experiment (3 DAS), seedlings of all genotypes had a similar size in root length with mean values approximately the same (Figure 4.3A). On the final day of the experiment at 9 DAS,

ga1-t seedlings had the shortest mean root length of 29.9 mm (SE = 0.471), followed by *ga1-t gai-td1* (mean = 33.7 mm, SE = 0.461), *ga1-t rga-28* (mean = 42 mm, SE = 0.649) and WT (mean = 48.3 mm, SE = 0.922). A similar trend was observed when plotting the distribution of root lengths for each genotype with boxplots (Figure 4.3C). These results implied there were differences between the root growth rates of these mutant lines, which was evident from plotting the mean root lengths for each genotype over time. The slope of the fitted lines indicated that WT seedlings had the highest average root growth rate, followed by *ga1-t rga-28*, *ga1-t gai-td1* and *ga1-t* (Figure 4.3A).

To test these findings statistically, the association between genotype and length over time was assessed using a GLMM with a *Gamma* family and *identity* link, which included the main effects of day and genotype, their interaction and a random effect of plate variability (Appendix 4.2A). The model output showed that root length between days was significantly different, with WT seedlings growing at a rate of 6.43 mm per day (Table 4.3). As found in previous experiments, there was a significant reduction in the root growth rate of *ga1-t* seedlings when compared to WT, with a decrease of 2.43 mm per day (t_3= -29.40, p<0.001). Furthermore, there were significant differences in the root growth rates of WT seedlings when compared to the double mutant lines, *ga1-t rga-28* and *ga1-t gai-td1*. For *ga1-t gai-td1* seedlings, the growth rate was 1.93 mm less than WT per day (t_3= -22.47, p<0.001), whilst *ga1-t rga-28* seedlings grew faster, with a growth rate 0.85 mm less than WT per day (t_3= -8.82, p<0.001). When comparing between these lines, the root growth rate of *ga1-t rga-28* seedlings was significantly greater than that of *ga1-t gai-td1*, with an increase of 1.15 mm per day (t_3= 10.7, p<0.001), whilst *ga1-t gai-td1* seedlings grew at significantly increased rate of 0.5 mm/day when compared to *ga1-t* (t_3= 5.08, p<0.001).

Genotype	Root growth rate (mm/day)	Standard Error	t-value	p-value
Col-0 (WT)	6.43	0.064	101.01	<0.001
ga1-t	4.00	0.077	52.10	<0.001
ga1-t gai-td1	4.50	0.080	55.96	<0.001
ga1-t rga-28	5.58	0.091	61.25	<0.001

Table 4.3: Daily root growth rates for each genotype as predicted by the statistical model (GLMM). For each calculation, there was always one degree of freedom. Levels of significance are represented by: * p<0.05, ** P<0.01 and *** p<0.001. The p-value refers to the difference in growth rate between days.

These differences could be visualised by plotting the predicted lines from the model for each genotype over the raw data (Figure 4.3B). The lines appeared to fit with the data and demonstrate differences between their slopes, showing a similar pattern as described for the mean values plotted over time

Figure 4.3 Analysis of root growth, meristem size, cortical cell number and cell production rate for *Col-0* WT, *ga1-t*, *ga1-t gai-td1* and *ga1-t rga-28* seedlings from 3 - 9 days after stratification (DAS). All of these lines were germinated on 2.5 μM of GA_3 and transferred to fresh plates 1 DAS. Results are represented by:

(A) Average root length for each genotype plotted over time fitted with a linear trendline

(B) The predicted lines for root length over time per genotype as determined by the statistical model used to analyse the data and plotted over the raw data values

(C) Boxplots for each genotype over time, with the final day enlarged for better visualisation of the distribution of root lengths. The boxplots show the median value as represented by the dividing line, as well as the lower and upper interquartile ranges, with whiskers extending 1.5 times the interquartile range.

(D) Boxplots of root meristem size for each genotype

(E) Boxplots of cortical cell number within the root meristem for each genotype

(F) Boxplots of cell production rate for each genotype

A

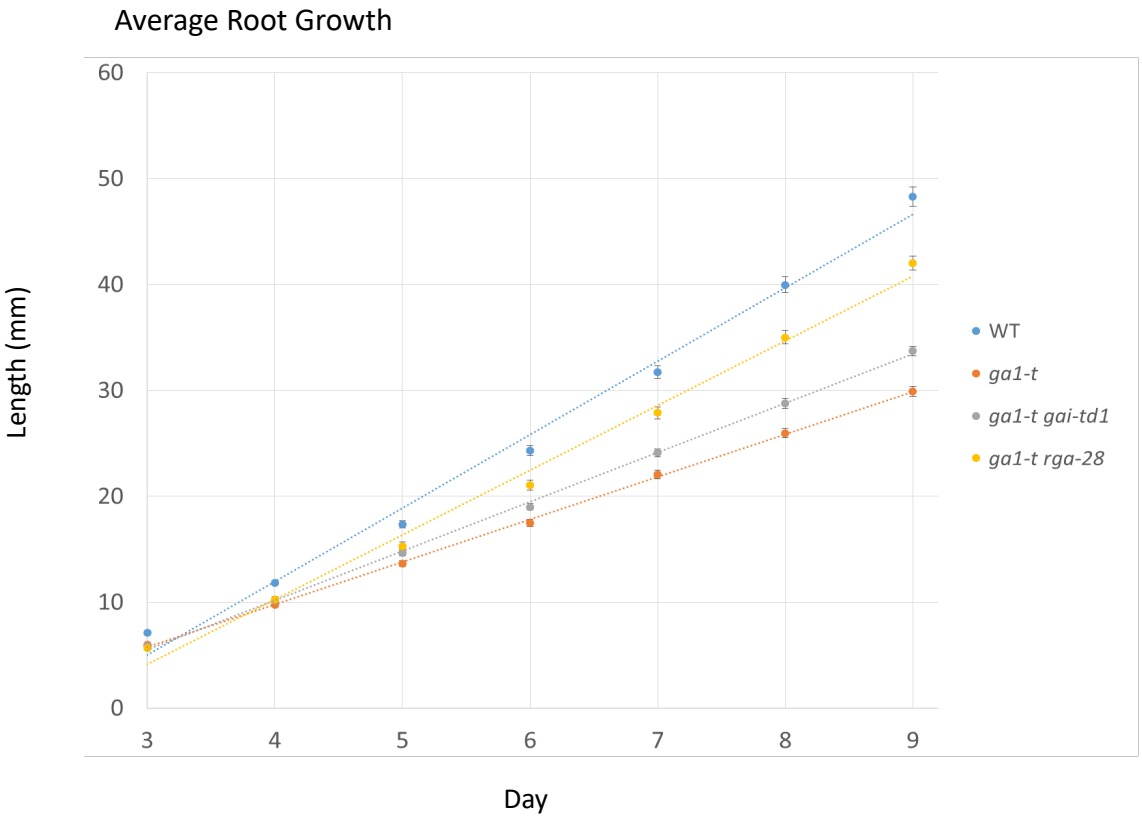
Average Root Growth
Length (mm)
60
50
40
30
20
10
0
3
4
5
6
7
8
9
Day
WT
ga1-t
ga1-t gai-td1
ga1-t rga-28

B

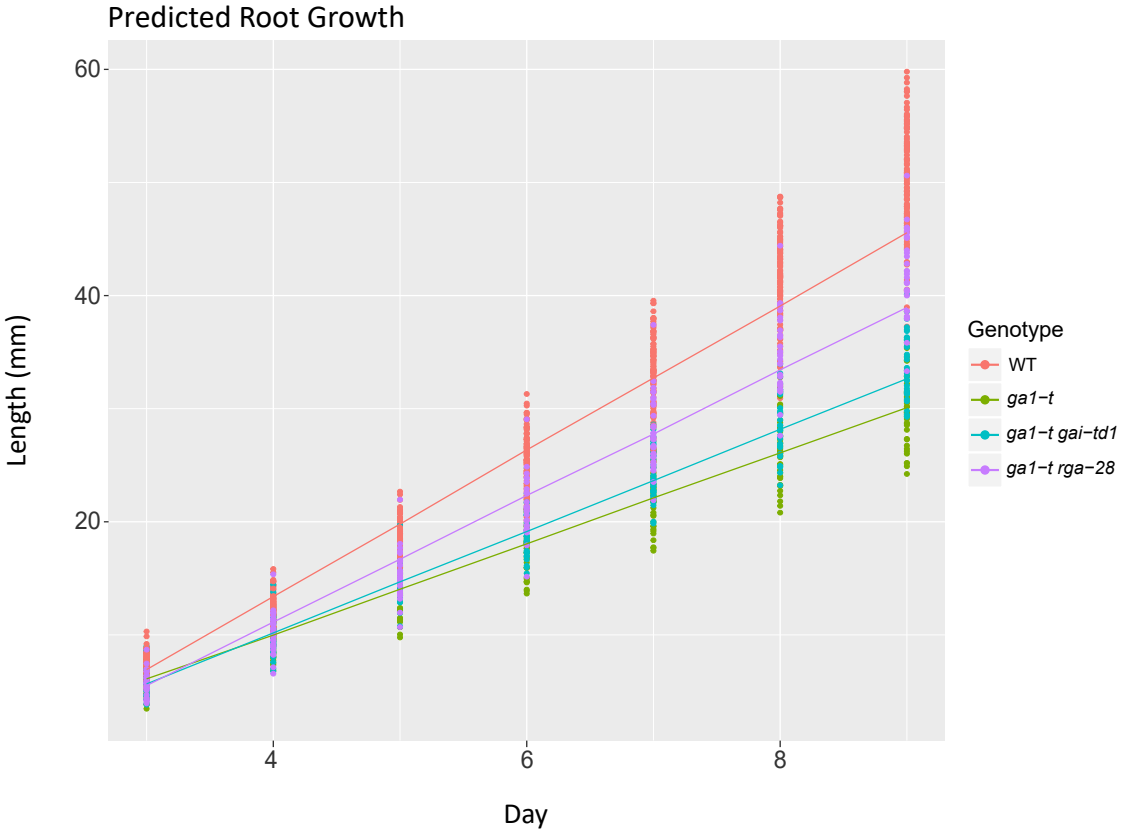
Predicted Root Growth
Length (mm)
60
40
20
4
6
8
Day
Genotype
WT
ga1−t
ga1−t gai−td1
ga1−t rga−28

C

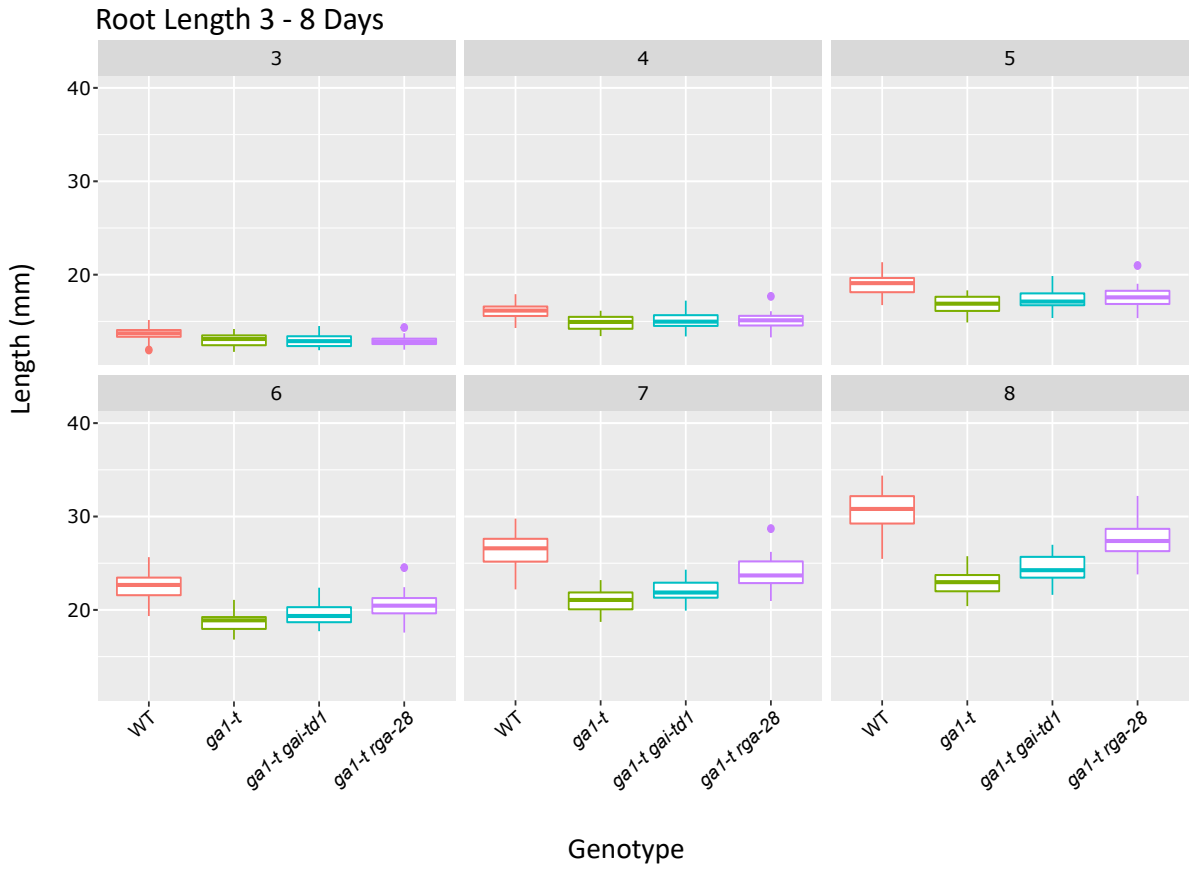
Root Length 3 - 8 Days
3
4
5
6
7
8
Length (mm)
40
30
20
WT
ga1-t
ga1-t gai-td1
ga1-t rga-28
Genotype

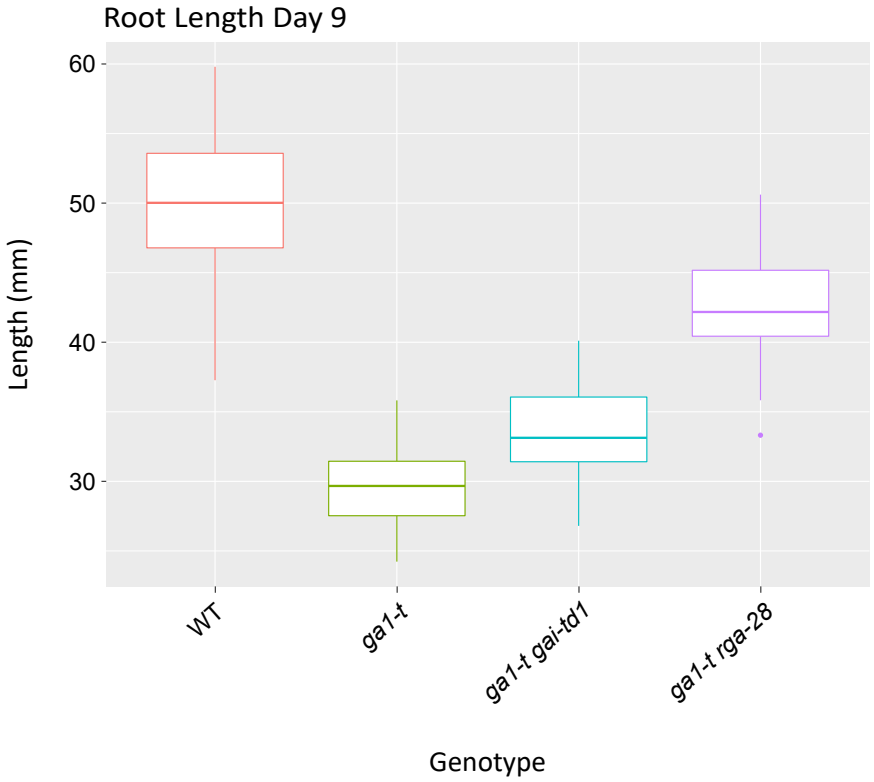
Root Length Day 9
Length (mm)
60
50
40
30
WT
ga1-t
ga1-t gai-td1
ga1-t rga-28
Genotype

D

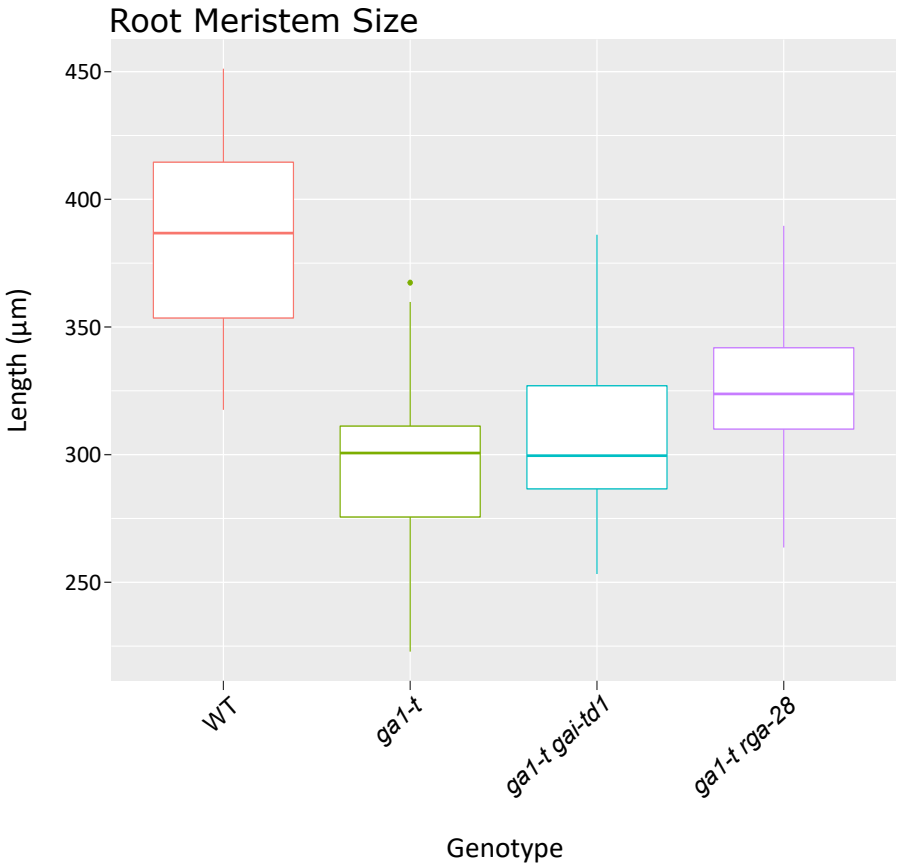
Root Meristem Size
Length (µm)
450
400
350
300
250
WT
ga1-t
ga1-t gai-td1
ga1-t rga-28
Genotype

E

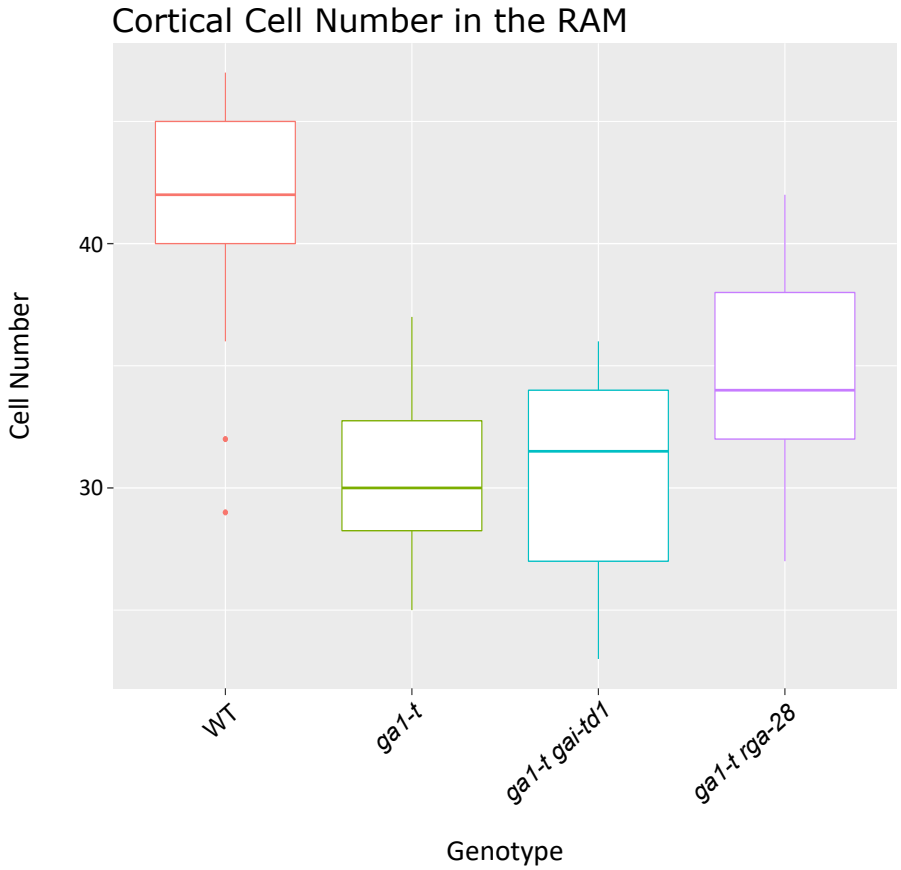
Cortical Cell Number in the RAM
Cell Number
40
30
WT
ga1-t
ga1-t gai-td1
ga1-t rga-28
Genotype

F

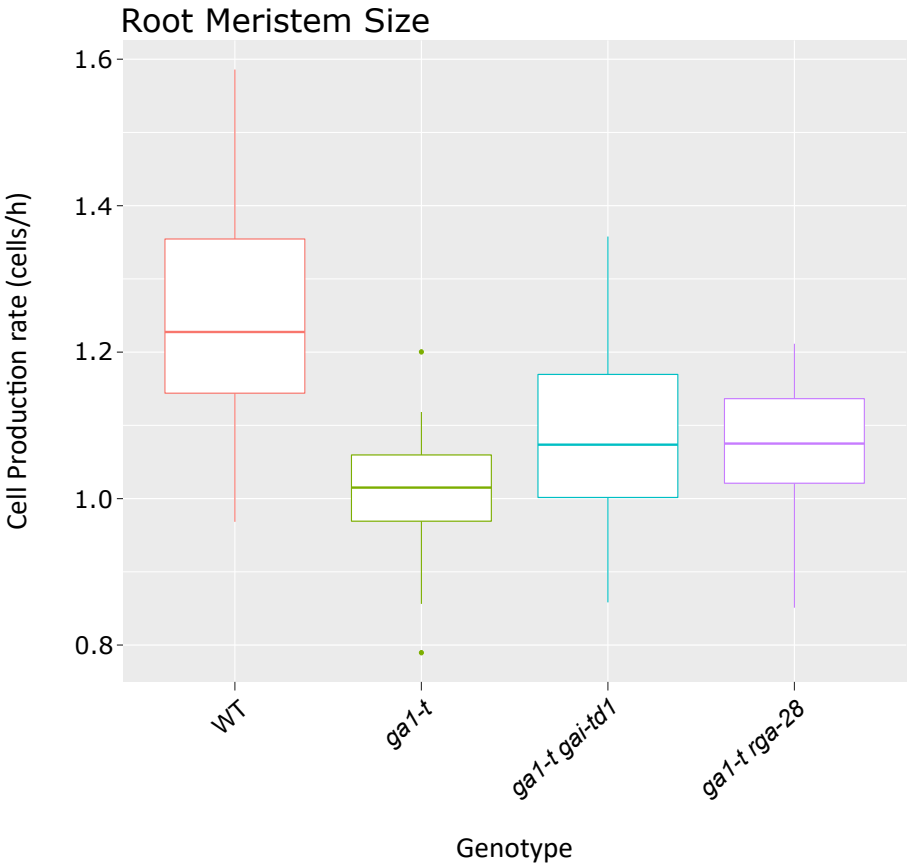
Root Meristem Size
Cell Production rate (cells/h)
1.6
1.4
1.2
1.0
0.8
WT
ga1-t
ga1-t gai-td1
ga1-t rga-28
Genotype

(Figure 4.3A,B). Both plots show a general trend of root growth for *ga1-t rga-28* seedlings being closer to that of WT, whilst the growth of *ga1-t gai-td1* seedlings was closer to that of the *ga1-t* mutant. Therefore, introduction of the null *rga* mutation into the *ga1-t* mutant background was able to rescue the reduced growth phenotype of *ga1-t* more substantially than introduction of the *gai* null mutation. These results support previous evidence that both RGA and GAI inhibit root growth via the GA signalling pathway, but RGA plays more of a dominant role in relation to regulation of this process (Fu and Harberd, 2003). This could be the result of a decreased rate of cell elongation and/or cell division.

To investigate further, the effect of these null mutations at the cellular level were examined in the region of active cell division. This was done by using confocal microscopy to image the RAM on the final day of the root growth assay at 9 DAS. The cortical cell layer was then analysed to determine meristem length and cortical cell number within this region. Fully elongated cortical cells were also imaged further along the root and measured in order to calculate the cell production rate of individual seedlings. Cell production rate is a measure of how many cells are produced per unit of time, which is simply calculated by dividing the growth rate of a seedling by the average length of its elongating cells (Baskin 2013, Rymen, 2010).

Overall, WT seedlings had a longer meristem and increased amount of cortical cells in this region when compared to that of *ga1-t*, *ga1-t gai-td1* and *ga1-t rga-28* seedlings (Figure 4.3D,E). Both cortical cell number and meristem length between these genotypes generally reflected the pattern found for their rates of root elongation, suggesting a relationship between these variables. Specifically, where there was a reduction in root elongation, there was also a corresponding reduction in meristem length and cortical cell number. In relation to meristem length, *ga1-t* and *ga1-t gai-td1* seedlings appeared to have the shortest meristem size, with mean values of 295.25 µm (SE = 5.04) and 310.56 µm (SE = 6.27), respectively. This was followed by *ga1-t rga-28* seedlings with a mean of 325.21 µm (SE = 4.27) and WT seedlings with a mean of 385.6 µm (SE = 6.78). Although the median values for meristem size between *ga1-t* and *ga1-t gai-td1* seedlings appeared to be similar, the boxplot for *ga1-t* seedlings was skewed by lower values, whereas the boxplot for *ga1-t gai-td1* seedlings was skewed by higher values (Figure 4.3D). This was consistent with the reduced rate of root elongation found for both of these lines, with *ga1-t* seedlings having a more substantial reduction in root elongation rate than *ga1-t gai-td1* seedlings. Furthermore, the increased meristem size for *ga1-t rga-28* and WT seedlings was also consistent with their increased rates of root elongation. In relation to cortical cell number, *ga1-t* and *ga1-t gai-td1* seedlings appeared to contain the least amount of cortical cells with both having the lowest mean value when rounded to the nearest whole number of 31 cells (SE = 0.46 and 0.72, respectively), *ga1-t rga-28* with a mean of 35 cells (SE = 0.59) and WT with a mean of 42 cells (SE =

0.74). Again, this pattern followed that of the differences for meristem length, as well as differences in their rate of elongation for these genotypes.

For statistical analysis, the association between meristem length and genotype was assessed with a linear mixed effects model (LMER), which included the main effect of length and the random effects of plate variability and whether the measurement was taken from the left or right cortical cell layer (Appendix 4.2B). The model output demonstrated that root meristem size was significantly different for all mutant genotypes when compared to WT, which had the largest predicted meristem size of 385.75 µm (Table 4.4). Specifically, *ga1-t* had a reduction of 90.94 µm in meristem length (t_3 = -10.81, p<0.001), followed by reduction of 76.59 µm for *ga1-t gai-td1* (t_3 = -8.78, p <0.001) and a reduction of 60.5 µm for *ga1-t rga-28* (t_3 = -7.29, p<0.001) when compared to WT. Furthermore, when comparing meristem size of *ga1-t* seedlings to that of *ga1-t rga-28*, there was a significant difference between them with *ga1-t* having a reduction of 30.44 µm in length (t_3 = -4.31, p<0.001). However, there was no significant difference in meristem length when comparing between *ga1-t* and *ga1-t gai-td1* seedlings (t_3 = -1.88, p = 0.06), even though *ga1-t* had a predicted meristem size 14.36 µm less than *ga1-t gai-td1*. Finally, there was a significant difference between *ga1-t gai-td1* and *ga1-t rga-28* with a reduction of 16.09 µm in meristem length for *ga1-t gai-td1* (t_3 = -2.16, p<0.05), thus implying that a reduction in meristem size is related to the differences found for the primary root growth rates of these lines.

Genotype	Meristem size (µm)	Standard Error
WT	385.75	6.377
ga1-t	294.81	5.835
ga1-t gai-td1	309.17	6.269
ga1-t rga-28	325.25	5.668

Table 4.4: Predicted root meristem size for each genotype determined by the statistical model (GLMM). For each calculation, there were three degrees of freedom (n-1).

For analysis of cortical cell number within the meristem of these lines, the association between cortical cell number and genotype was assessed with a GLMM with a *Poisson* family and an *identity* link, which included the main effect of cortical cell number and the random effect of whether the measurement was taken from the left or right cortical cell layer (Appendix 4.2C). As was the case for meristem size, the model output demonstrated that the meristems of WT seedlings contained greater than the other mutant genotypes. Both *ga1-t* and *ga1-t gai-td1* seedlings had meristems containing the least amount of cortical cells, with a predicted size of 11 cells less than WT (t_3 = -7.77, p<0.001 and t_3 = -7.37,

p<0.001, respectively), followed by *ga1-t rga-28* seedlings with a predicted size of 7 cells less than WT (t_3 = -4.64, p<0.001). Similar to the findings for meristem size, the amount of cortical cells compared between the meristems of *ga1-t* and *ga1-t gai-td1* seedlings was not significantly different (t_3 = 0.14, p = 0.888). However, there was a significant difference for cortical cell number when comparing the meristems of *ga1-t* and *ga1-t gai-td1* seedlings between that of *ga1-t rga-28*, with both containing a predicted size of approximately 4 cells less than *ga1-t rga-28* (t_3 = 3.44, p<0.001 and t_3 = 3.15, p<0.01, respectively). These results combined demonstrate that the differences found in the primary root growth rates between *ga1-t* and *ga1-t rga-28* seedlings were associated with a corresponding reduction in root meristem size and cortical cell number, thus implying that the process of cell division is altered in these lines. Whether these changes in meristem size were accompanied by changes in the rate of cell division remained unclear, but could easily be determined by measuring the rates of cell production for these lines.

Genotype	Cortical Cell Number	Standard Error
WT	42	1.124
ga1-t	31	0.896
ga1-t gai-td1	31	0.979
ga1-t rga-28	35	0.923

Table 4.5: Predicted cortical cell number for each genotype as determined by the statistical model (GLMM). Due to the discrete nature of this variable, the predicted values have been rounded to the nearest whole number. There were three degrees of freedom for each prediction (n-1).

To determine cell production rates between the aforementioned lines, the average growth rate of individual seedlings from each genotype was calculated and divided by the average size of their elongated cortical cells. The data was then visualised by plotting the distribution of cell production rate for each genotype with boxplots (Figure 4.3F). The plots indicated that WT seedlings had the highest median rate of cell production, whilst *ga1-t gai-td1* and *ga1-t rga-28* seedlings had reduced and relatively similar median values, followed by *ga1-t* seedlings with the lowest median and distribution of values. There were also differences between the mean values of cell production rate for these mutant genotypes when compared to WT. Indeed, the mean cell production rate for WT seedlings was 1.24 cells per hour (cells/h), whereas the means for *ga1-t*, *ga1-t gai-td1* and *ga1-t rga-28* seedlings were lower and did not appear to vary substantially, with values of 1.01 (SE = 0.023), 1.10 (SE = 0.032) and 1.07 (SE = 0.021) cells/h, respectively.

To examine these potential differences statistically, the association between cell production rate and genotype was assessed with a linear regression model (LM – Appendix 4.2D). The model output

demonstrated WT seedlings had the highest cell production rate with a predicted value of 1.22 cells/hour, which was significantly different to the mutant genotypes. Specifically, *ga1-t* seedlings had the lowest cell production rate in comparison to WT with a reduction of 0.24 cells/h (t_3 = -5, p<0.001), followed by *ga1-t rga-28* with a reduction of 0.17 cells/h (t_3 = -3.77, p<0.001) and *ga1-t gai-td1* with a reduction of 0.15 cells/h (t_3 = -3.1, p<0.01).

When comparing between these mutant genotypes, the cell production rate of *ga1-t* seedlings was significantly different to that of *ga1-t gai-td1* with a reduced rate of 0.09 cells/h (t_3 = 2.1, p<0.05), whereas there was no significant difference in the rate of this line when compared to seedlings of *ga1-t rga-28* (t_3 = 1.42, p = 0.161). Moreover, there was no significant difference between the cell production rates of *ga1-t gai-td1* seedlings when compared to that of *ga1-t rga-28* (t_3 = -0.71, 0.483). These results demonstrate that the proliferative performance of the meristem was reduced in all of the aforementioned mutant lines, particularly the *ga1-t* single null mutant, suggesting that cell division rates were negatively affected by the presence of this mutation. Furthermore, the fact that there was little variation between the cell production rates of *ga1-t gai-td1* and *ga1-t rga-28* seedlings, indicated that the differences found between their rates of primary root elongation must be attributable to changes in root meristem size to alter the process of cell division, and/or differences between their rates of cellular expansion.

Genotype	Cell Production Rate (cells/h)	Standard Error
WT	1.24	0.036
ga1-t	1.01	0.031
ga1-t gai-td1	1.1	0.031
ga1-t rga-28	1.07	0.03

Table 4.6: Predicted cell production rate for each genotype determined by a linear regression model. There were three degrees of freedom for each prediction (n-1). The rate of cell production for individual seedlings was calculated by dividing their hourly root growth rate by the average size of their elongating cortical cells.

4.1.3 Removal of GAI or RGA function in the RBR translational reporter line does not confer different root phenotypes

To investigate how GAI and RGA are related to the cell cycle in more detail, the previously described single null mutant lines, *gai-td1* and *rga-28*, were crossed to the RBR translational reporter line, pRBR::RBR-GFP. Crosses were generated to the F2 stage and genotyped in order to identify F3 lines homozygous for both genes. This was done to see whether introduction of an additional copy of RBR

in the absence of either GAI or RGA was sufficient to cause differences in their root growth rates. Indeed, previous research had shown that pRBR::RBR-GFP seedlings had a reduced meristem size when compared to WT, suggesting that the presence of RBR-GFP has an effect on the overall root growth phenotype (Magyer et al., 2012).

Once these crosses had been obtained, high-throughput root growth experiments using these lines alongside relevant controls (WT, *gai-td1*, *rga-28* and pRBR::RBR-GFP) were performed using the facilities provided by Wolfgang Busch at the Gregor Mendel Institute (GMI), Vienna. Here, they have developed a pipeline for growing seedlings and analysing root growth in a high-throughput manner, which controls for plate variability by grouping different genotypes together on a single plate and changing their positions across different plates (Slovak *et al.*, 2015). For each mutant line, a total of 24 seedlings were grown alongside WT and other mutant lines, distributed in different positons across 8 plates (i.e. 3 mutant seedlings grown against 3 WT and other mutant lines per plate). Primary root growth was then measured consecutively from 2-9 DAS using the root phenotyping pipeline. Furthermore, a series of treatment experiments were set up with GA and PAC to alter endogenous GA levels and examine the effect this had on the root growth phenotypes of these lines. Therefore, seeds from each genotype were plated out onto control growth media, as well as media supplemented with either 10 µM of GA_3 or 1 µM of PAC. Some of the lines in these experiments were *ga1* mutants and therefore required exogenous GA for germination. Furthermore, since PAC is a GA biosynthetic inhibitor, seeds that were treated with this compound may not germinate. Consequently, all seeds were pre-treated with 2.5 µM of GA_3 until they had germinated at 1 DAS and then transferred to the different treatment conditions.

In terms of the control treatment, primary root growth from 2-9 DAS across all genotypes was found to be linear (Figure4.4Ai). At the beginning of the experiment at 2 DAS, the mean values appeared to be relatively similar amongst the different genotypes, ranging between 2.78 mm and 3.88 mm (Figure 4.4Ai). By the end of the experiment at 9 DAS, the means for WT, *gai-td1* and *rga-28* seedlings were similar with values of 32.87 mm (SE = 1.089), 32.22 mm (SE = 1.338) and 31.87 mm (SE = 1.017), respectively. Whereas, the means for pRBR::RBR-GFP, pRBR::RBR-GFP *gai-td1* and pRBR::RBR-GFP *rga-28* seedlings were slightly reduced with values of 28.01 mm (SE = 0.717), 29.92 mm (SE = 0.808) and 29.21 mm (SE = 0.653), respectively. From examining the boxplot distribution of these lines, a similar trend was observed as described for the average values (Figure 4.4Ci). The boxplots indicated that RBR::RBR-GFP *gai-td1* seedlings had a higher median root length when compared to pRBR::RBR-GFP, although it was negatively skewed by an increased variability of lower root length values. Overall, there did not appear to be any substantial difference in root growth between the WT, *gai-td1* and *rga-*

Figure 4.4 Analysis of root growth for *Col-0* WT, *gai-td1*, *rga-28*, RBR::RBR-GFP, RBR::RBR-GFP *gai-td1* and RBR::RBR-GFP *rga-28* seedlings from 2-9 days after stratification (DAS). All of these lines were germinated on 2.5 µM of GA_3 and transferred to fresh plates 1 DAS. Seedlings were subject to different treatments: (i) control (ii) 10 µM of GA_3 and (iii) 1 µM of PAC and are represented by:

(A) Average root length for each genotype plotted over time fitted with a linear trendline

(B) The predicted lines for root length over time per genotype as determined by the statistical model used to analyse the data and plotted over the raw data values

(C) Boxplots for each genotype over time, with the final day enlarged for better visualisation of the distribution of root lengths. The boxplots show the median value as represented by the dividing line, as well as the lower and upper interquartile ranges, with whiskers extending 1.5 times the interquartile range.

A (i)

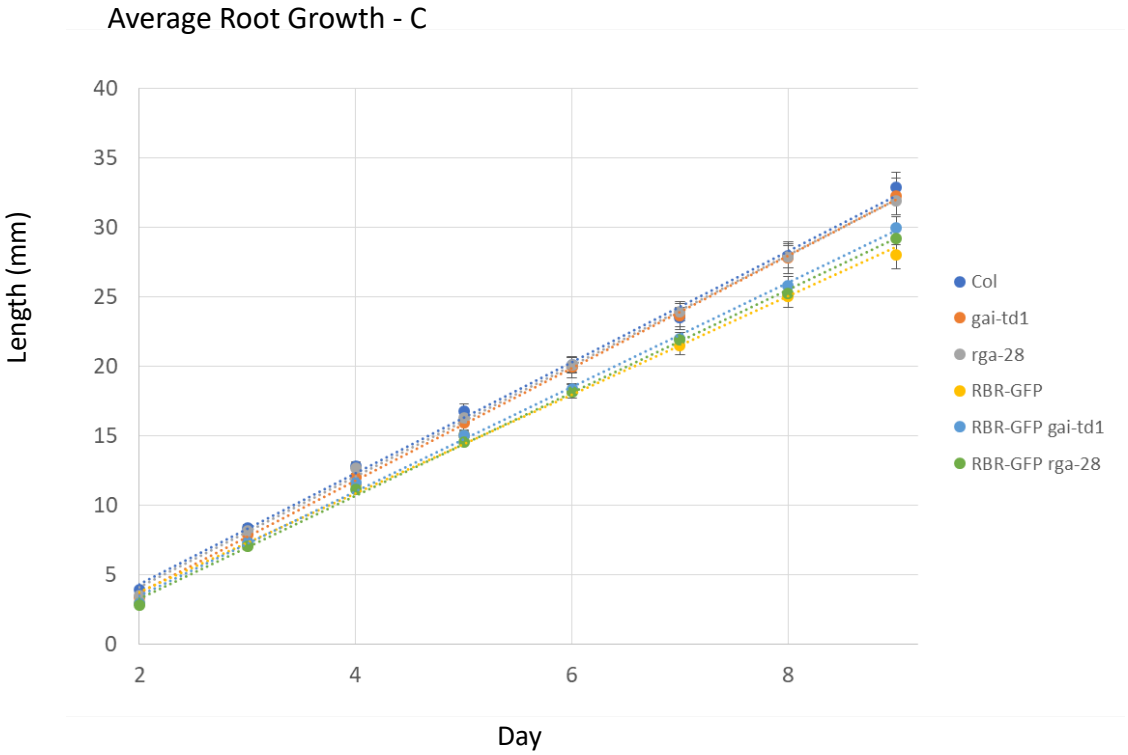
Average Root Growth - C
Length (mm)
40
35
30
25
20
15
10
5
0
2
4
6
8
Day
Col
gai-td1
rga-28
RBR-GFP
RBR-GFP gai-td1
RBR-GFP rga-28

B (i)

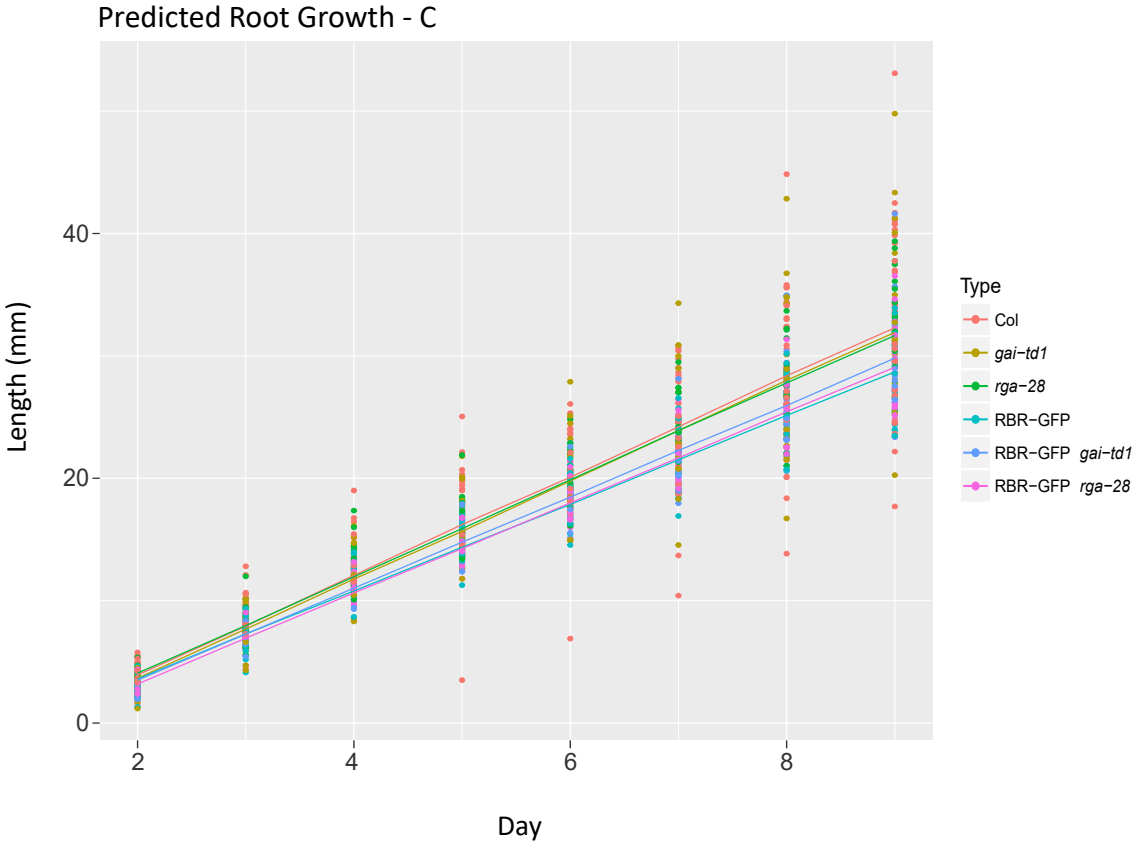
Predicted Root Growth - C
Length (mm)
40
20
0
2
4
6
8
Day
Type
Col
gai-td1
rga-28
RBR-GFP
RBR-GFP gai-td1
RBR-GFP rga-28

C (i)

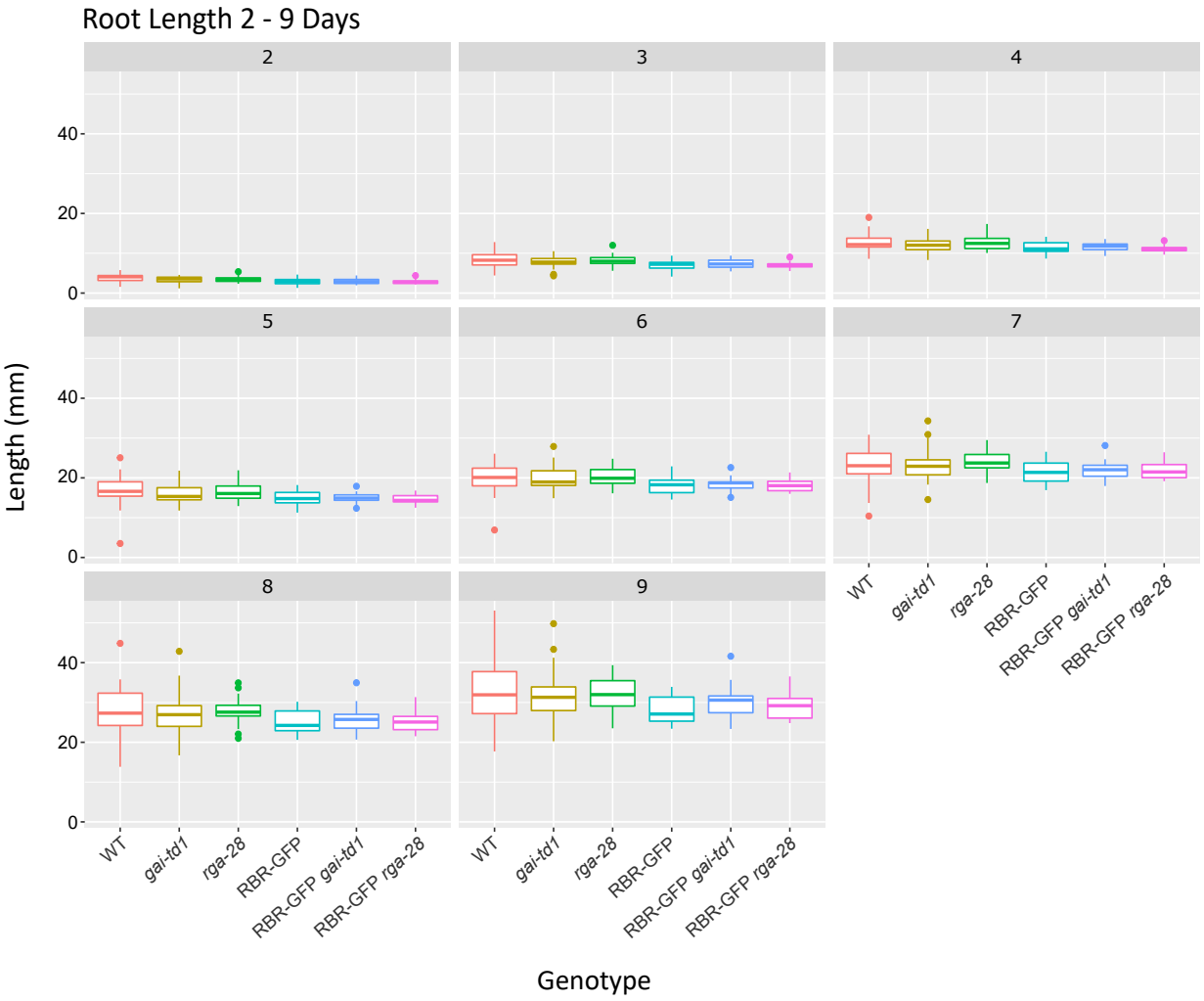
Root Length 2 - 9 Days
2
3
4
5
6
7
8
9
Length (mm)
0
20
40
WT
gai-td1
rga-28
RBR-GFP
RBR-GFP gai-td1
RBR-GFP rga-28
Genotype

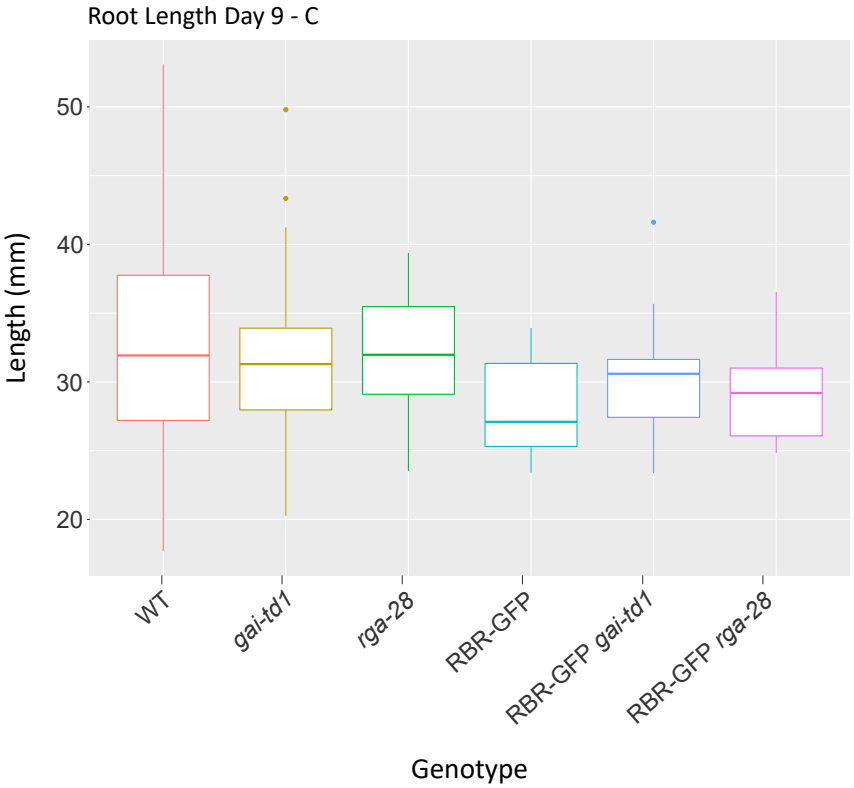
Root Length Day 9 - C
Length (mm)
20
30
40
50
WT
gai-td1
rga-28
RBR-GFP
RBR-GFP gai-td1
RBR-GFP rga-28
Genotype

A (ii)

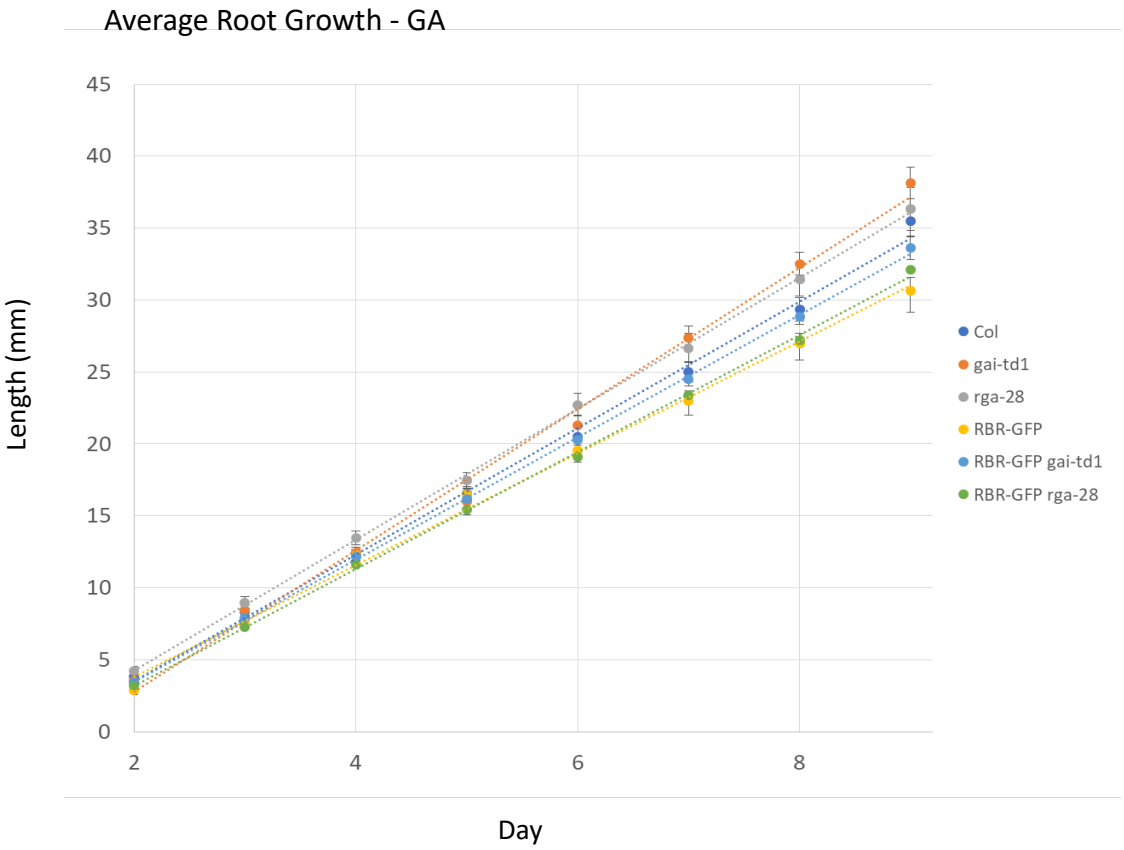
Average Root Growth - GA
Length (mm)
45
40
35
30
25
20
15
10
5
0
2
4
6
8
Day
Col
gai-td1
rga-28
RBR-GFP
RBR-GFP gai-td1
RBR-GFP rga-28

B (ii)

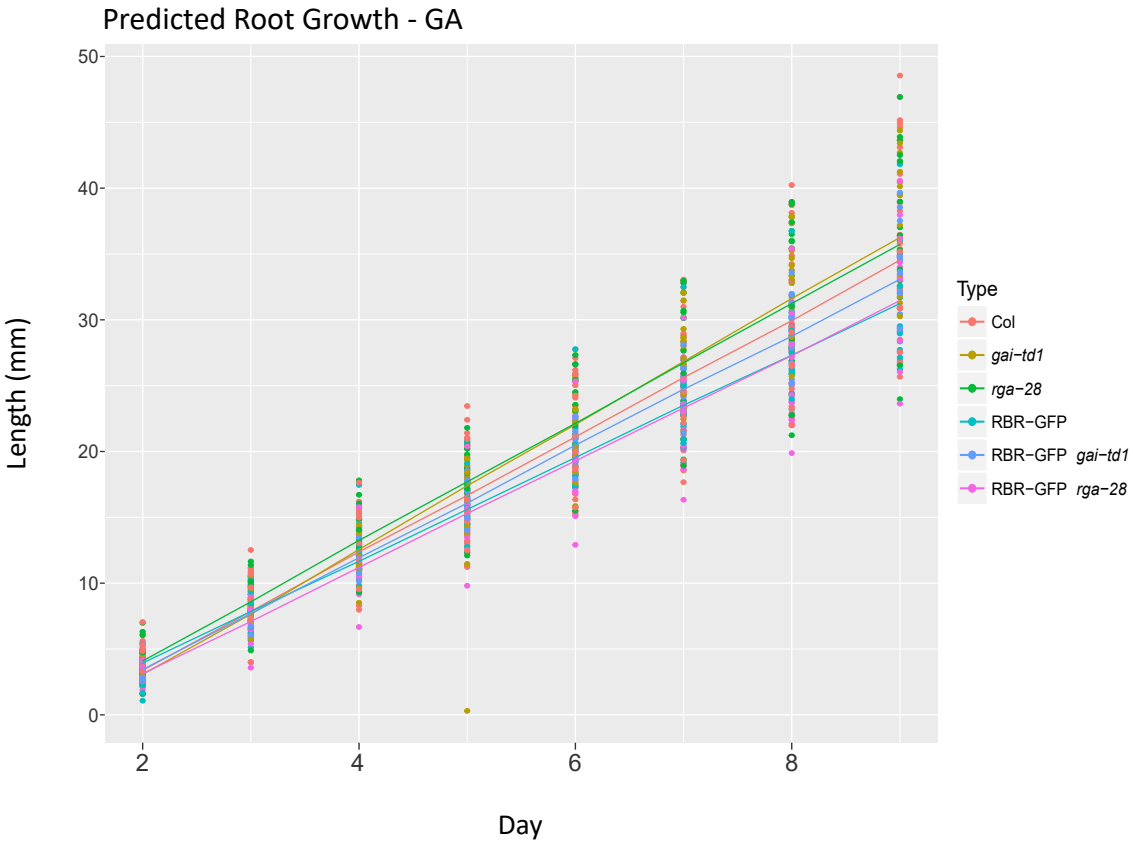
Predicted Root Growth - GA
Length (mm)
50
40
30
20
10
0
2
4
6
8
Day
Type
Col
gai-td1
rga-28
RBR-GFP
RBR-GFP gai-td1
RBR-GFP rga-28

C (ii)

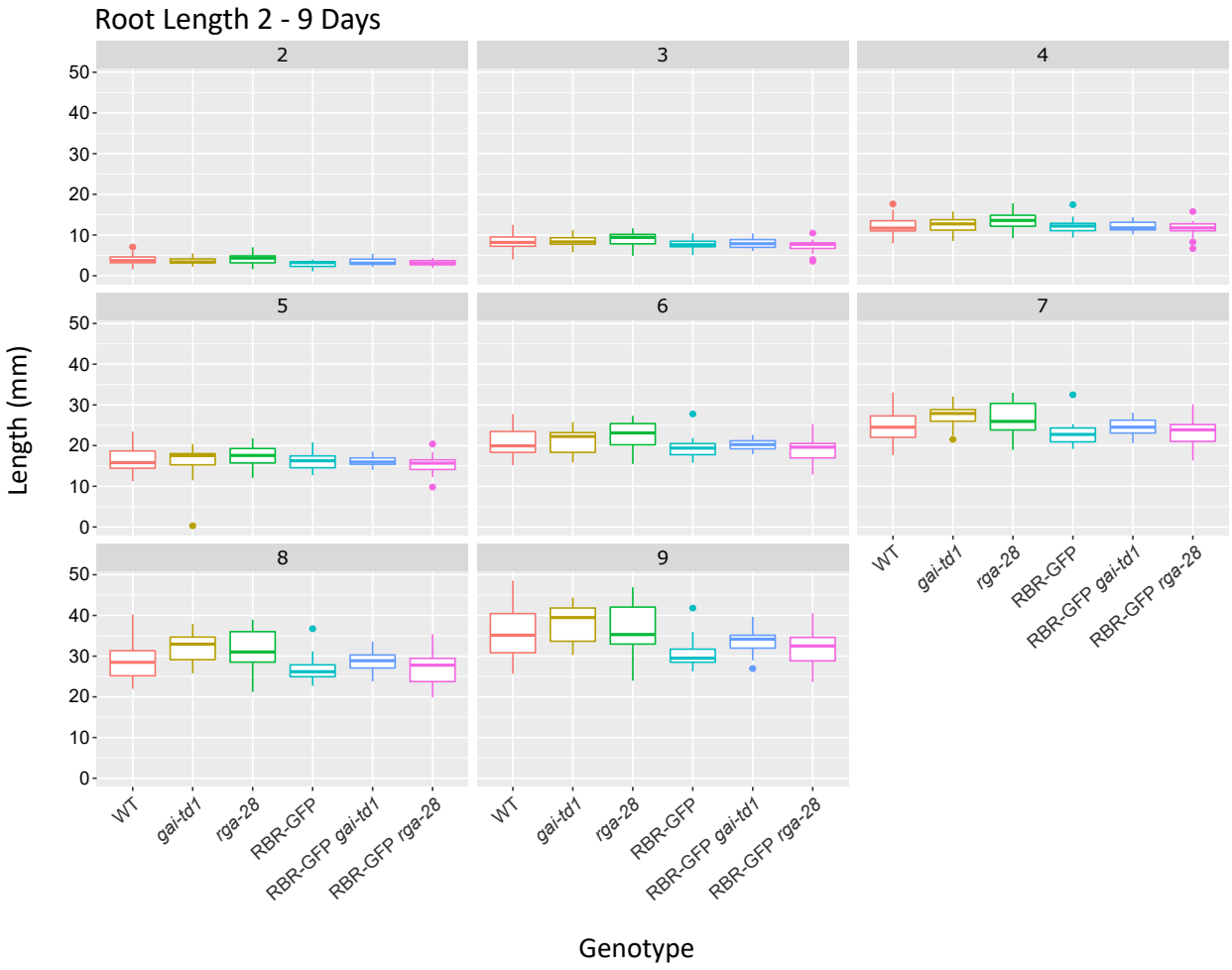
Root Length 2 - 9 Days
2
3
4
5
6
7
8
9
Length (mm)
0
10
20
30
40
50
WT
gai-td1
rga-28
RBR-GFP
RBR-GFP gai-td1
RBR-GFP rga-28
Genotype

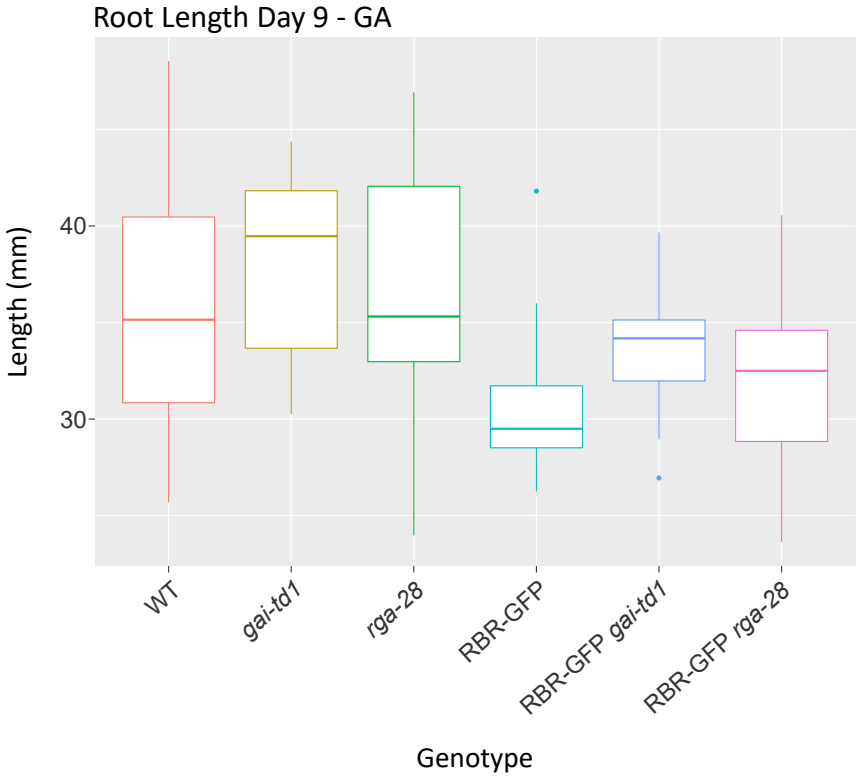
Root Length Day 9 - GA
Length (mm)
30
40
WT
gai-td1
rga-28
RBR-GFP
RBR-GFP gai-td1
RBR-GFP rga-28
Genotype

A (iii)

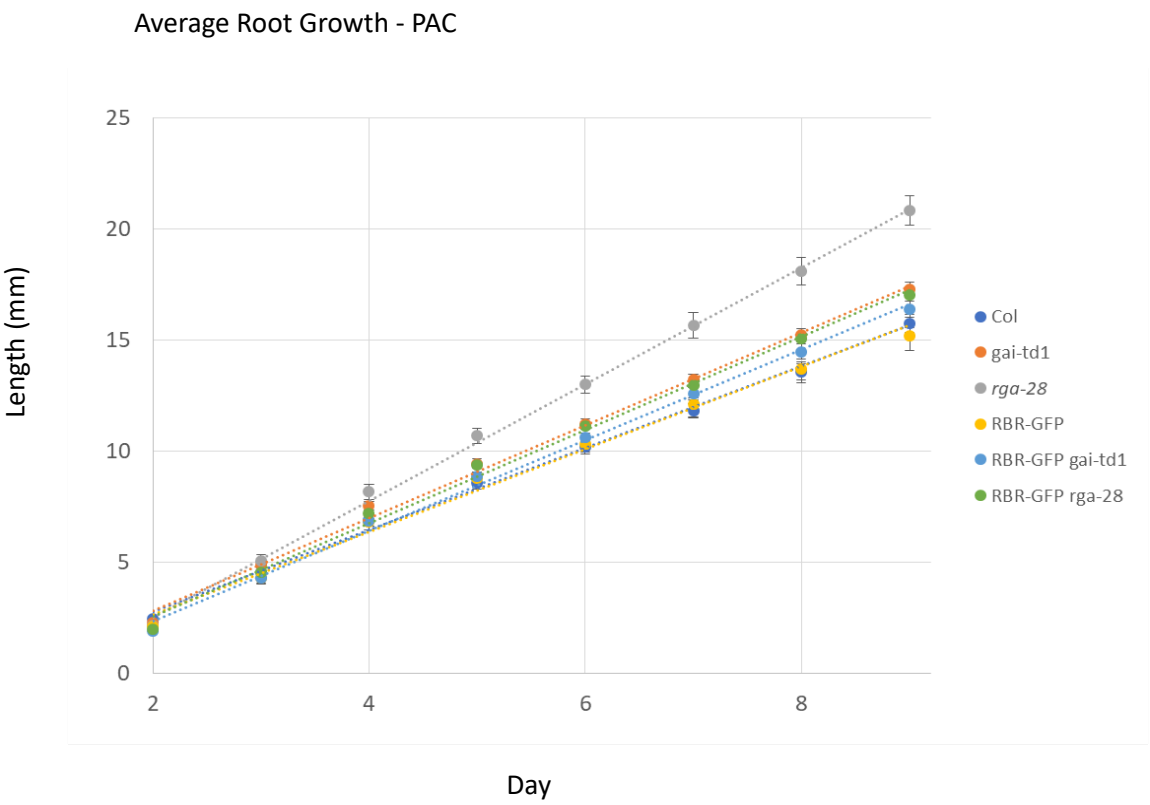
Average Root Growth - PAC
Length (mm)
25
20
15
10
5
0
2
4
6
8
Day
Col
gai-td1
rga-28
RBR-GFP
RBR-GFP gai-td1
RBR-GFP rga-28

B (iii)

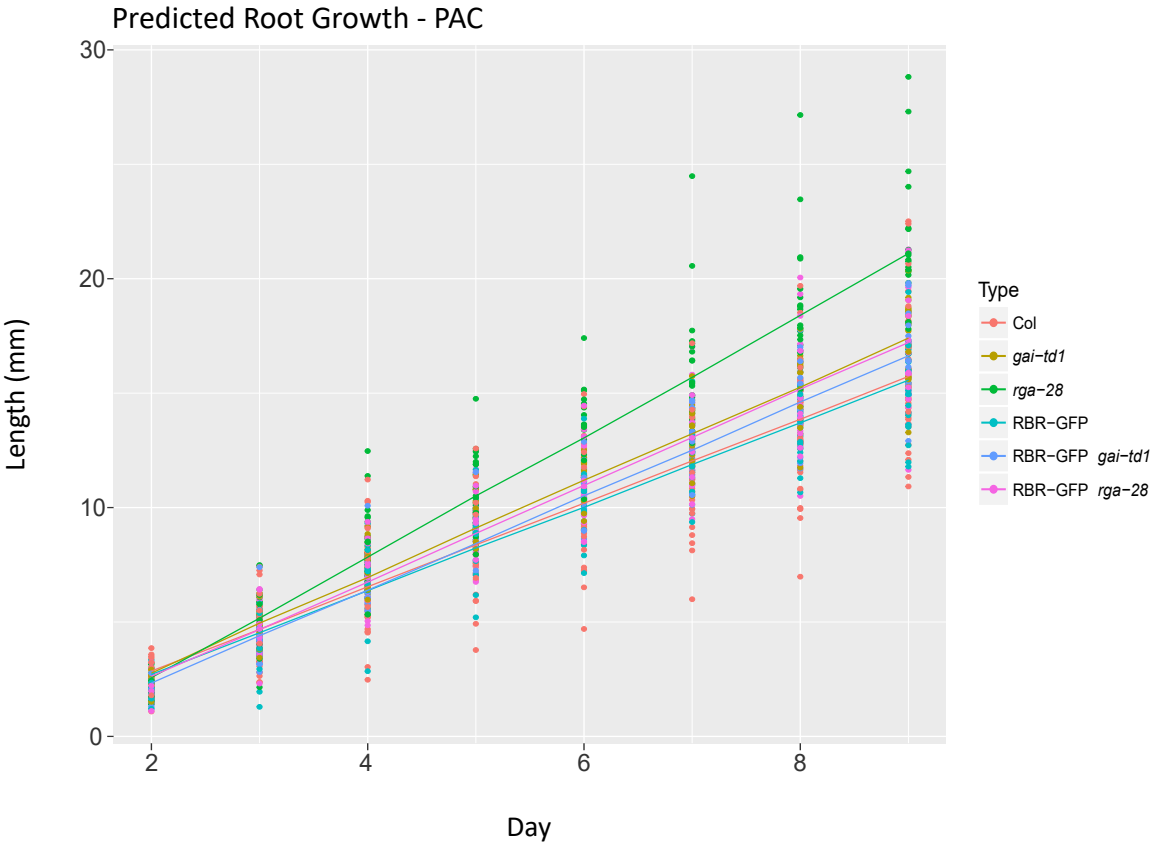
Predicted Root Growth - PAC
Length (mm)
30
20
10
0
2
4
6
8
Day
Type
Col
gai-td1
rga-28
RBR-GFP
RBR-GFP gai-td1
RBR-GFP rga-28

C (iii)

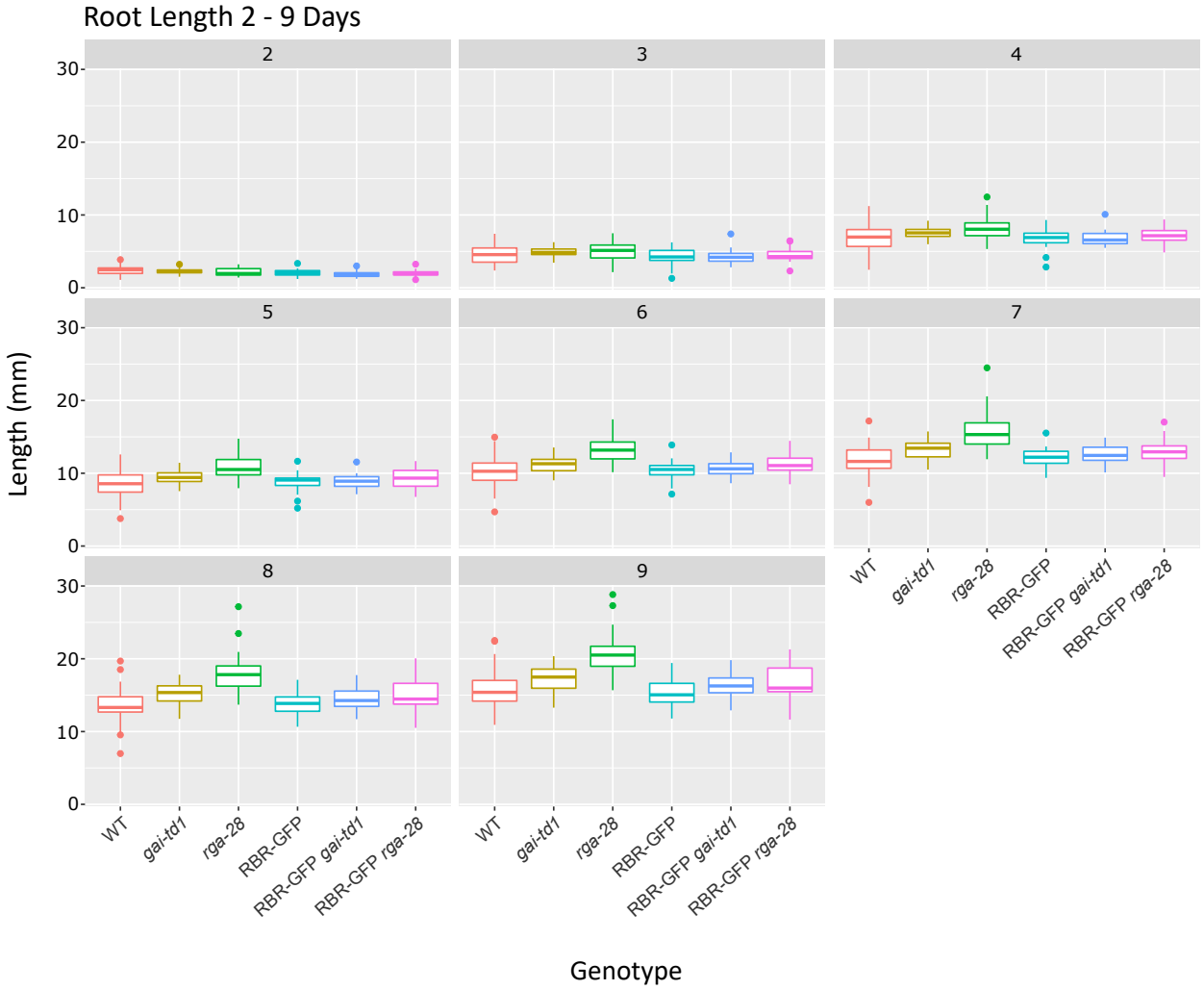
Root Length 2 - 9 Days
2
3
4
5
6
7
8
9
Length (mm)
0
10
20
30
WT
gai-td1
rga-28
RBR-GFP
RBR-GFP gai-td1
RBR-GFP rga-28
Genotype

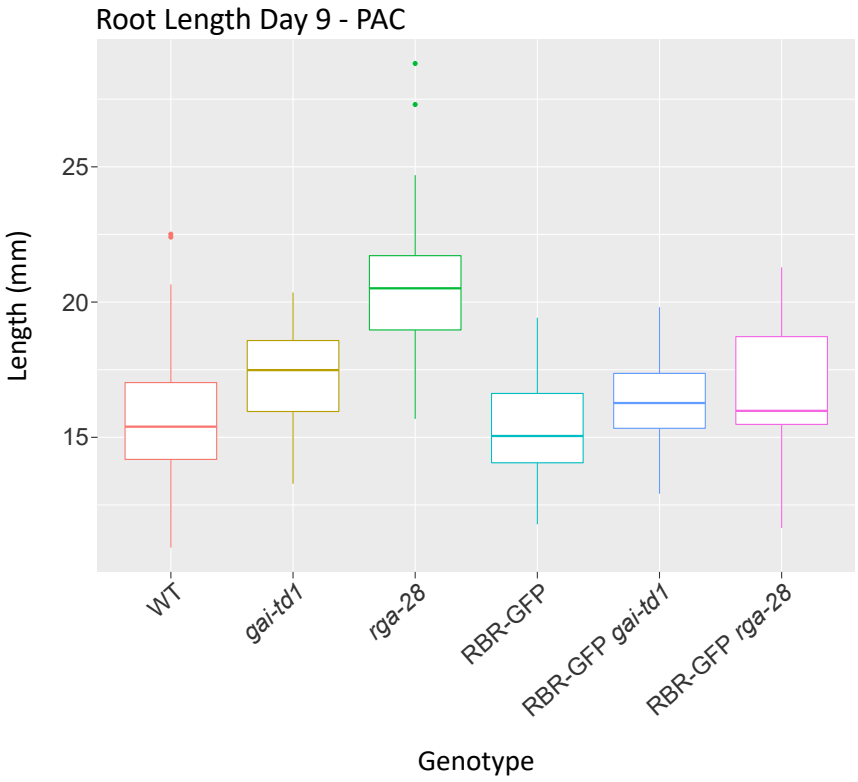
Root Length Day 9 - PAC
Length (mm)
15
20
25
WT
gai-td1
rga-28
RBR-GFP
RBR-GFP gai-td1
RBR-GFP rga-28
Genotype

D

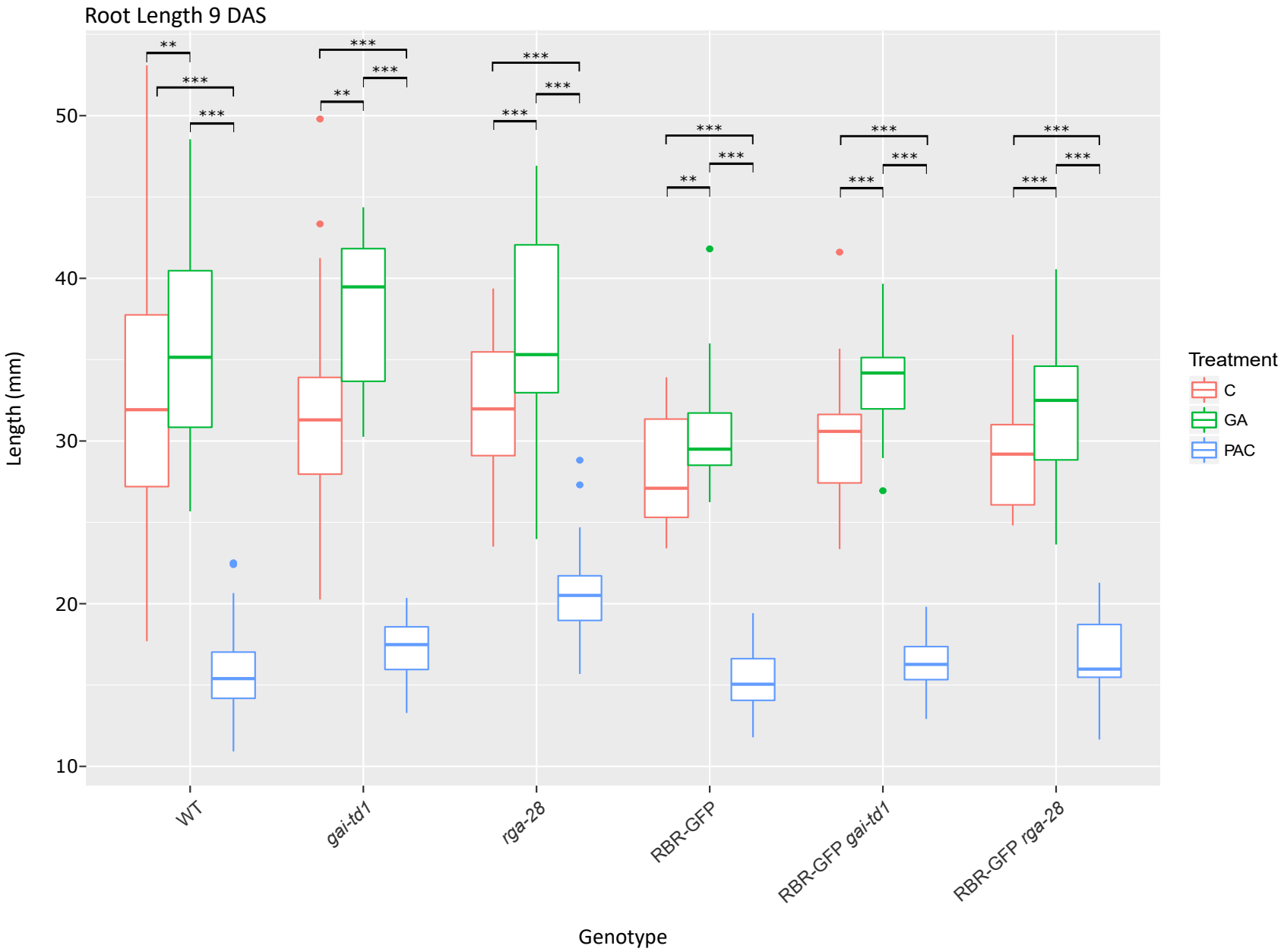
Root Length 9 DAS
Length (mm)
50
40
30
20
10
**
***
***
***
**
***
***
***
***
***
**
***
***
***
***
***
***
***
***
WT
gai-td1
rga-28
RBR-GFP
RBR-GFP gai-td1
RBR-GFP rga-28
Genotype
Treatment
C
GA
PAC

28 control lines as found in previous experiments. However, root growth for pRBR::RBR-GFP, pRBR::RBR-GFP *gai-td1* and pRBR::RBR-GFP *rga-28* seedlings did appear to be somewhat reduced in relation to the aforementioned controls, but did not vary substantially when comparing between them (Figure 4.4i).

To test these observations statistically, the association between root length and genotype was assessed with a LMER, which included the main effects of day and genotype, their interaction and a random effect of plate variability (Appendix 4.3A). The model output demonstrated that WT seedlings had a predicted root growth rate of 4.05 mm/day (Table 4.7), which was not significantly different to the predicted root growth rates of *gai-td1* (t_5 = -0.06, p = 0.949) and *rga-28* (t_5 = -0.72, p = 0.471). However, pRBR::RBR-GFP seedlings grew at a significantly decreased rate of 0.48 mm/day when compared to WT (t_5 = -3.57, p<0.001), followed by pRBR::RBR-GFP *rga-28* with a decrease of 0.36 mm/day (t_5 = -2.65, p<0.01) and pRBR::RBR-GFP *gai-td1* with a decrease of 0.29 mm/day (t_5 = -2.16, p<0.05). Analysis between these lines demonstrated no significant difference in the root growth rate of pRBR::RBR-GFP seedlings when compared to pRBR::RBR-GFP *gai-td1* (t_5 = 1.23, p = 0.22) and pRBR::RBR-GFP *rga-28* (t_5 = 081, p = 0.417), as well as no significant difference for pRBR::RBR-GFP *gai-td1* seedlings when compared to pRBR::RBR-GFP *rga-28* (t_5 = -0.42, p = 0.676).

Genotype	Root growth rate (mm/day)	Standard Error	t-value	p-value
WT (Col)	4.05	0.08	51.15	<0.001
gai-td1	4.05	0.11	37.28	<0.001
rga-28	3.96	0.11	35.94	<0.001
RBR::RBR-GFP	3.58	0.11	32.86	<0.001
RBR::RBR-GFP *gai-td1*	3.76	0.11	34.45	<0.001
RBR::RBR-GFP *rga-28*	3.70	0.11	34.07	<0.001

Table 4.7: Predicted daily root growth rates for each genotype from the control treatment determined by the statistical model (GLMM). For each calculation, there was one degree of freedom. Levels of significance are represented by: * p<0.05, ** P<0.01 and *** p<0.001. The p-value refers to the difference in growth rate between days.

Finally, the root growth rate of pRBR::RBR-GFP *gai-td1* seedlings was not significantly different to both *gai-td1* (t_5 = 1.84, p<0.1) and *rga-28* (t_5 = 1.25, p = 0.211). This was also the case for pRBR::RBR-GFP *rga-28* compared to *rga-28* (t_5 = 1.67, p <0.1), but there was a significant difference in the growth rate of pRBR::RBR-GFP *rga-28* compared to *gai-td1*, with a reduction of 0.35 mm/day (t_5 = 2.26, p<0.05). These differences can be visualised by plotting the predicted lines from the model for each genotype over the raw data (Figure 4.4Ci). To summarise, the root growth rates of the control lines, WT, *gai-td1*

and *rga-28* were relatively similar in the presence of endogenous GA levels. However, there was a reduction in root growth for pRBR::RBR-GFP, pRBR::RBR-GFP *gai-td1* and pRBR::RBR-GFP *rga-28* seedlings, but no significant differences when comparing between them. These findings imply that removal of RGA or GAI function in the pRBR::RBR-GFP translational reporter line does not confer different root phenotypes under these conditions. In general, the root growth rate of WT seedlings was lower than that of previous experiments, which may be indicative of different growth conditions (such as light intensity) as a result of growing these seedlings in a different environment.

In relation to the GA treatment, primary root growth from 2-9 DAS across all genotypes was found to be linear (Figure 4.4Aii). At the beginning of the experiment (2 DAS) the mean values across all genotypes did not appear to vary substantially, ranging between 2.88 – 4.21 mm. By 9 DAS *gai-td1* seedlings had the highest mean root length of 38.12 mm (SE = 1.101), followed by *rga-28* (mean = 36.31 mm, SE = 1.505), WT (mean = 35.48 mm, SE = 1.051), pRBR::RBR-GFP *gai-td1* (mean = 33.60 mm, SE = 0.792), pRBR::RBR-GFP *rga-28* (mean = 32.10 mm, SE = 0.996) and pRBR::RBR-GFP with the lowest mean of 30.66 mm (SE = 0.896). A similar trend was observed when plotting the data with boxplots for each genotype (Figure 4.4Cii). The variation of measurements around the median for WT, *gai-td1* and *rga-28* appeared to be greater than that of the other genotypes, as reflected by their increased standard errors when examining their mean values. In particular, the lower interquartile range for *gai-td1* was negatively skewed by an increased variability of lower root lengths, whereas the upper interquartile range for *rga-28* seedlings was positively skewed by an increased variability of higher root lengths.

Overall, there appeared to be a more substantial difference between the average root growth rates of WT, *gai-td1*, *rga-28* seedlings than the control treatment. Specifically, *gai-td1* had an increased average root growth rate in comparison to both *rga-28* and WT (Figure 4.4Aii). As was found for the control treatment, the average root growth rates of pRBR::RBR-GFP, pRBR::RBR-GFP *gai-td1* and pRBR::RBR-GFP *rga-28* seedlings were reduced in comparison to the aforementioned control lines. However, there was a slight increase in the growth of RBR::RBR-GFP *gai-td1* seedlings when compared to pRBR::RBR-GFP and pRBR::RBR-GFP *rga-28* (Figure 4.4Aii).

To test these observations statistically, the association between root length and genotype was assessed with a LMER, with the same parameters as defined for the control treatment (Appendix 4.3B). The model output demonstrated that WT seedlings had a predicted root growth rate of 4.43 mm/day (Table 4.8), which grew at a significantly reduced rate of 0.31 mm/day when compared to gai-td1 (t_5 = -2.24, $p<0.05$), but was not significantly different when compared to *rga-28* (t_5 = 0.67, p = 0.505). There was also no significant difference between the growth rates of *gai-td1* seedlings when

compared to *rga-28* (t_5 = -1.35, p = 0.179), even though the boxplots showed a difference between their median values and the predicted growth rate of *rga-28* was 0.22 mm/day less than *gai-td1*. When comparing the root growth rates of WT seedlings to pRBR::RBR-GFP, they grew at a significantly increased rate of 0.52 mm/day (t_5 = 3.66, p<0.001), followed by an increase of 0.38 mm/day when compared to pRBR::RBR-GFP *rga-28* (t_5 = 2.67, p<0.01). However, there was no significant difference in the root growth rates of WT and pRBR::RBR-GFP *gai-td1* seedlings (t_5 = 1.44, p = 0.149).

As expected, the model predicted that *gai-td1* seedlings had the highest root growth rate of 4.74 mm/day (Table 4.8), which was significantly different to pRBR::RBR-GFP with an increased rate of 0.83 mm/day (t_5 = 5.10, p<0.001), followed by pRBR::RBR-GFP *rga-28* with an increase of 0.69 mm/day (t_5 = 4.24, p<0.001) and pRBR::RBR-GFP *gai-td1* with an increase of 0.51 mm/day (t_5 = 3.19, p<0.01). Similar to the analysis of WT seedlings, *rga-28* seedlings grew at a significantly increased root growth rate of 0.62 mm/day in comparison to pRBR::RBR-GFP (t_5 = 3.74, p<0.001) and an increase of 0.47 mm/day when compared to pRBR::RBR-GFP *rga-28* (t_5 = 2.88, p<0.01), but there was no significant difference when comparing the growth of this line to RBR::RBR-GFP *gai-td1* (t_5 = -1.82, p = 0.069).

Genotype	Root growth rate (mm/day)	Standard Error	t-value	p-value
WT	4.43	0.08	55.02	<0.001
gai-td1	4.74	0.11	41.86	<0.001
rga-28	4.53	0.12	39.23	<0.001
pRBR::RBR-GFP	3.91	0.12	33.21	<0.001
pRBR::RBR-GFP *gai-td1*	4.23	0.11	37	<0.001
pRBR::RBR-GFP *rga-28*	4.05	0.12	34.64	<0.001

Table 4.8: Predicted daily root growth rates for each genotype from the GA treatment determined by the statistical model (GLMM). For each calculation, there was one degree of freedom. Levels of significance are represented by: * p<0.05, ** P<0.01 and *** p<0.001. The p-value refers to the difference in growth rate between days.

When analysing root growth rates between the pRBR::RBR-GFP lines, there was no significant difference for RBR::RBR-GFP compared to pPRBR::RBR-GFP *rga-28* (t_5 = 0.86, p = 0.39), as well as pRBR::RBR-GFP *gai-td1* compared to pRBR::RBR-GFP *rga-28* (t_5 = -1.09, p = 0.277). This was also found for pRBR::RBR-GFP compared to pRBR::RBR-GFP *gai-td1* (t_5 = 1.95, p = 0.051), which was not expected since the boxplots for root length at 9 DAS and the average root growth plots over time for these genotypes showed differences between them. However, it appears that the p-value as predicted by the model was just out of the range of significance, even though pRBR::RBR-GFP *gai-td1* seedlings had

an increased growth rate of 0.32 mm/day. Since there were no significant differences between the growth rates of these lines, this implies that removal of GAI or RGA function from the pRBR::RBR-GFP line does not confer different root phenotypes in the presence of increased GA levels. These differences can be visualised by plotting the predicted lines from the model for each genotype over the raw data (Figure 4.4Bii).

For the PAC treatment, root growth for all genotypes between 2-9 DAS was linear (Figure 4.4Aiii), but appeared to be substantially reduced when compared to both the control and the GA treatment (Figure 4.4D). At 2 DAS, the average root lengths across these lines appeared to be similar, ranging between 1.89 - 2.44 mm. By 9 DAS, there were more substantial differences between the average values with WT and pRBR::RBR-GFP seedlings having the shortest mean root lengths of 15.75 mm (SE = 0.402) and 15.19 mm (SE = 0.396), respectively. This was followed by pRBR::RBR-GFP *gai-td1* seedlings with a mean of 16.40 mm (SE = 0.358), RBR::RBR-GFP *rga-28* (mean = 17.02, SE = 0.516) and *gai-td1* (mean = 17.29, SE = 0.336). Finally, *rga-28* seedlings had the highest mean value of 20.85 (SE = 0.653). A similar of trend was observed when plotting the distribution of root lengths for each genotype with boxplots (Figure 4.4Ciii). The upper and lower interquartile ranges appeared to be closely distributed around the median for each genotype without being skewed, apart from the boxplot for pRBR::RBR-GFP *rga-28* seedlings that was positively skewed by an increased variation of larger root lengths. Overall, root growth of *rga-28* seedlings appeared to be substantially higher than that of the other genotypes, whilst WT and pRBR::RBR-GFP seedlings had the lowest root growth rates (Figure 4.4Aiii).

To test these observations statistically, the association between root length and genotype was assessed with a LMER, with the same parameters as defined for the control treatment (Appendix 4.3C). As expected, the model output demonstrated that *rga-28* seedlings had the highest predicted root growth rate of 2.64 mm/day (Table 4.9) that was significantly different to all the other genotypes. The greatest difference in growth rate when comparing this line was between RBR::RBR-GFP with a predicted decrease of 0.81 mm/day (t_5 = -9.6, p<0.001), followed by WT with a decrease of 0.8 mm/day (t_5 = -10.97, p<0.001), pRBR::RBR-GFP *gai-td1* with a decrease of 0.6 mm/day (t_5 = -7.19, p<0.001), *gai-td1* with a decrease of 0.56 mm/day (t_5 = -6.64, p<0.001) and pRBR::RBR-GFP *rga-28* with a decrease of 0.54 mm/day (t_5 = -.646, p<0.001). Both WT and pRBR::RBR-GFP had the lowest root growth rates of 1.84 mm/day (Table 4.9) that were not statistically different between them (t_5 = 0.06, p = 0.954). Furthermore, WT seedlings had a significantly decreased rate of 0.26 mm/day when compared to pRBR::RBR-GFP *rga-28* (t_5 = -3.56, p<0.001), followed by a reduction of 0.25 mm/day when compared to *gai-td1* (t_5 = -3.40, p<0.001) and a reduction of 0.2 mm/day in relation to pRBR::RBR-GFP *gai-td1* (t_5 = -2.78, p<0.01). There was also a significant difference in the predicted root growth rates of *gai-td1*

seedlings when compared to pRBR::RBR-GFP, with an increased rate of 0.25 mm/day (t_5 = 3, p<0.01). However, there was no significant difference for the root growth rate of *gai-td1* seedlings when compared to both pRBR::RBR-GFP *gai-td1* (t_5 = -0.54, p= 0.586) and pRBR::RBR-GFP *rga-28* (t_5 = 0.15, p = 0.877).

Genotype	Root growth rate (mm/day)	Standard Error	t-value	p-value
WT	1.84	0.043	42.90	<0.001
gai-td1	2.09	0.059	35.36	<0.001
rga-28	2.64	0.06	44.45	<0.001
pRBR::RBR-GFP	1.84	0.06	30.73	<0.001
pRBR::RBR-GFP *gai-td1*	2.04	0.06	34.61	<0.001
pRBR::RBR-GFP *rga-28*	2.10	0.06	35.29	<0.001

Table 4.9: Predicted daily root growth rates for each genotype from the PAC treatment determined by the statistical model (GLMM). For each calculation, there was one degree of freedom. Levels of significance are represented by: * p<0.05, ** P<0.01 and *** p<0.001. The p-value refers to the difference in growth rate between days.

Analysis of the root growth for pRBR::RBR-GFP seedlings revealed they had a significantly decreased rate of 0.27 mm/day when compared to pRBR::RBR-GFP *rga-28* (t_5 = -3.14, p<0.01), followed by a decreased rate of 0.2 mm/day when compared to pRBR::RBR-GFP *gai-td1* (t_5 = -2.46, p<0.05). However, there was no significant difference between the predicted root growth rates of pRBR::RBR-GFP *gai-td1* and pRBR::RBR-GFP *rga-28* seedlings (t_5 = 0.7, p = 0.486). These differences were visualised by plotting the predicted lines from the model for each genotype over the raw data (Figure 4.4Biii). Overall, the results showed that decreasing endogenous GA levels by treating with PAC resulted in different root growth phenotypes between WT, *gai-td1* and *rga-28* seedlings, with WT having the greatest reduction in root growth rate, followed by *gai-td1* and *rga-28*. These findings are reflective of previous experiments where removal of RGA/GAI function in a GA-biosynthetic mutant background partially rescued its reduced root growth phenotype. This is because DELLA levels for this line were already high due to a lack of GA inhibition, so removal of one of these proteins reduces their inhibitory effect on root growth. Furthermore, removal of either RGA or GAI function in the pRBR::RBR-GFP background was sufficient to partially rescue its reduced growth phenotype, but did not confer different root phenotypes when comparing between them, suggesting that they are functionally redundant in this context.

To analyse root growth rates for each genotype between treatments, the association between length and the specified genotype was assessed with an LMER, which included the main effects of day and

treatment, their interaction and a random effect of plate variability (Appendix 4.3D-H). The model outputs demonstrated that each genotype grew at a statistically reduced rate under PAC in comparison to both the control and GA treatment (Figure 4.4D). Furthermore, GA treatment resulted in a significantly increased root growth rates across all genotypes when compared to the control (Figure 4.4D). For more detailed analysis of predicted root growth rates and their differences between treatments please see Appendix 4.3I.

4.2.4 Removal of RGA and GAI function confers different root phenotypes when the cell cycle inhibitor, KRP2, is overexpressed

Since previously described experiments demonstrated that removal of either GAI or RGA function in the pRBR::RBR-GFP translational reporter line did not confer any differences between their root phenotypes, crosses were performed between the null mutant lines, *gai-td1* and *rga-28*, to the cell cycle overexpresser, 35S::KRP2-GFP. This was done to examine the effect of removing GAI and RGA function when the amount of un-phosphorylated RBR was substantially increased by overexpressing KRP2, which is an inhibitor of the CDK complexes that phosphorylate RBR. The 35S::KRP2-GFP line was also crossed to the *ga1-t* null mutant in order to examine the opposing effect of increased DELLA levels on the phenotype of this line. As mentioned previously, 35S::KRP2-GFP seedlings have a severely impaired growth phenotype, suggesting that their rate of root elongation is substantially reduced when compared to WT seedlings. The aforementioned crosses were therefore generated to examine potential differences between their root growth phenotypes in order to further our understanding of how GAI and RGA are related to the cell cycle. The F2 progeny were established and genotyped to identify lines homozygous for either *gai-td1*, *rga-28* or *ga1-t* (depending on the cross) and viewed under the microscope for GFP florescence to identify lines expressing KRP2-GFP. Once these lines were selected, multiple F3 seedlings from each cross were viewed under a florescent microscope to identify lines that were also homozygous for 35S::KRP2-GFP. In the case of *ga1-t* crossed to 35S::KRP2-GFP, F2 lines homozygous for *ga1-t* were identified, but none of the F3 populations examined were homozygous for 35S::KRP2-GFP. When taken to subsequent generations, this line was continually segregating for KRP2-GFP, thus implying that the homozygote for both *ga1-t* and 35S::KRP2-GFP was somehow lethal. Indeed, from examining the siliques of these plants, embryo lethality was observed (Figure 4.5). For the other crosses, double homozygote lines for both 35S::KRP2-GFP *rga-28* and 35S::KRP2-GFP *gai-td1* were obtained. It was noticed whilst growing these plants on soil that 35S::KRP2-GFP *rga-28* seedlings had a phenotype similar to that of WT, whilst 35S::KRP2-GFP *gai-td1* seedlings had a similar reduced growth phenotype to that of 35S::KRP2-GFP alone (Figure 4.8A).

Figure 4.5 Representative images of embryo lethality observed in siliques from plants homozygous for *ga1-t*, but segregating for 35S::KRP2-GFP. These plants were checked for GFP expression prior to transplanting to soil so they contain a single copy of 35S::KRP2-GFP. The white arrows indicate individual aborted embryos. A representative example of a WT silique is provided below showing no example of embryo lethality.

A

ga1-t 35SKRP2-GFP

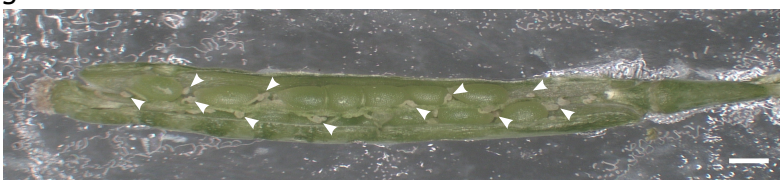

ga1-t 35SKRP2-GFP

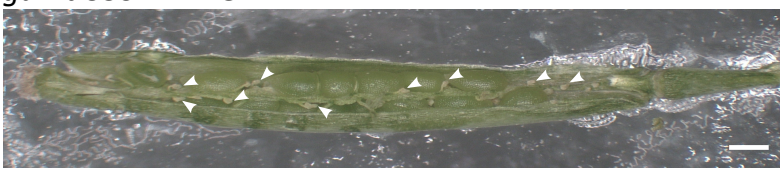

ga1-t 35SKRP2-GFP

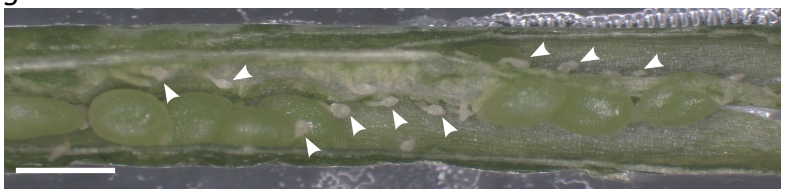

Col-0 WT

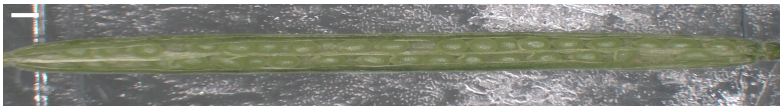

To investigate these phenotypic differences further, high-throughput root growth experiments of WT, 35S::KRP2-GFP, 35S::KRP2-GFP *gai-td1* and 35S::KRP2-GFP *rga-28* seedlings were performed using the same facilities provided by the GMI. For each mutant line, a total of 24 seedlings were grown alongside WT and other mutant lines, distributed in different positions across 8 plates (i.e. 3 mutant seedlings grown against 3 WT and other mutant lines per plate). Primary root growth was measured consecutively from 2-9 DAS using the previously described root phenotyping pipeline. Furthermore, a series of treatment experiments were set up to alter endogenous GA levels and examine the effect this had on the root growth phenotypes of these lines. As was done previously, all seeds were pre-treated with 2.5 µM of GA_3 until they had germinated at 1 DAS and then transferred to the different treatment conditions, including control growth media and the same media supplemented with either 10 µM of GA_3 or 1 µM of PAC.

In terms of the control treatment, primary root growth from 2-9 DAS across all genotypes was found to be linear (Figure 4.5Ai). On the first day of the experiment (2 DAS), seedlings of all genotypes had a similar size in root length with mean values approximately the same, ranging between 3.31 - 4.56 mm. On the final day of the experiment at 9 DAS, 35S::KRP2-GFP seedlings had the shortest mean root length of 23.02 mm (SE = 1.03), followed by 35S::KRP2-GFP *gai-td1* (mean = 28.55 mm, SE = 1.178), 35S::KRP2-GFP *rga-28* (mean = 33.39 mm, SE =0.842) and WT (mean = 34.97 mm, SE = 1.272) seedlings. A similar trend was also observed when plotting the median root lengths and interquartile ranges for each genotype with boxplots (Figure 4.5Ci). Overall, it appears there were substantial differences between the root growth rates of these mutant lines, which was evident from plotting the mean root lengths for each genotype over time (Figure 4.5Ai). The slope of the fitted lines indicated that WT seedlings had the highest average root growth rate followed by 35S::KRP2-GFP *rga-28,* 35S::KRP2-GFP *gai-td1* and 35S::KRP2-GFP.

To test these findings statistically, the association between length and genotype was assessed with a LMER, which included the main effects of day and genotype, their interaction and a random effect of plate variability (Appendix 4.4A). The model output showed that root length between days was significantly different, with WT seedlings growing at a rate of 4.15 mm per day (Table 4.10). As expected, there was a significant reduction in the root growth rate of 35S::KRP2-GFP seedlings when compared to WT, with a decrease of 1.52 mm per day (t_3= -10.32, $p<0.001$). Furthermore, 35S::KRP2-GFP *gai-td1* seedlings grew at a significantly reduced rate of 0.86 mm less than WT per day (t_3= -5.74, $p<0.001$). However, there was no significant difference between the root growth rate of 35S::KRP2-GFP *rga-28* seedlings, when compared to WT (t_3= -0.52, p = 0.601). When comparing between the different 35S::KRP2-GFP lines, the root growth rate of 35S::KRP2-GFP *rga-28* seedlings was

significantly greater than that of both 35S::KRP2-GFP *gai-td1* and 35S::KRP2-GFP, with an increase of 0.78 mm/day (t_3= 5.47, p<0.001) and 1.44 mm/day (t_3 = 10.26, p<0.001), respectively. Furthermore, 35S::KRP2-GFP *gai-td1* roots grew at a significantly increased rate of 0.66 mm/day when compared to 35S::KRP2-GFP (t_3 = 4.54, p<0.001). These differences are clearly demonstrated by plotting the predicted lines from the model for each genotype over the raw data (Figure 4.5Bi). Indeed, the lines appear to fit with the raw data plots, showing the same trends and similar slopes to the fitted lines for the mean root lengths plotted over time. To conclude, WT and 35S::KRP2-GFP *rga-28* seedlings had similar root growth rates, whereas 35S::KRP2-GFP *gai-td1* and 35S::KRP2-GFP seedlings had significantly reduced root growth rates. Therefore, removal of RGA function from the 35S::KRP2-GFP line is sufficient to rescue its reduced growth phenotype.

Genotype	Root growth rate (mm/day)	Standard Error	t-value	p-value
WT	4.15	0.108	38.58	<0.001
35S::KRP2-GFP	2.63	0.107	26.25	<0.001
35S::KRP2-GFP *gai-td1*	3.29	0.104	31.54	<0.001
35S::KRP2-GFP *rga-28*	4.08	0.098	41.44	<0.001

Table 4.10: Predicted daily root growth rates for each genotype from the control treatment determined by the statistical model (GLMM). For each calculation, there was one degree of freedom. Levels of significance are represented by: * p<0.05, ** P<0.01 and *** p<0.001. The p-value refers to the difference in growth rate between days.

For the GA treatment, primary root growth from 2-9 DAS across all genotypes was found to be linear (Figure 4.5Aii). On the first day of the experiment (2 DAS), seedlings of all genotypes had relatively similar sizes in mean root length with values ranging between 3.1 - 4.3 mm. On the final day of the experiment at 9 DAS, 35S::KRP2-GFP *gai-td1* seedlings had the shortest mean root length of 22.67 mm (SE =0.864), followed by 35S::KRP2-GFP (mean = 26.22 mm, SE = 1.018), 35S::KRP2-GFP *rga-28* (mean = 31.84 mm, SE = 1.133) and WT (mean = 36.05 mm, SE = 1.222). A similar trend was also observed when plotting the distribution of root lengths for this day with boxplots (Figure 4.5Bii). Most of the boxplots indicated that the data for each genotype was relatively condensed around themedian, but for WT seedlings the boxplot was negatively skewed by an increased variability of lower root lengths. Overall, these differences in growth are shown by plotting the mean root lengths for each genotype over time, with WT seedlings having the highest average root growth rate, followed by 35S::KRP2-GFP *rga-28,* 35S::KRP2-GFP and 35S::KRP2-GFP *gai-td1*. (Figure 4.5Aii).

To test these findings statistically, the association between length and genotype was assessed with a LMER, with the same parameters as defined for the control treatment (Appendix 4.4B). The model

Figure 4.6 Analysis of root growth for *Col-0* WT, 35S::KRP2-GFP, 35S::KRP2-GFP *gai-td1* and 35S::KRP2-GFP *rga-28* seedlings from 2-9 days after stratification (DAS). All of these lines were germinated on 2.5 µM of GA_3 and transferred to fresh plates 1 DAS. Seedlings were subject to different treatments: (i) control, (ii) 10 µM of GA_3 and (iii) 1 µM of PAC and are represented by:

(A) Average root length for each genotype plotted over time fitted with a linear trendline

(B) The predicted lines for root length over time per genotype as determined by the statistical model used to analyse the data and plotted over the raw data values

(C) Boxplots for each genotype over time, with the final day enlarged for better visualisation of the distribution of root lengths. The boxplots show the median value as represented by the dividing line, as well as the lower and upper interquartile ranges, with whiskers extending 1.5 times the interquartile range.

A (i)

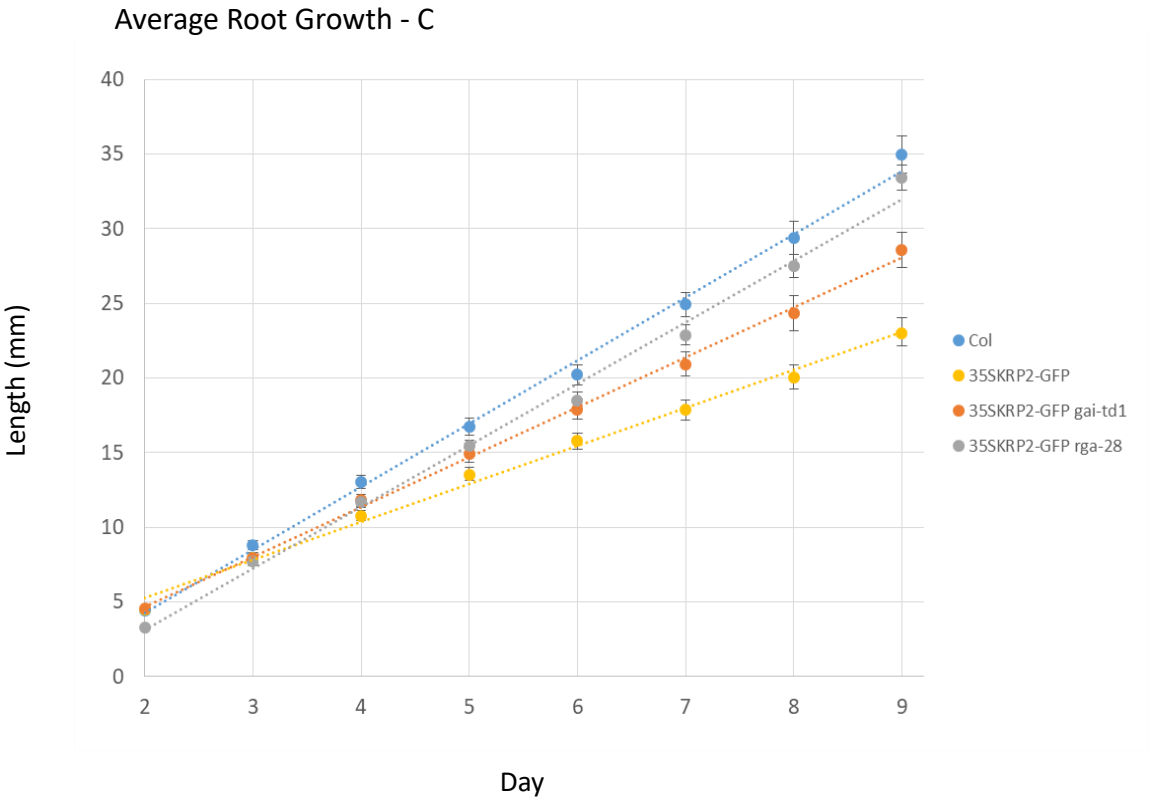
Average Root Growth - C
Length (mm)
Day
Col
35SKRP2-GFP
35SKRP2-GFP gai-td1
35SKRP2-GFP rga-28

B (i)

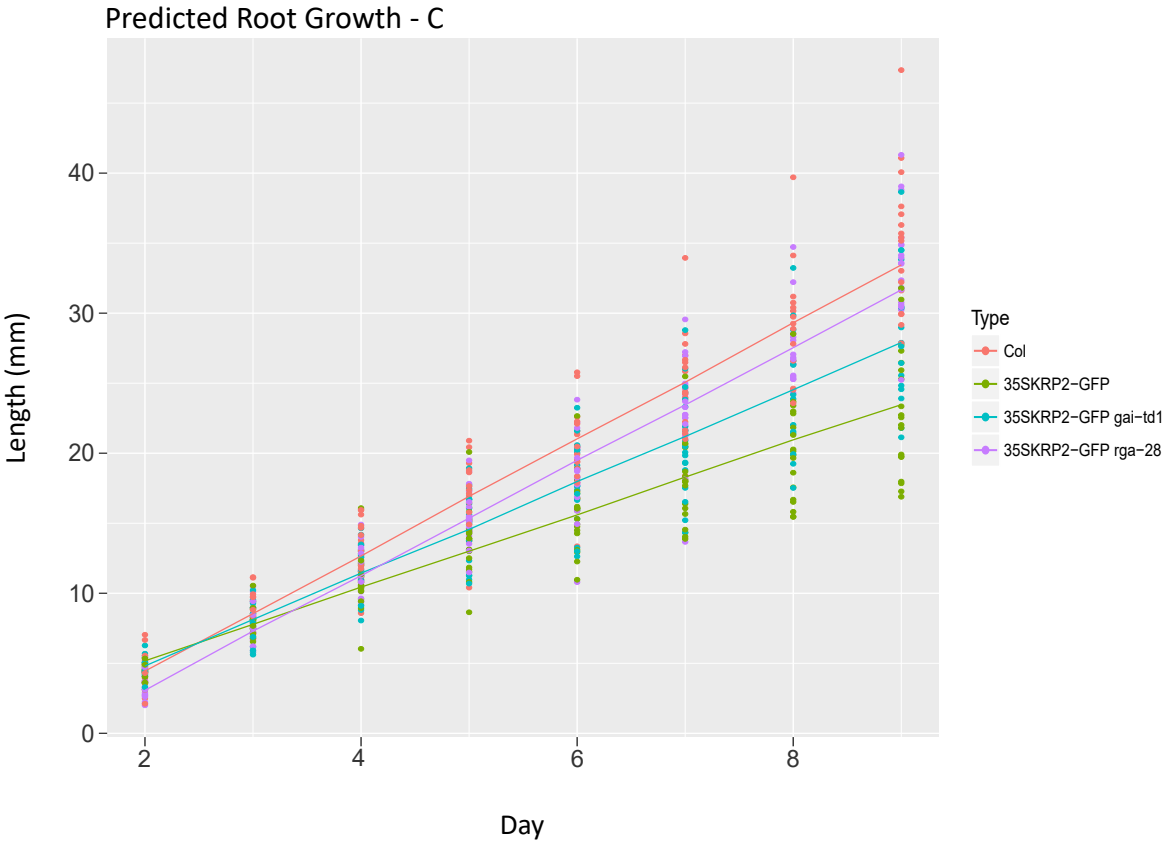
Predicted Root Growth - C
Length (mm)
Day
Type
Col
35SKRP2-GFP
35SKRP2-GFP gai-td1
35SKRP2-GFP rga-28

C (i)

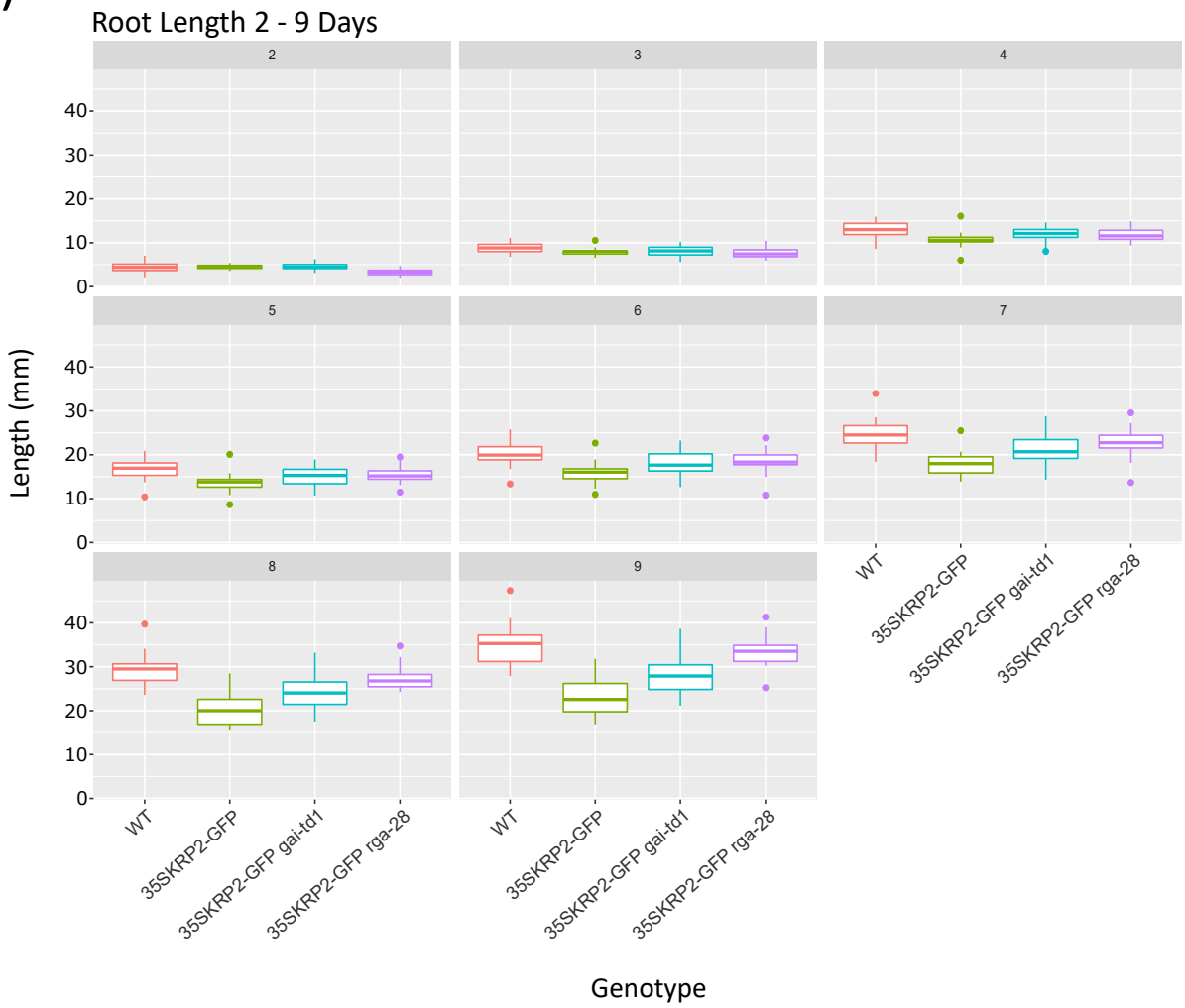
Root Length 2 - 9 Days
2
3
4
5
6
7
8
9
Length (mm)
0
10
20
30
40
WT
35SKRP2-GFP
35SKRP2-GFP gai-td1
35SKRP2-GFP rga-28
Genotype

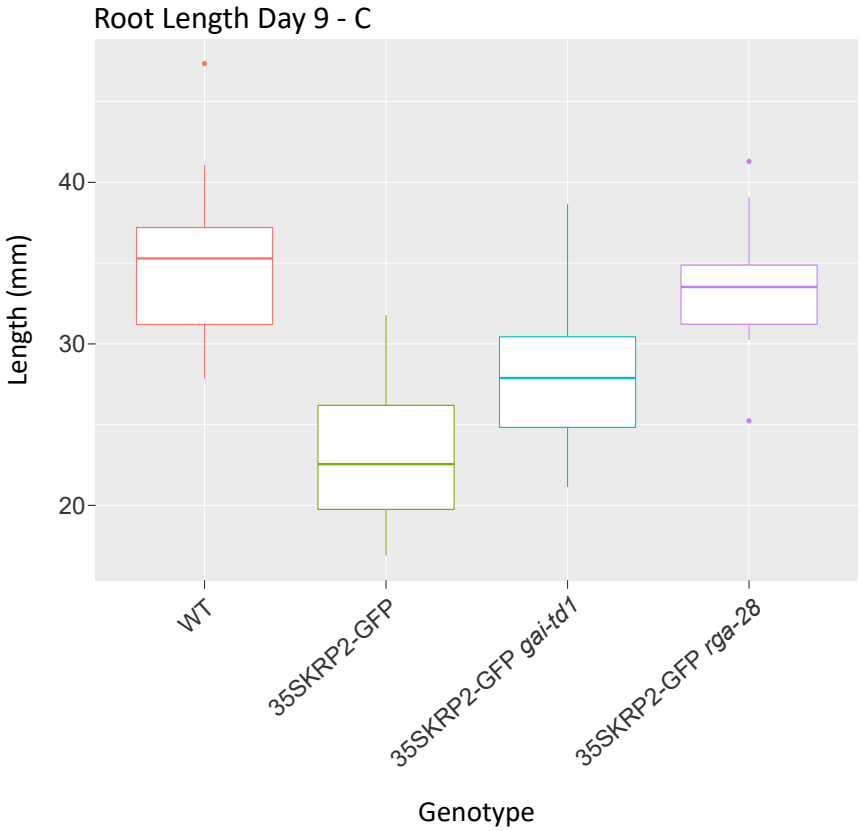
Root Length Day 9 - C
Length (mm)
20
30
40
WT
35SKRP2-GFP
35SKRP2-GFP gai-td1
35SKRP2-GFP rga-28
Genotype

A (ii)

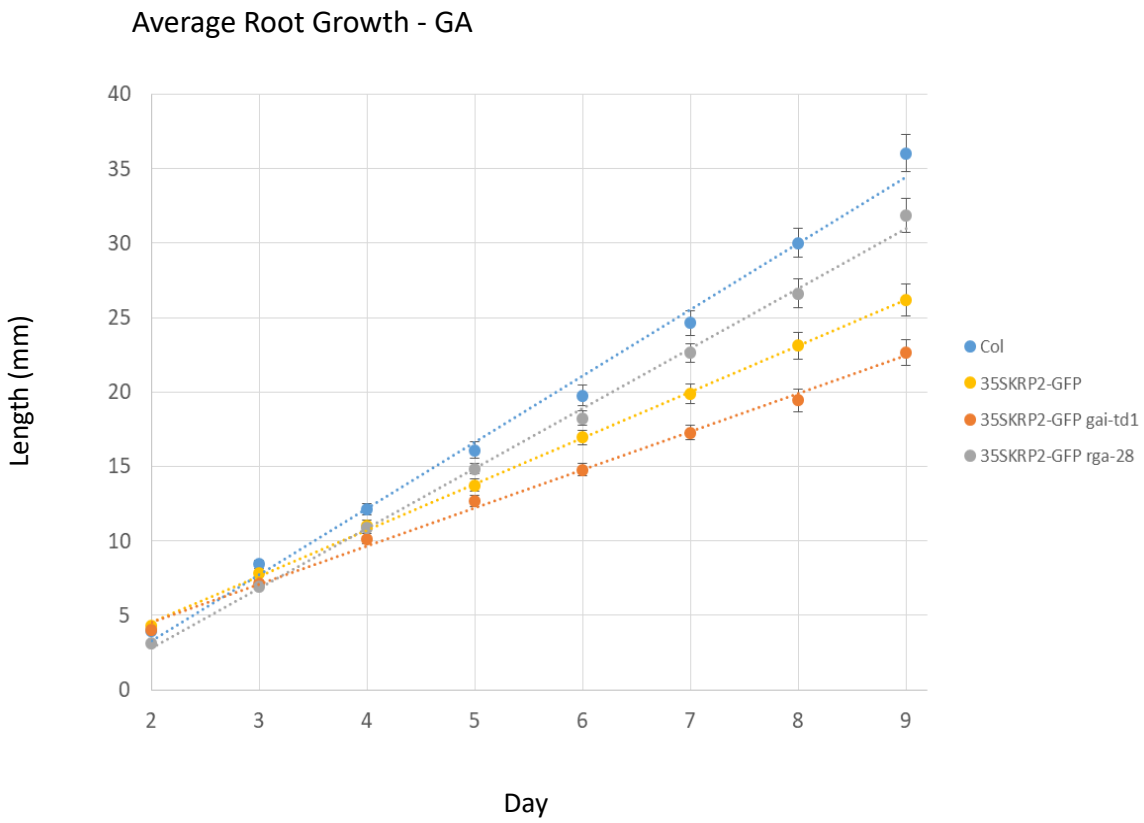
Average Root Growth - GA
Length (mm)
40
35
30
25
20
15
10
5
0
2
3
4
5
6
7
8
9
Day
Col
35SKRP2-GFP
35SKRP2-GFP gai-td1
35SKRP2-GFP rga-28

B (ii)

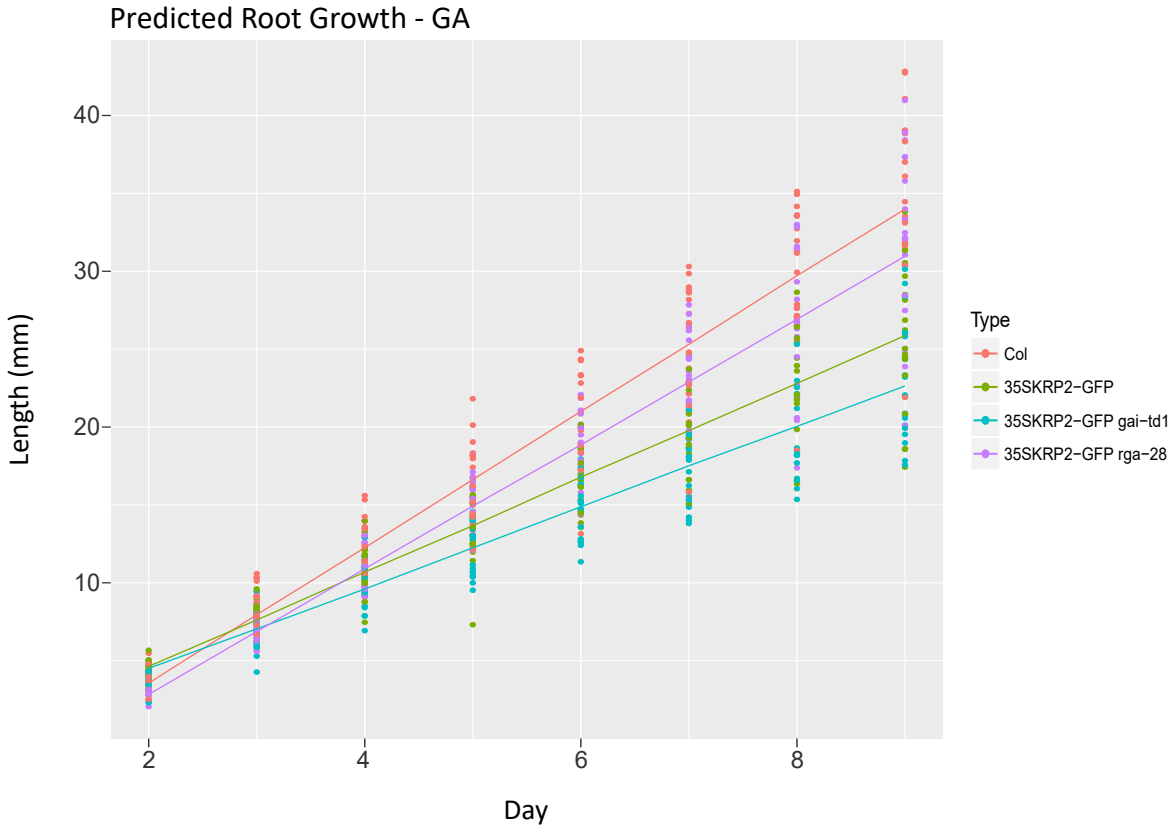
Predicted Root Growth - GA
Length (mm)
40
30
20
10
2
4
6
8
Day
Type
Col
35SKRP2-GFP
35SKRP2-GFP gai-td1
35SKRP2-GFP rga-28

C (ii)

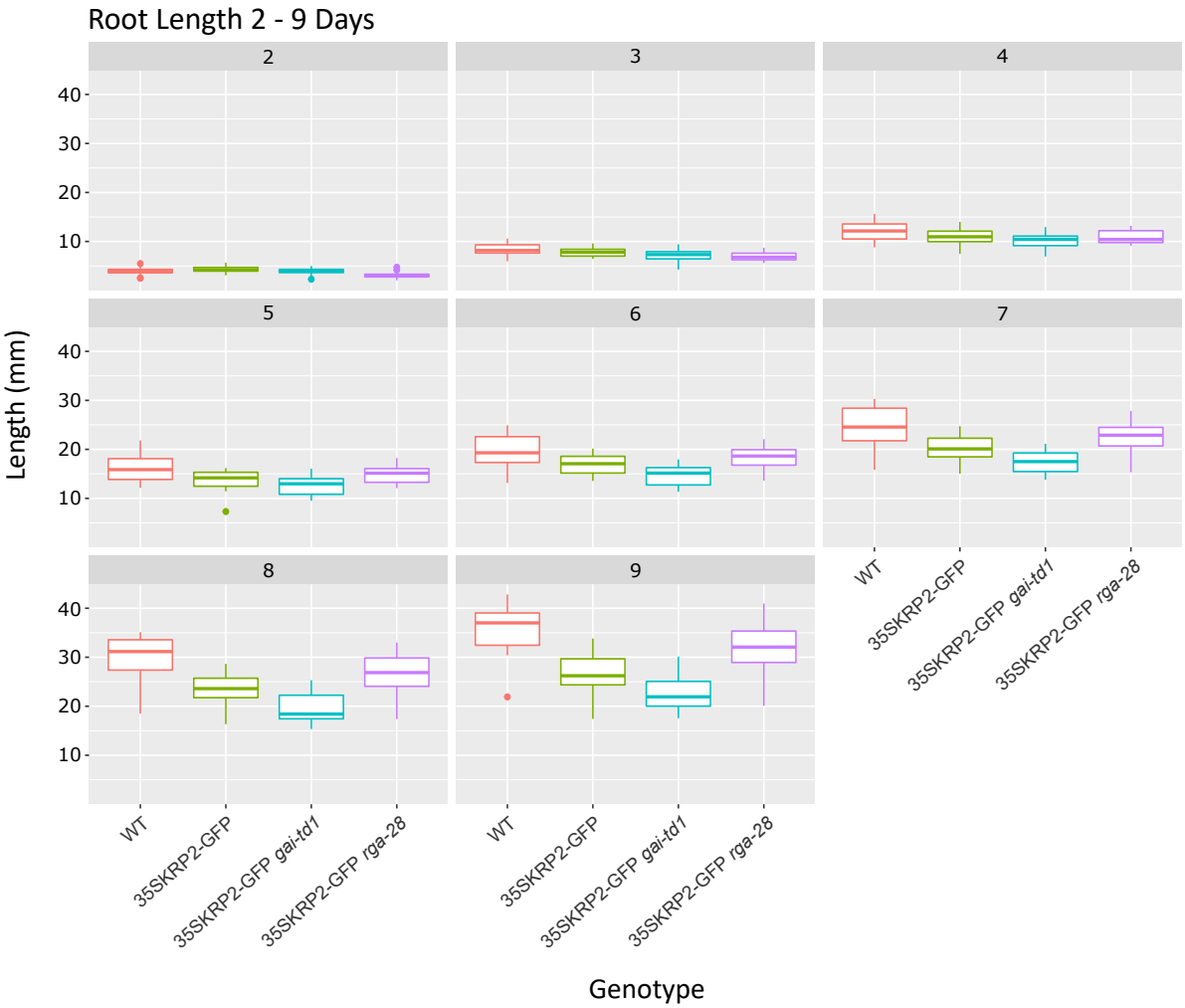
Root Length 2 - 9 Days
2
3
4
5
6
7
8
9
Length (mm)
40
30
20
10
WT
35SKRP2-GFP
35SKRP2-GFP gai-td1
35SKRP2-GFP rga-28
Genotype

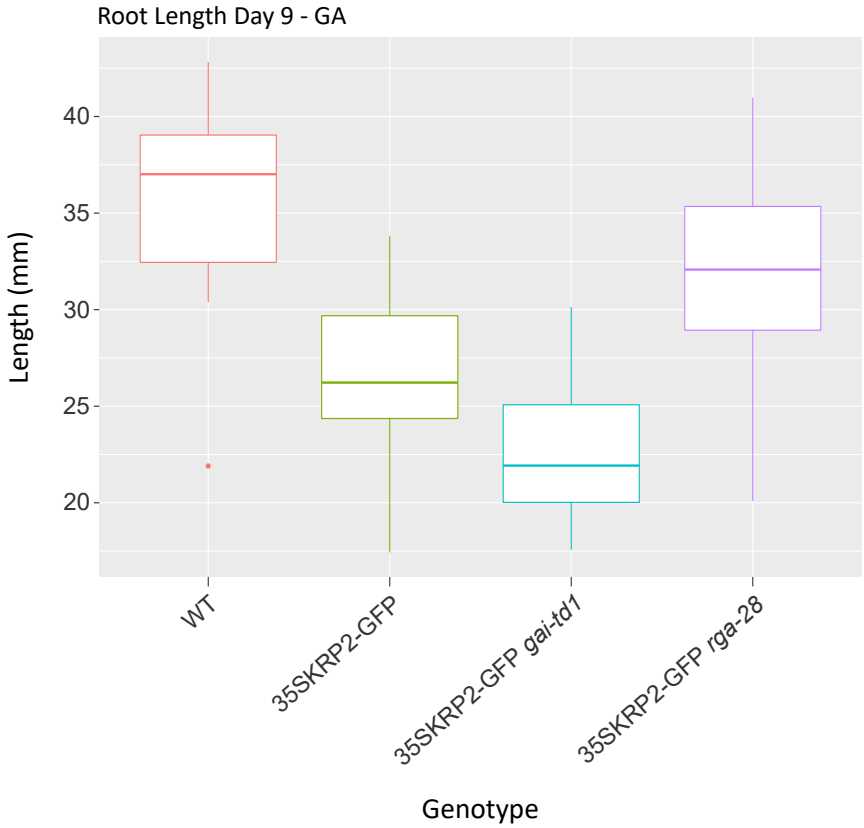
Root Length Day 9 - GA
Length (mm)
40
35
30
25
20
WT
35SKRP2-GFP
35SKRP2-GFP gai-td1
35SKRP2-GFP rga-28
Genotype

A (iii)

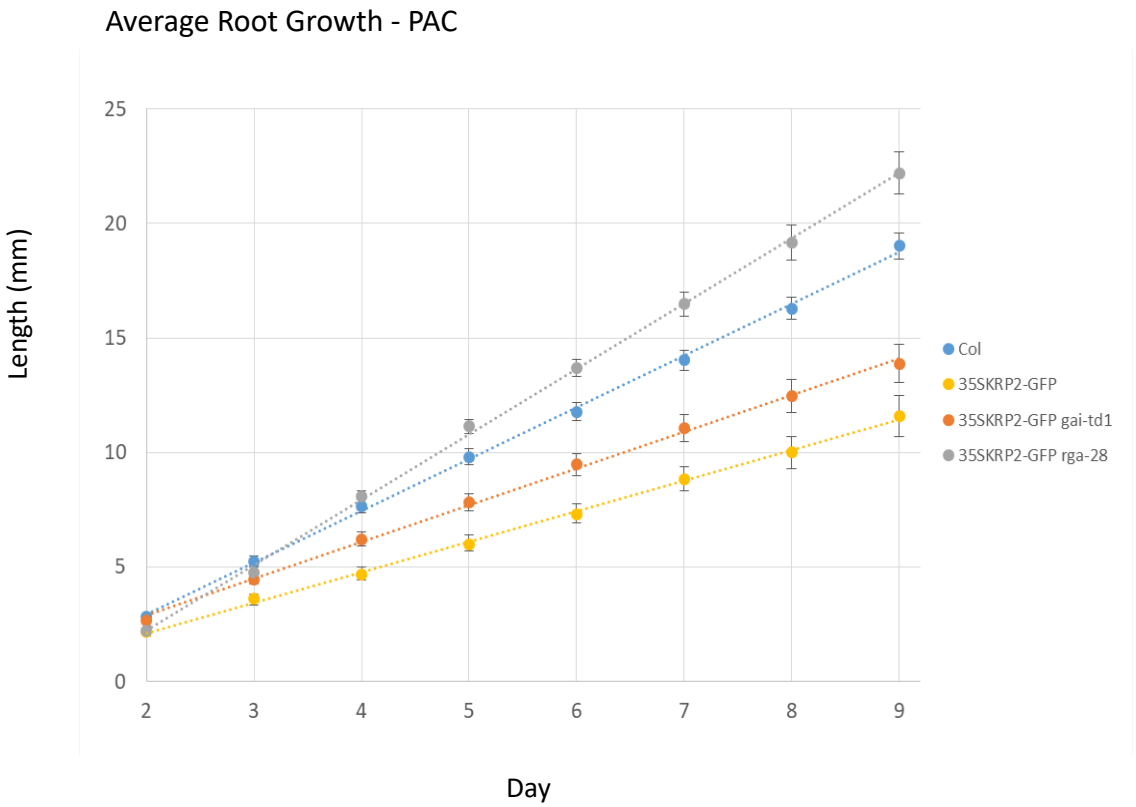
Average Root Growth - PAC
Length (mm)
25
20
15
10
5
0
2
3
4
5
6
7
8
9
Day
Col
35SKRP2-GFP
35SKRP2-GFP gai-td1
35SKRP2-GFP rga-28

B (iii)

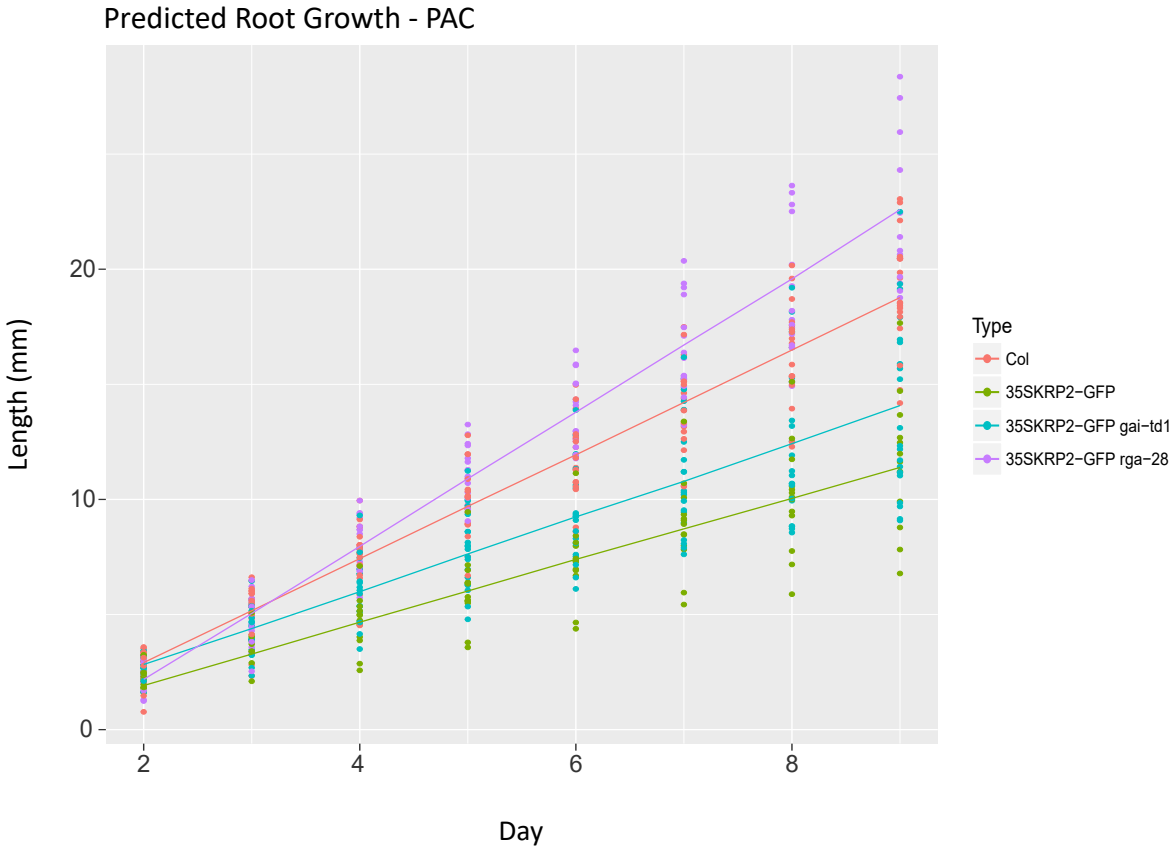
Predicted Root Growth - PAC
Length (mm)
20
10
0
2
4
6
8
Day
Type
Col
35SKRP2-GFP
35SKRP2-GFP gai-td1
35SKRP2-GFP rga-28

C (iii)

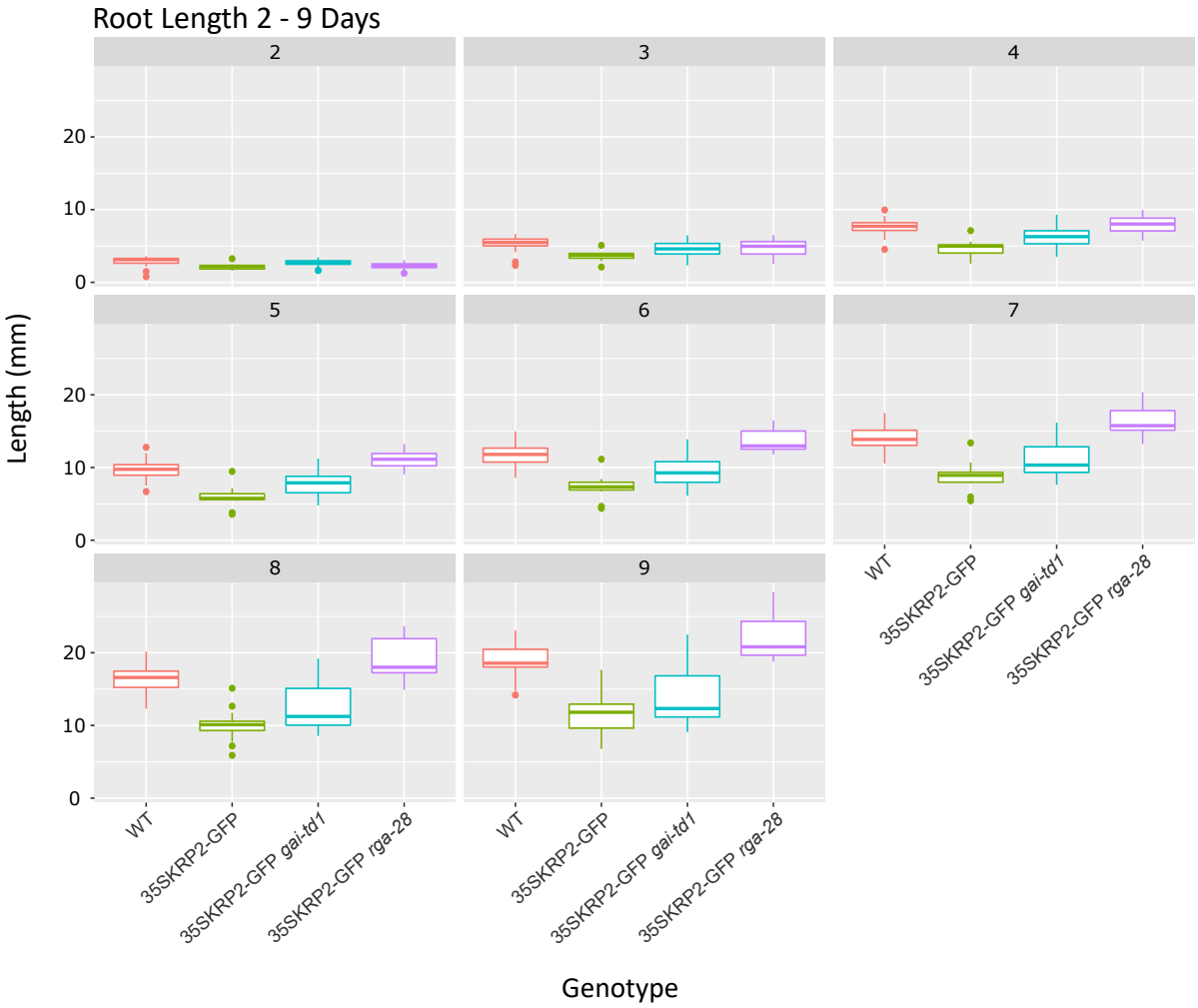
Root Length 2 - 9 Days
2
3
4
5
6
7
8
9
Length (mm)
0
10
20
WT
35SKRP2-GFP
35SKRP2-GFP gai-td1
35SKRP2-GFP rga-28
Genotype

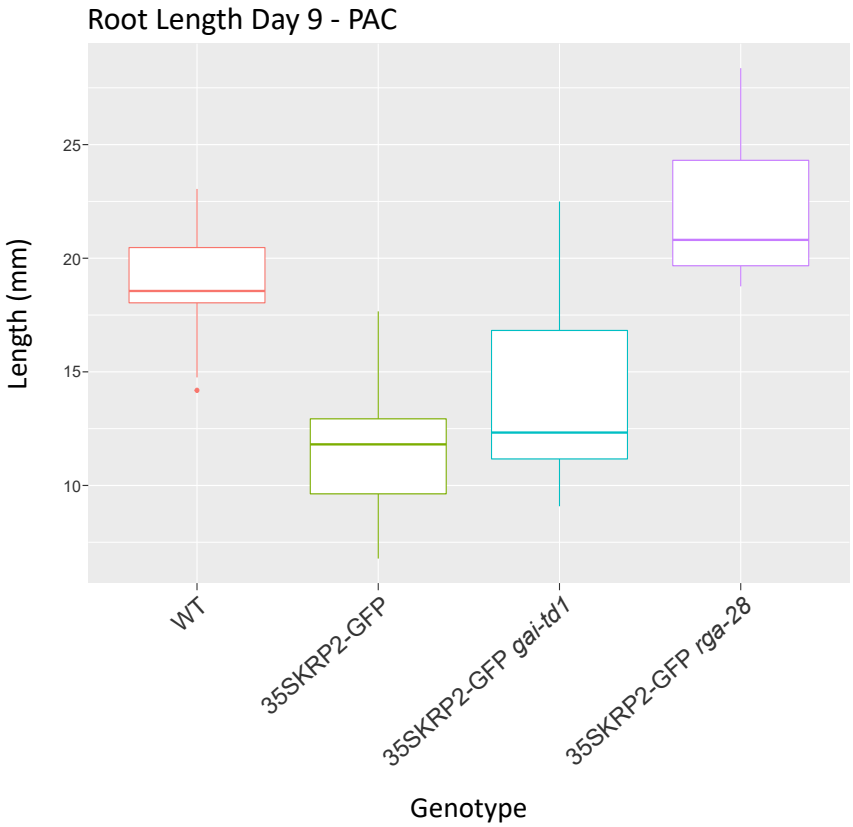
Root Length Day 9 - PAC
Length (mm)
10
15
20
25
WT
35SKRP2-GFP
35SKRP2-GFP gai-td1
35SKRP2-GFP rga-28
Genotype

D

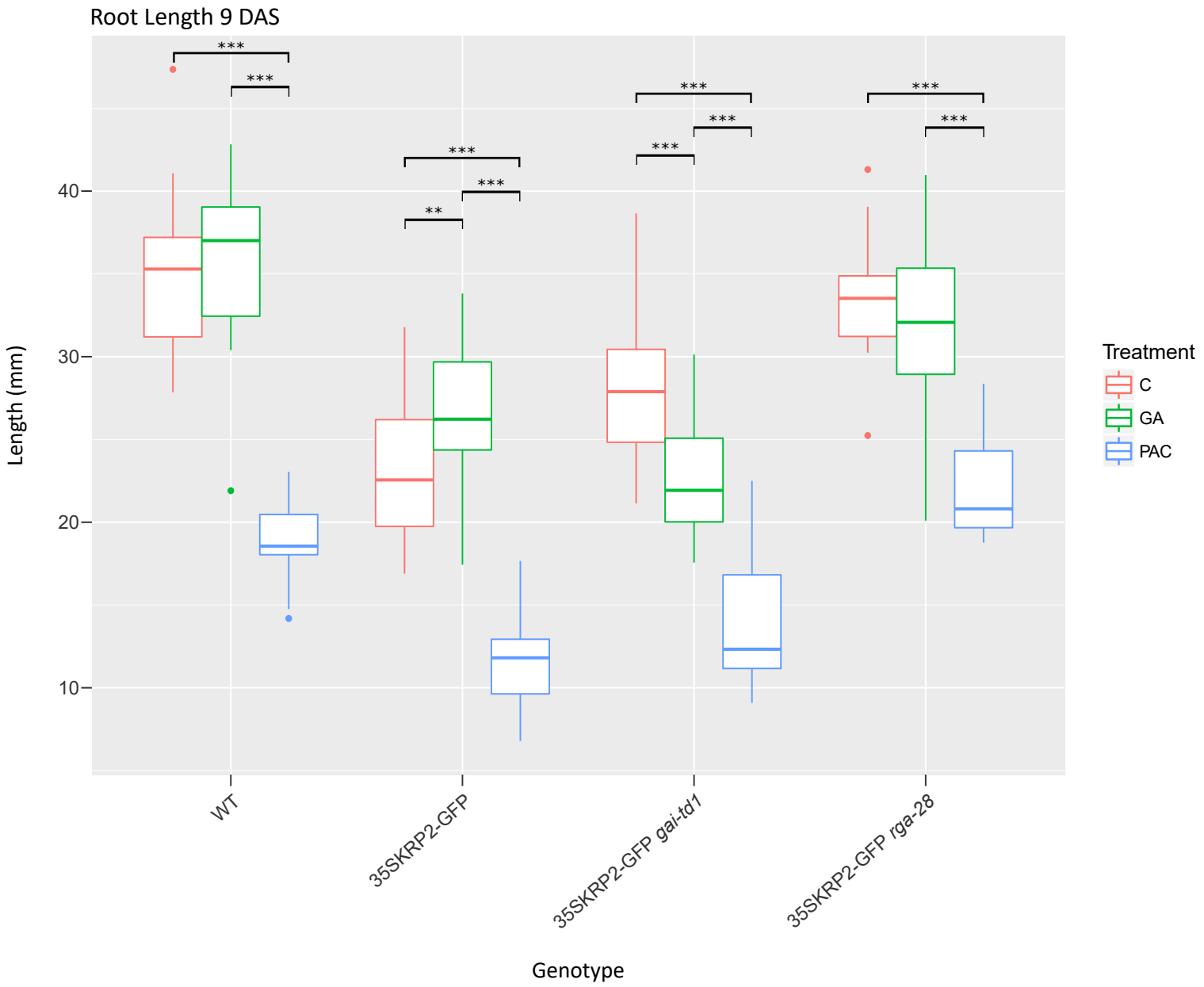
Root Length 9 DAS
Length (mm)
40
30
20
10
***
***
***
***
**
***
***
***
***
***
WT
35SKRP2-GFP
35SKRP2-GFP gai-td1
35SKRP2-GFP rga-28
Genotype
Treatment
C
GA
PAC

outcome showed that root length between days was significantly different, with WT seedlings growing at a rate of 4.36 mm per day (Table 4.11). As was found for the control treatment, there was a significant reduction in the root growth rate of 35S::KRP2-GFP seedlings when compared to WT, with a decrease of 1.33 mm per day (t_3= -9.54, p<0.001). In contrast to the control treatment, 35S::KRP2-GFP *gai-td1* seedlings had the lowest root growth rate in comparison to all the other genotypes and grew at a significantly reduced rate of 1.76 mm less than WT per day (t_3= -12.74, p<0.001). Furthermore, there was a significant difference in the growth rates of 35S::KRP2-GFP *rga-28* seedlings when compared to WT, which grew at a reduced rate of 0.35 mm/day (t_3= -2.57, p = <0.05). When comparing between the different 35S::KRP2-GFP lines, the root growth rate of 35S::KRP2-GFP *rga-28* was significantly greater than both 35S::KRP2-GFP *gai-td1* and 35S::KRP2-GFP, with an increase of 1.42 mm/day (t_3 = 10.11, p<0.001) and 0.97 mm/day (t_3= 6.96, p<0.001), respectively. Furthermore, 35S::KRP2-GFP *gai-td1* roots grew at a significantly decreased rate of 0.43 mm/day when compared to 35S::KRP2-GFP (t_3 = 3.07, p<0.01).

Genotype	Root growth rate (mm/day)	Standard Error	t-value	p-value
WT	4.36	0.096	45.26	<0.001
35S::KRP2-GFP	3.03	0.10	30.24	<0.001
35S::KRP2-GFP *gai-td1*	2.60	0.099	26.22	<0.001
35S::KRP2-GFP *rga-28*	4.01	0.098	40.99	<0.001

Table 4.11: Predicted daily root growth rates for each genotype from the GA treatment determined by the statistical model (GLMM). For each calculation, there was one degree of freedom. Levels of significance are represented by: * p<0.05, ** P<0.01 and *** p<0.001. The p-value refers to the difference in growth rate between days.

By plotting these differences as the predicted lines for each genotype over the raw data, it was evident they had similar slopes to the fitted lines for the mean values plotted over time (Figure 4.4Bii). As for the control treatment, WT seedlings had the highest root growth rate, followed by 35S::KRP2-GFP *rga-28* seedlings. The difference between these growth rates appeared to more substantial than the control treatment as demonstrated by their significant differences. Furthermore, 35S::KRP2-GFP *gai-td1* seedlings had the lowest root growth rate, followed by 35S::KRP2-GFP, which was the opposite finding to the control treatment. Overall, the recuse phenotype observed for 35S::KRP2-GFP *rga-28* seedlings was still present under this treatment.

In terms of PAC treatment, primary root growth from 2-9 DAS across all genotypes was found to be linear (Figure 4.5Aii). On the first day of the experiment (2 DAS), seedlings of all genotypes had a similar size in root length with mean values approximately the same, ranging between 2.17 - 2.84 mm.

On the final day of the experiment at 9 DAS, 35S::KRP2-GFP seedlings had the shortest mean root length of 11.61 mm (SE =0.875), followed by 35S::KRP2-GFP *gai-td1* (mean = 13.88 mm, SE = 0.836), WT (mean = 19.03 mm, SE = 0.562) and 35S::KRP2-GFP *rga-28* (mean = 22.21 mm, SE = 0.906) seedlings. A similar trend was also observed when plotting the distribution of root lengths for each genotype for this day with boxplots (Figure 4.5Cii). However, the boxplots for WT, 35S::KRP2-GFP *gai-td1* and 35S::KRP2-GFP *rga-28* were positively skewed by an increased variation in higher root lengths above the median value. Overall, it was evident from plotting the mean root lengths over time that 35S::KRP2-GFP *rga-28* seedlings had the highest average root growth rate followed by WT, 35S::KRP2-GFP *gai-td1* and 35S::KRP2-GFP seedlings (Figure 4.5Aii). Furthermore, root growth under this treatment appeared to be substantially reduced for all of these genotypes when compared to both the control and GA treatment (Figure 4.5D). This implies that endogenous DELLA accumulation in the root for all of these lines is normally repressed by the presence of endogenous GA.

To test these findings statistically, the association between length and genotype was assessed with a LMER, with the same parameters as defined for the control treatment (Appendix 4.4C). The model output revealed that root length was significantly different between days, with WT seedlings growing at a rate of 2.26 mm per day (Table 4.12). In contrast to the control and GA treatment, 35S::KRP2-GFP *rga-28* seedlings had the highest root growth rate that was significantly different when compared to WT, with an increased rate of 0.65 mm/per day ($t_3 = 6.06$, $p<0.001$). Similar to the control, 35S::KRP2-GFP seedlings had the lowest predicted root growth rate that was significantly different to WT, with a decrease of 0.91 mm/day ($t_3 = -8.13$, $p<0.001$). Moreover, 35S::KRP2-GFP *gai-td1* grew at a significantly decrease root growth rate of 0.65 mm/day ($t_3 = -6.39$, $p<0.001$).

When comparing between the different 35S::KRP2-GFP lines, the root growth rate of 35S::KRP2-GFP *rga-28* was significantly greater than both 35S::KRP2-GFP *gai-td1* and 35S::KRP2-GFP, with an increase of 1.3 mm/day ($t_3 =12.32$, $p<0.001$) and 1.56 mm/day ($t_3= 13.54$, $p<0.001$), respectively. Furthermore, 35S::KRP2-GFP *gai-td1* roots grew at a significantly increased rate of 0.26 mm/day when compared to 35S::KRP2-GFP ($t_3 = 2.33$, $p<0.05$). These differences in growth rates were visualised by plotting the predicted lines from the model over the raw data for each genotype, demonstrating the same trend and similar slopes as described for the mean lengths plotted over time (Figure 4.5Biii). To conclude, the root phenotypes of the aforementioned lines were all significantly different when comparing between them with 35S::KRP2-GFP *rga-28* seedlings having the highest root growth rate followed by WT, 35S::KRP2-GFP *gai-td1* and 35S::KRP2-GFP seedlings.

Genotype	Root growth rate (mm/day)	Standard Error	t-value	p-value
WT	2.26	0.073	30.76	<0.001
35S::KRP2-GFP	1.35	0.084	16.01	<0.001
35S::KRP2-GFP *gai-td1*	1.6	0.071	22.67	<0.001
35S::KRP2-GFP *rga-28*	2.91	0.078	37.08	<0.001

Table 4.12: Predicted daily root growth rates for each genotype from the PAC treatment determined by the statistical model (GLMM). For each calculation, there was one degree of freedom. Levels of significance are represented by: * p<0.05, ** P<0.01 and *** p<0.001. The p-value refers to the difference in growth rate between days.

To analyse root growth rates for each genotype between treatments, the association between length and the specified genotype was assessed with an LMER, which included the main effects of day and treatment, their interaction and a random effect of plate variability (Appendix 4.4D-G). The model outputs demonstrated that each genotype grew at significantly decreased rates under PAC in comparison to both the control and GA treatment (Figure 4.4D). The fact that 35S::KRP2-GFP *rga-28* seedlings had the highest root growth rate from this treatment contrasted with the findings from the control and GA treatment where WT seedlings had the highest root growth rate. Therefore, PAC treatment conferred opposing root phenotypes for WT and 35S::KRP2-GFP *rga-28* seedlings when compared to the control. For the GA treatment, opposing root phenotypes where also found for 35S::KRP2-GFP *gai-td1* and 35S::KRP2-GFP seedlings when compared to the control. Specifically, 35S::KRP2-GFP *gai-td1* seedlings grew at a significantly increased rate of 0.69 mm/day (t_2 = 5.4, p<0.001) for the control when compared to GA treatment, whereas 35S::KRP2-GFP seedlings grew at a significantly decreased rate of 0.4 mm/day (t_2 = -3.21, p<0.01). However, there were no significant differences for the root growth rates of WT (t_2 = 1.45, p = 0.148) and 35S::KRP2-GFP *rga-28* (t_2 = -0.53, p = 0.593) seedlings when comparing between these treatments. Across all of these treatments there was a general trend of 35S::KRP2-GFP *rga-28* roots having in increased growth rate in comparison to 35S::KRP2-GFP *gai-td1* and growing at a similar rate to WT seedlings. Therefore, loss of RGA function in the 35S::KRP2-GFP line is able to rescue its reduced growth phenotype.

To assess the validity of these findings, these experiments were repeated. The rescue phenotype observed for 35S::KRP2-GFP *rga-28* seedlings in the previous experiment remained consistent throughout the different treatments (Figure 4.6). However, there was no significant difference between the growth rates of 35S::KRP2-GFP and 35S::KRP2-GFP *gai-td1* seedlings for both the control (t_3 = -0.313, p = 0.755) and GA (t_3 = -0.698, p = 485) treatment (Figure 4.6D). This may have been due

Figure 4.7 Analysis of repeated root growth experiment for *Col-0* WT, 35S::KRP2-GFP, 35S::KRP2-GFP *gai-td1* and 35S::KRP2-GFP *rga-28* seedlings from 2-9 days after stratification (DAS). All of these lines were germinated on 2.5 µM of GA_3 and transferred to fresh plates 1 DAS. Seedlings were subject to different treatments: (i) control, (ii) 10 µM of GA_3 and (iii) 1 µM of PAC and are represented by:

(A) Average root length for each genotype plotted over time fitted with a linear trendline

(B) The predicted lines for root length over time per genotype as determined by the statistical model used to analyse the data and plotted over the raw data values

(C) Boxplots for each genotype over time, with the final day enlarged for better visualisation of the distribution of root lengths. The boxplots show the median value as represented by the dividing line, as well as the lower and upper interquartile ranges, with whiskers extending 1.5 times the interquartile range.

A (i)

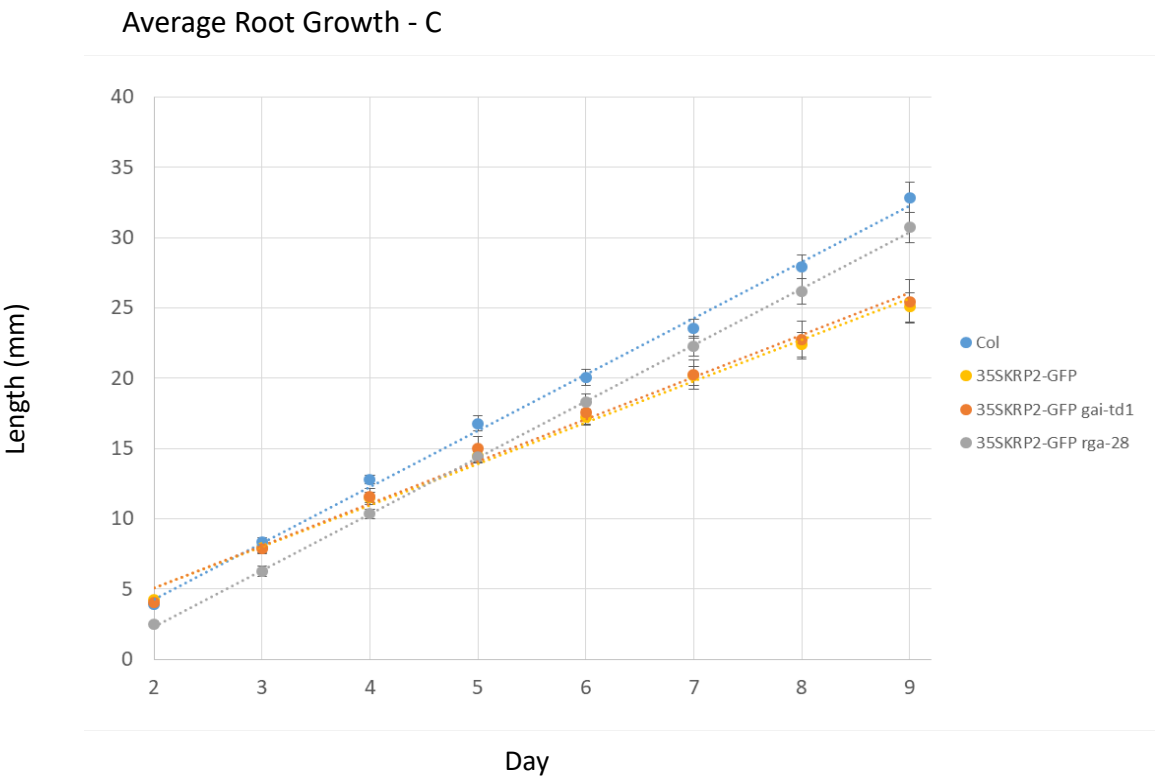
Average Root Growth - C
Length (mm)
40
35
30
25
20
15
10
5
0
2
3
4
5
6
7
8
9
Day
Col
35SKRP2-GFP
35SKRP2-GFP gai-td1
35SKRP2-GFP rga-28

B (i)

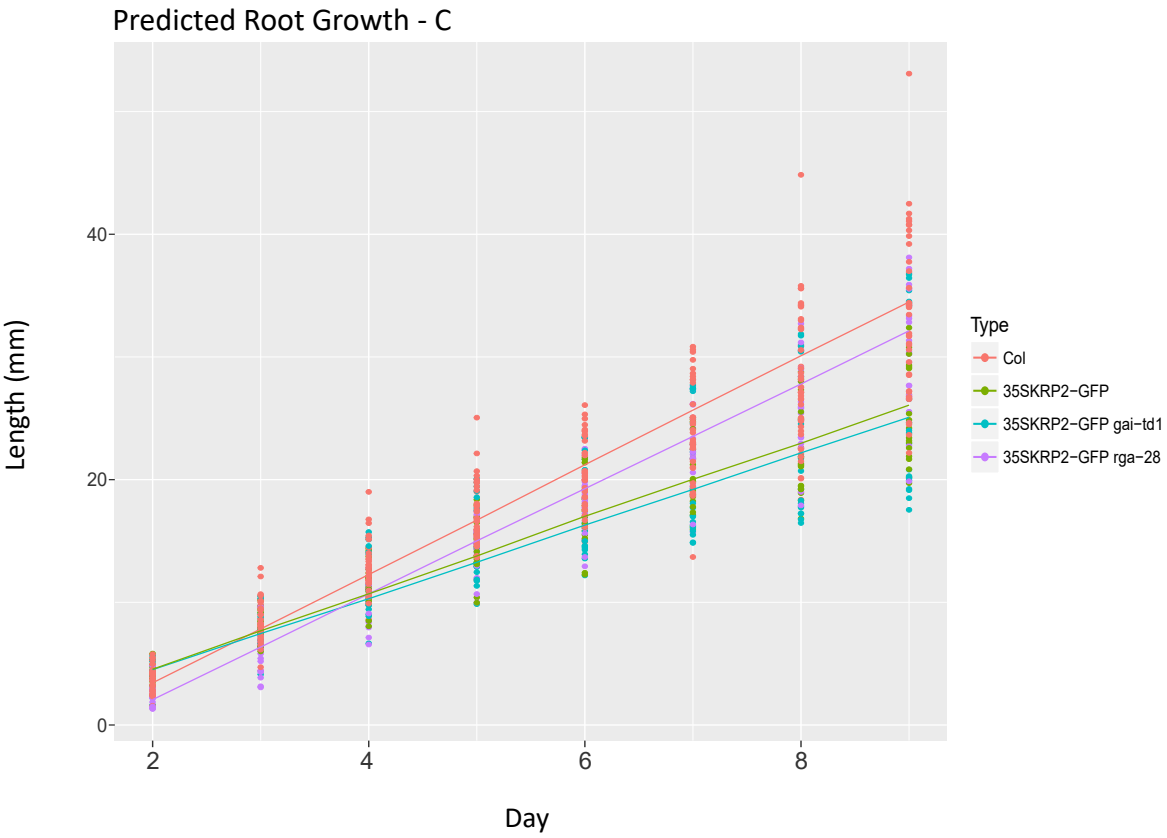
Predicted Root Growth - C
Length (mm)
40
20
0
2
4
6
8
Day
Type
Col
35SKRP2-GFP
35SKRP2-GFP gai-td1
35SKRP2-GFP rga-28

C (i)

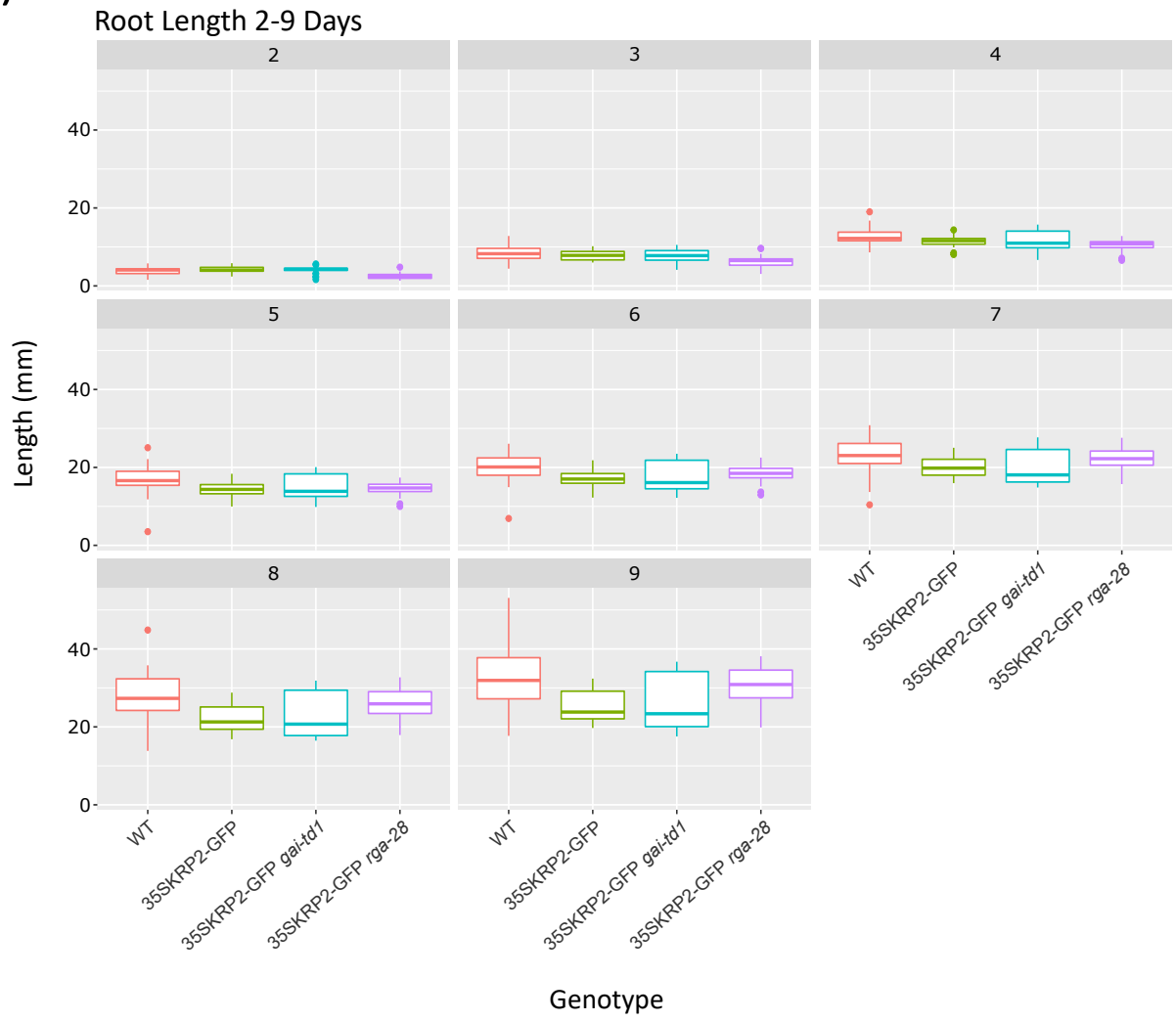
Root Length 2-9 Days
2
3
4
5
6
7
8
9
Length (mm)
0
20
40
WT
35SKRP2-GFP
35SKRP2-GFP gai-td1
35SKRP2-GFP rga-28
Genotype

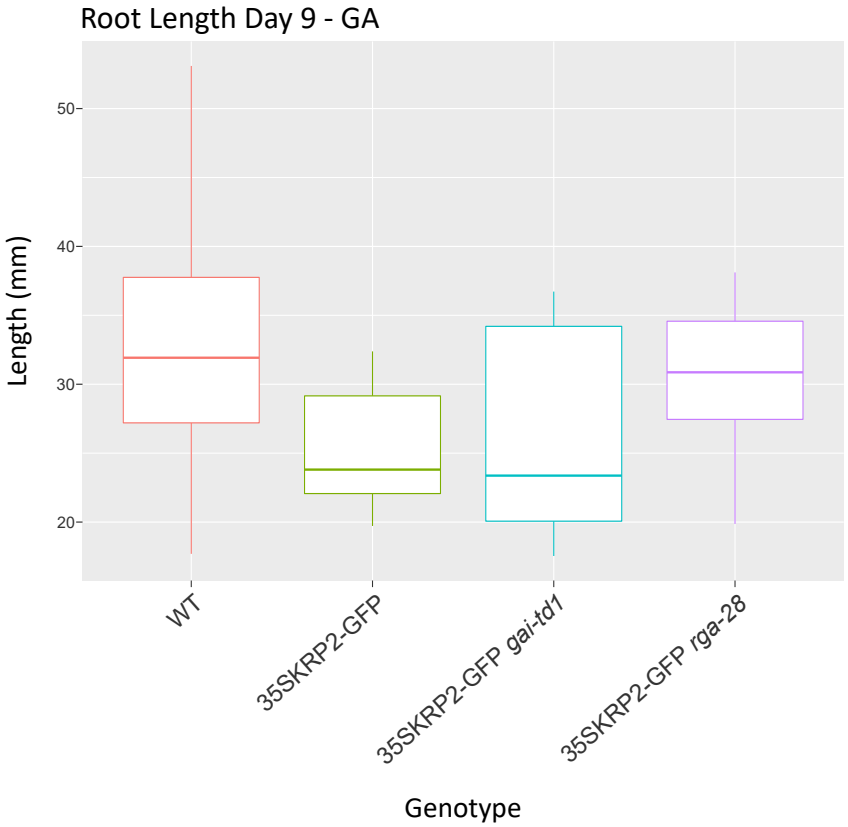
Root Length Day 9 - GA
Length (mm)
20
30
40
50
WT
35SKRP2-GFP
35SKRP2-GFP gai-td1
35SKRP2-GFP rga-28
Genotype

B (ii)

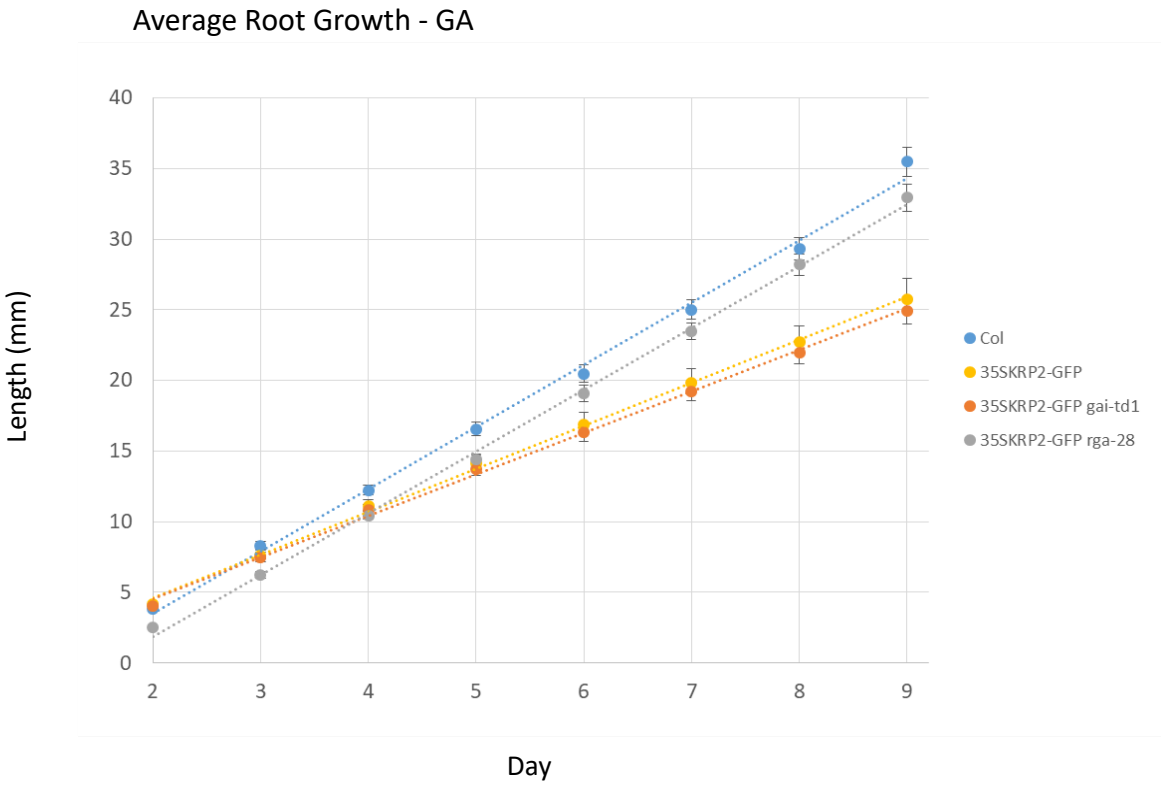
Average Root Growth - GA
Length (mm)
40
35
30
25
20
15
10
5
0
2
3
4
5
6
7
8
9
Day
Col
35SKRP2-GFP
35SKRP2-GFP gai-td1
35SKRP2-GFP rga-28

C (ii)

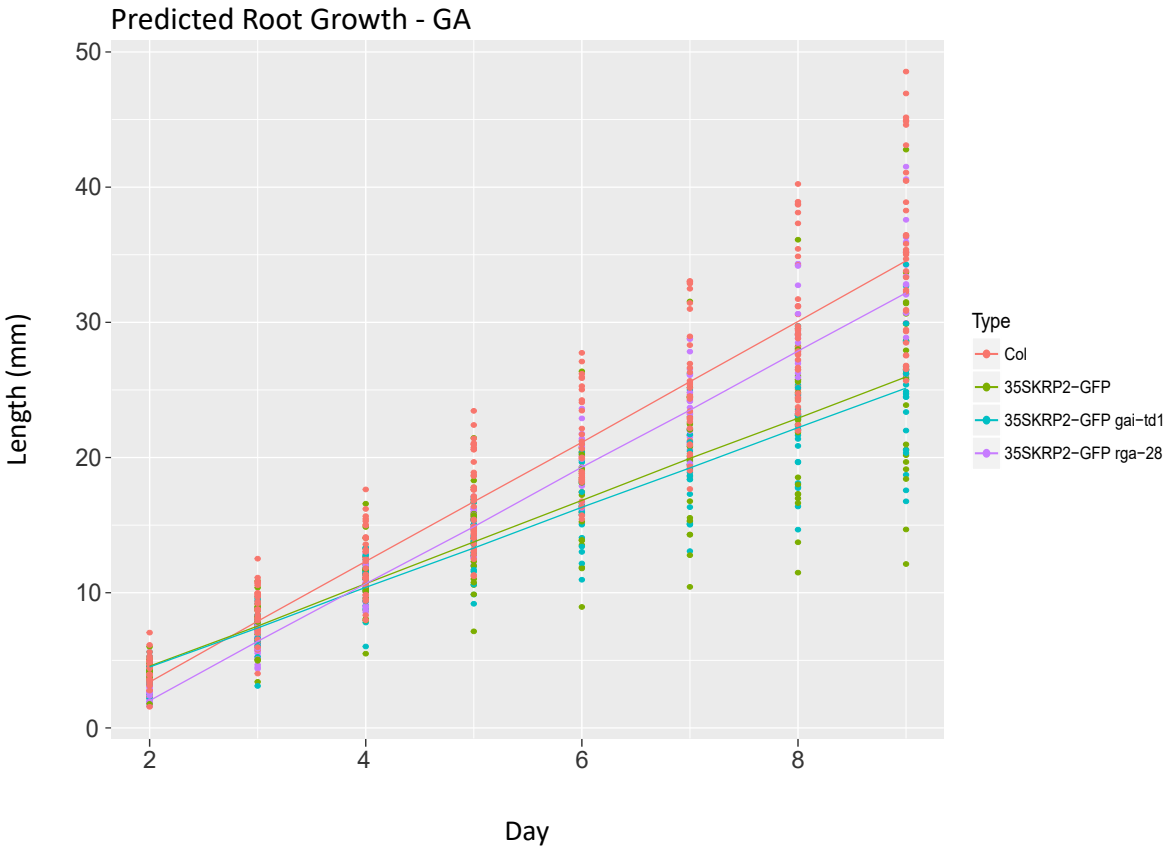
Predicted Root Growth - GA
Length (mm)
50
40
30
20
10
0
2
4
6
8
Day
Type
Col
35SKRP2-GFP
35SKRP2-GFP gai-td1
35SKRP2-GFP rga-28

C (ii)

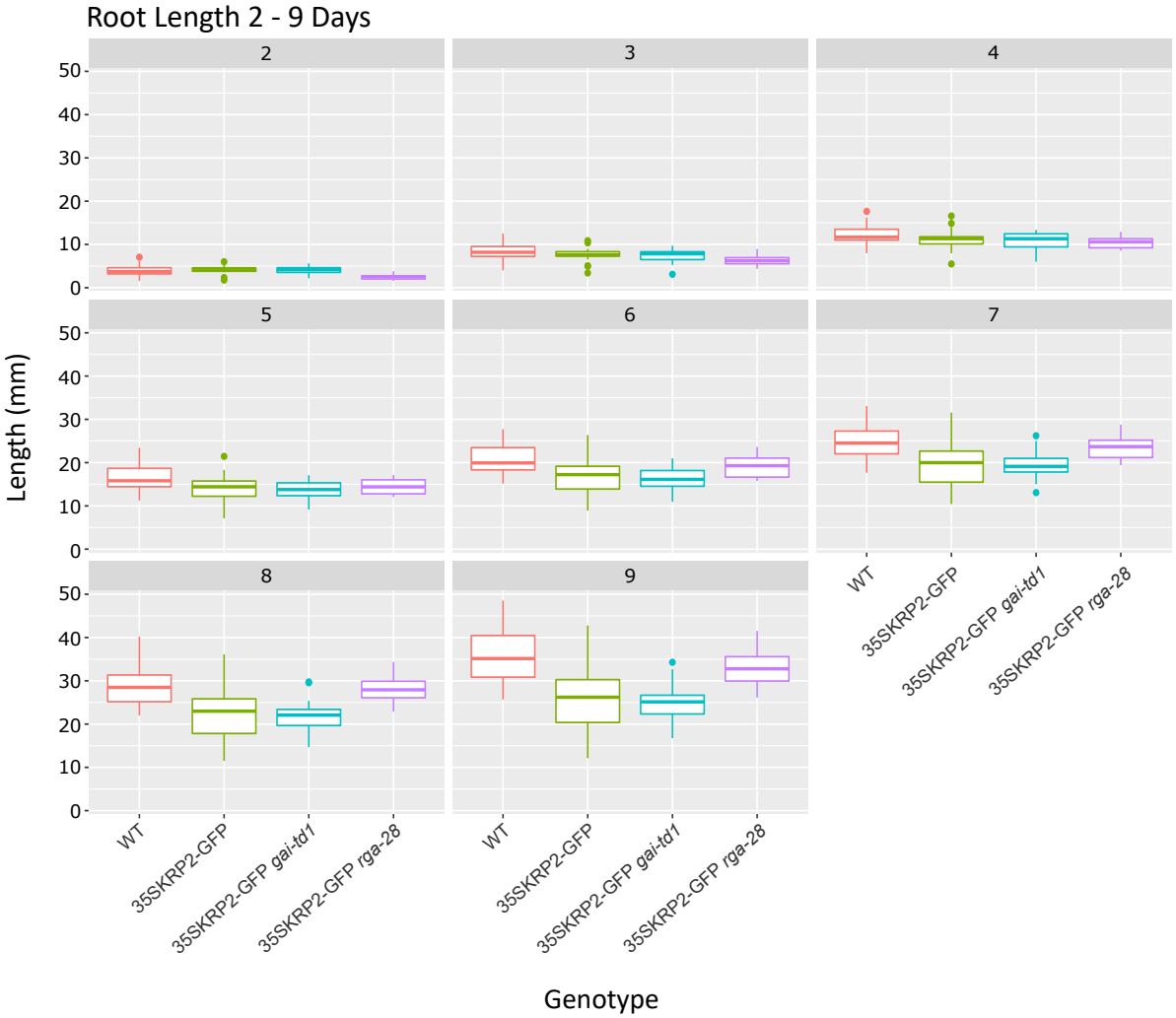
Root Length 2 - 9 Days
2
3
4
5
6
7
8
9
Length (mm)
0
10
20
30
40
50
WT
35SKRP2-GFP
35SKRP2-GFP gai-td1
35SKRP2-GFP rga-28
Genotype

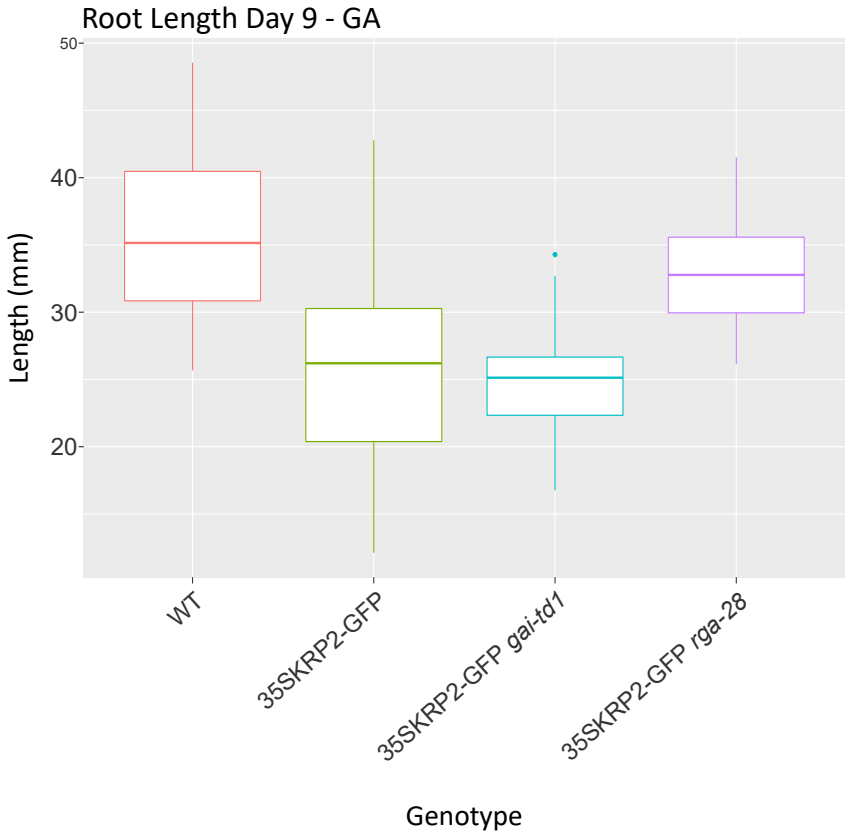
Root Length Day 9 - GA
Length (mm)
20
30
40
50
WT
35SKRP2-GFP
35SKRP2-GFP gai-td1
35SKRP2-GFP rga-28
Genotype

A (iii)

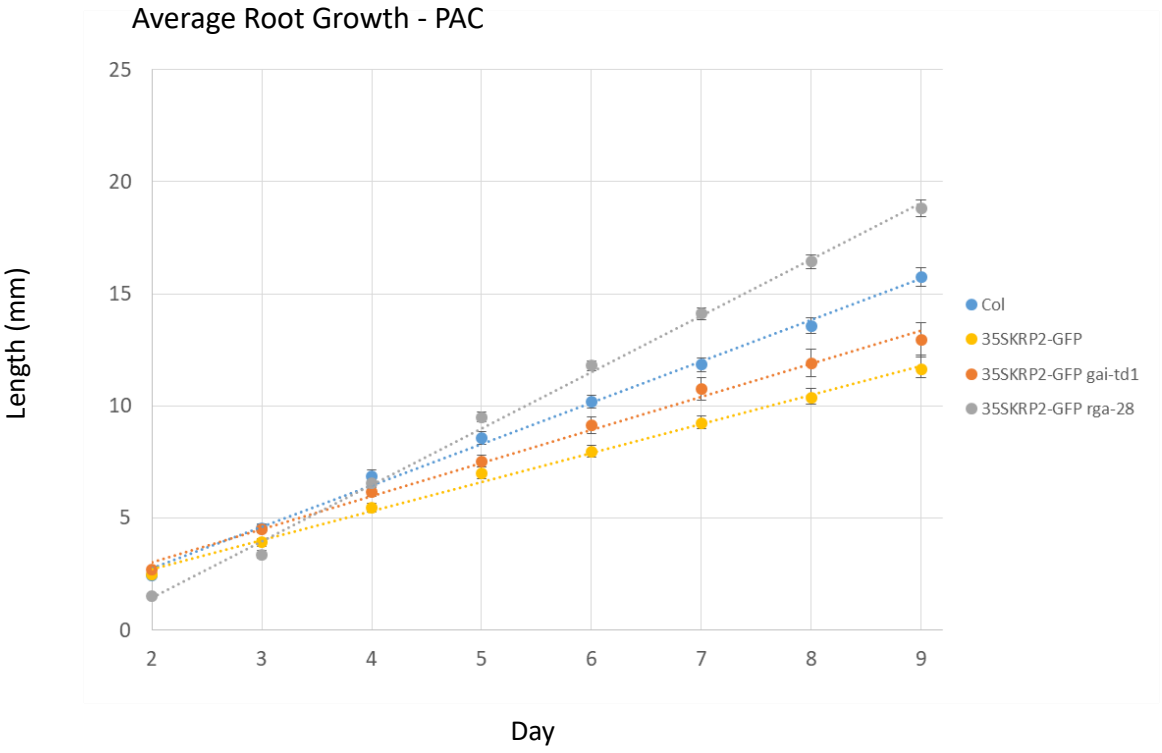
Average Root Growth - PAC
Length (mm)
25
20
15
10
5
0
2
3
4
5
6
7
8
9
Day
Col
35SKRP2-GFP
35SKRP2-GFP gai-td1
35SKRP2-GFP rga-28

B (iii)

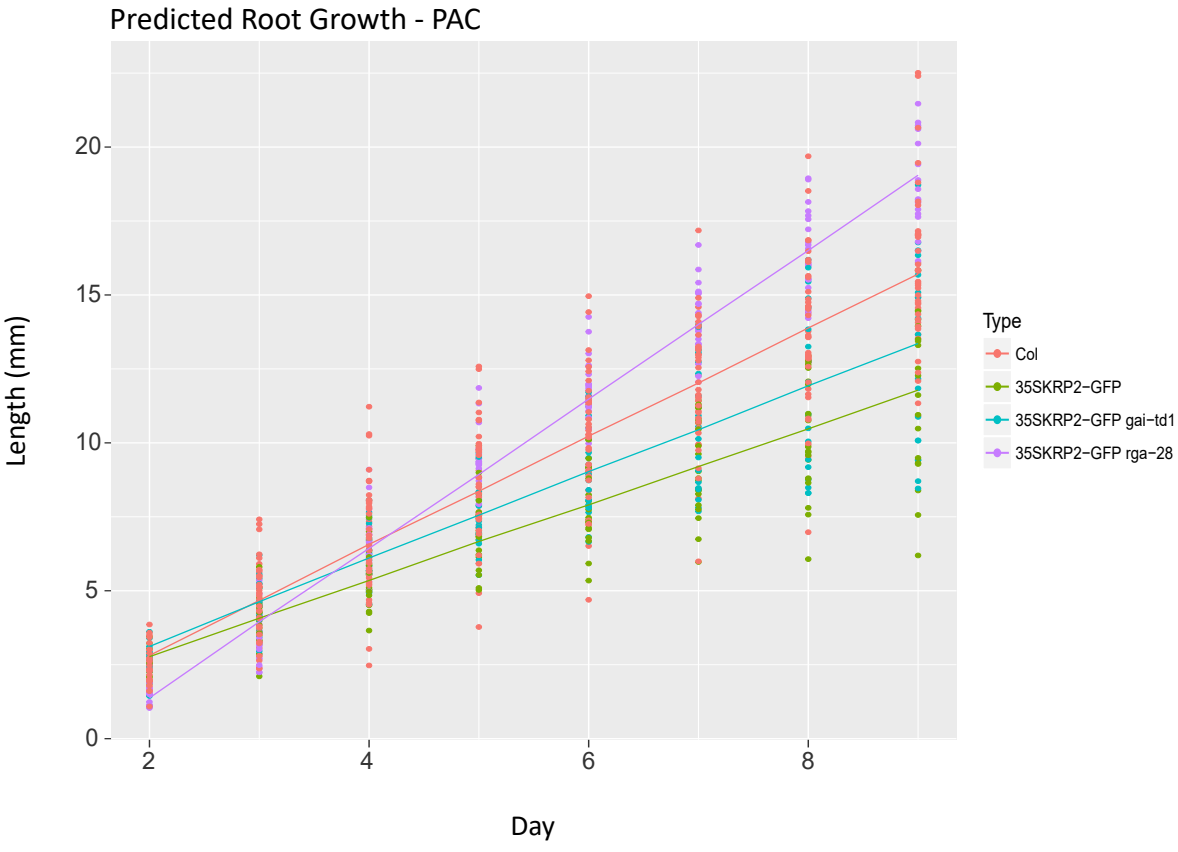
Predicted Root Growth - PAC
Length (mm)
20
15
10
5
0
2
4
6
8
Day
Type
Col
35SKRP2-GFP
35SKRP2-GFP gai-td1
35SKRP2-GFP rga-28

C (iii)

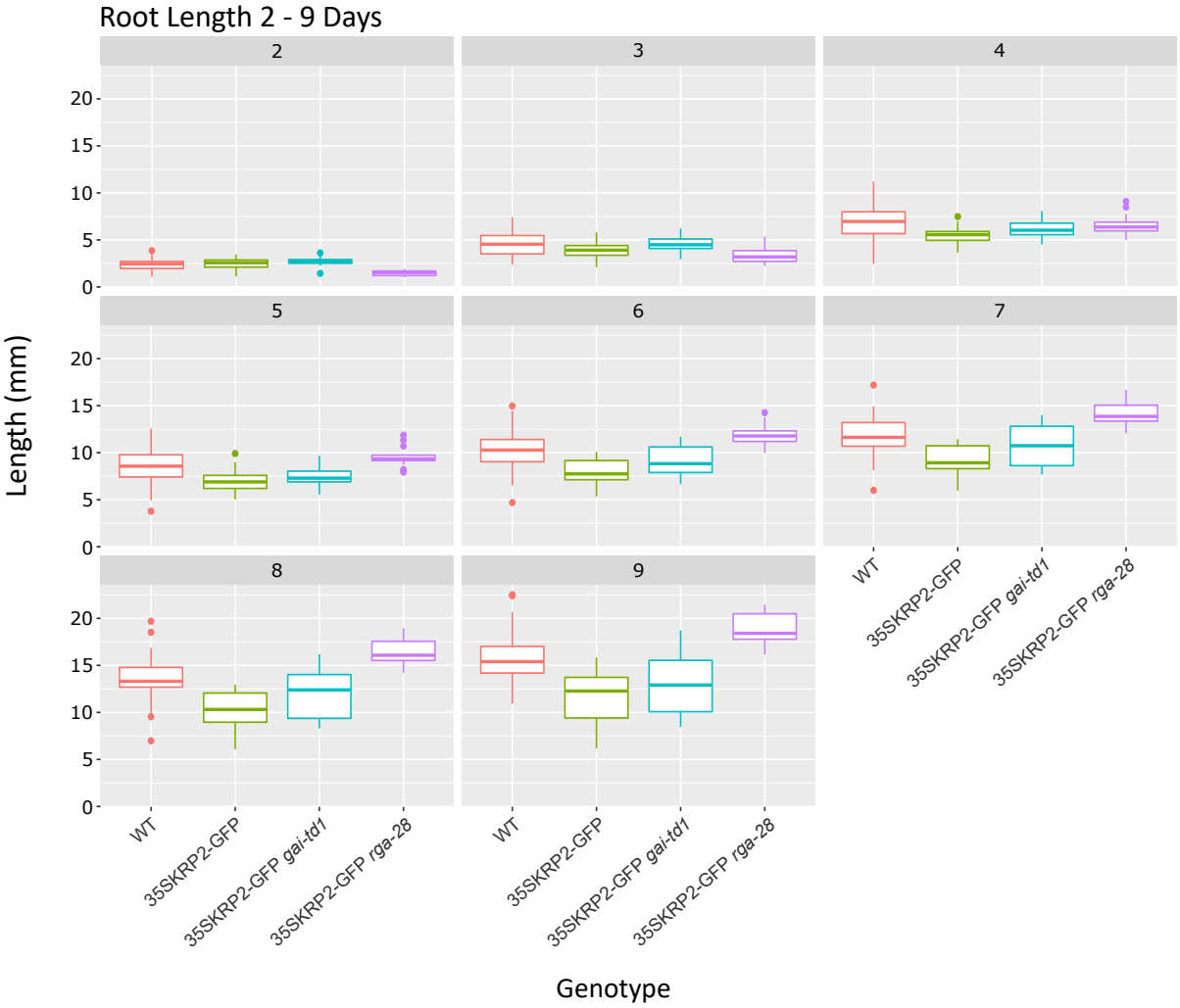
Root Length 2 - 9 Days
2
3
4
5
6
7
8
9
Length (mm)
0
5
10
15
20
WT
35SKRP2-GFP
35SKRP2-GFP gai-td1
35SKRP2-GFP rga-28
Genotype

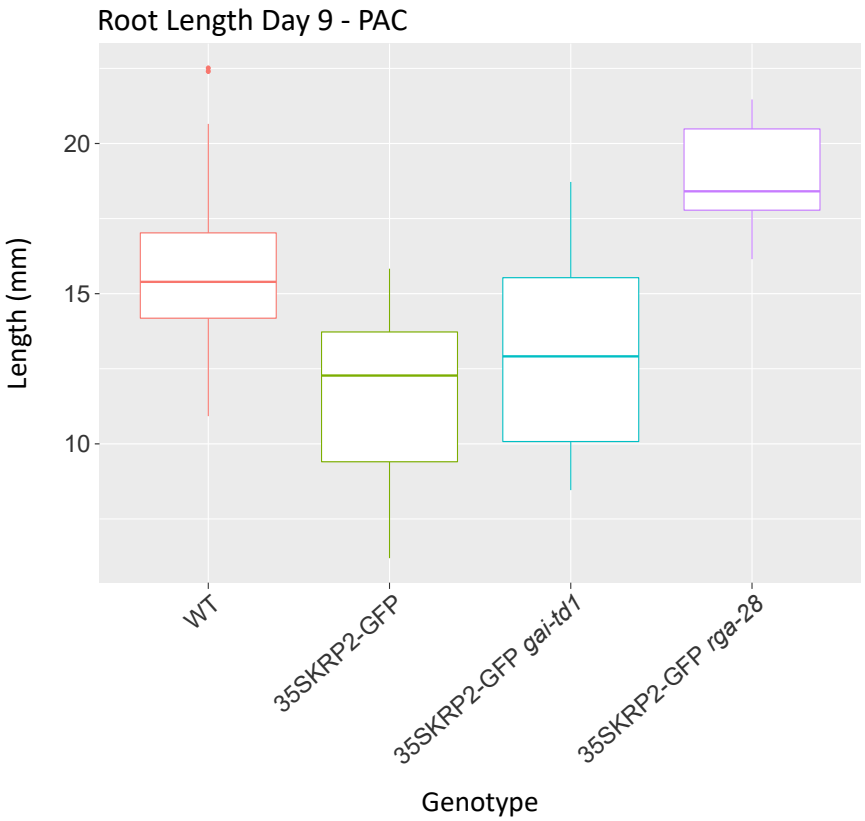
Root Length Day 9 - PAC
Length (mm)
10
15
20
WT
35SKRP2-GFP
35SKRP2-GFP gai-td1
35SKRP2-GFP rga-28
Genotype

D

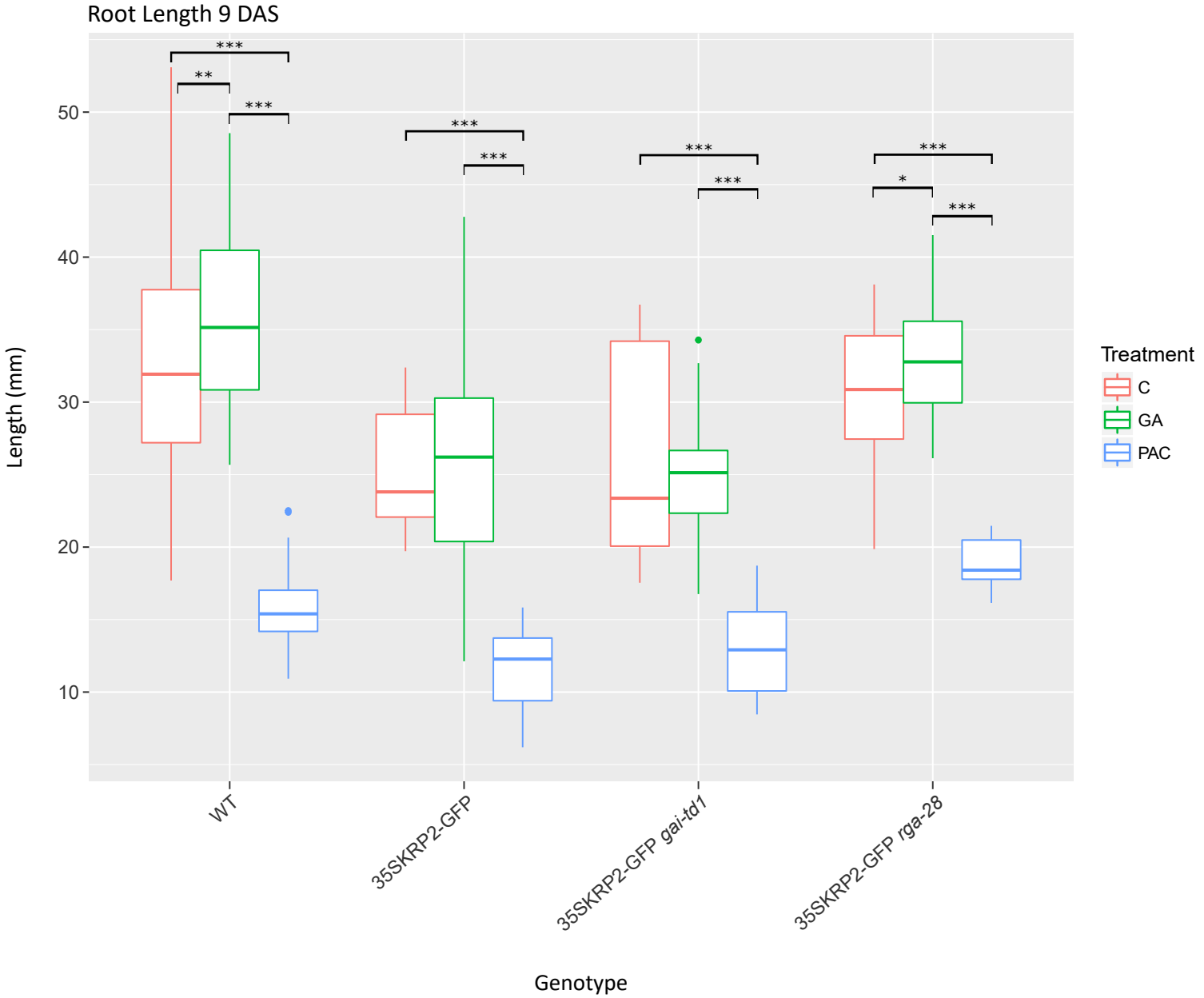
Root Length 9 DAS
Length (mm)
50
40
30
20
10
***
**
***
***
***
***
***
*
***
WT
35SKRP2-GFP
35SKRP2-GFP gai-td1
35SKRP2-GFP rga-28
Genotype
Treatment
C
GA
PAC

to an increased variation of larger root lengths for 35S::KRP2-GFP *gai-td1* for the control treatment, as well as an increased variation of smaller root lengths for 35S::KRP2-GFP for the GA treatment (Figure 4.6D). Furthermore, there was a significant difference in root growth rates of WT seedlings when comparing the control to the GA treatment, with a decreased rate of 0.38 mm/day (t_2 = -3.06, $p<0.01$) and for 35S::KRP2-GFP *rga-28* seedlings, with a decreased rate of 0.25 mm/day (t_2 = -2.24, $p<0.05$). Otherwise, significant differences between these genotypes and different treatments were similar to those described for the original experiment (Figure 4.5 & 4.6D). These results combined demonstrate that there was a consistent rescued root growth phenotype observed for 35S::KRP2-GFP *rga-28* seedlings in relation to the growth of 35S::KRP2-GFP, whereas this was not consistently observed for 35S::KRP2-GFP *gai-td1*. Therefore, the presence of RGA is somehow important for the function of KRP2, suggesting that they are associated with each other. Whether removal of RGA function affected the expression of *KRP2* at the transcript level and/or the accumulation of KRP2 at the protein level, required further investigation.

Transcriptional analysis of these lines by qPCR revealed that the relative expression of both *KRP2* and *GFP* for 35S::KRP2-GFP *rga-28* seedlings was less than 35S::KRP2-GFP and 35S::KRP2-GFP *gai-td1* (Figure 4.7B). This suggests that *KRP2* is regulated at a transcriptional level by RGA. This analysis also showed that the abundance of *KRP2* relative to WT was increased ten-fold and the amount of *GFP* relative to 35S::KRP2-GFP was approximately 0.7 for this line. Even though the phenotype of 35S::KRP2-GFP *rga-28* was similar to that of WT, it still appeared to contain relatively high transcript levels of *KRP2* and *GFP*. Therefore, these results imply that KRP2 is also regulated at a protein level and RGA is associated with this process. Indeed, the amount of GFP protein detected in this line by western blot analysis appeared to be less than 35S::KRP2-GFP and 35S::KRP2-GFP *gai-td1* (Figure 4.8D). To test whether RGA regulates KRP2 protein levels directly, a putative interaction between these two proteins was tested with Co-Immunoprecipitation (Co-IP). An initial result was found when pulling down GFP-tagged protein from an extract of whole 35S::KRP2-GFP seedlings and probing the resulting pull-down with an anti-RGA antibody (Figure 4.8C). Although this Co-IP was repeated multiple times, a subsequent positive result was never obtained. Regardless of this factor, it is evident that removal of RGA function from 35S::KRP2-GFP negatively affected the transcriptional expression of *KRP2* and production of its corresponding protein. This analysis and the distinctive recue phenotype observed for 35S::KRP2-GFP *rga-28* seedlings indicates that the reduced accumulation of KRP2 protein is not just attributable to a reduction in its corresponding transcript levels. Therefore, *KRP2* is regulated by RGA on multiple levels, which may be controlled by different molecular pathways.

Figure 4.8 Analysis of the rescue phenotype similar to WT observed for 35S::KRP2-GFP *rga-28* in relation to 35S::KRP2-GFP, 35S::KRP2-GFP *gai-td1*.

(A) Images of WT, 35S::KRP2-GFP *rga-28*, 35S::KRP2-GFP *gai-td1* and 35S::KRP2-GFP plants at 29 days-after-stratification (DAS).

(B) Abundance of *KRP2* transcripts for 35S::KRP2-GFP, 35S::KRP2-GFP *gai-td1* and 35S::KRP2-GFP *rga-28* seedlings relative to WT (left). Abundance of *GFP* transcripts for 35S::KRP2-GFP *gai-td1* and 35S::KRP2-GFP *rga-28* seedlings relative to 35S::KRP2-GFP (right). All qPCR analysis was performed on cDNA extracted from seedlings grown for 7 DAS. The charts represent the average relative abundance from three independent repeats and the standard errors between these experiments.

(C) Co-Immunoprecipitation (Co-IP) on a total protein extract of 35S::KRP2-GFP whole seedlings. Extracts were incubated with GFP-Trap beads (Chromotek) to pulldown GFP-tagged protein. The resulting samples were run an 8% SDS gel, including 40 µg of starting material (Input), 20 µl of the unbound/post-bound fraction (PB) and 20 µl of the from the pull-down extract (Elute). On the left: Western blot analysis with an anti-RGA antibody (Agrisera, Sweden) was used for detection of RGA protein. On the right: Western blot analysis using an anti-GFP (Torrey Pines) antibody to visualise the efficiency of the pull-down for KRP2-GFP.

(D) Western blot analysis of total protein extracts for WT, 35S::KRP2-GFP, 35S::KRP2-GFP *gai-td1* 35S::KRP2-GFP *rga-28* seedlings at 7 DAS. 20ug of each protein extract was run on an 8% SDS gel. The membrane was probed with an anti-GFP antibody for detection of KRP2-GFP.

A

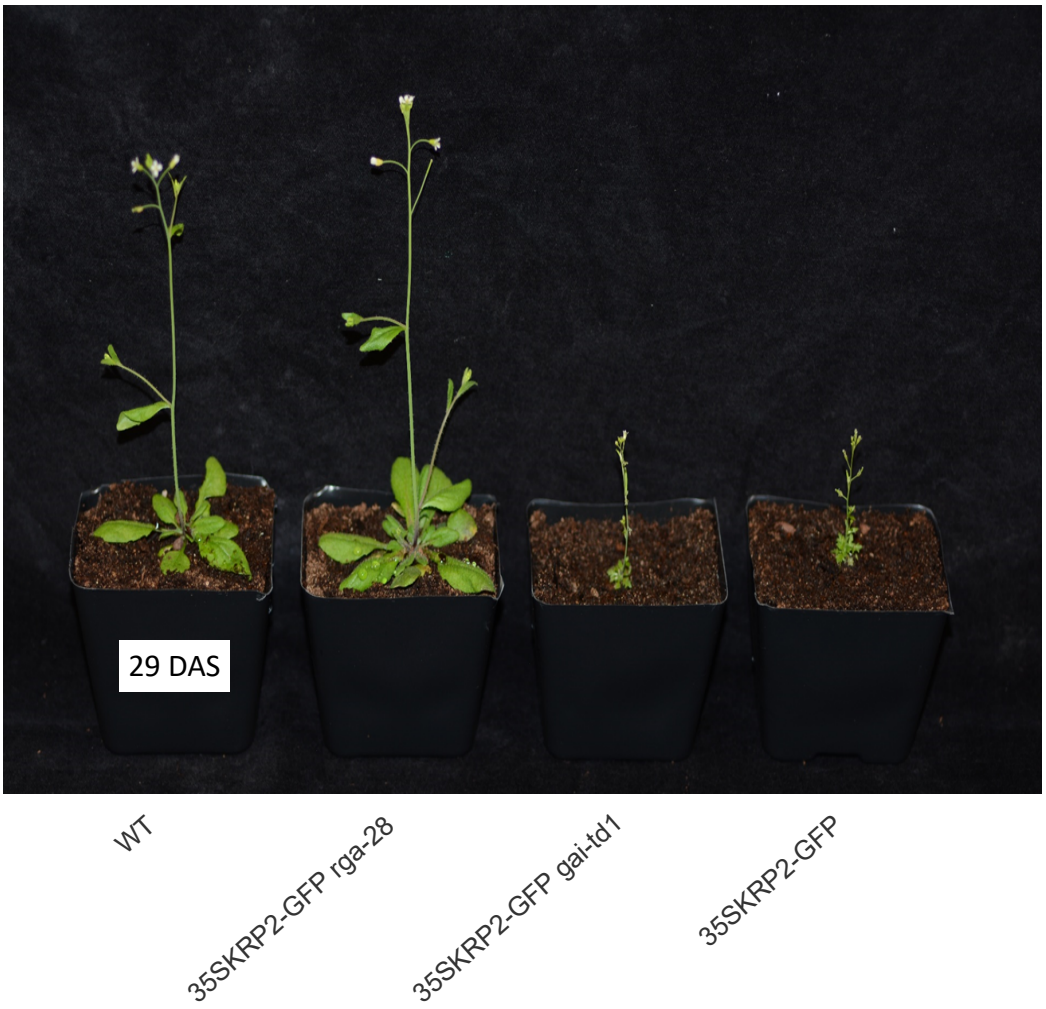
29 DAS
WT
35SKRP2-GFP rga-28
35SKRP2-GFP gai-td1
35SKRP2-GFP

B

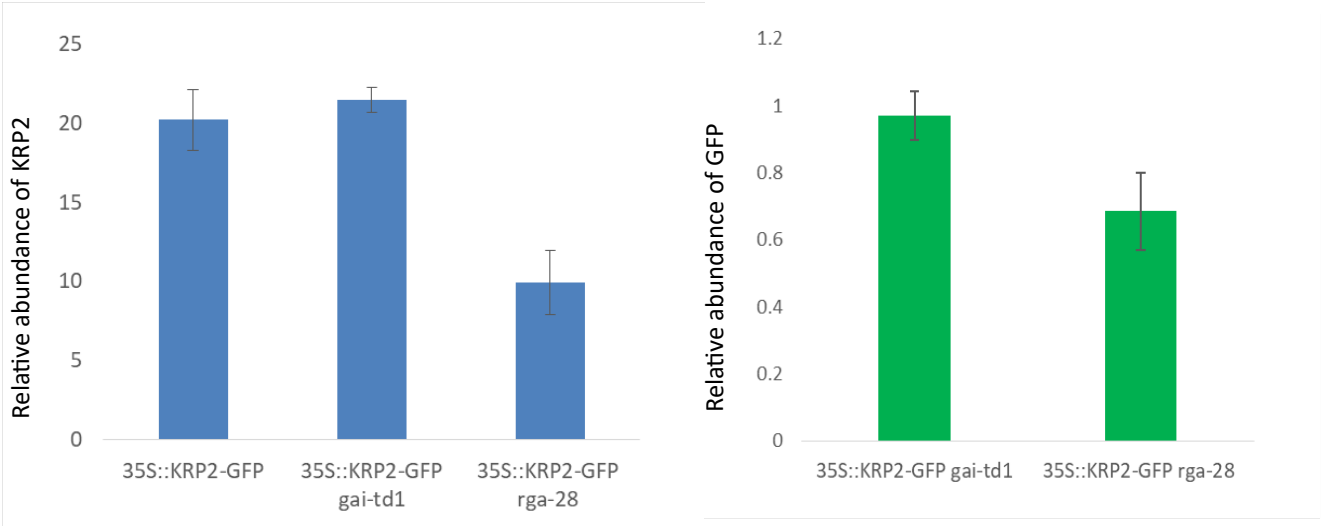
Relative abundance of KRP2
25
20
15
10
5
0
35S::KRP2-GFP
35S::KRP2-GFP gai-td1
35S::KRP2-GFP rga-28
Relative abundance of GFP
1.2
1
0.8
0.6
0.4
0.2
0
35S::KRP2-GFP gai-td1
35S::KRP2-GFP rga-28

C

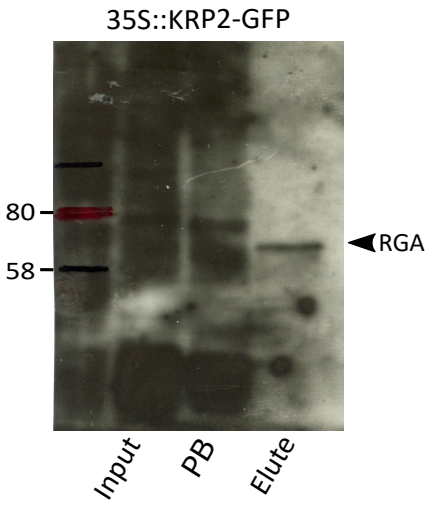

1° = αRGA 1:1000
2° = GAR 1:20,000

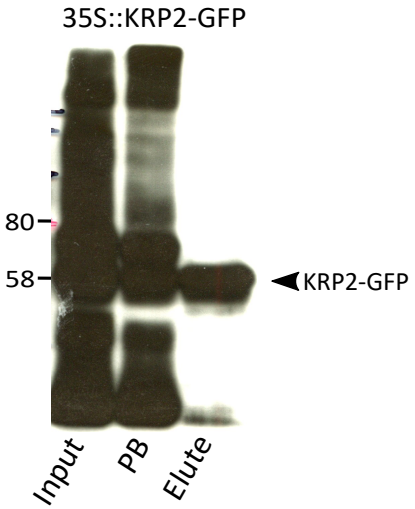

1° = αGFP 1:3000
2° = GAR 1:20,000

D

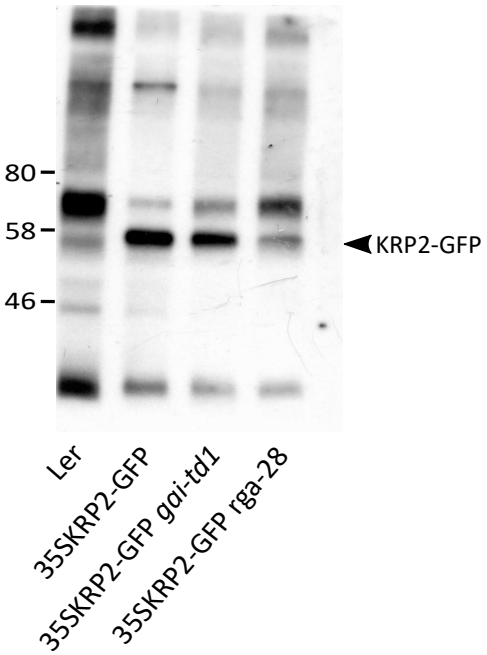

1° = αGFP 1:3000
2° = GAR 1:20,000

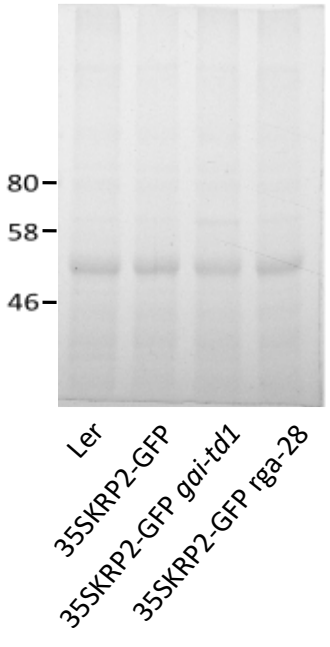

Loading control

Discussion:

The root growth rates of the single null mutants, *gai-td1* and *rga-28*, were assessed in relation to WT and no difference was found between them, suggesting a level of redundancy for RGA and GAI in relation to regulation of root growth. However, differences were found when growing these lines on both PAC and GA indicating that they confer different root growth phenotypes when endogenous GA levels are altered. More specifically, *rga-28* seedlings had an increased root growth rate relative to *gai-td1* when grown on PAC, whilst *gai-td1* seedlings had an increased growth rate relative to *rga-28* when grown on GA. Furthermore, by crossing these null mutants to the GA biosynthetic mutant, *ga1-t*, the conditions for the PAC treatment could essentially be mimicked without exogenous input. Root growth experiments of these homozygous lines revealed that *ga1-t rga-28* seedlings had an increased root growth rate relative to that of *ga1-t gai-td1*. Together, these results imply that RGA plays a more dominant role than GAI with respect to regulation of root growth via the GA signalling pathway. This could either be due to a difference between their function or a difference between their levels of accumulation. Nevertheless, it was evident that removal of either GAI or RGA function was sufficient to partially rescue the reduced growth phenotype of the *ga1-t* single null mutant. To ascertain whether this was due to an increased rate of cell division, the cellular phenotype of these roots were examined by measuring meristem size, cortical cell number and cell production rate for *ga1-t gai-td1* and *ga1-t rga-28* seedlings and compared to WT and *ga1-t* controls.

Root growth rate is dependent on changes in the elemental expansion rate, as well as the length of the growth zone. Just as root elongation is dependent on these parameters, so too the cell production rate is dependent on two analogous parameters: the rate of cell production and the number of dividing cells (Baskin 2013). The number of dividing cells is usually defined as the length of the meristem and tends to be the main parameter that varies when determining differences in root growth acclimation due to changes in cell division. Unfortunately, cell division rates are rarely reported for root growth experiments, but it should be more commonplace to accompany often reported changes in root meristem size. Although cell division rates can be difficult to obtain, cell production rates are relatively easy to measure and provide an indication of the proliferative performance of the meristem. Measuring this parameter alongside measurements of root meristem size therefore provides a better understanding of how a plant adapts to its environment by altering the process of cell division and to determine how these changes are instigated.

In relation to meristem size and cortical cell number, both were reduced significantly for the roots of *ga1-t* seedlings when compared to WT. Moreover, cell production rates for this line were significantly reduced, thus supporting previously reported findings (Achard *et al.*, 2009). In accordance with the

partial rescue phenotype observed for roots of *ga1-t rga-28* seedlings, both meristem size and cortical cell number were significantly increased in relation to *ga1-t,* but significantly reduced in relation to WT. Furthermore, cell production rate for this line was significantly reduced in relation to WT, but there was no difference in relation to *ga1-t*. Therefore, the increased growth rate observed for *ga1-t rga-28* seedlings when compared to *ga1-t* was associated with an increase in meristem size and cortical cell number i.e. the number of dividing cells, rather than changes in the rate of cell division. Conversely, meristem size and cortical cell number for *ga1-t* and *ga1-t gai-td1* seedlings were not significantly different when comparing between them. However, there was a difference between their cell production rates, with *ga1-t* seedlings having a reduced rate in comparison *ga1-t gai-td1*. These findings imply that the increased growth rate observed for *ga1-t gai-td1* seedlings when compared to *ga1-t* was the result of an increased rate of cell production, rather than alterations in the number of dividing cells. Finally, since there was a significant increase in meristem size and cortical cell number for *ga1-t rga-28* seedlings in relation to *ga1-t gai-td1,* but no difference in their cell production rates, the differences between their observed root growth phenotypes must have been a result of an increased number of dividing cells in the meristem. To conclude, it is evident that RGA and GAI do alter the process of cell division either by reducing the number of dividing cells in the meristem and/or by decreasing the rate of cell production. However, the molecular mechanisms behind these processes are still poorly understood.

To further our understanding of how these DELLA proteins are associated with cell division, root growth experiments of the aforementioned single null mutants crossed to the pRBR::RBR-GFP translational report line were conducted in the presence and absence of PAC and GA. Although there were significant reductions in the growth rates of pRBR::RBR-GFP, pRBR::RBR-GFP *gai-td1* and pRBR::RBR-GFP *rga-28* seedlings when compared to WT, there were no significant differences between the growth rates of pRBR::RBR-GFP *gai-td1* and pRBR::RBR-GFP *rga-28* across all treatments. Previous reports showed that root meristem size for pRBR::RBR-GFP seedlings was reduced in relation to WT (Magyar *et al.*, 2012) so this would explain the reduced growth phenotypes observed for these lines. For PAC treatment, removal of either RGA or GAI function was sufficient to partially rescue this reduced growth phenotype, but with no difference between them. However, rescue phenotypes were also observed for the roots of *gai-td1* and *rga-28* control seedlings when compared to WT under this treatment, although there were differences between them. Either this means that there is no association between GAI/RGA and RBR, or that GAI and RGA are functionally redundant in relation to RBR. To clarify, the double mutant for *gai-td1 rga-28* crossed to pRBR::RBR-GFP could be generated and incorporated into these experiments to assess their root growth rates in comparison to the single null mutants crossed to pRBR::RBR-GFP. However, since the pRBR::RBR-GFP only contains an

additional copy of RBR and is not overexpressed more substantially, perhaps the effect of removing GAI and RGA function on root growth for this line was too minimal to be observed from these experiments. Unfortunately, a line that overexpresses RBR was not obtainable, but others that indirectly increase the levels of RBR because they affect the amount of RBR phosphorylation were. For example, the 35S::KRP2-GFP cell-cycle overexpresser line increases the amount of unphosphorylated RBR by inhibiting CDK complexes.

From root growth experiments of crosses generated between 35S::KRP2-GFP to either *gai-td1* or *rga-28*, it was evident there were differences in their root growth phenotypes across all treatments. Indeed, 35S::KRP2-GFP *rga-28* seedlings had consistently increased root growth rates when compared to 35S::KRP2-GFP *gai-td1* that were similar to that of WT. Conversely, roots of 35S::KRP2-GFP *gai-td1* seedlings tended to grow at a similar rate to that of 35S::KRP2-GFP seedlings alone. Therefore, it appears that GAI and RGA are functionally different in this context, since loss of RGA function counteracted the reduced root growth phenotype of 35S::KRP2-GFP, whereas loss of GAI did not. These results imply that either native *RGA* stabilises KRP-GFP at the transcriptional and/or protein level or that KRP2 somehow requires native RGA to sit in a complex with it, or vice versa. Transcriptional analysis of KRP2 and GFP levels were analysed for this line and showed that both levels were reduced when compared to 35S::KRP2-GFP and 35S::KRP2-GFP *gai-td1*, therefore suggesting that *RGA* regulates *KRP2* at a transcriptional level. In support of this finding, a recent paper published by Serrano-Mislata et al. (2017), discovered with Chip-Seq that a GA-resistant form of RGA binds to and upregulates the levels of *KRP2* in the inflorescence tip (where flowers initiate) of *Arabidopsis* plants. Hence, RGA restricts shoot meristem size as a result of direct upregulation of *KRP2*. These experiments were based on previous findings that *KRP2* abundance was upregulated in the GA biosynthetic mutant, *ga1-3* (Achard *et al.*, 2009).

Since a putative binding between RGA and KRP2 was inconstantly found, there is no definitive evidence so far to suggest that they form a complex. However, the relative transcript levels of both *KRP2* and *GFP* were substantially high, but the phenotype of these seedlings were still similar to WT, which suggests that KRP2 protein accumulation levels are somehow being degraded in the absence of RGA. To conclude, as had been demonstrated recently in the shoot (Serrano-Mislata *et al.*, 2017), it appears that RGA is able to indirectly restrict cell division in the root by directly upregulating endogenous levels of KRP2. Furthermore, RGA also appears to affect the level of KRP2 protein accumulation, leading to its degradation when RGA function has been removed. Neither of these observations was made for GAI, suggesting that RGA and GAI are functionally different in relation to how they restrict cell division and therefore root growth.

Chapter 5

Evidence supporting an interaction between GAI and RBR exists in mitotic cells of *Arabidopsis* roots

Chapter 5 – Evidence supporting an interaction between GAI and RBR exists in mitotic cells of *Arabidopsis* roots

Introduction

As previously mentioned in Chapter 1, GAI and RGA are the main DELLA proteins in *Arabidopsis* that repress growth. Their mechanism is to act as transcriptional regulators that repress the GA signalling pathway. RBR regulates the G_1 to S transition of the plant cell cycle by binding with E2F/DP proteins and preventing the expression of E2F regulated genes. This interaction is controlled by the level of kinase activity by CDK/Cyclin complexes that phosphorylate RBR, thereby releasing it from E2F and initiating E2F-regulated genes that allow the transition to S-Phase.

It has been shown that a variety of different proteins containing the LxCxE motif are able to bind Rb via its corresponding binding pocket (Lee *et al.*, 1998). This indicates that the Leu-Cys-Glu residues of this motif are key to the binding of proteins to RBR, whilst the intervening "x" between these residues can in principle be any amino acid type. GAI contains the aforementioned motif and thus implies a putative binding affinity for RBR. Furthermore, a closely related GRAS protein known as SCARECROW (SCR) has been shown to bind RBR via its LxCxE motif with yeast-two-hybrid assay (Cruz-Ramírez *et al.*, 2012). There are a variety of *in silico*, *in vitro* and *in vivo* ways to demonstrate an interaction between two proteins. However, it depends on the nature of the interaction as to what method is the best one to select for testing.

In silico protein modelling is a useful way of primarily testing a putative protein-protein interaction. This usually relies on the availability of a crystal structure for each protein of interest. However, crystal structures can be notoriously difficult to obtain. There is currently no available crystal structure for RBR in *Arabidopsis*, particularly since most research has been focused on the human Rb protein. Homology modelling is a way of predicting the 3D structure of a protein by using its primary amino acid sequence and combining it with a comparative 3D crystal structure (template) of a different protein from the Protein Data Bank (PDB), when a crystallographic structure is not available (Berman *et al.*, 2000; Martí-Renom *et al.*, 2000; Gomaa *et al.*, 2007). The method relies on the fact that the protein secondary structure (3D structure) is highly conserved among homologous proteins that share a certain identity in their amino acids primary sequence and an identity higher than 45% will give a reliable homology model in terms of 3D structure.

One of the most commonly used biochemical techniques for testing protein-protein interactions *in vivo* is co-immunoprecipitation (Co-IP). This involves using a specific antibody to target a protein of interest and "pull-down" or immunoprecipitate intact protein complexes from a crude extract. The

resulting protein complexes can then be resolved by SDS-PAGE (sodium dodecyl sulfate-polyacrylamide gel electrophoresis) and subjected to western blot analysis to detect putative binding partners. Therefore, antibodies specific to the target protein and the putative binding partner are required to perform a Co-IP. If protein-specific antibodies are not available for this purpose, antibodies targeted to homologous proteins from other organisms might also be able to detect the protein of interest. If no suitable antibody is available, one can potentially be made by expressing the full-length coding sequence, or a particular region of the target protein in bacteria. The expressed protein can then be purified and used to generate antibodies either in-house (if the facilities are available) or by outsourcing to a commercial company that specialises in antibody production.

To investigate a putative binding between GAI and RBR, preliminary Co-IP experiments were performed in collaboration with Prof. Malcolm Bennett from the School of Biosciences, University of Nottingham. The pull-down was performed with an anti-GFP antibody on nuclei extracted from root cultures of the previously mentioned translational reporter lines, pGAI::GAI-GFP and pRGA::GFP-RGA (Silverstone *et al.*, 2001; Fleck and Nicholas P. Harberd, 2002). At the time, it was unknown as to whether there was a commercially available *Arabidopsis*-specific antibody for RBR, so a human Rb antibody was used for detection of this protein from the pulled-down extract. RBR was successfully detected in the eluted fraction of the pGAI::GAI-GFP protein extract, but not for pRGA::GFP-RGA (Figure 4.1). However, these eluted fractions were not subsequently probed with an anti-GFP antibody to ensure that the pull-down of GFP-tagged protein had actually worked. Moreover, a wild-type (WT) control was not incorporated into these experiments to control for unspecific binding of other proteins. Regardless of these factors, the results were promising and provided a rationale for investigating the putative interaction with this type of method.

As well as this experimental finding, a particular type of *in vitro* method was used to test the interaction by Prof. Rishikesh Bhalerao from the Umeå Plant Science Centre, Sweden. This involved transfecting *Arabidopsis* protoplasts with expression constructs driven by the 35S cauliflower mosaic virus (CaMV) for GAI, RGA and RBR (Figure 4.2). Protoplasts are plant cells that have had their cell walls completely or partially removed by either mechanical or enzymatic means in order to allow the uptake of macromolecules, such as DNA, RNA and protein. The different constructs generated for this experiment included WT versions of RBR, GAI with the LxCxE motif and RGA with the MxCxE motif, as well as GAI with a mutated motif to GxGxG. Other constructs included fusion proteins of the GAI and RGA N-terminus containing the different aforementioned versions of this motif fused to the C-terminus of the opposing protein. Furthermore, constructs containing truncated forms of GAI with either the LxCxE motif or the mutated GxGxG motif were also included in these experiments.

Figure 5.1 Evidence for the putative interaction between GAI/RGA and RBR. This was demonstrated with different types of biochemical methods as follows:

(A) Co-immunoprecipitation (Co-IP) experiments indicating a putative interaction between GAI and RBR. The pull-down was performed on nuclei preps of root cultures from pGAI::GAI-GFP and pRGA::GFP-RGA seedlings. Western blot analysis was either performed with a:

  (i) Human anti-RB antibody or
  (ii) Phospho-specific human anti-RB antibody.

(B) Transfection of *Arabidopsis* protoplasts with a sinlge RBR construct and different GAI/RGA constructs containing either their native LxCxE (W) motif for GAI and MxCxE (R) for RGA, or a mutated form of the motif, GxGxG (m). All constructs were driven by the 35S CaMV promotor for overexpression and are represented by the diagrams provided.

  (i) Results from Co-IP experiments using the transfected protoplasts expressing the aforementioned constructs are provided
  (ii) RBR protein was HA-tagged, whilst GAI/RGA constructs were myc-tagged. For the top row of results, pull-downs were performed with an anti-myc antibody and the western blot (WB) was probed with an anti-HA antibody. For the next row, the pull-down and WB was performed the other way around. The following row shows the control for protoplasts transformed with HA-RBR only that have been pulled-down with an anti-HA antibody and probed on a WB with an anti-myc antibody. The inputs for each experiment are also provided that have been probed with their corresponding tag-specific antibody.

A.i

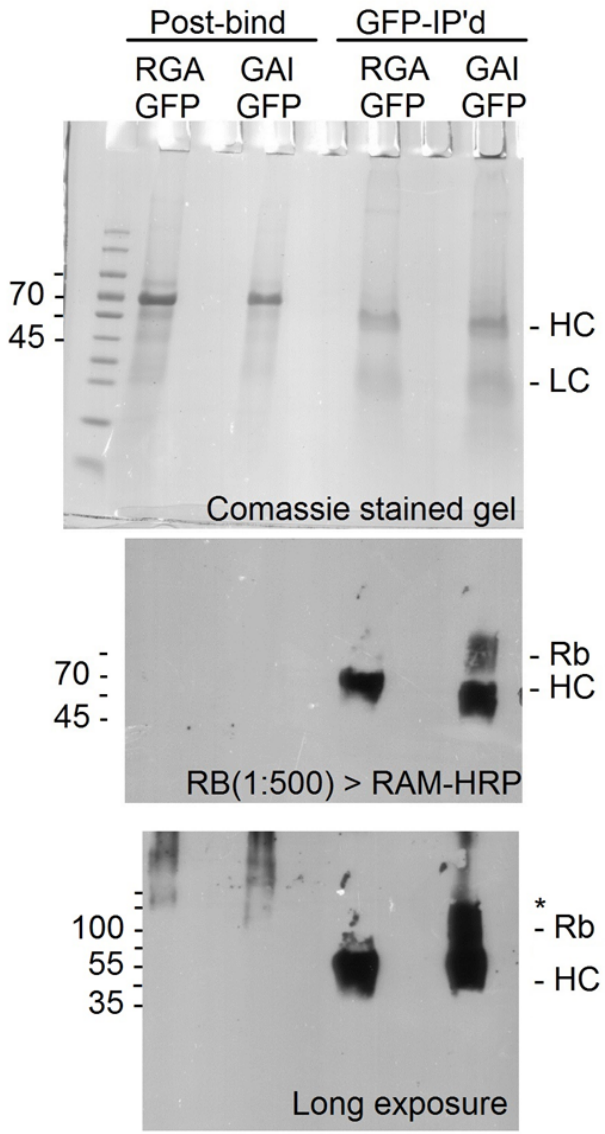
Post-bind
GFP-IP'd
RGA GFP
GAI GFP
RGA GFP
GAI GFP
70
45
- HC
- LC
Comassie stained gel
70
45
- Rb
- HC
RB(1:500) > RAM-HRP
100
55
35
*
- Rb
- HC
Long exposure

A.ii

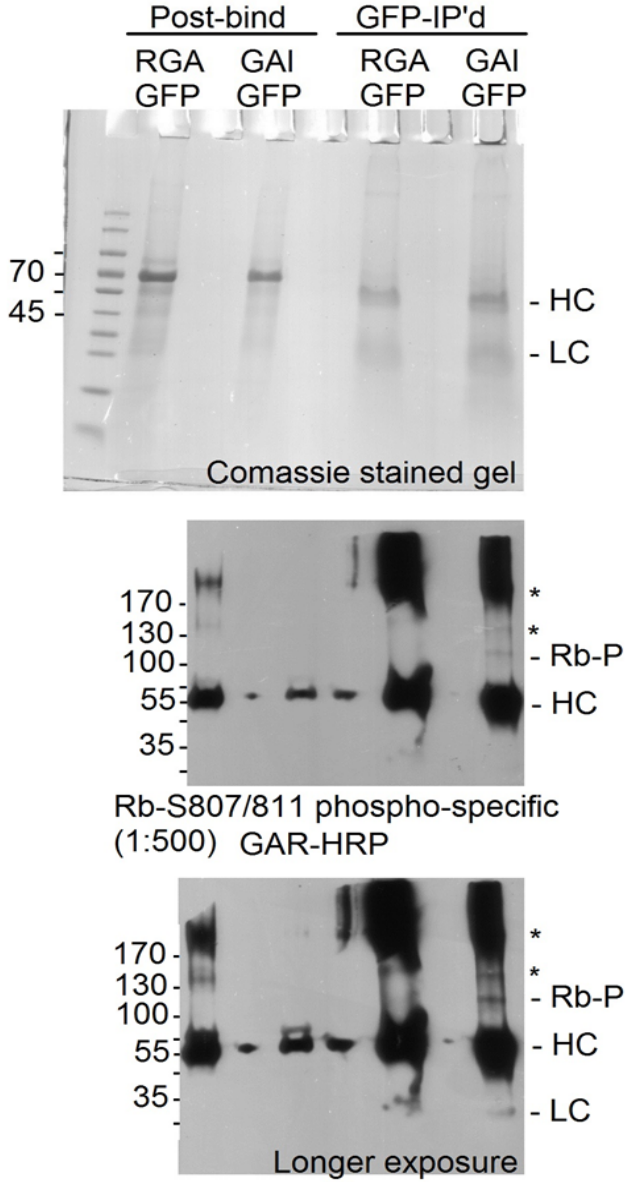
Post-bind
GFP-IP'd
RGA GFP
GAI GFP
RGA GFP
GAI GFP
70
45
- HC
- LC
Comassie stained gel
170
130
100
55
35
*
*
- Rb-P
- HC
Rb-S807/811 phospho-specific
(1:500) GAR-HRP
170
130
100
55
35
*
*
- Rb-P
- HC
- LC
Longer exposure

B (i)

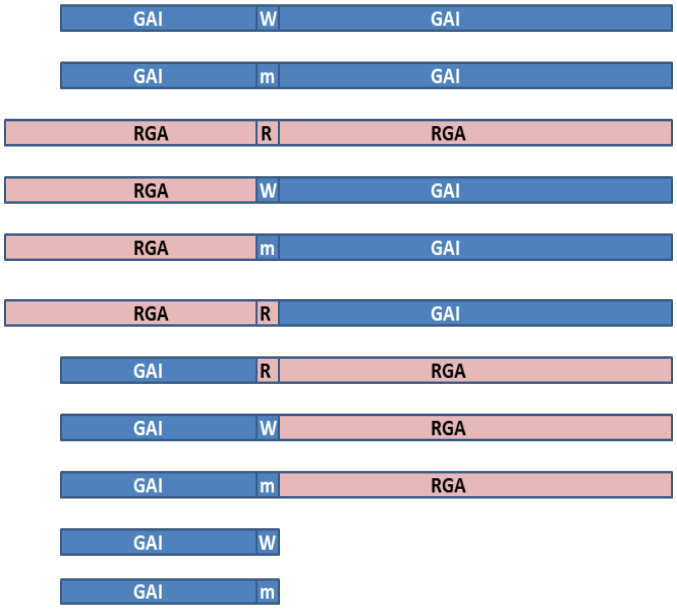

W = LxCxE
m = GxGxG
R = MxCxE

B (ii)

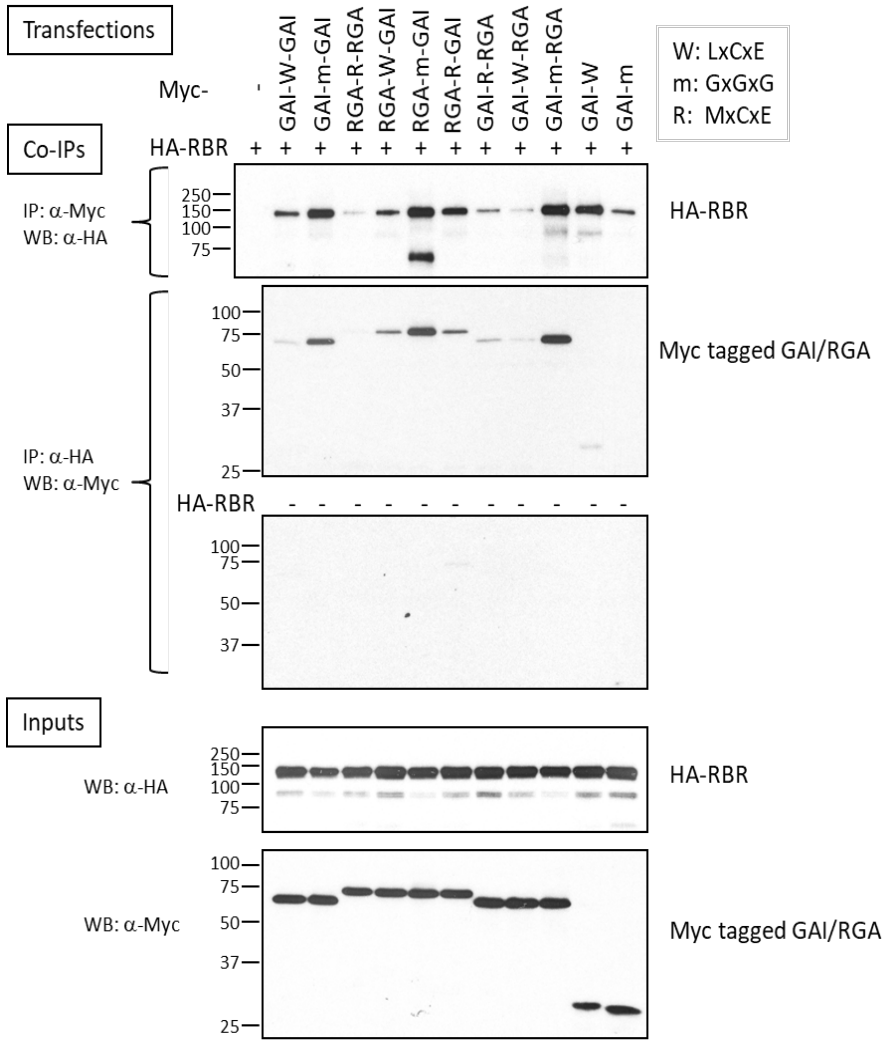

The results demonstrated that GAI in its native form binds more strongly to RBR than native RGA. A binding was also demonstrated when the GAI protein was truncated, but still included the native LxCxE motif. However, unexpected findings were reported when the GAI motif was mutated to GxGxG, which had a greater binding affinity to RBR than the native form. This was also observed for the construct expressing the RGA N-terminal containing this motif fused to the GAI C-terminal and vice versa. The most likely explanation for these findings is that glycine can destabilise α-helixes, so mutating this motif to contain these residues may have prevented the resulting protein from folding properly and therefore rendered it to be un-functional, causing it to aggregate as a result. Irrespective of these unexpected results, the experiments generally support the hypothesis that GAI binds to RBR and demonstrated that RGA can also bind, but to a weaker extent. This experiment also revealed information on potential regions, other than the GAI motif itself that might be important for enhancing this binding affinity. Indeed, when the N-terminus of RGA either contained its native form of the motif or the LxCxE motif fused to the C-terminus of the GAI, these fusion proteins bound to RBR to a greater extent than when the fusion proteins were constructed the other way round i.e. the GAI C-terminal fused to the RGA N-terminal with either of these motifs. Therefore, the C-terminal region of GAI is potentially more important for enhancing the binding of this protein to RBR. 3D protein modelling of this interaction could be one way of clarifying these results further so that the molecular structure of both proteins and how they fit together can be visualised.

Another biochemical method used to test for protein interactions is a GST pull-down assay. This involves fusing the target protein (bait) to a molecular tag, glutathione-s-transferase (GST). The fusion protein can then be cloned into an isopropyl-beta-D-thiogalactoside (IPTG)-inducible construct for expression in bacteria. The resulting bacterial culture is then lysed to release total protein content and incubated with glutathione sepharose beads to purify by affinity the GST fusion protein from the lysate. This glutathione sepharose matrix bound to the GST fusion protein can then be incubated with a crude or purified protein extract containing the putative binding partner (prey). Complexes recovered from the beads can then be resolved with SDS-PAGE and analysed with western blot analysis.

Alternatively to these biochemical methods, protein interactions can be probed *in situ* with microscopy using fluorescent lifetime imaging (FLIM) and by measuring the Förster resonance energy transfer (FRET) between two fluorophores. FLIM generates images based on the excited state decay rates of a fluorescent sample (Gadella *et al.*, 1993). When a fluorophore is excited, it will remain in this state for a period of time before returning to its resting state and emitting a photon as a result. The fluorescence lifetime is therefore defined as the average time that a fluorophore remains in this excited state. Because the lifetimes of individual fluorophores are being measured rather than their

emission spectra, it is a more robust way of capturing an image and has several advantages over intensity-based methods, such as being independent of concentration. FLIM is performed with a single wavelength and can be measured in two different ways: in the frequency domain or a time domain. A common way of determining FLIM in the time domain is to use Time-Correlated Single Photon Counting. This incorporates the use of a pulsed laser to excite individual photons and a specialised single-photon detector to measure the time between photon excitation and detection.

FRET is a distance dependent method of measuring the radiationaless energy transfer from an excited donor fluorophore to a suitable acceptor fluorophore through dipole-dipole interactions. Since the fluorescence lifetime of a fluorophore is dependent on both radiative (i.e. fluorescence) and non-radiative (i.e. quenching, FRET) processes, the lifetime of the donor decreases as a result of energy transfer from the donor molecule to the acceptor molecule. Protein-protein interactions can therefore be tested using FLIM/FRET analysis by labelling both proteins with a suitable pair of fluorescent molecules. The donor fluorescent dye must have a shorter excitation/emission spectra than the acceptor and there must also be an overlap between the excitation spectra of the donor and the emission spectra (absorption) of the acceptor. This spectral overlap allows FRET to occur so long as the donor and acceptor are within close proximity of each other (< 10nm). Special filter combinations can then be used to image these proteins at the cellular level to determine the average lifetime of the donor on its own and the donor in the presence of the acceptor.

Here, I report on the incorporation of the aforementioned techniques to develop and expand upon initial findings of an interaction between GAI/RGA and RBR and the interpretation of these results.

5.1 Results

5.1.1 The GAI LxCxE motif and the RGA MxCxE motif is evolutionarily conserved in higher plants

In order to examine the relevance of the GAI LxCxE motif in plants and assess if it has been evolutionarily conserved between different plant species, a tBlastn search for homologues of the *Arabidopsis thaliana* GAI amino acid sequence (AtGAI) was performed. A tBlastn search is an online tool available on the National Center for Biotechnology Information (NCBI) website that allows the user to identify homologous protein sequences. This is done by inputting an amino acid sequence and querying it against a translated nucleotide sequence database, which dynamically translates in all six reading frames on both strands. It also enables the user to define specific parameters such as the type of database and the type of organism/taxon to search. In this query, the refseq_genomic database was specified because it contains a set of well annotated and comprehensive sequences that provide a stable reference for comparative genomics (O'Leary *et al.*, 2016). The tBlastn search resulted in some

Figure 5.2 Amino acid (aa) sequence alignments for GAI and RGA. Alignments are colour coded by consensus sequence identity. Aa's that share 100% identity between all of the aligned sequences are white, whereas aa's are graded from light to dark shades of grey depending on their percentage identity respective to the other aligned sequences. The motif of interest is highlighted in light-blue.

(A) Result of a tBlastn search for GAI (TAIR: AT1G14920) homologues showing the highly conserved LxExC motif. The major crops, rice (*Oryza sativa*), maize (*Zea mays*), wheat (*Triticum aestivum*), barley (*Hordeum vulgare*) and the common liverwort, *Marchantia polymorpha*, have also been included.

(B) Result of a tBlastn search for RGA (TAIR: AT2G01570) homologues showing the highly conserved MxCxE motif.

(C) Result of an alignment for the SCR, GAI and RGA protein sequences showing the variation for the LxCxE motif and surrounding aa's between them.

(D) Phylogenetic analysis of selected GAI and RGA homologues from the tBlastn search. The phylogeny was constructed using an Unweighted Pair Group Method with Arithmetic Mean (UPGMA) and a bootstrap value of 1000 replicates.

A

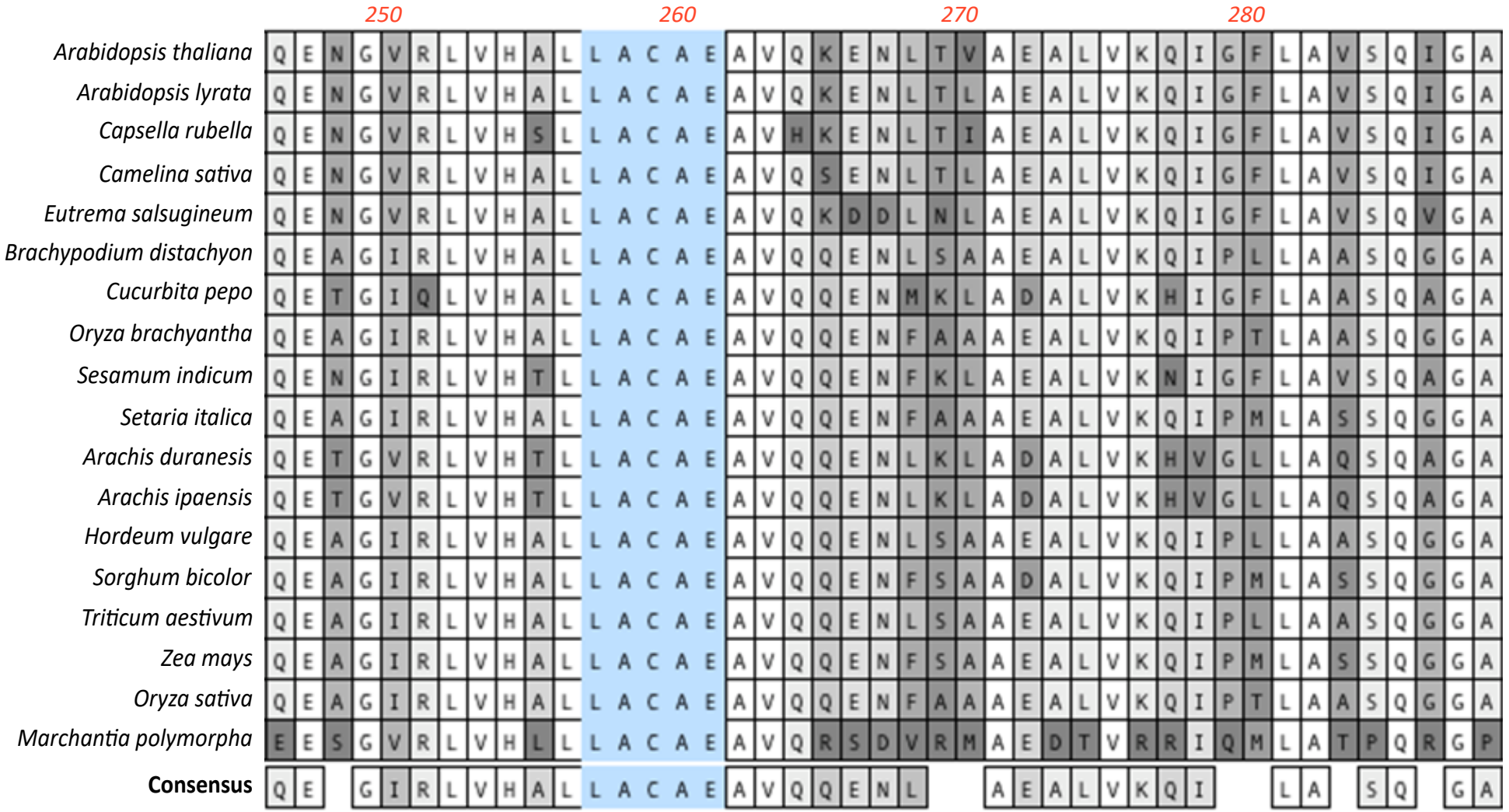
250
260
270
280
Arabidopsis thaliana
Arabidopsis lyrata
Capsella rubella
Camelina sativa
Eutrema salsugineum
Brachypodium distachyon
Cucurbita pepo
Oryza brachyantha
Sesamum indicum
Setaria italica
Arachis duranesis
Arachis ipaensis
Hordeum vulgare
Sorghum bicolor
Triticum aestivum
Zea mays
Oryza sativa
Marchantia polymorpha
Consensus

B

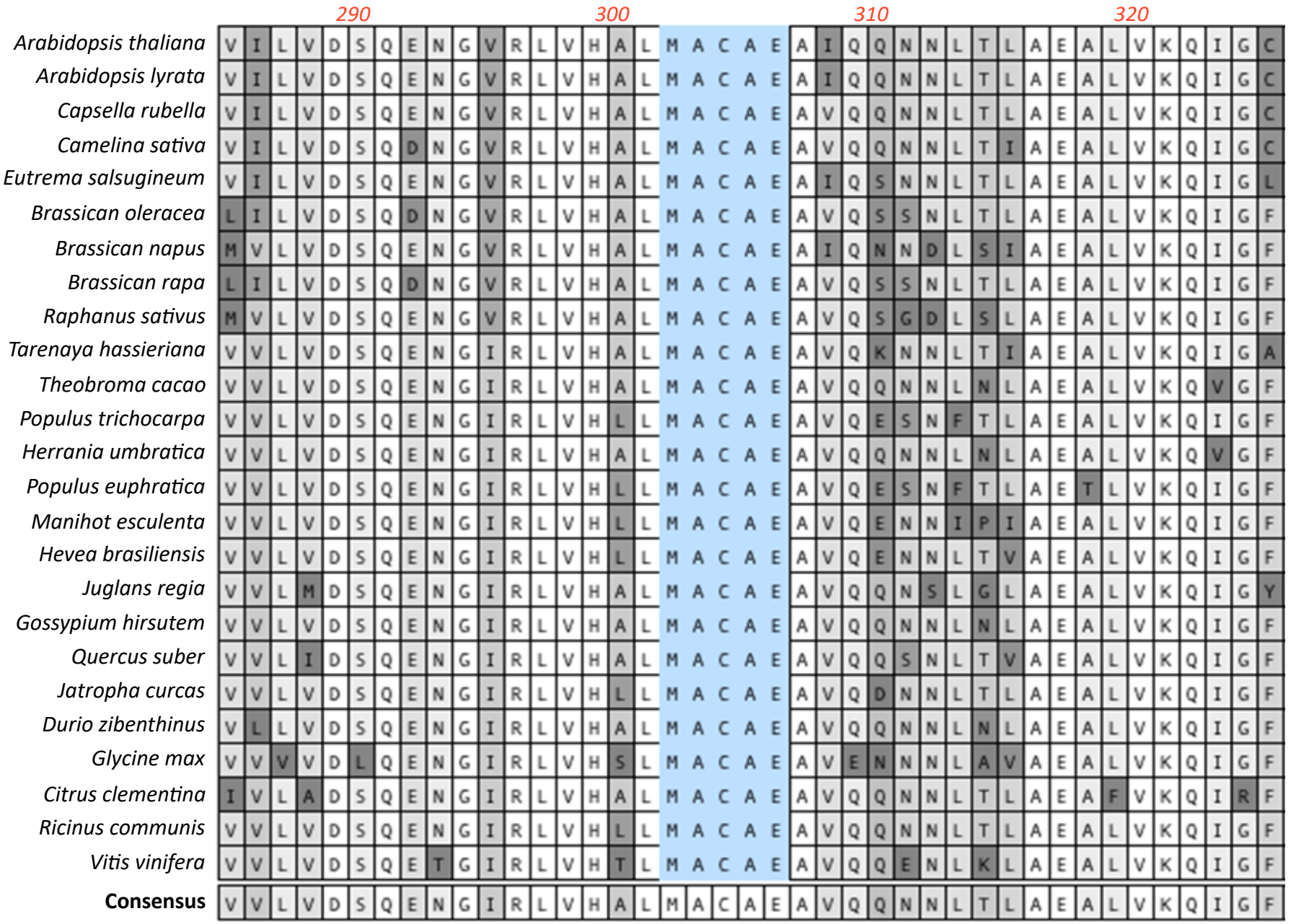
290
300
310
320
Arabidopsis thaliana VILVDSQENGVRLVHALMACAEAIQQNNLTLAEALVKQIGC
Arabidopsis lyrata VILVDSQENGVRLVHALMACAEAIQQNNLTLAEALVKQIGC
Capsella rubella VILVDSQENGVRLVHALMACAEAVQQNNLTLAEALVKQIGC
Camelina sativa VILVDSQDNGVRLVHALMACAEAVQQNNLTIAEALVKQIGC
Eutrema salsugineum VILVDSQENGVRLVHALMACAEAIQSNNLTLAEALVKQIGL
Brassican oleracea LILVDSQDNGVRLVHALMACAEAVQSSNLTLAEALVKQIGF
Brassican napus MVLVDSQENGVRLVHALMACAEAIQNNDLSIAEALVKQIGF
Brassican rapa LILVDSQDNGVRLVHALMACAEAVQSSNLTLAEALVKQIGF
Raphanus sativus MVLVDSQENGVRLVHALMACAEAVQSGDLSLAEALVKQIGF
Tarenaya hassieriana VVLVDSQENGIRLVHALMACAEAVQKNNLTIAEALVKQIGA
Theobroma cacao VVLVDSQENGIRLVHALMACAEAVQQNNLNLAEALVKQVGF
Populus trichocarpa VVLVDSQENGIRLVHLLMACAEAVQESNFTLAEALVKQIGF
Herrania umbratica VVLVDSQENGIRLVHALMACAEAVQQNNLNLAEALVKQVGF
Populus euphratica VVLVDSQENGIRLVHLLMACAEAVQESNFTLAETLVKQIGF
Manihot esculenta VVLVDSQENGIRLVHLLMACAEAVQENNIPIAEALVKQIGF
Hevea brasiliensis VVLVDSQENGIRLVHLLMACAEAVQENNLTVAEALVKQIGF
Juglans regia VVLMDSQENGIRLVHALMACAEAVQQNSLGLAEALVKQIGY
Gossypium hirsutem VVLVDSQENGIRLVHALMACAEAVQQNNLNLAEALVKQIGF
Quercus suber VVLIDSQENGIRLVHALMACAEAVQQSNLTVAEALVKQIGF
Jatropha curcas VVLVDSQENGIRLVHLLMACAEAVQDNNLTLAEALVKQIGF
Durio zibenthinus VLLVDSQENGIRLVHALMACAEAVQQNNLNLAEALVKQIGF
Glycine max VVVVDLQENGIRLVHSLMACAEAVENNNLAVAEALVKQIGF
Citrus clementina IVLADSQENGIRLVHALMACAEAVQQNNLTLAEAFVKQIRF
Ricinus communis VVLVDSQENGIRLVHLLMACAEAVQQNNLTLAEALVKQIGF
Vitis vinifera VVLVDSQETGIRLVHTLMACAEAVQQENLKLAEALVKQIGF
Consensus VVLVDSQENGIRLVHALMACAEAVQQNNLTLAEALVKQIGF

C

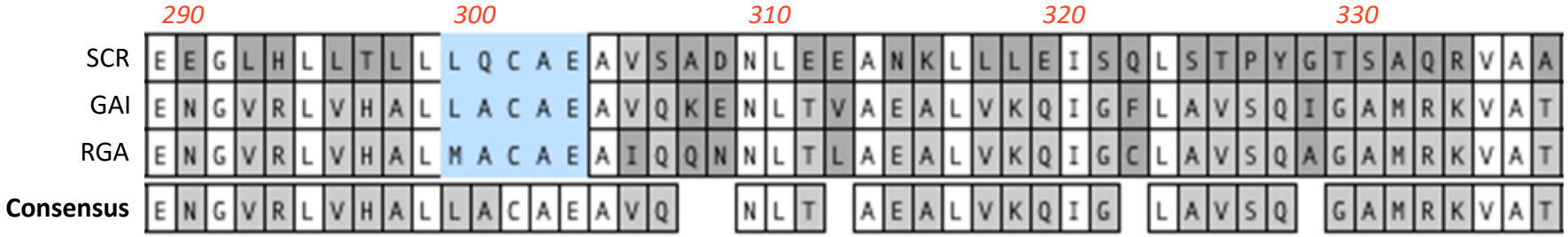

D

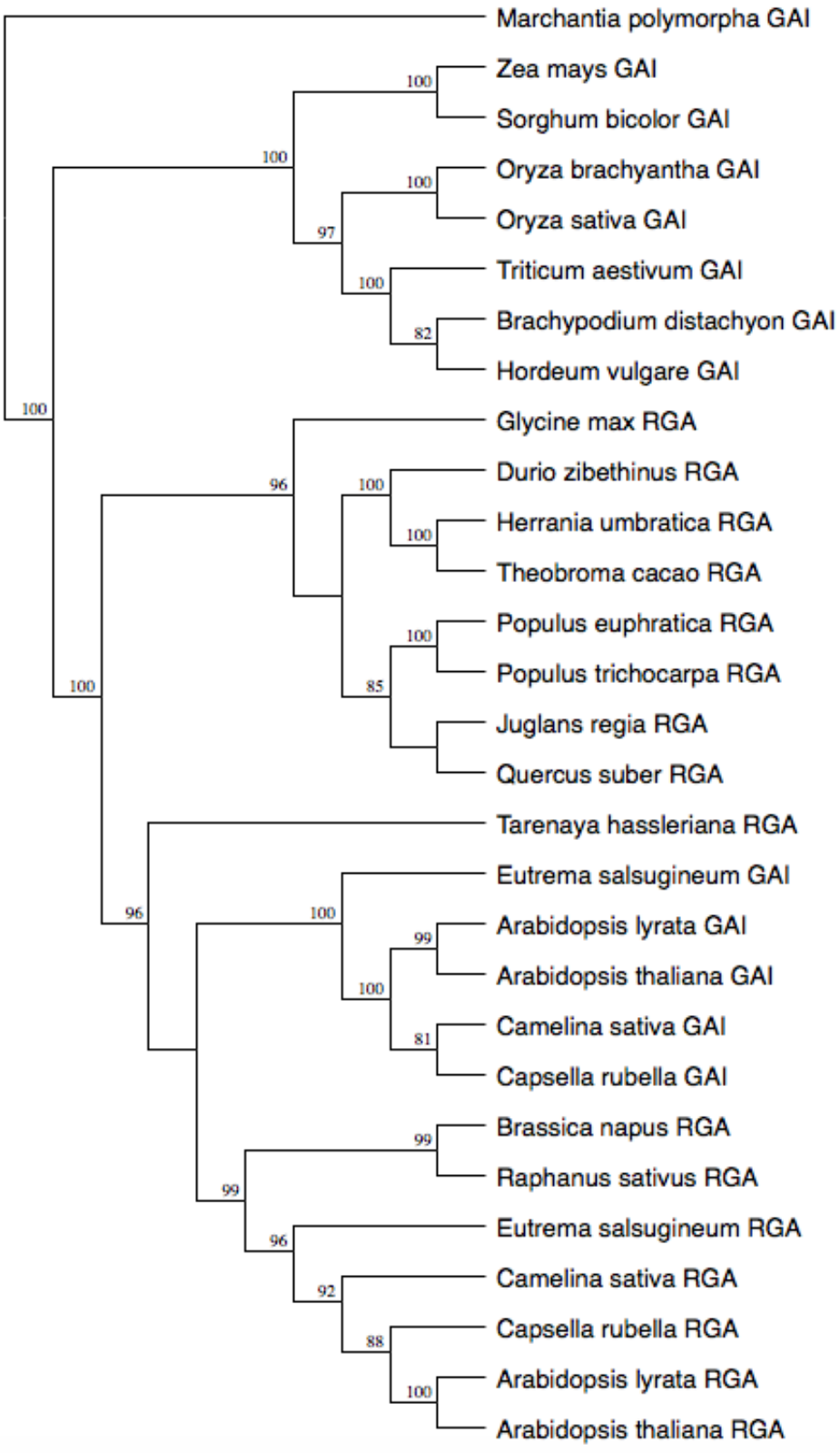
Marchantia polymorpha GAI
Zea mays GAI
Sorghum bicolor GAI
Oryza brachyantha GAI
Oryza sativa GAI
Triticum aestivum GAI
Brachypodium distachyon GAI
Hordeum vulgare GAI
Glycine max RGA
Durio zibethinus RGA
Herrania umbratica RGA
Theobroma cacao RGA
Populus euphratica RGA
Populus trichocarpa RGA
Juglans regia RGA
Quercus suber RGA
Tarenaya hassleriana RGA
Eutrema salsugineum GAI
Arabidopsis lyrata GAI
Arabidopsis thaliana GAI
Camelina sativa GAI
Capsella rubella GAI
Brassica napus RGA
Raphanus sativus RGA
Eutrema salsugineum RGA
Camelina sativa RGA
Capsella rubella RGA
Arabidopsis lyrata RGA
Arabidopsis thaliana RGA
100
100
100
97
100
82
100
96
100
100
100
85
96
100
99
100
81
99
99
96
92
88
100

homologous RGA sequences being highlighted. These homologs were probably selected because they are closely related to GAI. This was only noticed after aligning the top 20 sequences with the highest percentage identity and upon identifying the region where the LxCxE motif was situated. Some of the sequences contained the mutated form of the RGA motif, MxCxE, so these were traced back to the original protein to ensure that they were RGA homologs and were subsequently removed.

For some plants, their genome only codes for a single DELLA protein that is homologous to AtGAI, such as *SLR1* in rice, *Rht* in wheat, *SLN1* in barley and *D8* in maize (Winkler and Freeling, 1994; Peng *et al.*, 1999; Ikeda *et al.*, 2001; Chandler *et al.*, 2002). The sequences for these four major monocot crop species were obtained and included in the alignment in order to establish whether the LxCxE motif is conserved between monocots and dicots. A DELLA-like sequence from a more ancient plant model organism, *Marchantia polymorphia*, was also included in the alignment to establish whether this motif existed in early land plants. The results indicated that the motif is highly conserved between all of these plant species, including the monocotyledons (Figure 5.3A). Interestingly, there was no DELLA motif present in the *Marchantia* protein sequence, but the LxCxE motif was found. This would suggest that a GA mechanism may not have existed in early land plants and probably evolved later on in more complex plant species, such as the angiosperms. Not only were the key L-C-E amino acid residues conserved, but so were the intervening "x" amino acids, as alanine (Ala) in both cases. Furthermore, the amino acids surrounding this motif, both upstream and downstream were also highly conserved. The overall sequence that was conserved between all species was: L**LACAE**AV (where LxCxE is highlighted in bold). The fact that there is no variation for this motif between both monocots and dicots suggests that there is some sort of functional relevance for it. Therefore, it may be the case that these adjacent amino acids are also important for the binding affinity with RBR. There were also highly conserved regions preceding the LxCxE motif up to six amino acids away, apart from in the closely related species, *Capsella rubella* that had a single point mutation from Alu-Ser positioned two amino acids before the motif. Overall, it is clear that LxCxE motif in GAI has been evolutionarily conserved between higher plants, as well as surrounding regions with little variation when comparing between homologues.

Since RGA contains a variation of this motif, in which the Leu is replaced with a methionine (M), it is also useful to examine conservation of the MxCxE motif between species. RGA homologues only exist in dicots, so a tBLastn search using the AtRGA amino acid sequence was performed with eudicots specified and the same refseq_genomic database as selected for GAI. The MxCxE motif was found to be highly conserved between the top 25 homologous sequences that were obtained and aligned as a result of this search (Figure 5.3B). As in the case of the LxCxE motif in GAI the "x" amino acid in the MxCxE motif was Ala, which was also highly conserved between different species. Furthermore, some

of the amino acids surrounding this motif were highly conserved including a Leu that proceeds it and an Ala that comes after it. However, the variability surrounding this motif appeared to be greater than that of GAI homologues, especially at the position of two aa's before. Overall, it appears that the GAI LxCxE motif is evolutionarily conserved amongst monocots and dicots, whilst the RGA MxCxE motif is evolutionarily conserved to dicots only.

Phylogenetic analysis using some of these GAI- and RGA-like sequences indicate that GAI has been evolutionarily conserved from early land plants and that RGA occurred as a result of gene duplication in the eudicotyledons (Figure 5.3D). Interestingly, there is a group of species from the Rosid clade of flowering plants that have lost their GAI homologues, but have retained an RGA equivalent all with MxCxE motifs. This was observed in species ranging from soybean (*Glycine max*), English walnut (*Juglans regia*) and oak trees to rapeseed (*Brassica napus*) and Chinese cabbage (*Brassica rapa*). These observations were confirmed by investigating the type of DELLA proteins that exist in each individual species, either by further BLAST searches of specified genomes, or by searching the current literature around this subject. For example, a paper published in 2014 on genome-wide analysis of GRAS proteins in *Brasicca rapa*, demonstrated by comparing its genome with that of *Arabidopsis thaliana*, that they have RGA homologues but not GAI (Song *et al.*, 2014). The phylogenetic tree implies that species with both RGA and GAI homologues may have acquired them through multiple gene duplication events. If a GAI-RBR interaction is found, whilst an RGA-RBR interaction is not, then perhaps the LxCxE/MxCxE has influenced this function and therefore the evolution of their genes.

To assess differences between these motifs in relation to the closely related GRAS protein, SCR, a known binding partner for RBR, an alignment between these three proteins was performed (Figure 5.3C). From this alignment, the preceding Leu occurring prior to the motif and the Ala that follows immediately after, are conserved between these proteins. For RGA the following aa is an Isoleucine (I), whereas for SCR and GAI it is a Valine (V). In terms of the motif itself, the intervening aa's for GAI and RGA are the same, whereas the aa that follows the first Leu of the LxCxE motif for SCR is a Glutamine (Q) instead of an Ala. Regardless of these differences, it is evident that both GAI and SCR share the conserved LxCxE motif, whilst RGA does not. The fact that they all have the same preceding Leu to this motif and Ala just after, implies that these aa may also be important for SCR, RGA and GAI function, whether they bind to RBR or not.

5.1.2 Homology modelling of interaction between GAI and RGA reveals it can exist

As mentioned previously, there is currently no available crystal structure of *Arabidopsis* RBR, so homology modelling was used as a way to demonstrate an interaction *in silico*. The modelling was performed by Dr Salvatore Ferla from the School of Pharmacy and Pharmaceutical Sciences, Cardiff

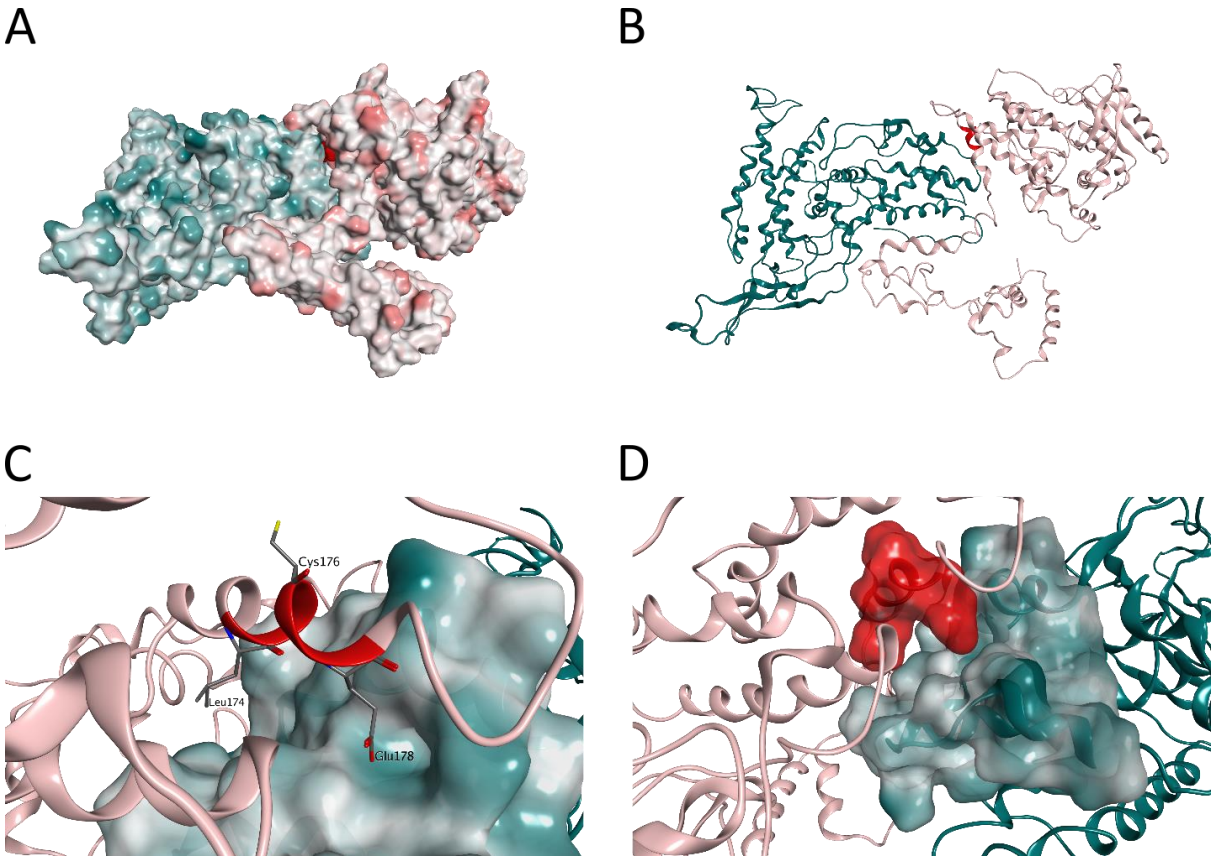

Figure 5.3: A 3D protein homology model of the interaction between GAI (pink) and RBR (blue) via the LxCxE motif (red) and represented as (A) the molecular surface of both proteins, (B) the ribbon surface, (C) a close-up of the LxCxE motif ribbon structure with the key amino acids (aa) shown and (D) a close-up of the molecular surface of the LxCxE motif bound to the corresponding binding pocket. For the RBR 3D structure, the *Arabidopsis thaliana* RBR (AtRBR) amino acid sequence was combined with the crystal structure of the A and B box of the human RB as a template. For the GAI 3D structure, the *Arabidopsis thaliana* GAI aa sequence was combined with the crystal structure for the first 113 aa's of AtGAI and the crystal structure of the GRAS domain from a related protein, SCL7 in rice (*Oryza sativa*). The N-terminal of the GAI protein is located to the bottom right of diagrams A and B.

University, who specialises in this type of method. The most identical protein with crystal structures available was the human RB with a 26% identity. Although several crystal structures for this protein were available, few of them were in the un-phosphorylated active form and they were only of the A and B box, where the corresponding binding site for the LxCxE motif resides. For this reason, the AtRBR amino acid sequence was obtained together with the human Rb crystal structure of the A and B box (C. Lee *et al.*, 2002) and aligned to generate a final 3D model. The crystal structure for the first 113 aa of *Arabidopsis* GAI was available on PDB, but this doesn't include the LxCxE motif, which starts at 174 aa (Murase et al. 2008). A protein blast search revealed a 34% identity between GAI and the crystal structure of the GRAS domain of SCL7 in rice (*Oryza sativa*) (Li *et al.*, 2016). The GRAS domain contains

the LxCxE motif. Thus, the primary amino acid sequence for GAI was obtained together with the two aforementioned crystal structures and aligned to generate a 3D model. The interaction was then modelled using a protein-protein docking tool by selecting the LxCxE motif as the ligand and the corresponding binding pocket as the receptor (Figure 5.3). The resulting homology model demonstrated that the putative interaction between the LxCxE motif of GAI and a corresponding binding pocket of RBR is indeed possible. Furthermore, it demonstrated that as well as this motif, a large region of the GAI protein remains in contact with the RBR protein. For a more detailed description of these methods and results see section 2.4.2.

5.1.3 Testing for a putative interaction between GAI/RGA and RBR using immunoprecipitation techniques

As mentioned earlier, a closely related GRAS family protein known as SCR was found to interact with RBR using a yeast-two-hybrid assay. Since this method was able to demonstrate a binding affinity between these two proteins, it was initially used by other researchers to investigate the putative interaction between GAI/RGA and RBR. Unfortunately, results from these experiments were reported to be inconclusive (Angela Marchbank, personal communication). As mentioned previously, unpublished data from Nottingham University had investigated the interaction using Co-IP's. They found evidence for a positive binding between GAI-GFP and RBR, but not GFP-RGA. However, all the necessary controls weren't included, such as the use of a WT line as a negative control for the pull-down of GFP and probing the membrane with an anti-GFP antibody to assess whether GFP-tagged protein had been pulled-down.

To assess the validity of these findings, the experiments were repeated with the necessary controls in place. The initial Co-IP experiment was performed on nuclei preps of root cultures from the previously described translational reporter lines, pGAI::GAI-GFP and pRGA::GFP-RGA (Silverstone *et al.*, 2001; Fleck and Nicholas P. Harberd, 2002). This means that seedlings of these lines were grown in conical flasks containing root growth media for a period of 3-4 weeks under no light conditions, in order to induce root growth only. Since previous evidence implied a putative interaction between GAI and RBR may occur in the root, root cultures were grown as a way of bulking up the levels of target protein complexes. Nuclei preps were performed to extract nuclei from the root cultures, since all proteins of interest had previously been shown to be nuclear-localised (see Chapter 3). This technique is useful for concentrating nuclear-localised target protein, as well as removing other unwanted proteins from the total extract. This can help reduce the amount of unspecific binding when using polyclonal antibodies to pull-down and probe these extracts during the Co-IP.

Once nuclei preps had been obtained from root cultures of pGAI::GAI-GFP, pRGA::GFP-RGA and WT (Ler) seedlings, the extracts were incubated with a GFP antibody followed by magnetic-coated agarose beads conjugated to Protein A (the GFP antibody was generated in rabbit – see Chapter 2) to pull-down GFP-tagged protein and assess whether there was any unspecific binding to the beads themselves. From western blot analysis of these nuclei preps, the level of GAI protein detected was lower than the level of RGA (Figure 5.4). Although total protein content was not quantified prior to loading of the gel, the amount of starting material for each extract was similar between samples. For the initial Co-IP result obtained at Nottingham University, a human RB antibody was used to detect RBR protein on a western blot. This antibody was obtained and tested on total protein extracts of whole seedlings, but was unable to detect a corresponding band, even though the same conditions were used as originally described. Initial attempts were made to express a peptide of *Arabidopsis* RBR in *E.coli* in order to make a species-specific antibody that was much more suitable for this purpose. However, it was eventually discovered that a commercially available *Arabidopsis thaliana* RBR antibody (AtRBR1) had already been developed (Magyar *et al.*, 2012). The results from Co-IP experiments performed under these conditions revealed that RBR could be detected in the input samples, but not in the unbound fraction (post-bind) after the pull-down and neither in the elute for all samples (Figure 5.5A,B). These experiments were repeated multiple times, without successful detection of RBR in the eluted fraction (Table 5.1).

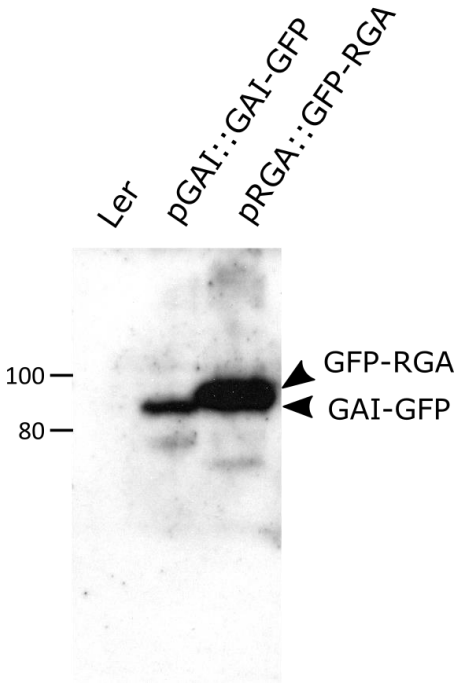

Figure 5.4 Western blot analysis on nuclear extracts using an anti-GFP antibody to detect GAI-GFP and GFP-RGA fusion protein in *Arabidopisis thaliana*. Nuclei preps were performed on WT, pGAI::GAI-GFP and pRGA::GFP-RGA root cultures in the *Ler* ecotype. Samples were separated on an 8% SDS gel and probed with anti-GFP antibody (Torey Pines) followed by a HRP-conjugated goat anti-rabbit IgG secondary antibody (Santa Cruz).

Since it was difficult to obtain a large amount of GAI protein from these nuclei preps of roots cultures, different types of growth conditions were investigated in order to try and optimise the total GAI concentration. Moreover, even though the same protocol and growth conditions were followed, the root cultures did not grow very well when compared to the ones grown at Nottingham University. Analysis of GAI expression in *Arabidopsis* roots (Chapter 3) indicated that GAI expression in this organ was generally low, being concentrated mainly in the RAM. Therefore, to increase the chance of detection, multiple individual seedlings of the pGAI::GAI-GFP line were grown together to perform nuclei preps on this material. Two methods were adopted for this purpose: seedlings grown on GM root plates and seedlings grown hydroponically (see Chapter 2 for details). After 7 days of growth (7 DAS), the roots were separated from the shoots and the resulting plant matter was weighed prior to nuclear extraction. Samples were then run on an SDS gel and probed with an anti-GFP antibody. Western blot analysis revealed that higher amounts of GAI-GFP protein could be detected in the condition where seedlings were grown on plates, whereas GFP-RGA protein levels appeared to be the same between both conditions (Figure 5.5D). Nuclei preps from shoots of pGAI::GAI-GFP seedlings were also included to assess the prevalence GAI-GFP levels and compare between growth conditions. The shoots of pGAI::GAI-GFP seedlings had higher GAI-GFP levels when grown hydroponically, but they still appeared to be lower than the levels found for roots grown on plates (Figure 5.5D).

Western blot analysis using the AtRBR1 antibody revealed that for Ler (WT) seedlings the amount of RBR protein appeared to be relatively similar between the growth conditions (Figure 5.3c). However, for pGAI::GAI-GFP and pRGA::GFP-RGA seedlings, higher RBR levels were detected when seedlings were grown on plates, compared to seedlings grown hydroponically. Nuclei preps on the shoots of pGAI::GAI-GFP seedlings were also tested for RBR expression, but there was less RBR protein detectable in both experimental conditions. Overall, it appeared that growing seedlings on plates was the best experimental condition to use for obtaining highest amounts of GAI-GFP, GFP-RGA and RBR protein in the aforementioned lines.

Co-IP's using these extracts were performed and repeated multiple times, but no bands corresponding to the size of RBR were observed in the elute for all samples. Moreover, a large amount of seed (approximately 1 ml) was required to obtain enough starting material for nuclear extraction, particularly since the roots were much lighter than the shoot, so it was difficult to bulk these lines up sufficiently to maintain these experiments. Therefore, nuclei preps were performed on whole seedlings rather than roots alone in order to bulk up the amount of material extracted for Co-IP experiments. To reduce the amount of steps involved and the incubation time during this process, commercially available magnetic-coated agarose beads conjugated to a GFP antibody (GFP-Trap) were used instead of a GFP antibody followed by Protein A beads. Since previous Co-IP attempts were

Figure 5.5 Immunoblot analysis of pull-down and root growth experiments to investigate the putative interaction between GAI/RGA and RBR in *Arabidopsis*.

(A) Results from Co-IP experiments performed on nuclei preps of root cultures for WT, pGAI::GAI-GFP and pRGA::GFP-RGA seedlings in the *Ler* ecotype. The pull-down was performed by incubating nuclear extracts with magnetic beads conjugated to a GFP antibody (GFP-Trap, Chromotek). The resulting samples were separated on an 8% SDS gel, including 40 µg of starting material (Input), 20 µl of the unbound/post-bound fraction (PB) and 20 µl from the pull-down extract (Elute).

    (i) Western blot analysis was performed using an AtRBR1 antibody for detection of RBR protein, with an approximate size of 125 kDa
    (ii) The loading control for the Co-IP experiment.

(B) Western blot analysis on nuclei preps of root and shoot (S) cultures for WT, pGAI::GFP-GAI and RGA::GFP-GAI seedlings grown in different conditions to increase levels of target protein from extracts used for Co-IP experiments. Seedlings were either grown on plates containing growth media, or hydroponically (H). 20 µl of each nuclear extract was separated on an 8% SDS and transferred to a PVDF membrane.

    (i) The membrane was probed with an AtRBR (Agrisera) antibody for detection of RBR protein.
    (ii) The membrane was probed with an anti-GFP antibody for detection of GAI-GFP and GFP-RGA protein.

(C) Results from Co-IP experiments performed on total protein extracts of WT, pGAI::GAI-GFP, pRGA::GFP-RGA, pE2FA::E2FA-GFP and 35S::GAI-GFP whole seedlings. Extracts were incubated with GFP-Trap beads (Chromotek) to pulldown GFP-tagged protein. The resulting samples were run an 8% SDS gel, including 40 µg of starting material (Input), 20 µl of the unbound/post-bound fraction (PB) and 20 µl of the from the pull-down extract (Elute).

    (i) Western blot analysis using an AtRBR1 antibody (Agrisera) was performed for detection of RBR protein.
    (ii) Western blot analysis using an anti-GFP antibody (Torrey Pines) to visualise the pull-down efficiency for GAI-GFP, GFP-RGA and E2FA-GFP protein.

(D) Results from Co-IP experiments performed on whole seedling total protein extracts of 35S::GAI-GFP and E2FA::E2FA-GFP seedlings. Extracts were incubated with GFP-Trap beads (Chromotek) to pulldown GFP-tagged protein. The resulting samples were separated on an 8% SDS gel, including 40 µg of starting material (Input), 20 µl of the unbound/post-bound fraction (PB) and 20 µl from the pull-down extract (Elute).

    (i) Western blot analysis using an AtRBR1 antibody was performed for detection of RBR protein
    (ii) Western blot analysis using an anti-GFP antibody to visualise the pull-down efficiency for GAI-GFP and E2FA-GFP protein.

A (i)

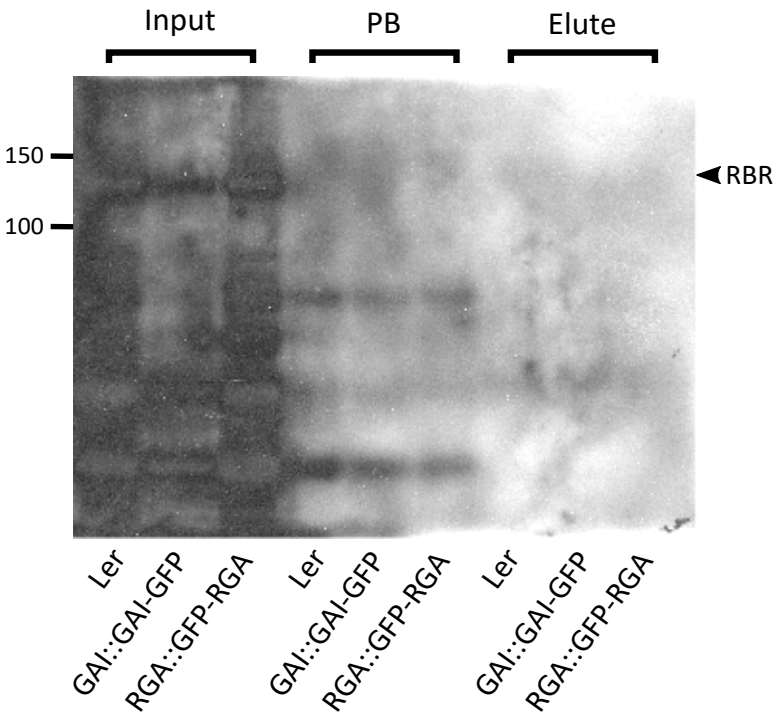

1° = αGFP 1:3000
2° = GAR 1:20,000

A (ii)

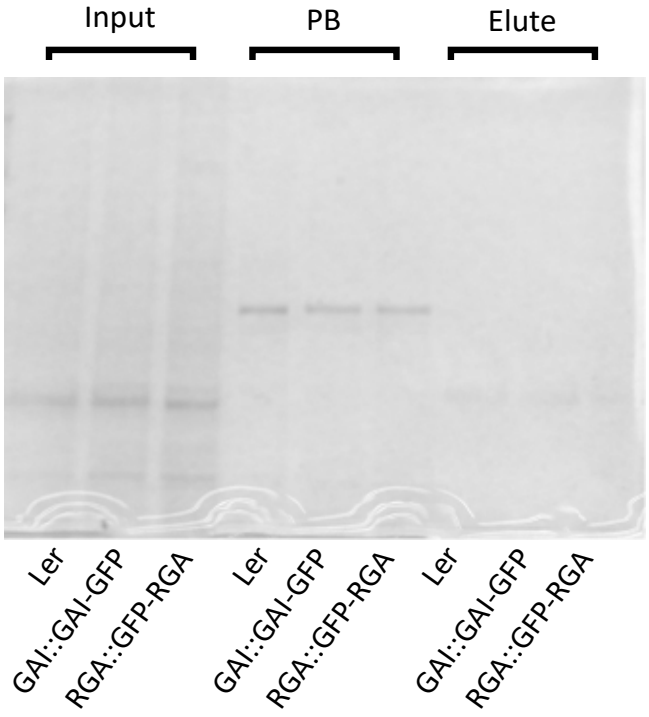

Loading control

B (i)

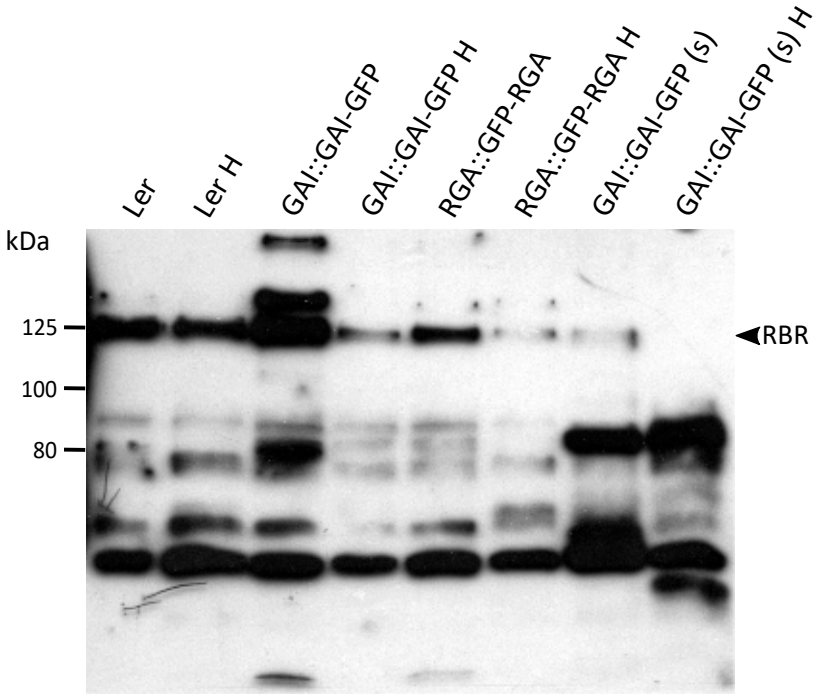

1° = αRBR 1:6000
2° = GAC 1:20,000

B (ii)

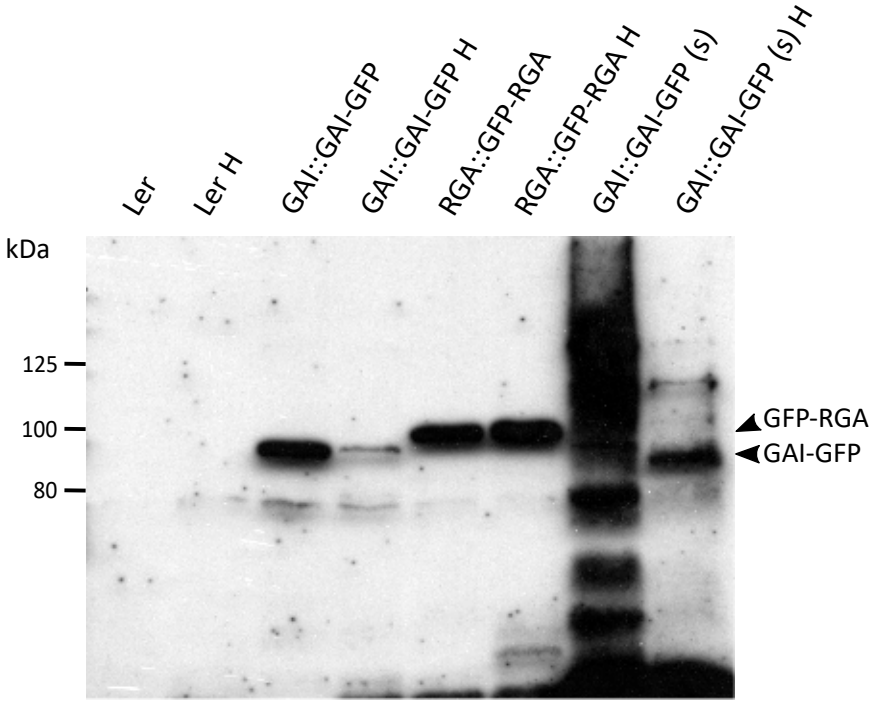

1° = αGFP 1:3000
2° = GAR 1:20,000

C

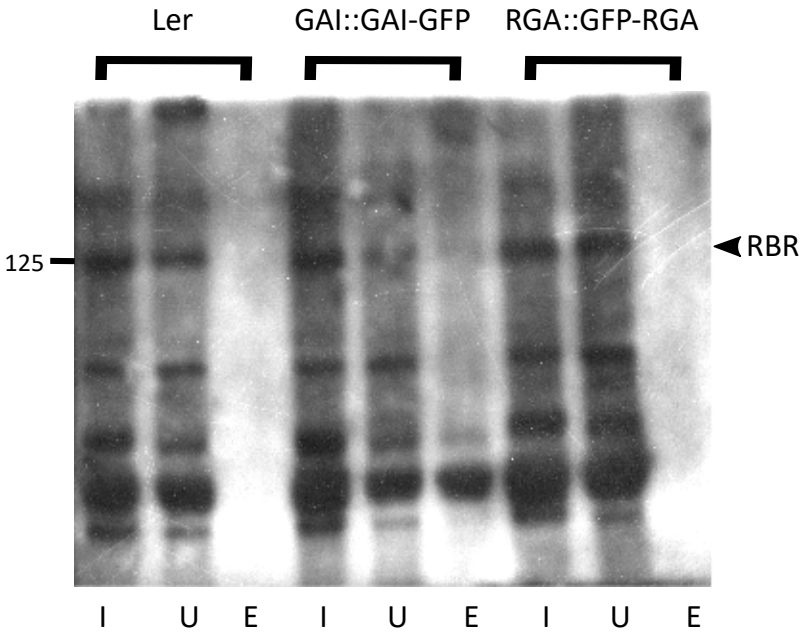

1° = αRBR 1:6000
2° = GAC 1:20,000

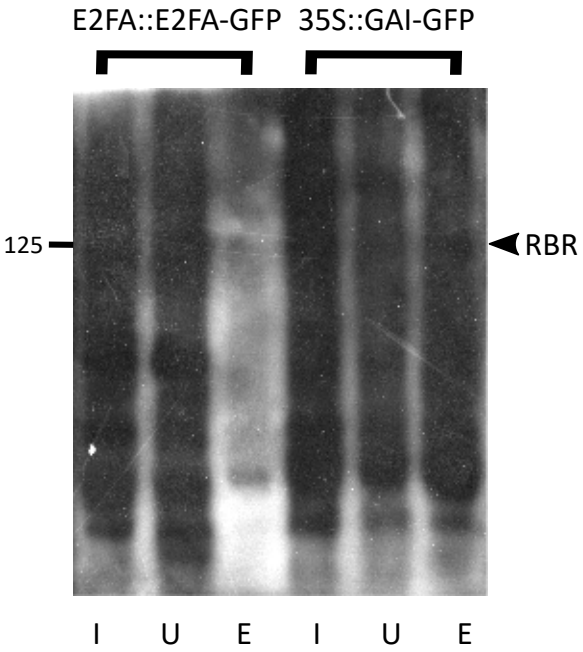

1° = αRBR 1:6000
2° = GAC 1:20,000

D

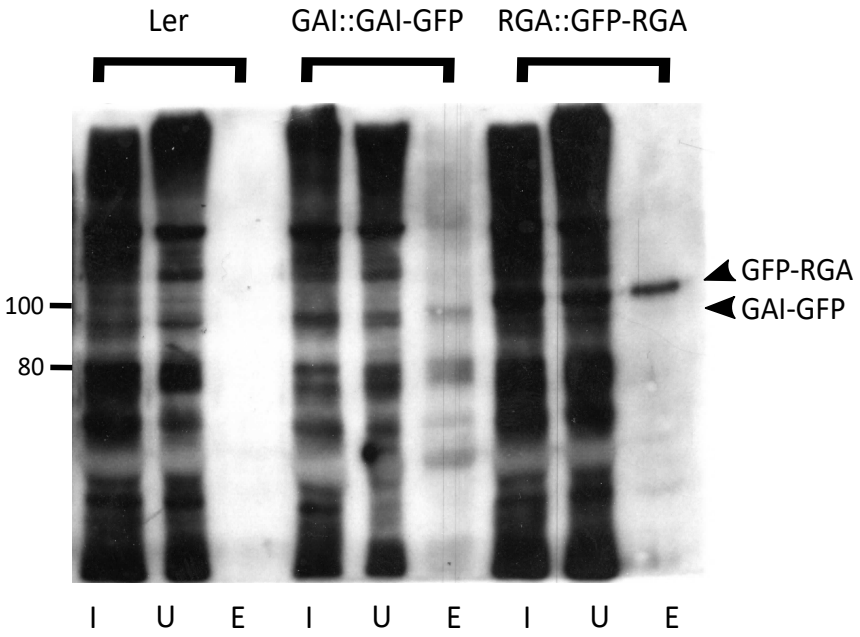

1° = αGFP 1:3000
2° = GAR 1:20,000

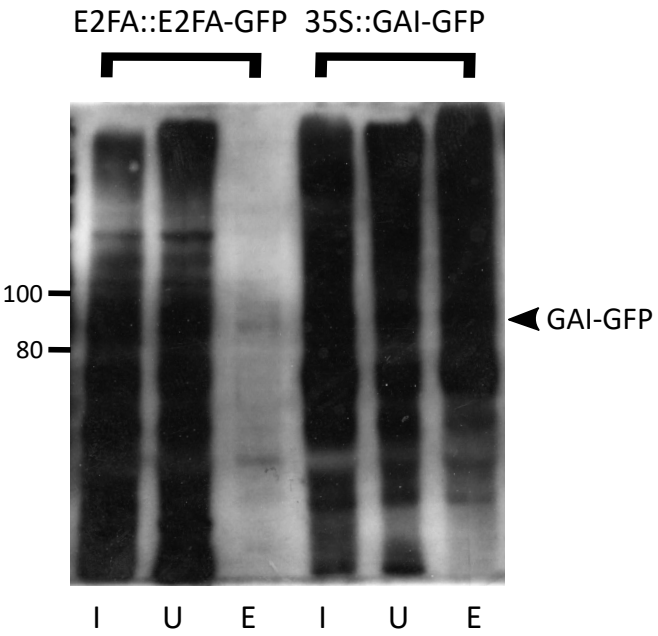

1° = αGFP 1:3000
2° = GAR 1:20,000

E (i)

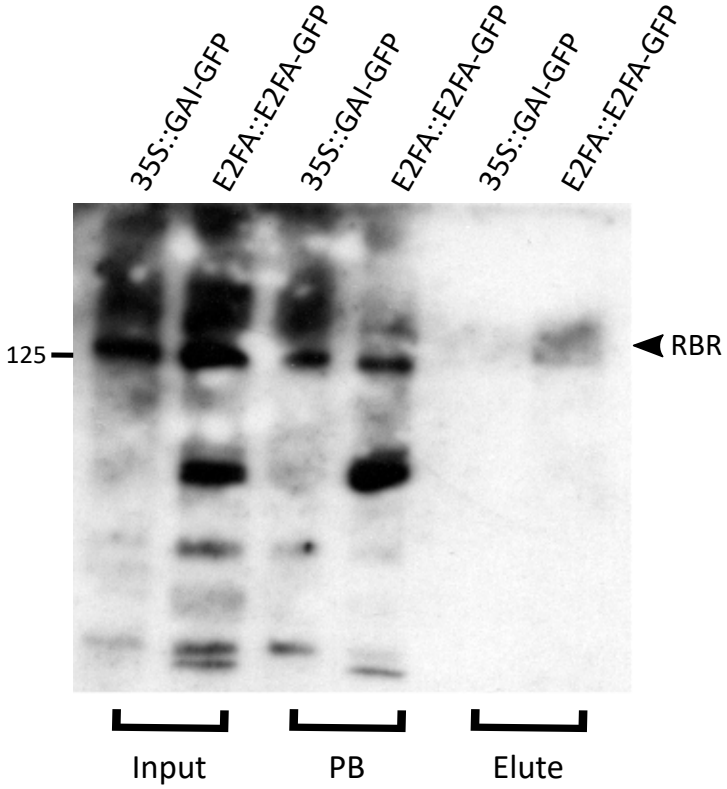

1° = αRBR 1:6000
2° = GAC 1:20,000

E (ii)

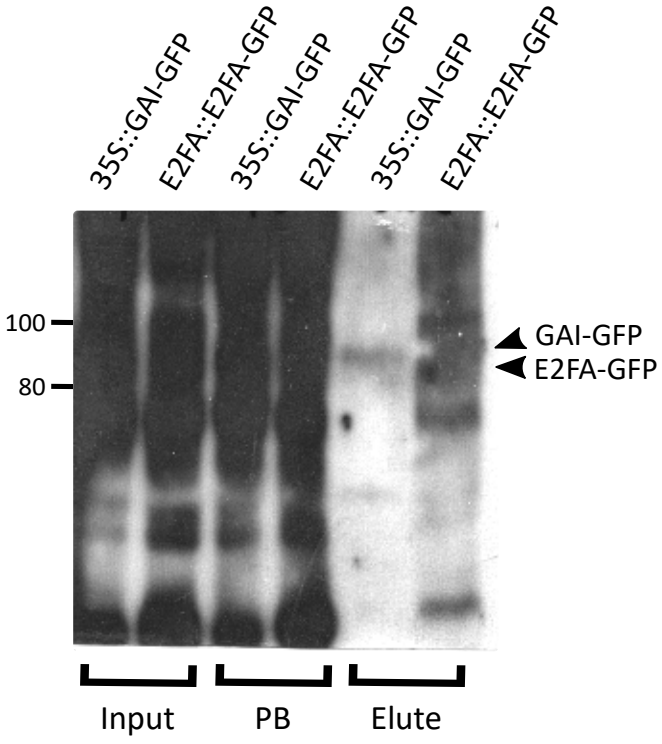

1° = αGFP 1:3000
2° = GAR 1:20,000

unsuccessful in demonstrating a positive binding, it was difficult to infer whether this was an indication that the pull-down itself did not work or that the interaction doesn't exist. To test this further, a known binding partner for RBR was incorporated into subsequent Co-IP experiments as a positive control. Magyar et al., 2012 had shown that E2FA-GFP can bind to RBR, so the translational reporter line described in this paper, pE2FA::E2FA-GFP, was obtained from the authors. A positive binding between GAI/RGA and RBR using these methods was not found, but this was also the case for the positive control suggesting that the pull-down itself wasn't working.

To adapt this protocol further, total protein extracts were performed on whole seedlings instead of nuclei preps. This was done for WT (Ler), pGAI::GAI-GFP, pRGA::GFP-RGA and pE2FA::E2FA-GFP seedlings, as well as incorporating the 35S::GAI-GFP line to try and increase the expression of GAI-GFP. This time around, a very faint band corresponding to the size of RBR was observed in the elute for both pGAI::GAI-GFP and 35S::GAI-GFP (Figure 5.5E). However, the positive control failed to work during this experiment, suggesting that perhaps the pull-down itself was variable in its efficiency. Indeed, when probing the membrane with an anti-GFP antibody, there wasn't a clear band corresponding to the approximate size of the target protein being pulled-down across all samples, although it was found for pGAI::GAI-GFP and 35S::GAI-GFP seedlings (Figure 5.5F). Therefore, these results are indicative of a genuine interaction between GAI-GFP and RBR. However, subsequent repeats of this particular experiment did not reproduce the same result consistently.

In one particular experiment using total protein extracts from whole seedlings, the pull-down was performed using the 35S::GAI-GFP and pE2FA::E2FA-GFP lines only. A band corresponding to the size of RBR was detected in the pull-down of the positive control, E2FA-GFP (Figure 5.5F). There also appeared to be a slight mark in the pull-down of the experimental sample for GAI-GFP, but it was very faint and may not have been a genuine result. It may have been due to unspecific binding of the AtRBR1 antibody to the membrane itself, which was a consistent problem that arose as a result of using this particular antibody. When probing the membrane with an anti-GFP antibody, a band corresponding to the approximate size of GAI-GFP and E2FA-GFP was detected, suggesting that the pull-down of both of these proteins had worked (Figure 5.5G). Again, subsequent repeats of this experiment failed to generate the same result, particularly in relation to successful detection of a control band in the elute corresponding to the size of E2FA-GFP.

Another way to investigate the interaction was to perform the Co-IP's the other way round to the aforementioned methods by pulling down RBR or RBR-GFP from total protein extracts. Firstly, protein extracts from whole seedlings of the previously described translational reporter line pRBR::RBR-GFP (Chapter 3) were obtained alongside WT (Col) seedlings as a control. Both extracts were then

incubated with GFP-Trap beads in an attempt to pull down RBR-GFP for the experimental sample and to determine proteins that bind un-specifically to the beads in the case of the control. Western blot analysis was used to probe the membrane with an anti-GAI antibody, which was also able to cross-react and therefore detect RGA protein. Bands were detected in the elute for both the control and experimental samples, but none corresponding to size of GAI or RGA. Finally, in an attempt to bulk up endogenous levels of RBR protein, whole seedling protein extracts from the previously described cell cycle overexpresser lines, 35S::KRP2-GFP and G54 (see Chapter 4 for details) were obtained. The Co-IP was performed by pulling down RBR protein with the AtRBR1 antibody, incubating with IgY resin (because the AtRBR1 was made in chickens), running the resulting extracts on an SDS gel and probing with the same anti-GAI antibody as used previously.

Overall, even though the Co-IP protocol was optimised as much as possible using a variety of different protein extracts and pull-downs, it appeared that this particular choice of methodology was not sufficient to demonstrate a reproducible binding affinity between the proteins of interest. This was the case when testing the putative interaction between GAI/RGA and RBR, as well as the control of E2FA. Perhaps these types of interactions are too transient to be shown with this type of technique and/or the overall protein levels were too low. Alternatively, the pull-down itself was not very efficient at purifying target protein. An overview of all the different experiments conducted is provided overleaf (Table 5.1).

Plant lines	Plant material	Protein extract	Pull-down	Result
Ler, pGAI::GAI-GFP and pRGA::GFP-RGA	Root cultures	Nuclei preps	anti-GFP antibody (Abcam, ab290) and protein A magnetic beads	No binding found for all samples (apart from initial result obtained at Nottingham University)
Ler, pGAI::GAI-GFP and pRGA::GFP-RGA	Roots	Nuclei preps	GFP-Trap magnetic coated agarose beads (Chromotek)	No positive binding found
Ler, pGAI::GAI-GFP, pRGA::GFP-RGA and pE2FA::E2FA-GFP	Whole seedlings	Nuclei preps	GFP-Trap magnetic coated agarose beads (Chromotek)	No positive binding found
Ler, pGAI::GAI-GFP, pRGA::GFP-RGA, pE2FA::E2FA-GFP and 35S::GAI-GFP	Whole seedlings	Total protein	GFP-Trap magnetic coated agarose beads (Chromotek)	A positive binding between GAI and RBR was demonstrated, but unable to repeat. A positive binding between E2FA and RBR was also found, but unable to repeat
Col-0 and pRBR::RBR-GFP	Whole seedlings	Total protein	GFP-Trap magnetic coated agarose beads (Chromotek)	No positive binding found and unspecific binding was detected for both the WT control and experimental sample
35S::KRP2-GFP and G54	Whole seedlings	Total protein	antiRBR1 (Agrisera) and IgY agarose beads	Unspecific bands were detected in the elute, but background binding was too prevalent to detect bands corresponding to the approximate size of GAI/RGA

Table 5.1 A summary of Co-IP experiments performed to investigate an interaction between GAI/RGA and RBR

5.1.4 Testing for a putative interaction between GAI/ RGA and RBR with a GST pull-down assay

Since various Co-IP attempts proved difficult to detect consistently an interaction between GAI/RGA and RBR, a GST pull-down assay was adopted as an alternative method. A construct specific for this procedure had previously been developed by Huntley *et al.* (1998) containing a coding sequence for maize (*Zea mays*) RBR, ZmRb-1 (see Chapter 2 for details). The protocol for expression of this vector in bacteria had been optimised and described by the authors (Huntley *et al.*, 1998). It was therefore decided to use this construct, termed pGEX-ZmRb-1, for this purpose since RBR is evolutionarily conserved between these species (Gutzat et al., 2012).

Firstly, the construct was expressed in two different types of *E.coli* cells (DG1 and DH5α) to optimise the amount of ZmRb-1 accumulation and compare between them. The same construct without the ZmRb-1 insert (GST-only vector) was also expressed in *E.coli* cells (DG1) as a negative control to assess for unspecific binding to the GST resin during the pull-down assay. For the GST-only vector, it was evident that after 4 hours after IPTG induction, a band corresponding to the approximate size of GST (~ 25 kDa) had increased when compared to the un-induced control (Figure 5.6A). For the pGEX-ZmRb-1 vector, a band corresponding to the approximate size of ZmRB-1 (~ 100 kDa) was detected, but it was difficult to observe a definite increase in the amount of protein produced over the 4 hours after IPTG induction (Figure 5.6A). There also did not appear to be much difference between expression in DG1 and DH5α cells.

After induction, the bacterial cells for each construct were lysed in order to extract target protein from the lysate by incubating with GST resin. After incubation, a small amount of each extract was then run on an SDS gel against BSA standards (ranging from 0.5 - 10 µg) in order to visualise GST-purified protein and to roughly estimate the concentration for the pull-down experiment (Figure 5.6B). For GST resin only, there was only a single band corresponding to the predicted size of GST and the amount was between 5-10 µg (10 µl was loaded onto the gel in this case). For ZmRb-1 fused to GST (ZmRb-1-GST), there were bands of various sizes, one of which corresponded to the approximate size of the fusion protein. The amount appeared to be much lower than that of the GST resin only, being approximately 1 µg (20µl was loaded onto the gel).

The pull-down assay was performed by incubating approximately 1 µg of ZmRB-1-GST fusion protein resin (or GST resin alone as the control) with a total protein extract from whole seedlings of 35S::GAI-GFP and E2FA::E2FA-GFP. The resin was then loaded onto an SDS gel for western blot analysis. Firstly, western blot analysis was performed with and anti-GFP antibody in order to detect both GAI-GFP and E2FA- GFP (Figure 5.6C). For the GST only sample incubated with a protein extract from E2FA::E2FA-

Figure 5.6 GST pull-down assay using maize (Zea mays) GST_RBR1 (GST_ZmRB) fusion protein expressed in bacteria and purified using GST resin.

(A) Analysis of IPTG induction of a GST_ZmRB and GST only construct expressed in DG1 and/or DH5α *E.coli* cells. The total duration of the induction was 4 hours at 30°C, with 1 ml aliquots of bacterial cells taken every hour after induction and before IPTG induction as the un-induced control (0 hours). Samples were separated on a 10% SDS and 8% SDS gel for GST and GST_ZmRB, respectively. Protein fraction were visualised by coomassie blue staining.

(B) Analysis of GST and GST_ZmRB protein after purification by incubating the bacterial lysate with GST resin. Both the supernatant and the GST resin bound to purified protein for each construct were run alongside BSA standards (10-0.5 µg) on an 8% SDS gel. Protein fraction were visualised by coomassie blue staining.

(C) Western blot analysis of GST pull down experiments using GST and GST_ZmRB resin. Samples were separated on a 10% SDS gel and transferred to a PVDF membrane. For detection of GFP-tagged protein, membranes were incubated with an anti-GFP antibody (Torey Pines) and HRP-conjugated goat anti-rabbit IgG secondary antibody (Santa Cruz). For detection of GAI and GAI-GFP protein, membranes were incubated with an anti-GAI antibody (Nottingham University) and HRP-conjugated rabbit anti-sheep IgG (Santa Cruz) secondary antibody.

A

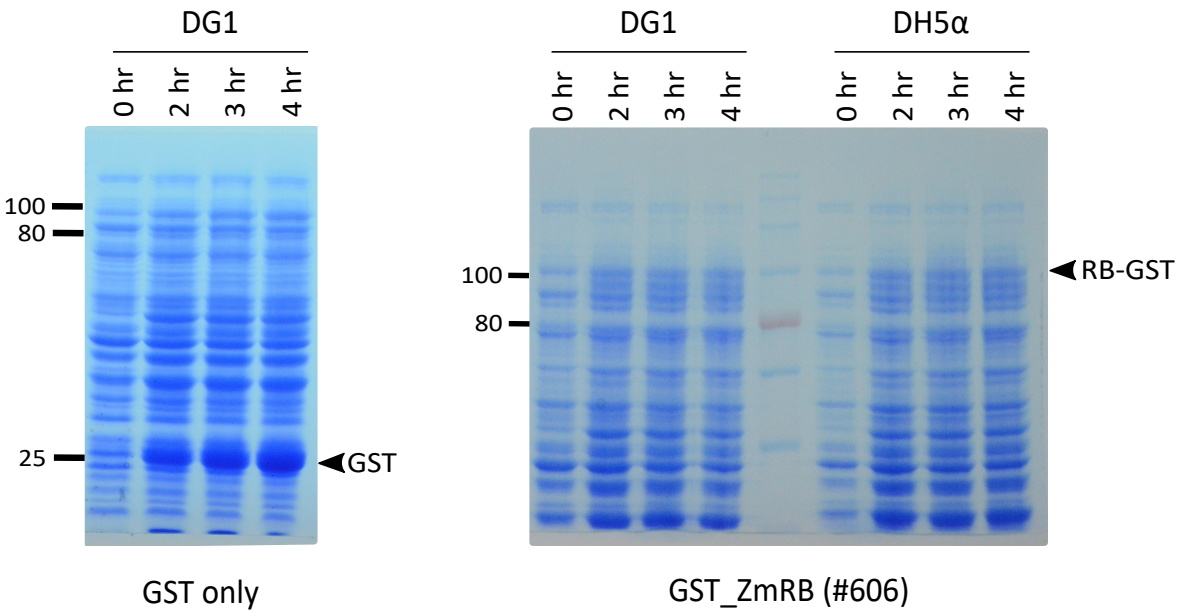
DG1
0 hr
2 hr
3 hr
4 hr
100
80
25
GST
GST only
DG1
DH5α
0 hr
2 hr
3 hr
4 hr
100
80
RB-GST
GST_ZmRB (#606)

B

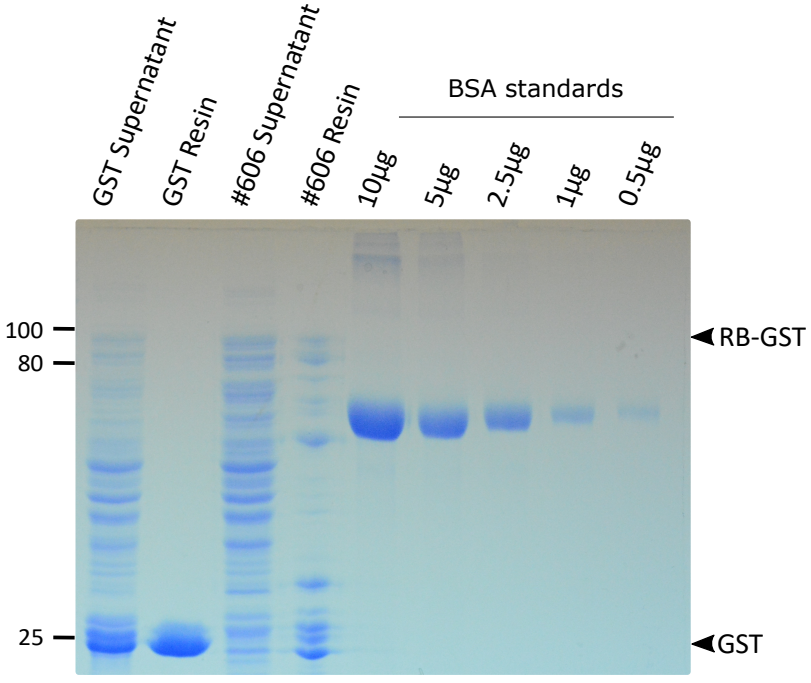
GST Supernatant
GST Resin
#606 Supernatant
#606 Resin
BSA standards
10µg
5µg
2.5µg
1µg
0.5µg
100
80
25
RB-GST
GST

C

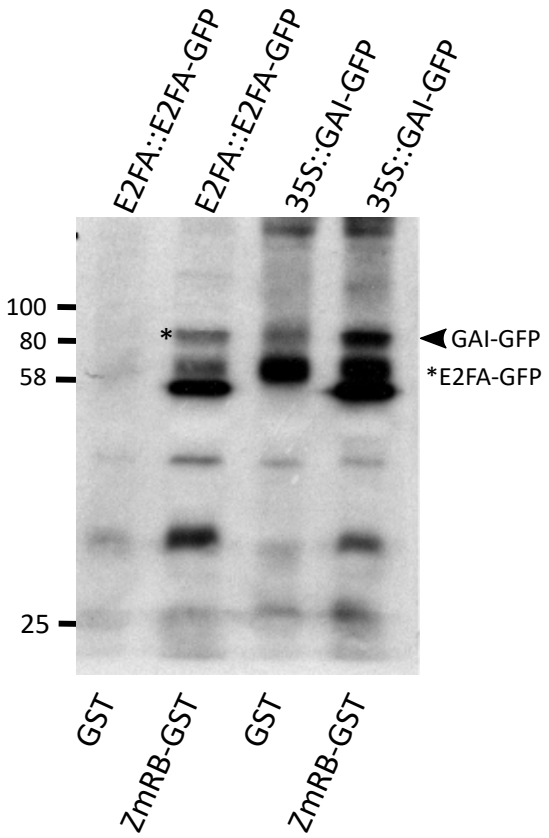

1° = αGFP 1:3000
2° = GAR 1:20,000

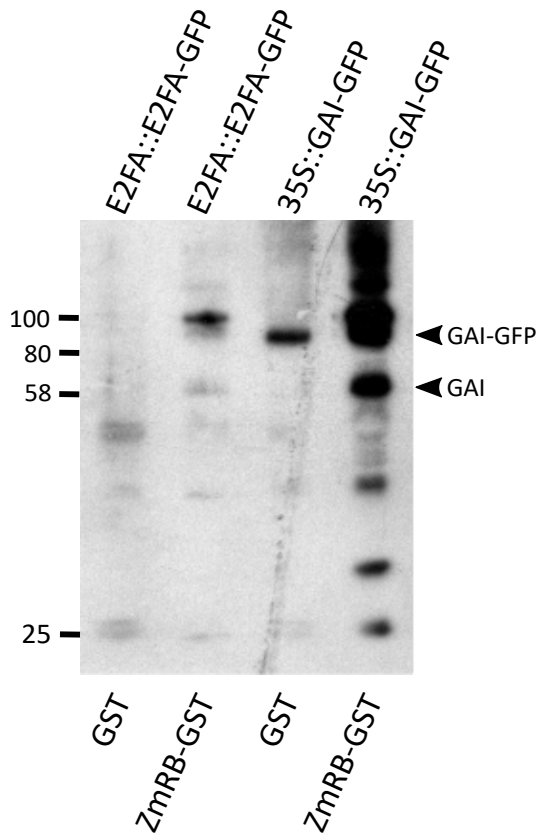

1° = αGAI 1:2000
2° = GAR 1:25,000

GFP seedlings, some bands were detected, but they were all very faint and there was no band corresponding to the approximate size of E2FA-GFP (~ 83 kDa) as expected. For the E2FA::E2FA-GFP extract incubated with ZmRb-1-GST resin, the same background bands were observed for the control, but some of them with a higher intensity. Additional bands were also detected for this sample that were not observed in the GST only control. One of these bands corresponded to the approximate size of E2FA-GFP, suggesting that an interaction between this fusion protein and ZmRBR exists. Another band of higher intensity at around 58 kDa was detected, as well as one between this and the putative band for E2FA-GFP. These are most likely to be other interacting factors that had been pulled out of the protein extract and detected by unspecific binding of the GFP antibody, due to it being polyclonal and therefore able to interact with other epitopes. For the 35S::GAI-GFP protein extract incubated with GST only resin, there were more bands with a higher intensity when compared to the GST-only pull-down of pE2FA::E2FA-GFP. In particular, there was a band of high intensity corresponding to approximately 65 kDa and also a band above that corresponding to the approximate size of GAI-GFP (~85 kDa). In the experimental condition of 35S::GAI-GFP incubated with ZmRb-1-GST resin, a band corresponding to this size was also visualised, but with a higher intensity. Even though there was a band in the GST-only control condition, the fact that the intensity in the experimental condition was higher could still be indicative of an interaction between GAI-GFP and ZmRBR-1. Another band approximately 58 kDa in size, was detected in the experimental condition for 35S::GAI-GFP and pE2FA::E2FA-GFP, but did not appear in the control for both samples. As mentioned earlier, this was probably another ZmRBR-1 interacting factor being pull-down and detected un-specifically.

To investigate these findings further and to detect endogenous GAI (as well as GAI-GFP) western blot analysis was performed using an anti-GAI antibody (Figure 5.6C). For GST-only resin incubated with the pE2FA::E2FA-GFP protein extract, very few bands were detected and they were very faint. When this protein extract was incubated with ZmRb-1-GST, a faint band that did not come up in the GST-only control was detected and corresponded to the approximate size of GAI (58 kDa). Another unspecific band of higher intensity was also detected, which was approximately 110 kDa. For the GST-only resin incubated with 35S::GAI-GFP there were some very faint bands detected, as in the case of the E2FA::E2FA-GFP control condition. There was also a band of higher intensity with an approximate size corresponding to GAI-GFP. This matches the observation made when the same sample was probed with and anti-GFP antibody. However, there wasn't a band corresponding to the approximate size of GAI alone, suggesting that unspecific binding to the GST resin alone could be the result of the GFP tag being present. In the experimental condition of 35S::GAI-GFP incubated with ZmRb-1-GST, there was a definitive band approximately the size of GAI, as well as one approximately the size of

GAI-GFP. This band also had a higher intensity when compared to the GST-only control. This experiment was repeated and similar results were obtained.

Since the GST-Assay appeared to demonstrate a positive binding between ZmRb-1 and GAI/GAI-GFP (and E2FA-GFP as a positive control), an attempt to generate a construct for GST expression of *Arabidopsis* RBR1 (AtRBR1). For this purpose, the same GST construct as described previously was used and the full-length AtRBR1 coding sequence (CDS) from Col-0 cDNA was amplified. This CDS was then ligated into the GST vector and expressed in bacteria following the same protocol that was used for the expression of ZmRb-1. Unfortunately, the AtRBR1-GST protein formed inclusion bodies and it was not possible to optimise the protocol sufficiently to push it into soluble fraction.

5.1.5 FLIM/FRET analysis reveals a positive binding between GAI and RBR in mitotic cells, but not RGA and RBR

To investigate the putative binding of RBR to GAI in *Arabidopsis* further, a FLIM/FRET analysis approach using confocal microscopy was adopted. This technique is particularly useful because it means one can visualise exactly where an interaction takes place in a spatial context at the cellular level, such as in dividing cells of the RAM where we suspect the interaction between GAI and RBR to be localised. Furthermore, the method does not rely on a high concentration of target protein, which is particularly useful in the case of GAI where overall concentration levels were found to be low (Chapter 3). It may be the case that the traditional Co-IP technique was not the best way to test for the interaction because of the transient expression of GAI, which would explain why it had proved difficult to demonstrate. In order to apply FLIM/FRET analysis, translational reporter lines that encode each protein of interest tagged with an appropriate fluorophore had to be obtained. This means that for each protein-protein interaction being tested, there needed to be a spectral overlap between the excitation spectra of the donor and emission spectra of the acceptor fluorophores used to tag the proteins of interest. Typical combinations include cyan fluorescent protein/yellow FP (CFP/YFP) and GFP/RFP.

Since translational reporter lines for both *GAI* and *RGA* that incorporates a GFP tag (pGAI::GAI-GFP and pRGA::GFP-RGA – see Chapter 2 and 3 for details) were already available, it was decided to use them for FLIM/FRET analysis. A suitable FRET partner was then obtained from a collaborator; an unpublished translational reporter line for RBR tagged with RFP, pRBR::RBR-RFP (Prof. Ben Scheres, Wageningen University, Netherlands). In order to combine the GFP-tagged donor protein with the acceptor, crosses were performed between the aforementioned pGAI::GAI-GFP/pRGA::GFP-RGA and pRBR::RBR-RFP lines. Crosses were also performed with pRBR::RBR-RFP to a translational reporter for E2FA-GFP, pE2FA::E2FA-GFP (Magyer et al., 2012), as a positive control. RBR had previously been

shown to bind E2FA-GFP biochemically with Co-IP's, thereby preventing the progression to S-phase by inhibiting the expression of E2FA regulated genes (Magyar *et al.*, 2012). For each cross, attempts to obtain F3 lines that were homozygous for both translational reporter lines were made. After subsequent attempts, it was only possible to reach lines that were homozygous for the donor (GFP-tagged protein), but segregating for the acceptor (RFP-tagged protein). This was the case for all of the crosses performed, but the presence of RBR-RFP for each seedling could be easily determined using fluorescent microscopy prior to obtaining the FLIM image. Where RBR-RFP was absent in the sample, this provided a sibling donor control, so it turned out to be beneficial that each cross was segregating for RFP. After generating these crosses, they were plated onto GM root and grown until 4-5 DAS. For each individual seedling, confocal microscopy and Time-Correlated Single Photon Counting by means of a pulsed laser was used to obtain FLIM images of the root tip. This was performed on seedlings expressing the donor only and the donor in the presence of the acceptor. Additional controls were also used for FLIM images, including seedlings expressing 35S::GFP to determine the lifetime of GFP only and WT seedlings to control for any autofluorescence in the root.

The resulting images were analysed with the SymphoTime software used to obtain the FLIM images. However, analysis using this software proved to be difficult due to the prevalence of a short-lifetime autofluorescent component concentrated around the root tip. This component prevented further image processing, such as determining FRET efficiencies. Although the software still enabled us to determine fluorescent lifetime values for individual components, the results were highly variable and difficult to interpret between images. A consequential collaboration was established with Prof. Wolfgang Langbein and Dr. Francesco Masia in the School of Physics and Astronomy, Cardiff University, who have developed a specific algorithm for non-negative factorisation of FLIM images. The method is called FSC^3, "Factorization into Spectra and Concentrations of Chemical Components" (Masia *et al.*, 2013). Each FLIM image constitutes a range of lifetime values that are based on the differences in excited decay rates from a florescent sample. The fluorescent lifetime value represents the average amount of time a molecule, such as a fluorophore, remains in an excited state. The FCS^3 method takes the sum of these decay curves with various amplitudes and decomposes the data into a linear combination of different components of a given spectra. This concept is analogous to an RGB image consisting of a range of different colours due to each individual pixel being composed of three colour components, red, green and blue. Just as an RGB image can be broken down into its individual components, so too can a FILM image using this factorisation method. Non-negative factorisation is a matrix decomposition technique that consists of mathematical algorithms used to factorise a matrix into multiple matrices, assuming that they are composed of non-negative elements. By applying this method to FLIM images, the different decay curves and therefore lifetimes of these components can

Figure 5.7 FLIM images of the root meristem of 4-day-old seedlings expressing the donor only and the donor in the presence of the acceptor.

(A) FLIM images of GAI-GFP only (donor) and GAI-GFP with RBR-RFP (donor and acceptor) that have been factorised by the FCS^3 method into three components.

(B) Decay curves for each component that have been colour coded. The green curve represents non-interacting GFP present localised to the nuclei in both images. The blue curve represents autofluorescence from cell cytosol, present in both sample and showing a sub-resolution decay (limited by the system response). The red curve represents interacting GAI-GFP and RBR-RFP localised to the cell nuclei and co-localised with GFP only in the sample where the Rb is tagged with RFP. Colour coding for the decay curves corresponds with that of the above images (A). Yellow regions in the picture of GAI-GFP with RBR-RFP indicates the localisation of the FRET signal i.e. the shorter decay curve than non-interacting GAI-GFP.

(E) Representative FLIM images of WT, pGAI::GAI-GFP and pGAI::GAI-GFP X pRBR::RBR-GFP seedlings showing the observed stabilisation of GAI-GFP in the presence of RBR-RFP.

(F) Representative FLIM images of WT, RGA::GFP-RGA and RGA::GFP-RGA X RBR::RBR-GFP seedlings showing no obvious stabilisation effect of GFP-RGA in the presence of RBR-RFP. The grey legend (top right) represents the intensity of the image by the number of photon counts (cnts), whilst the colour legend (bottom right) represents the range of average lifetime values (ns).

A

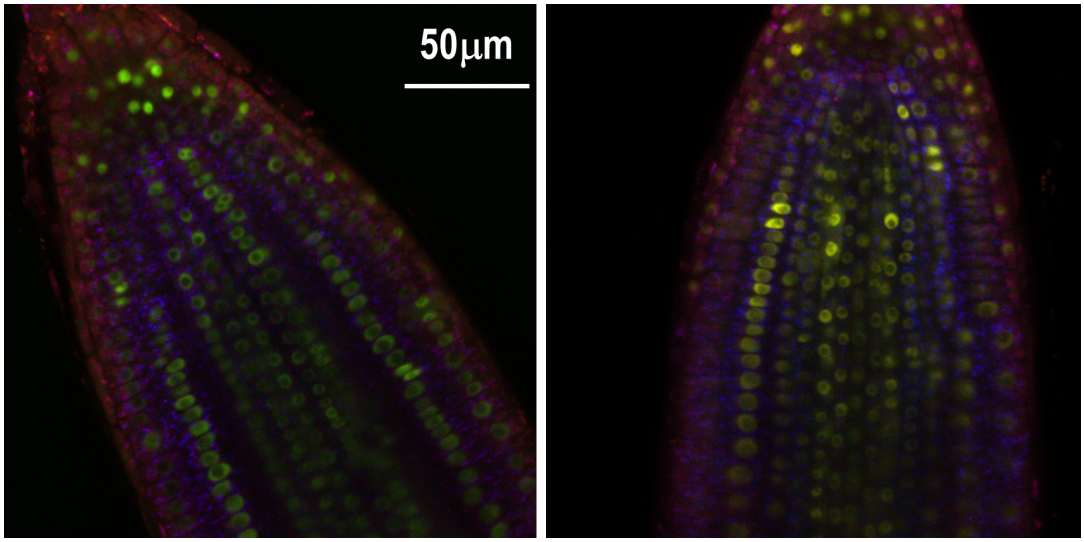

GAI-GFP (Donor)

GAI-GFP (Donor)
+ RBR-RFP (Acceptor)

B

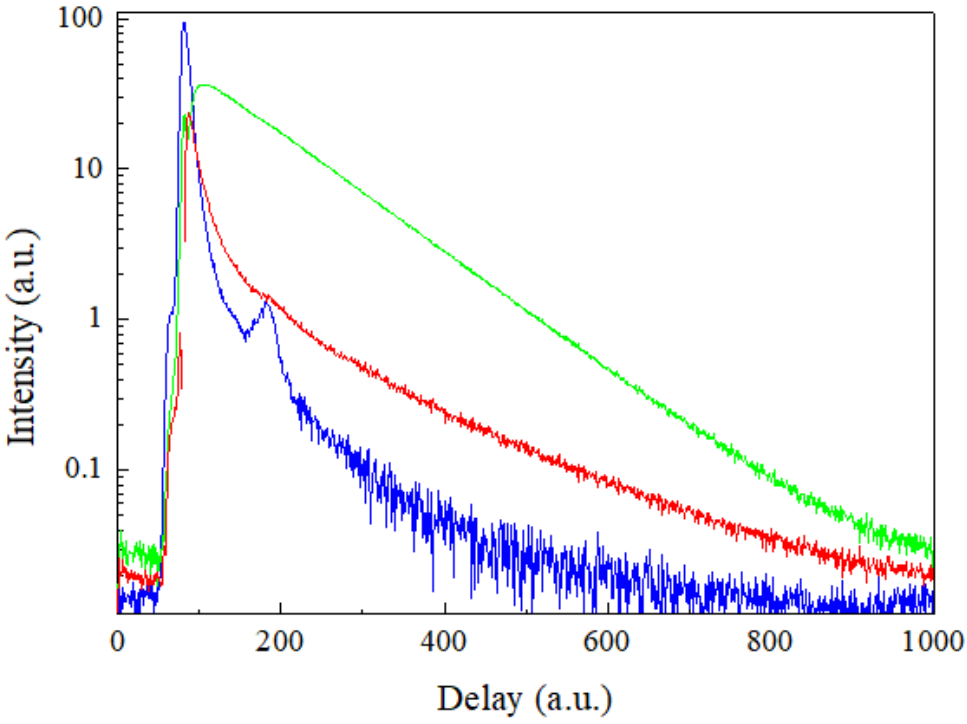

C

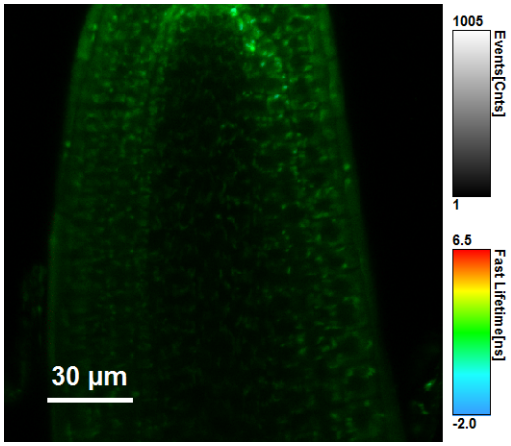

WT

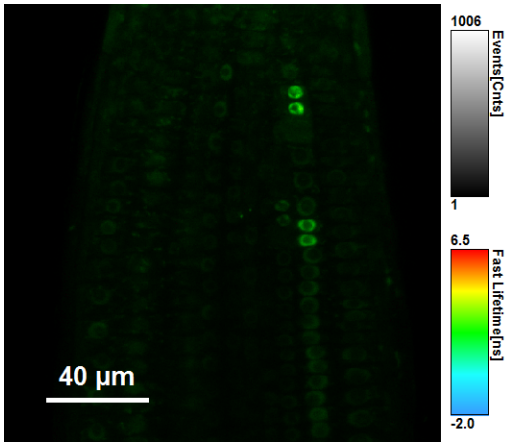

GAI-GFP

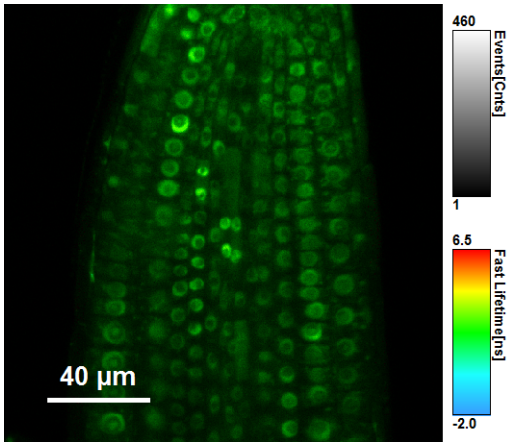

GAI-GFP x RBR-RFP

D

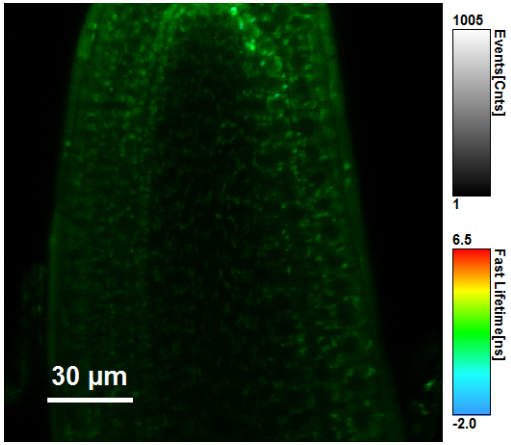

WT

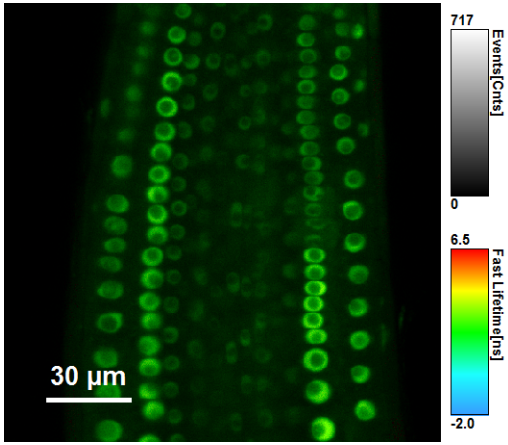

GFP-RGA

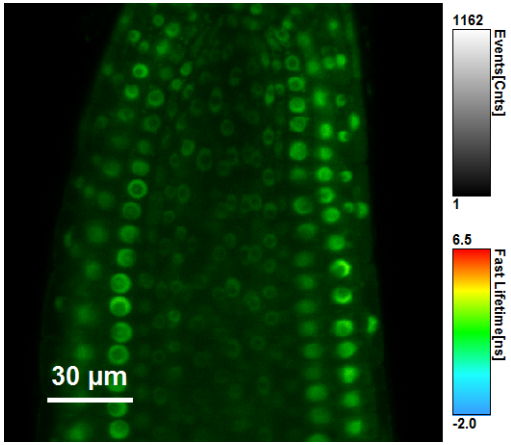

GFP-RGA x RBR-RFP

be determined and compared using images of the donor only and the donor in the presence of the acceptor. Our collaborators found a third component that was only present in the images of the root tip where both the donor and acceptor were present (Figure 5.7A,B). Specifically, the component was localised to the cell nuclei and co-localized with GFP only in the sample where the RBR-RFP was also present. This decay curve was shorter than that of the second component found for non-interacting GFP localised the cell nuclei and present in both samples. Since the decay was much faster than the case of non-interacting donors, these results demonstrate the occurrence of FRET and therefore imply a putative interaction between GAI-GFP and RBR-RFP.

5.1.6 Increased levels of RBR stabilises GAI-GFP, but not GFP-RGA

An observation was made when acquiring FLIM images of a stabilisation of GAI-GFP levels in the presence of RBR-RFP. This was discovered when comparing the FLIM images of seedlings expressing pGAI::GAI-GFP alone and pGAI::GAI-GFP co-expressed with pRBR::RBR-RFP. A consistent pattern was observed in which the expression of GAI-GFP appeared to be present in more nuclei of cells in the root tip of seedlings co-expressed with RBR-RFP when compared to GAI-GFP alone (Figure 5.7C). On the other hand, a stabilisation of GFP-RGA was not found in the presence of RBR-RFP (Figure 5.7D). To support this further, confocal images of GFP expression for pGAI::GAI-GFP, pGAI::GAI-GFP x pRBR::RBR-RFP, pRGA::GFP-RGA and pRGA::GFP-RGA x pRBR::RBR-RFP were obtained. However, the results from this experiment did not show a definitive stabilisation in the overall levels of both GAI-GFP and GFP-RGA, probably because it is not as sensitive as FLIM.

Discussion

The putative binding between GAI and RBR has been demonstrated with FLIM/FRET analysis. The fact that a stabilisation of GAI-GFP occurred in the presence of RBR-RFP, supports the hypothesis of this binding affinity and suggests that RBR stabilises GAI by preventing it from targeted degradation whilst they interact. Previous analysis had shown that GAI-GFP levels are transiently expressed during root development and that highest expression was observed just after cell division, during the G_1 phase of the cell cycle (Chapter 3). Furthermore, GA treatment experiments (Chapter 3) caused an overall reduction in GAI-GFP levels, apart from in these subset of adjacent cells. These observations imply that GAI is controlled by RBR in a cell-cycle dependent manner. This would explain why trying to demonstrate the interaction with traditional Co-IP methods proved difficult; because it is only occurring in a few cells at a time contained within the proximal meristem. Therefore, the amount of GAI protein obtained from protein extracts would be very small in relation to the total protein content, even when nuclei preps of root cultures were performed in an attempt to concentrate its accumulation levels further. Perhaps the interaction is also occurring in other regions of the plant,

such as the shoot meristem where cell division also takes place. Even if this was the case, the transient nature of this interaction and the fact that the regions of cell division in either the root or shoot are so small in relation the overall architecture of plant, would make it practically impossible to prove using these types of methods. Even when GAI-GFP protein was constitutively expressed, consistent Co-IP results demonstrating a positive binding were difficult to achieve.

Attempts to overexpress the GAI protein by using the 35S::GAI-GFP line did prove particularly useful for the GST-Assay using the maize RBR protein overexpressed in *E.coli* cells. By combining a total protein extract of these seedlings with ZmRBR1-GST, a positive binding was implied along with the corresponding control, E2FA-GFP. However, the results were not definitive since it appeared that GAI-GFP was also pulled down for the GST-only control. To clarify, these experiments could also be performed in conjunction with a negative control, such as protein extracts from seedlings expressing the null mutant allele, *gai-td1*. Western blot analysis could then be performed with an anti-GAI antibody in order to determine whether a band corresponding to GAI was found for this line. If no band is detected for the null *gai* mutant, but a band corresponding to GAI is detected for 35S::GAI-GFP (as found in previous experiments), then this would provide a better indication that the result is genuine.

Overall, it appears that there are some convincing results to indicate a putative binding between GAI and RBR, especially from the FLIM/FRET analysis. However, this analysis is still ongoing and should therefore be considered as preliminary until more data from these images are obtained. Although the factorisation algorithm is working to separate these FLIM images into different components, there are still some issues for effectively separating the short life-time components from each other. Furthermore, the actual mechanism for this putative binding is yet to be tested. Since a positive *in situ* binding had only recently been demonstrated, experiments involving mutational analysis of the suspected binding motif, LxCxE, had not been performed. Once the data from these FLIM images has been confirmed, the next stage would be to generate a transgenic translational reporter line for GAI-GFP with a mutated LxCxE motif and cross this to the pRBR::RBR-RFP to perform FLIM/FRET analysis on roots of these seedlings. For this purpose, a construct has been developed to contain the GAI promoter and the GAI coding sequence (CDS) fused to GFP, with a mutated motif as described by Cruz Ramirez *et al.* 2012, who mutated the LxCxE motif in SCR to AxCxE. This mutation was incorporated into the GAI sequence by designing specific primers for overlap extension PCR, which is a method used for introducing targeted mutations. The resulting fragment was ligated into a specific vector that is compatible for *Arabidopsis* transformation.

From the alignments for homologous GAI and RGA protein sequences, it was evident that not only was the LxCxE motif in GAI evolutionarily conserved, but also the preceding Leu and the following Ala and Val. Perhaps these amino acid residues also influence the binding of GAI to RBR. A paper published in 2005 by Singh *et al.*, investigated the binding affinity of LxCxE peptides derived from viral oncoproteins known to interact with the pocket domain of the human RB. For this purpose, they used a multi-method approach using direct *in vitro* experiments, such as NMR spectroscopy, mass spectrometry and isothermal titration calorimetry. By systematically substituting the amino acids flanking the LxCxE motif, the authors found that the strength of the binding was dependent on these residues. Specifically, any positively charged "x" amino acid in the xLxCxExxx sequence weakened the binding such that the interactions were more transient as a result (Singh *et al.*, 2005). Positive amino acids include Arg. Since GAI, SCR and RGA protein all contain Arg in their respective LxCxE or MxCxE motifs and after, perhaps this influences their ability to bind RBR. Indeed, it could potentially contribute to the transient nature of the GAI/RBR interaction.

The protein homology modelling indicated that the GAI/RBR interaction via the LxCxE motif was indeed possible. However, this result should be considered as speculative because there was only a 26% shared identity between the human RB crystal structure of the A/B binding pocket and *Arabidopsis* RBR. Moreover, there was also only a 34% shared identity between the crystal structure of the SCL7 GRAS domain in rice and the corresponding domain for AtGAI. As mentioned earlier, the method relies on the fact that homologous proteins share a primary amino acid sequence with an identity higher than 45% for the homology model to be reliable in terms of its 3D structure. Since neither of these proteins had this level of percentage identity between their regions of homologous crystal structures, the 3D model may not be completely reliable. However, it at least provides an indication of the possibility of an interaction occurring, but probably nothing more than that.

To conclude, a variety of different methods have been attempted in order to test the putative interaction between GAI/RGA and RBR. The most effective way of demonstrating this interaction so far was *in situ* FLIM/FRET analysis of the Arabidopsis roots expressing GFP- and RFP- tagged fusion proteins of the suspected interacting partners. Even though this method has been the most effective so far, the analysis is not complete and there are also issues with this method in terms if definitely identifying FRET. This could be for a variety of reasons such as the high prevalence of the short-lifetime component interfering with the analysis, or the actual confirmation of the proteins. For FRET to be effectively determined, the proteins of interest have to be within a certain distance of each other (<10 nm). The GFP- or RFP- tag may also interfere with the conformation and/or localisation of these proteins. Furthermore, the factorisation (FCS^3) algorithm being used to analyse FLIM images is a new type of method that is still in progress. This is the first time that the algorithm has been applied to

biological data so there are refinements that are still being made to improve it. If it turns out the method does not work for these type of images, then other types of methods will be investigated. A recent paper demonstrated FRET between YFP- and RFP-tagged combinations of three co-expressed transcription factors known to interact in the root meristem (Long *et al.*, 2017). Here, they used a method termed as phasor plots to fit the FLIM data of *Arabidopsis* seedlings expressing different constructs for SCARECROW (SCR), SHORTROOT (SHR) and JACKDAW (JKD). The authors describe how they were able to optimise their approach of *in vivo* FLIM/FRET analysis under these physiological conditions to determine interactions between these proteins in a spatially distinct context (Long *et al.*, 2017). Therefore, if the factorisation method proves too difficult to optimise then a similar approach as described in the aforementioned paper will be adopted.

Chapter 6

Discussion

Chapter 6 – Discussion

Root growth is a fundamental developmental process for defining the overall growth of a plant. Understanding the molecular mechanisms that regulate root growth is therefore useful for enhancing food security. With an ever increasing population and a lack of available arable land, there is a subsequent demand to produce more food by increasing crop productivity. The DELLA's have already played a pivotal part in developing new crop varieties with an increased yield. Indeed, they were the key components associated with the Green Revolution, because the semi-dwarfed wheat and rice varieties selected for greater yields were DELLA mutants that had altered responses to GA signalling. Since organ growth is determined by tight coordination of cell division and differentiation, it is important to further our understanding of how they are regulated and integrated. Cell division is essential to maintaining growth because it allows a continuous source of cells in the meristem that later enter the transition zone for differentiation. Hence, the root apical meristem comprises a stem cell niche that continually produces new cells to undergo further divisions in the proximal meristem – the region of active cell division. This is controlled by a variety of cell-cycle regulators associated with different stages of the cell cycle. RBR is the key regulatory component that controls the G_1-to-S transition of the mitotic cell cycle. Furthermore, increasing evidence suggests that RBR acts as a molecular hub to integrate cell division and differentiation by responding to developmental and environmental cues (Harashima and Sugimoto, 2016).

DELLA proteins influence growth because they are negative regulators of GA signalling, which promotes various developmental and growth processes, including root elongation. There is mounting evidence to suggest that DELLAs integrate multiple signalling pathways by acting as co-transcriptional regulators and/or interacting with regulatory proteins (Lor and Olszewski, 2015; Davière and Achard, 2016). Consequently, DELLA proteins have diverse roles during the plant life cycle by integrating and conveying a variety of developmental and external signals. The main regulators of root growth with respect to the GA pathway are GAI and RGA (Fu and Harberd, 2003). Since the rate of cell division and differentiation determines root growth, RGA and GAI must be associated with these processes. Whether they directly or indirectly link to the cell cycle is still not clearly understood.

What is evident for all of these aforementioned proteins is that they are very promiscuous in their ability to bind with other regulatory factors, either at the transcriptional or protein level. Therefore, there may be a cross-over between their molecular pathways. Here, a specific link between GAI/RGA and RBR was investigated in an attempt to uncover how the DELLAs relate to cell division control. Specifically, a putative binding between GAI and RBR was tested based on the fact that GAI contains an LxCxE motif and that a variety of different proteins bind RBR via this motif. The discovery that the

closely related SCR protein binds to RBR in this way was also promising (Cruz Ramirez et al. 2012). Various experiments were performed to investigate this putative interaction, including assessing the expression and protein accumulation levels of *GAI*, *RGA* and *RBR* in the root, kinematic analysis of root growth experiments for specific lines associated with these genes and finally, testing the interaction itself with a variety of different methods. Here, I will attempt to summarise the results of these experiments and what they mean on a broader scale.

6.1 GAI and RGA inhibit cell proliferation in the root apical meristem

It had previously been reported that GAI and RGA repress root growth (Fu & Harberd 2003), but an indication as to whether this was due to a decreased rate of cell division was not provided. However, when examining the roots of the GA-deficient mutant, *ga1-3*, meristem size and cell production rates were significantly reduced (Ubeda-Tomás *et al.*, 2009). DELLA levels for this line are substantially increased due to the absence of their negative regulator, GA, so the observed phenotypic differences may be attributable to this factor. Since both GAI and RGA were found to accumulate in the root meristem (Chapter 3), this would imply that theres a functional relevance for this localisation. . As root growth had been reported to be repressed by GAI and RGA, it seems logical that this was in part due to a decreased rate of cell division, as well as cell elongation. Most of the current knowledge on how GA promotes growth via the DELLA pathway is in relation to their effect on cellular elongation rather than cell division (Ubeda-Tomás *et al.*, 2008). Indeed, gibberellin had been reported to accumulate in elongating endodermal cells of the root meristem, whilst the distribution of GFP-RGA was complementary to GA in both the meristem and elongating cells (Shani *et al.*, 2013).

Similar to the analysis of the aforementioned *ga1-3* line, the effect of GAI and RGA on the cell division was first investigated by analysing meristem size, cortical cell number and cell production rate for the double null mutants, *ga1-t gai-td1* and *ga1-t rga-28*. Root growth for similar null mutants in a different ecotype (Ler) had previously been reported to partially rescue the reduced growth phenotype of a single biosynthetic GA mutant, *ga1-3* (Fu & Harberd 2003). Specifically, removal of RGA function in this mutant background demonstrated a rescue phenotpye to a greater degree than removal of GAI. The same observations were made for these experiments (Chapter 4), in which *ga1-t rga-28* seedlings grew more similarly to WT and had a significantly increased growth rate to *ga1-t gai-td1*, which in turn grew faster than *ga1-t*. When analysing their cell production rates in relation to WT, both were decreased, but there was no difference when comparing between them. However, *ga1-t gai-td1* had a significantly increased cell production rate than *ga1-t*, whilst *ga1-t rga-28* did not. Meristem size and cortical cell number was also reduced for both of these lines, but *ga1-t gai-td1* had a more substantial decrease, which was similar to that of the *ga1-t* control. Therefore, removal of either GAI

or RGA function in the biosynthetic GA mutant, *ga1-t*, demonstrated that cell division rates were partially rescued, but to varying degrees. Specifically, removal of RGA affected cell division in the root meristem to a greater extent than GAI due to an increased meristem size and cortical cell number. These results suggest that both proteins negatively affect the rate of cell division in the RAM either by restricting the number of dividing cells or by reducing the rate of cell production. When observing accumulation of GAI-GFP and GFP-RGA in the root meristem, RGA intensity appeared to be higher and more consistently expressed throughout the proximal meristem and transition zone (Chapter 3). On the other hand, GAI-GFP accumulation was transient and localised more specifically to the apical end of the meristem. Perhaps this explains why GAI had less of a negative impact on the rate of cell division than RGA. More likely, these results may collectively infer that RGA and GAI have different functions in relation to how they regulate cell division.

6.2 GAI binds to RBR is a reporter of the G_1 phase of the mitotic cell cycle

From observations that GAI-GFP accumulation in the root meristem was transient, it was also noted that the nature of this accumulation appeared to be in a cell-cycle-dependent context. Indeed, GAI-GFP was consistently observed in two adjacent cells of the proximal meristem that appeared to have just undergone mitosis. Cells that had just undergone mitosis were identified by their small size in comparison to neighbouring cells. The smaller size occurs following the final stage of mitosis, cytokinesis, whereby the parent cell splits into two daughter cells, forming a new cell wall between them. To investigate this finding further, the GAI::GAI-GFP translational reporter was crossed to an S-G_2-M-mCherry reporter and the F1 progeny was observed. GAI-GFP accumulation was consistently observed in cells where mCherry intensity was either low or barely detectable at all, suggesting that it accumulates specifically at the G_1 stage of the cell cycle. Therefore, there is potential to use this reporter line as a marker for this particular phase of the cell cycle.

More importantly, these findings support the hypothesis that GAI binds to RBR, since both proteins accumulate in similar regions of the root meristem (Chapter 3) and RBR regulates the G_1-to-S transition. To test the interaction itself, a variety of different methods were adopted. Initially, Co-IPs were used for this purpose because preliminary results from a collaborator had been able to demonstrate a binding in this way. Furthermore, the transient nature of GAI-GFP accumulation had not yet been observed. On reflection, it seems that Co-IPs were not the best method to demonstrate this interaction for this reason and also because GAI-GFP accumulation was generally low (Chapter 3 & 5). Even when GAI-GFP was constitutively expressed, the meristem comprises a very small part of

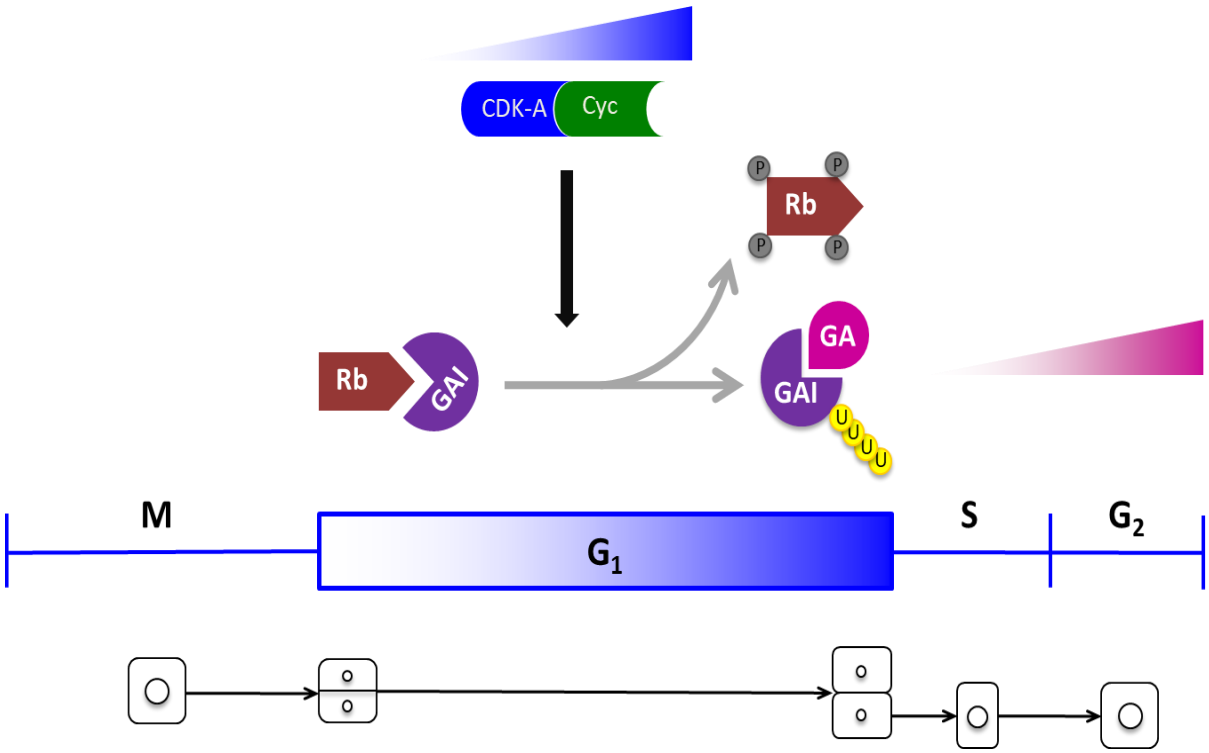

Figure 6.1 Schematic of the interaction between GAI and RBR in the context of the cell cycle. At the beginning of the G_1-phase, CDK/Cyclin kinase levels are low thus preventing phosphorylation of RBR. During this stage, RBR binds to and stabilises GAI by preventing it from targeted degradation by polyubiquitination. The interaction is disrupted by increasing levels of kinase activity which phosphorylates RBR. GAI is then subsequently degraded after its disassociation from RBR in the presence of increasing GA levels. The different stages of the cell cycle, including mitosis (M), S- and G_2- phase are specified in relation to G_1. Diagrams of a cell undergoing the process of cell division during these phases are included below.

the root and if the interaction is only occurring in this region, it would be almost impossible to demonstrate with such techniques. When the interaction was tested with a GST-assay, the results suggested the GAI/RBR interaction existed, but was not conclusive since GAI-GFP was also detected in the GST only control. The most promising results were obtained from FLIM/FRET analysis of *Arabidopsis* roots expressing the translational reporter, GAI::GAI-GFP as the donor and this line crossed with the translational reporter, RBR::RBR-RFP to combine the donor with the acceptor. Applying the factorisation method to FLIM images of the root meristem for these lines revealed an additional component for the donor in the presence of the acceptor, with a shorter lifetime than the corresponding component for the donor only. This was also the case when close-up FLIM images were analysed of a few cells in the meristem. Moreover, a stabilisation effect was observed where GAI-GFP accumulated in more cells within the root meristem in the presence of RBR-RFP. Therefore, not only does RBR appear to bind with GAI in mitotic cells, but it also stabilises the levels of GAI. Perhaps this is because RBR prevents GAI from targeted degradation by GA whilst bound to it. Indeed, when roots expressing *GAI-GFP* both under its own promoter and when constitutively expressed by the 35S CaMV promoter, are treated with PAC (an inhibitor of GA), the levels of GAI-GFP accumulation were increased (Chapter 3). Consequently, although GA is mainly localised to elongating endodermal cells as mentioned earlier, it may also acting in the root apical meristem to regulate DELLA levels.

Although a binding between GAI and RBR was demonstrated with FLIM/FRET analysis, the results are preliminary and analysis of these images is still underway. The analysis has proved more difficult due to the presence of auto-fluorescence in root meristem leading to detection of a very short-lifetime component. Furthermore, the mechanism for this binding is yet to be determined. As mentioned previously, the interaction was investigated due to the presence of an LxCxE motif for GAI. In order to test whether the binding occurs via this motif, a transgenic line could be generated to contain a translational reporter of GAI-GFP with a mutated LxCxE motif and crossed to RBR::RBR-RFP. This mutant-based approach, combined with FLIM/FRET analysis would indicate the interaction occurs at the LxCxE motif if FRET is not detected in this case. The type of mutation should be considered carefully, especially since preliminary experiments of transfected *Arabidopsis* protoplasts using different GAI/RGA constructs revealed that mutating the motif to GxGxG caused possible protein aggregation (discussed in Chapter 5). In the paper that showed SCR binds RBR via the LxCxE motif, they mutated it to AxCxE, which was sufficient to retain the proteins functionality, but prevented it from binding to RBR (Cruz Ramirez et al. 2012). Therefore, it would make sense to correspondingly mutate the GAI motif to the same one as described by the authors of this paper. Indeed, it necessary to retain GAI functionality and only disrupt its binding affinity for RBR i.e. without altering its secondary protein structure, in order to demonstrate that the interaction occurs at this motif.

6.3 Evidence to suggest that RGA directly upregulates *KRP2* to regulate root growth

To investigate the effect of a putative interaction between GAI/RGA and RBR on root growth, various crosses were made between *gai* and *rga* null mutants to lines associated to the G_1 phase of the cell cycle. For one particular cross between *rga-28* and an overexpresser of an inhibitor of the cell cycle, 35S::KRP2-GFP, an interesting phenotype was observed. Normally, 35S::KRP2-GFP seedlings exhibit a characteristic phenotype of severely stunted growth, small serrated leaves and in some cases, infertility. Indeed, from personal use of this line, it was often difficult to generate crosses with them. However, once a homozygous line for 35S::KRP2-GFP *rga-28* had been identified, the phenotype appeared to be similar to that of WT plants. On the other hand, the homozygous line for 35S::KRP2-GFP *gai-td1* demonstrated a similar phenotype to that of 35S::KRP2-GFP plants alone. Collectively, these observations implied that removal of RGA function from the 35S::KRP2-GFP line rescued its distinctive phenotype, whilst removal of GAI function did not. To investigate this further, root growth of WT, 35S::KRP2-GFP, 35S::KRP2-GFP *rga-28* and 35S::KRP2-GFP *gai-td1* seedlings was performed, as well as qPCR experiments in order to determine their transcript levels. Analysis of root growth for these lines demonstrated that (1) overexpression of KRP2, which inhibits kinase activity, resulted in a reduced root growth phenotype (2) introduction of the *rga-28* null mutation rescued this reduced growth phenotype and (3) introduction of the *gai-td1* null mutation did not have the same effect. This suggests that root growth is regulated by kinase activity and RGA directly or indirectly regulates the *KRP2* pathway at a transcriptional and/or a protein level. Measuring the relative transcriptional abundance for these lines revealed the levels of *KRP2* and *GFP* for 35S::KRP2-GFP *rga-28* seedlings were reduced in comparison to 35S::KRP2-GFP and 35S::KRP2-GFP *gai-td1*. However, there was still a ten-fold increase in *KRP2* levels relative to WT and only a reduction of a 0.3 for *GFP* relative 35S::KRP2-*GFP*. This result was compelling, considering that the phenotype of 35S::KRP2-GFP *rga-28* seedlings was similar to WT, but still expressed high levels of *KRP2* and *GFP*. Therefore, the take-home message from these findings is that RGA positively regulates *KRP2* at both the transcriptional and protein level.

The fact that a homozygous line was never obtained for *ga1-t* 35S::KRP2-GFP and aborted embryos were observed in siliques of plants homozygous for *ga1-t*, but segregating for 35S::KRP2-GFP, would suggest that overexpression of DELLA's and KRP2 leads to embryo lethality. These observations contrast with the suppressed phenotype observed when RGA function was removed from 35S::KRP2-GFP and further supports the hypothesis that RGA upregulates levels of *KRP2*. Hence, regulation of DELLA accumulation is essential for normal plant growth and development because it promotes the expression of *KRP2*, which inhibits cell proliferation. Indeed, it has been shown that *KRP2* is upregulated in the GA-biosynthetic mutant, *ga1-3* (Achard *et al.*, 2009).

To complement these findings, a recently published paper investigating how DELLA's restrict growth in the inflorescence meristem, found with Chip-Seq analysis that a GA-resistant form of RGA directly upregulates *KRP2* levels by binding to its promoter (Serrano-Mislata *et al.*, 2017).

Transgenic plants expressing this GA-resistant form of RGA, pRGA:GFP-rgaΔ17, have a 17 bp deletion within the DELLA motif of this protein, which prevents it from targeted degradation by the GA pathway (Dill and Sun, 2001; Dill *et al.*, 2001). These plants, known as gain-of-function mutants, exhibit a semi-dwarfed phenotype with defects in stem growth and shoot apical meristem size (SAM). Indeed, the authors reported that seedlings expressing pRGA:GFP-rgaΔ17 and a *gai* semi-dominant mutant containing the same 17 bp deletion, had a reduced shoot meristem size (Serrano-Mislata *et al.*, 2017). Consequently, they decided to use both of the aforementioned lines by crossing them to a *krp2* loss-of-function mutant to assess the effect this would have on the SAM. They found the reduced meristem size for the *gai* mutant was fully supressed to normal size, whereas it was only partially restored for pRGA:GFP-rgaΔ17. Furthermore, stem elongation for both of these lines was not affected by removal of KRP2 function, suggesting that the DELLAs regulate meristem size independently of their mechanisms for regulating stem growth (Serrano-Mislata *et al.*, 2017).

In the root meristem, KRP2-GFP accumulation is localised mainly to elongating cells, whilst it has low levels in the proximal meristem (Sanz *et al.*, 2011). Therefore, rather than restricting the rate of cell proliferation in the root meristem, RGA is more likely to upregulate *KRP2* expression in elongating cells. As in the case of the shoot, perhaps RGA restricts root meristem size by directly upregulating *KRP2* in elongating cells by inhibiting the rate of elemental expansion. This hypothesis is compelling, especially considering that GFP-RGA accumulation in the root was also observed in elongating cells, as well as the meristem (Chapter 3). To investigate this further, Chip-Seq analysis could be performed specifically on root tissues of *Arabidopsis* seedlings expressing the aforementioned RGA dominant-negative mutant. Moreover, measurements of cell production rate and root meristem size could be determined for primary roots of WT, 35S::KRP2-GFP, 35S::KRP2-GFP *rga-28* seedlings to investigate whether the rate of cell division for 35S::KRP2-GFP *rga-28* is rescued in relation to 35S::KRP2-GFP.

6.4 GAI and RGA are functionally different in relation to the cell cycle

Although GAI and RGA share a 82% amino acid sequence identity (Dill and Sun, 2001), it is evident that they have distinct, as well as overlapping roles, in relation to their regulation of plant growth and development. By investigating a putative interaction between GAI/RGA and RBR, it has emerged that RGA and GAI differentially regulate cell proliferation through different molecular mechanisms. Indeed, the DELLAs have diverse and multiple functions because they are able to transcriptionally regulate

genes, as well as directly binding to regulatory protein partners (discussed in Chapter 1). The research described here has shown a potential mechanism for GAI and RGA in regulating the cell cycle on multiple levels. Firstly, a putative interaction between GAI and RBR has been implied with FLIM/FRET analysis. Secondly, a potential link between RGA and the cell cycle inhibitor, *KRP2*, has been revealed from root phenotyping experiments and transcriptional analysis of these lines. Moreover, the expression and accumulation patterns of GAI and RGA within the root meristem appears to be substantially different, with GAI accumulating in a cell-cycle-dependent transient manner and RGA accumulation being more consistently expressed in both the meristem and elongating cells. It would be beneficial to understand the reason for these differences further by confirming the putative GAI/RBR interaction *in situ* and performing the suggested Chip-Seq and kinematic analysis in relation to RGA. Nevertheless, there is still some way to go in terms of understanding how these putative interactions are integrated and coordinated to regulate the cell cycle. It is likely that other interacting partners are involved in these mechanisms of control, especially since DELLAs do not contain any identifiable DNA binding domains and have been shown to act as co-transcriptional regulators (Lor and Olszewski, 2015). Unravelling these mechanisms will be a challenge, since both DELLAs and RBR impinge on multiple developmental pathways. Regardless, the results demonstrated here are compelling and provide a strong indication that both GAI and RGA are not only associated with cell elongation, but also cell proliferation and that there are clear differences in their function.

References

Abrahams, S., Cavet, G., Oakenfull, E. A., Carmichael, J. P., Shah, Z. H., Soni, R. and Murray, J. A. H. (2001) 'A novel and highly divergent Arabidopsis cyclin isolated by complementation in budding yeast', *Biochimica et Biophysica Acta (BBA) - Molecular Cell Research*, 1539(1), p. 1–6.

Ach, R. A., Durfee, T., Miller, A. B., Taranto, P., Hanley-Bowdoin, L., Zambryski, P. C. and Gruissem, W. (1997) 'RRB1 and RRB2 encode maize retinoblastoma-related proteins that interact with a plant D-type cyclin and geminivirus replication protein.', *Molecular and cellular biology*, 17(9), p. 5077–86.

Achard, P., Gusti, A., Cheminant, S., Alioua, M., Dhondt, S., Coppens, F., Beemster, G. T. S. and Genschik, P. (2009) 'Gibberellin signaling controls cell proliferation rate in Arabidopsis.', *Current biology : CB*. Elsevier Ltd, 19(14), p. 1188–93.

Alberts, B., Johnson, A., Lewis, J., Morgan, D., Raff, M., Roberts, K. and Walter, P. (2015) *Molecular Biology of the Cell*. 6th edn. New York: Garland Science.

An, F., Zhang, X., Zhu, Z., Ji, Y., He, W., Jiang, Z., Li, M. and Guo, H. (2012) 'Coordinated regulation of apical hook development by gibberellins and ethylene in etiolated Arabidopsis seedlings', *Cell Research*. Nature Publishing Group, 22(5), p. 915–927.

Ariizumi, T., Lawrence, P. K. and Steber, C. M. (2011) 'The Role of Two F-Box Proteins, SLEEPY1 and SNEEZY, in Arabidopsis Gibberellin Signaling', *Plant Physiology*. American Society of Plant Biologists, 155(2), p. 765–775.

Azumi, Y., Liu, D., Zhao, D., Li, W., Wang, G., Hu, Y. and Ma, H. (2002) 'Homolog interaction during meiotic prophase I in Arabidopsis requires the SOLO DANCERS gene encoding a novel cyclin-like protein', *The EMBO Journal*, 21(12), p. 3081 LP-3095.

Bai, M.-Y., Shang, J.-X., Oh, E., Fan, M., Bai, Y., Zentella, R., Sun, T. and Wang, Z.-Y. (2012) 'Brassinosteroid, gibberellin and phytochrome impinge on a common transcription module in Arabidopsis', *Nat Cell Biol*. Nature Publishing Group, a division of Macmillan Publishers Limited. All Rights Reserved., 14(8), p. 810–817.

Baskin, T. I. (2013) 'Patterns of root growth acclimation: constant processes, changing boundaries', *Wiley Interdisciplinary Reviews: Developmental Biology*. John Wiley & Sons, Inc., 2(1), p. 65–73.

Beemster, G. T. S. (1998) 'Analysis of Cell Division and Elongation Underlying the Developmental Acceleration of Root Growth in Arabidopsis thaliana', *PLANT PHYSIOLOGY*, 116(4), p. 1515–1526.

Benková, E. and Hejátko, J. (2008) 'Hormone interactions at the root apical meristem', *Plant Molecular Biology*, 69(4), p. 383–396.

van den Berg, C., Willemsen, V., Hendriks, G., Weisbeek, P. and Scheres, B. (1997) 'Short-range control of cell differentiation in the Arabidopsis root meristem', *Nature*. Macmillan Magazines Ltd., 390(6657), p. 287–289.

Berman, H. M., Westbrook, J., Feng, Z., Gilliland, G., Bhat, T. N., Weissig, H., Shindyalov, I. N. and Bourne, P. E. (2000) 'The Protein Data Bank', *Nucleic Acids Research*. Oxford, UK: Oxford University Press, 28(1), p. 235–242.

Bewley, J. D., Bradford, K. J., Hilhorst, H. W. M. and Nonogaki, H. (2013) 'Development and Maturation', in *Seeds*. 3rd edn. New York: Springer-Verlag, p. 27–83.

Biedermann, S., Harashima, H., Chen, P., Heese, M., Bouyer, D., Sofroni, K. and Schnittger, A.

(2017) 'The retinoblastoma homolog RBR1 mediates localization of the repair protein RAD51 to DNA lesions in Arabidopsis', *The EMBO Journal*, 36, p. 1279–1297.

Bird, D. A., Buruiana, M. M., Zhou, Y., Fowke, L. C. and Wang, H. (2007) 'Arabidopsis cyclin-dependent kinase inhibitors are nuclear-localized and show different localization patterns within the nucleoplasm', *Plant Cell Reports*, 26(7), p. 861–872.

Blilou, I., Xu, J., Wildwater, M., Willemsen, V., Paponov, I., Friml, J., Heidstra, R., Aida, M., Palme, K. and Scheres, B. (2005) 'The PIN auxin efflux facilitator network controls growth and patterning in Arabidopsis roots', *Nature*. Macmillian Magazines Ltd., 433(7021), p. 39–44.

Boniotti, M. B. and Gutierrez, C. (2001) 'A cell-cycle-regulated kinase activity phosphorylates plant retinoblastoma protein and contains, in Arabidopsis, a CDKA/cyclin D complex', *The Plant Journal*. Blackwell Science Ltd, 28(3), p. 341–350.

Borghi, L., Gutzat, R., Fütterer, J., Laizet, Y., Hennig, L. and Gruissem, W. (2010) 'Arabidopsis RETINOBLASTOMA-RELATED is required for stem cell maintenance, cell differentiation, and lateral organ production.', *The Plant cell*, 22(6), p. 1792–811.

Briones-Moreno, A., Hernández-García, J., Vargas-Chávez, C., Romero-Campero, F. J., Romero, J. M., Valverde, F. and Blázquez, M. A. (2017) 'Evolutionary Analysis of DELLA-Associated Transcriptional Networks', *Frontiers in Plant Science*. Frontiers Media S.A., 8, p. 626.

Buer, C. S., Sukumar, P. and Muday, G. K. (2006) 'Ethylene Modulates Flavonoid Accumulation and Gravitropic Responses in Roots of Arabidopsis', *Plant Physiology*, 140(4), p. 1384 LP-1396.

Chandler, P. M., Marion-Poll, A., Ellis, M. and Gubler, F. (2002) 'Mutants at the Slender1 Locus of Barley cv Himalaya. Molecular and Physiological Characterization', *Plant Physiology* , 129(1), p. 181–190.

Chen, Z., Hafidh, S., Poh, S. H., Twell, D. and Berger, F. (2009) 'Proliferation and cell fate establishment during Arabidopsis male gametogenesis depends on the Retinoblastoma protein', *Proceedings of the National Academy of Sciences* , 106(17), p. 7257–7262.

Chinnam, M. and Goodrich, D. W. (2011) 'Chapter 5 - RB1, Development, and Cancer', in Dyer, M. A. (ed.) *Current Topics in Developmental Biology*. Academic Press, p. 129–169.

Churchman, M. L., Brown, M. L., Kato, N., Kirik, V., Hülskamp, M., Inzé, D., De Veylder, L., Walker, J. D., Zheng, Z., Oppenheimer, D. G., Gwin, T., Churchman, J. and Larkin, J. C. (2006) 'SIAMESE, a Plant-Specific Cell Cycle Regulator, Controls Endoreplication Onset in Arabidopsis thaliana', *The Plant Cell* , 18(11), p. 3145–3157.

Claeys, H., De Bodt, S. and Inzé, D. (2014) 'Gibberellins and DELLAs: central nodes in growth regulatory networks.', *Trends in plant science*, 19(4), p. 231–9.

Colebrook, E. H., Thomas, S. G., Phillips, A. L. and Hedden, P. (2014) 'The role of gibberellin signalling in plant responses to abiotic stress', *The Journal of Experimental Biology*, 217(1), p. 67 LP-75.

Conway, G. (1997) *The Doubly Green Revolution: Food For All in the 21st Century*. London: Penguin Books.

Cruz-Ramírez, A. *et al.* (2012) 'A bistable circuit involving SCARECROW-RETINOBLASTOMA integrates cues to inform asymmetric stem cell division.', *Cell*, 150(5), p. 1002–15.

Cruz-Ramírez, A., Díaz-Triviño, S., Wachsman, G., Du, Y., Arteága-Vázquez, M., Zhang, H., Benjamins, R., Blilou, I., Neef, A. B., Chandler, V. and Scheres, B. (2013) 'A SCARECROW-RETINOBLASTOMA Protein Network Controls Protective Quiescence in the Arabidopsis Root Stem

Cell Organizer', *PLOS Biology*. Public Library of Science, 11(11), p. e1001724-.

Cui, H. and Benfey, P. N. (2009) 'Interplay between SCARECROW, GA and LIKE HETEROCHROMATIN PROTEIN 1 in ground tissue patterning in the Arabidopsis root', *Plant Journal*, 58(6), p. 1016–1027.

Davière, J.-M. and Achard, P. (2013) 'Gibberellin signaling in plants.', *Development (Cambridge, England)*, 140(6), p. 1147–51.

Davière, J.-M. and Achard, P. (2016) 'A Pivotal Role of DELLAs in Regulating Multiple Hormone Signals', *Molecular Plant*. Elsevier, 9(1), p. 10–20.

Daviere, J.-M., Wild, M., Regnault, T., Baumberger, N., Eisler, H., Genschik, P. and Achard, P. (2014) 'Class I TCP-DELLA interactions in inflorescence shoot apex determine plant height.', *Current biology : CB*. England, 24(16), p. 1923–1928.

Desvoyes, B., de Mendoza, A., Ruiz-Trillo, I. and Gutierrez, C. (2014) 'Novel roles of plant RETINOBLASTOMA-RELATED (RBR) protein in cell proliferation and asymmetric cell division.', *Journal of experimental botany*, 65(10), p. 2657–66.

Desvoyes, B., Ramirez-Parra, E., Xie, Q., Chua, N.-H. and Gutierrez, C. (2006) 'Cell Type-Specific Role of the Retinoblastoma/E2F Pathway during Arabidopsis Leaf Development', *Plant Physiology* , 140(1), p. 67–80.

Dewitte, W. and Murray, J. A. H. (2003) 'The Plant Cell Cycle', *Annual Review of Plant Biology*. Annual Reviews, 54(1), p. 235–264.

Dewitte, W., Riou-Khamlichi, C., Scofield, S., Healy, J. M. S., Jacqmard, A., Kilby, N. J. and Murray, J. A. H. (2003) 'Altered Cell Cycle Distribution, Hyperplasia, and Inhibited Differentiation in Arabidopsis Caused by the D-Type Cyclin CYCD3', *The Plant Cell*. American Society of Plant Biologists, 15(1), p. 79–92.

Dick, F. A. and Rubin, S. M. (2013) 'Molecular mechanisms underlying RB protein function', *Nature reviews. Molecular cell biology*, 14(5), p. 297–306.

Dill, A., Jung, H. S. and Sun, T. P. (2001) 'The DELLA motif is essential for gibberellin-induced degradation of RGA.', *Proceedings of the National Academy of Sciences of the United States of America*, 98(24), p. 14162–7.

Dill, A. and Sun, T. (2001) 'Synergistic Derepression of Gibberellin Signaling by Removing RGA and GAI Function in Arabidopsis thaliana', *Genetics*, 159(2), p. 777–785.

Dill, A., Thomas, S. G., Hu, J., Steber, C. M. and Sun, T. (2004) 'The Arabidopsis F-Box Protein SLEEPY1 Targets Gibberellin Signaling Repressors for Gibberellin-Induced Degradation', 16(June), p. 1392–1405.

Du, Y. and Scheres, B. (2018) 'Lateral root formation and the multiple roles of auxin', *Journal of Experimental Botany*, 69(2), p. 155–167.

Durfee, T., Feiler, H. S. and Gruissem, W. (2000) 'Retinoblastoma-related proteins in plants: homologues or orthologues of their metazoan counterparts?', *Plant molecular biology*, 43(5–6), p. 635–42.

Dyson, T. (1996) *Population and Food: Global Trends and Future Prospects*. Routledge, London.

Ebel, C., Mariconti, L. and Gruissem, W. (2004) 'Plant retinoblastoma homologues control nuclear proliferation in the female gametophyte', *Nature*, 429(6993), p. 776–780.

Endo, M., Nakayama, S., Umeda-Hara, C., Ohtsuki, N., Saika, H., Umeda, M. and Toki, S. (2012)

'CDKB2 is involved in mitosis and DNA damage response in rice', *The Plant Journal*. Oxford, UK: Blackwell Publishing Ltd, 69(6), p. 967–977.

Evans, L. T. (1993) *Crop Evolution, Adaptation and Yield*. Cambridge: Cambridge Univ. Press.

Evans, L. T. (1998) *Feeding the Ten Billion: Plants and Population Growth*, *Cambridge University Press*.

Feng, S., Martinez, C., Gusmaroli, G., Wang, Y., Zhou, J., Wang, F., Chen, L., Yu, L., Iglesias-Pedraz, J. M., Kircher, S., Schäfer, E., Fu, X., Fan, L.-M. and Deng, X. W. (2008) 'Coordinated regulation of Arabidopsis thaliana development by light and gibberellins.', *Nature*. Nature Publishing Group, 451(7177), p. 475–9.

Fisher, D. L. and Nurse, P. (1996) 'A single fission yeast mitotic cyclin B p34cdc2 kinase promotes both S-phase and mitosis in the absence of G1 cyclins.', *The EMBO Journal*, 15(4), p. 850–860.

Fleck, B. and Harberd, N. P. (2002) 'Evidence that the Arabidopsis nuclear gibberellin signalling protein GAI is not destabilised by gibberellin', *Plant Journal*, 32, p. 935–947.

Fleck, B. and Harberd, N. P. (2002) 'Evidence that the Arabidopsis nuclear gibberellin signalling protein GAI is not destabilised by gibberellin', *The Plant Journal*. Blackwell Science Ltd, 32(6), p. 935–947.

Fobert, P. R., Gaudin, V., Lunness, P., Coen, E. S. and Doonan, J. H. (1996) 'Distinct classes of cdc2-related genes are differentially expressed during the cell division cycle in plants.', *The Plant Cell*, 8(9), p. 1465–1476.

Francis, D. (2009) 'What ' s New in the Plant Cell Cycle ?'

French, A. P., Wilson, M. H., Kenobi, K., Dietrich, D., Voß, U., Ubeda-Tomás, S., Pridmore, T. P. and Wells, D. M. (2012) 'Identifying biological landmarks using a novel cell measuring image analysis tool: Cell-o-Tape', *Plant Methods*, 8(1), p. 7.

Fridman, Y., Elkouby, L., Holland, N., Vragović, K., Elbaum, R. and Savaldi-Goldstein, S. (2014) 'Root growth is modulated by differential hormonal sensitivity in neighboring cells', *Genes & Development*. Cold Spring Harbor Laboratory Press, 28(8), p. 912–920.

Friend, S. H., Bernards, R., Rogelj, S., Weinberg, R. A., Rapaport, J. M., Albert, D. M. and Dryja, T. P. 'A human DNA segment with properties of the gene that predisposes to retinoblastoma and osteosarcoma.', *Nature*, 323(6089), p. 643–6.

Friml, J., Vieten, A., Sauer, M., Weijers, D., Schwarz, H., Hamann, T., Offringa, R. and Jurgens, G. (2003) 'Efflux-dependent auxin gradients establish the apical-basal axis of Arabidopsis', *Nature*. Macmillian Magazines Ltd., 426(6963), p. 147–153.

Fu, X. and Harberd, N. P. (2003) 'Auxin promotes Arabidopsis root growth by modulating gibberellin response.', *Nature*, 421(6924), p. 740–3.

Fukaki, H., Okushima, Y. and Tasaka, M. B. T.-I. R. of C. (2007) 'Auxin-Mediated Lateral Root Formation in Higher Plants', in. Academic Press, p. 111–137.

Fukazawa, J., Teramura, H., Murakoshi, S., Nasuno, K., Nishida, N., Ito, T., Yoshida, M., Kamiya, Y., Yamaguchi, S. and Takahashi, Y. (2014) 'DELLAs Function as Coactivators of GAI-ASSOCIATED FACTOR1 in Regulation of Gibberellin Homeostasis and Signaling in Arabidopsis', *The Plant Cell Online* .

Fulcher, N. and Sablowski, R. (2009) 'Hypersensitivity to DNA damage in plant stem cell niches', *Proceedings of the National Academy of Sciences*, 106(49), p. 20984–20988.

Furukawa, T., Curtis, M. J., Tominey, C. M., Duong, Y. H., Wilcox, B. W. L., Aggoune, D., Hays, J. B. and Britt, A. B. (2010) 'A shared DNA-damage-response pathway for induction of stem-cell death by UVB and by gamma irradiation', *DNA Repair*, 9(9), p. 940–948.

Gadella, T. W. J., Jovin, T. M. and Clegg, R. M. (1993) 'Fluorescence lifetime imaging microscopy (FLIM): Spatial resolution of microstructures on the nanosecond time scale', *Biophysical Chemistry*, 48(2), p. 221–239.

Galbraith, D. W., Harkins, K. R. and Knapp, S. (1991) 'Systemic Endopolyploidy in <em>Arabidopsis thaliana</em&gt';, *Plant Physiology*, 96(3), p. 985 LP-989.

Gale, M. D. & Youssefian, S. (1985) *in Progress in Plant Breeding*. Butterworths, London: ed. Russell, G. E.

Gallego-Bartolomé, J., Arana, M. V, Vandenbussche, F., Žádníková, P., Minguet, E. G., Guardiola, V., Van Der Straeten, D., Benkova, E., Alabadí, D. and Blázquez, M. A. (2011) 'Hierarchy of hormone action controlling apical hook development in Arabidopsis', *The Plant Journal*. Blackwell Publishing Ltd, 67(4), p. 622–634.

Gallego-Bartolomé, J., Kami, C., Fankhauser, C., Alabadí, D. and Blázquez, M. A. (2011) 'A Hormonal Regulatory Module That Provides Flexibility to Tropic Responses', *Plant Physiology* , 156(4), p. 1819–1825.

Gallego-Bartolomé, J., Minguet, E. G., Grau-Enguix, F., Abbas, M., Locascio, A., Thomas, S. G., Alabadí, D. and Blázquez, M. A. (2012) 'Molecular mechanism for the interaction between gibberellin and brassinosteroid signaling pathways in Arabidopsis', *Proceedings of the National Academy of Sciences of the United States of America*. National Academy of Sciences, 109(33), p. 13446–13451.

Gomaa, M. S., Simons, C. and Brancale, A. (2007) 'Homology model of 1α,25-dihydroxyvitamin D3 24-hydroxylase cytochrome P450 24A1 (CYP24A1): Active site architecture and ligand binding', *The Journal of Steroid Biochemistry and Molecular Biology*, 104(1), p. 53–60.

Goodrich, D. W. and Lee, W.-H. (1993) 'Molecular characterization of the retinoblastoma susceptibility gene', *Biochimica et Biophysica Acta (BBA) - Reviews on Cancer*, 1155(1), p. 43–61.

Grafi, G., Burnett, R. J., Helentjaris, T., Larkins, B. A., DeCaprio, J. A., Sellers, W. R. and Kaelin, W. G. (1996) 'A maize cDNA encoding a member of the retinoblastoma protein family: involvement in endoreduplication.', *Proceedings of the National Academy of Sciences of the United States of America*, 93(17), p. 8962–7.

Griffiths, J., Murase, K., Rieu, I., Zentella, R., Zhang, Z.-L., Powers, S. J., Gong, F., Phillips, A. L., Hedden, P., Sun, T. and Thomas, S. G. (2006) 'Genetic characterization and functional analysis of the GID1 gibberellin receptors in Arabidopsis.', *The Plant cell*, 18(12), p. 3399–414.

Gruissem, W. (2007) 'Function of the Retinoblastoma-related Protein in Plants', in *Annual Plant Reviews Volume 32: Cell Cycle Control and Plant Development*. Blackwell Publishing Ltd, p. 164–186.

Gutzat, R., Borghi, L., Fütterer, J., Bischof, S., Laizet, Y., Hennig, L., Feil, R., Lunn, J. and Gruissem, W. (2011) 'RETINOBLASTOMA-RELATED PROTEIN controls the transition to autotrophic plant development', *Development*, 138(14), p. 2977–2986.

Hacham, Y., Holland, N., Butterfield, C., Ubeda-Tomas, S., Bennett, M. J., Chory, J. and Savaldi-Goldstein, S. (2011) 'Brassinosteroid perception in the epidermis controls root meristem size', *Development (Cambridge, England)*. Company of Biologists, 138(5), p. 839–848.

Harada, J. J., Belmonte, M. F. and Kwong, R. W. (2010) 'Plant Embryogenesis (Zygotic and Somatic)',

in *Encyclopedia of Life Sciences*. John Wiley & Sons, Ltd.

Harashima, H., Dissmeyer, N. and Schnittger, A. (2013) 'Cell cycle control across the eukaryotic kingdom', *Trends in Cell Biology*. Elsevier, 23(7), p. 345–356.

Harashima, H. and Sugimoto, K. (2016) 'Integration of developmental and environmental signals into cell proliferation and differentiation through RETINOBLASTOMA-RELATED 1.', *Current opinion in plant biology*. England, 29, p. 95–103.

Hedden, P. and Thomas, S. G. (2012) 'Gibberellin biosynthesis and its regulation', *Biochemical Journal*, 444(1), p. 11–25.

Heim, R., Cubitt, a B. and Tsien, R. Y. (1995) 'Improved green fluorescence.', *Nature*, p. 663–664.

Helariutta, Y., Fukaki, H., Wysocka-Diller, J., Nakajima, K., Jung, J., Sena, G., Hauser, M.-T. and Benfey, P. N. (2000) 'The SHORT-ROOT Gene Controls Radial Patterning of the Arabidopsis Root through Radial Signaling', *Cell*, 101(5), p. 555–567.

Heo, J.-O., Chang, K. S., Kim, I. A., Lee, M.-H., Lee, S. A., Song, S.-K., Lee, M. M. and Lim, J. (2011) 'Funneling of gibberellin signaling by the GRAS transcription regulator scarecrow-like 3 in the Arabidopsis root.', *Proceedings of the National Academy of Sciences of the United States of America*, 108(5), p. 2166–71.

Hirano, K., Asano, K., Tsuji, H., Kawamura, M., Mori, H., Kitano, H., Ueguchi-Tanaka, M. and Matsuoka, M. (2010) 'Characterization of the Molecular Mechanism Underlying Gibberellin Perception Complex Formation in Rice', *The Plant Cell*. American Society of Plant Biologists, 22(8), p. 2680–2696.

Hirano, K., Kouketu, E., Katoh, H., Aya, K., Ueguchi-Tanaka, M. and Matsuoka, M. (2012) 'The suppressive function of the rice DELLA protein SLR1 is dependent on its transcriptional activation activity', *The Plant Journal*. Blackwell Publishing Ltd, 71(3), p. 443–453.

Horvath, B. M., Kourova, H., Nagy, S., Nemeth, E., Magyar, Z., Papdi, C., Ahmad, Z., Sanchez-Perez, G. F., Perilli, S., Blilou, I., Pettkó-Szandtner, A., Darula, Z., Meszaros, T., Binarova, P., Bogre, L. and Scheres, B. (2017) 'Arabidopsis RETINOBLASTOMA RELATED directly regulates DNA damage responses through functions beyond cell cycle control', *The EMBO Journal*. Hoboken: John Wiley and Sons Inc., 36(9), p. 1261–1278.

Hou, X., Lee, L. Y. C., Xia, K., Yan, Y. and Yu, H. (2010) 'DELLAs modulate jasmonate signaling via competitive binding to JAZs.', *Developmental cell*. United States, 19(6), p. 884–894.

Hou, X., Lee, L. Y. C., Xia, K., Yan, Y. and Yu, H. (2016) 'DELLAs Modulate Jasmonate Signaling via Competitive Binding to JAZs', *Developmental Cell*. Elsevier, 19(6), p. 884–894.

Huntley, R., Healy, S., Freeman, D., Lavender, P., de Jager, S., Greenwood, J., Makker, J., Walker, E., Jackman, M., Xie, Q., Bannister, a J., Kouzarides, T., Gutiérrez, C., Doonan, J. H. and Murray, J. a (1998) 'The maize retinoblastoma protein homologue ZmRb-1 is regulated during leaf development and displays conserved interactions with G1/S regulators and plant cyclin D (CycD) proteins.', *Plant molecular biology*, 37(1), p. 155–69.

Ikeda, A., Ueguchi-Tanaka, M., Sonoda, Y., Kitano, H., Koshioka, M., Futsuhara, Y., Matsuoka, M. and Yamaguchi, J. (2001) 'slender Rice, a Constitutive Gibberellin Response Mutant, Is Caused by a Null Mutation of the SLR1 Gene, an Ortholog of the Height-Regulating Gene GAI/RGA/RHT/D8', *The Plant Cell* , 13(5), p. 999–1010.

Inzé, D. and De Veylder, L. (2006) 'Cell Cycle Regulation in Plant Development', *Annual Review of Genetics*. Annual Reviews, 40(1), p. 77–105.

Dello Ioio, R., Linhares, F. S., Scacchi, E., Casamitjana-Martinez, E., Heidstra, R., Costantino, P. and Sabatini, S. (2007) 'Cytokinins Determine Arabidopsis Root-Meristem Size by Controlling Cell Differentiation', *Current Biology*. Elsevier, 17(8), p. 678–682.

Itoh, H., Ueguchi-Tanaka, M., Sato, Y., Ashikari, M. and Matsuoka, M. (2002) 'The Gibberellin Signaling Pathway Is Regulated by the Appearance and Disappearance of SLENDER RICE1 in Nuclei', *The Plant Cell* , 14(1), p. 57–70.

Iuchi, S., Suzuki, H., Kim, Y.-C., Iuchi, A., Kuromori, T., Ueguchi-Tanaka, M., Asami, T., Yamaguchi, I., Matsuoka, M., Kobayashi, M. and Nakajima, M. (2007) 'Multiple loss-of-function of Arabidopsis gibberellin receptor AtGID1s completely shuts down a gibberellin signal', *The Plant Journal*, 50(6), p. 958–966.

J. Morris, E. and J. Dyson, N. (2001) *Morris EJ, Dyson NJ.. Retinoblastoma protein partners. Adv Cancer Res 82: 1-54*, *Advances in cancer research*.

Jaillais, Y. and Chory, J. (2010) 'Unraveling the paradoxes of plant hormone signaling integration.', *Nature structural & molecular biology*. Nature Publishing Group, 17(6), p. 642–5.

Jakoby, M. and Schnittger, A. (2004) 'Cell cycle and differentiation.', *Current opinion in plant biology*. England, 7(6), p. 661–669.

Johnston, A. J. and Gruissem, W. (2009) 'Gametophyte differentiation and imprinting control in plants: Crosstalk between RBR and chromatin', *Communicative & Integrative Biology*. Landes Bioscience, 2(2), p. 144–146.

Johnston, A. J., Matveeva, E., Kirioukhova, O., Grossniklaus, U. and Gruissem, W. (2008) 'A Dynamic Reciprocal RBR-PRC2 Regulatory Circuit Controls Arabidopsis Gametophyte Development', *Current Biology*, 18(21), p. 1680–1686.

Johnston, A. J., Matveeva, E., Kirioukhova, O., Grossniklaus, U. and Gruissem, W. (2009) 'A Dynamic Reciprocal RBR-PRC2 Regulatory Circuit Controls Arabidopsis Gametophyte Development', *Current Biology*. Elsevier, 18(21), p. 1680–1686.

Joubes, J. and Chevalier, C. (2000) 'Endoreduplication in higher plants.', *Plant molecular biology*. Netherlands, 43(5–6), p. 735–745.

Joubès, J., Chevalier, C., Dudits, D., Heberle-Bors, E., Inzé, D., Umeda, M. and Renaudin, J.-P. (2000) 'CDK-related protein kinases in plants', *Plant Molecular Biology*, 43(5), p. 607–620.

Kapulnik, Y., Delaux, P.-M., Resnick, N., Mayzlish-Gati, E., Wininger, S., Bhattacharya, C., Sejalon-Delmas, N., Combier, J.-P., Becard, G., Belausov, E., Beeckman, T., Dor, E., Hershenhorn, J. and Koltai, H. (2011) 'Strigolactones affect lateral root formation and root-hair elongation in Arabidopsis.', *Planta*. Germany, 233(1), p. 209–216.

Kapulnik, Y., Resnick, N., Mayzlish-Gati, E., Kaplan, Y., Wininger, S., Hershenhorn, J. and Koltai, H. (2011) 'Strigolactones interact with ethylene and auxin in regulating root-hair elongation in Arabidopsis.', *Journal of experimental botany*. England, 62(8), p. 2915–2924.

Kawamura, K., Murray, J. A. H., Shinmyo, A. and Sekine, M. (2006) 'Cell Cycle Regulated D3-type Cyclins form Active Complexes with Plant-specific B-type Cyclin-dependent Kinase in vitro', *Plant Molecular Biology*, 61(1), p. 311–327.

Kieffer, M., Neve, J. and Kepinski, S. (2010) 'Defining auxin response contexts in plant development', *Current Opinion in Plant Biology*, 13(1), p. 12–20.

Knudsen, E. S. and Knudsen, K. E. (2006) 'MINIREVIEW Retinoblastoma Tumor Suppressor: Where Cancer Meets the Cell Cycle'.

Kobayashi, K. *et al.* (2015) 'Transcriptional repression by MYB3R proteins regulates plant organ growth', *The EMBO Journal*. Chichester, UK: John Wiley & Sons, Ltd, 34(15), p. 1992–2007.

Kong, L. J., Orozco, B. M., Roe, J. L., Nagar, S., Ou, S., Feiler, H. S., Durfee, T., Miller, A. B., Gruissem, W., Robertson, D. and Hanley-Bowdoin, L. (2000) 'A geminivirus replication protein interacts with the retinoblastoma protein through a novel domain to determine symptoms and tissue specificity of infection in plants.', *The EMBO journal*, 19(13), p. 3485–95.

Koorneef, M., Elgersma, A., Hanhart, C. J., Loenen-Martinet, E. P., Rijn, L. and Zeevaart, J. A. D. (1985) 'A gibberellin insensitive mutant of Arabidopsis thaliana', *Physiologia Plantarum*, 65(1), p. 33–39.

Koornneef, M. and Meinke, D. (2010) 'The development of Arabidopsis as a model plant', *The Plant Journal*. Blackwell Publishing Ltd, 61(6), p. 909–921.

Koornneef, M. and van der Veen, J. H. (1980) 'Induction and analysis of gibberellin sensitive mutants in Arabidopsis thaliana (L.) heynh.', *TAG. Theoretical and applied genetics. Theoretische und angewandte Genetik*, 58(6), p. 257–63.

Koressaar, T. and Remm, M. (2007) 'Enhancements and modifications of primer design program Primer3', *Bioinformatics*, 23(10), p. 1289–1291.

Kumar, M., Pandya-Kumar, N., Kapulnik, Y. and Koltai, H. (2015) 'Strigolactone signaling in root development and phosphate starvation', *Plant Signaling & Behavior*. Taylor & Francis, 10(7), p. e1045174.

Di Laurenzio, L., Wysocka-Diller, J., Malamy, J. E., Pysh, L., Helariutta, Y., Freshour, G., Hahn, M. G., Feldmann, K. A. and Benfey, P. N. (1996) 'The SCARECROW gene regulates an asymmetric cell division that is essential for generating the radial organization of the Arabidopsis root.', *Cell*, 86(3), p. 423–33.

Lee, C., Chang, J. H., Lee, H. S. and Cho, Y. (2002) 'Structural basis for the recognition of the E2F transactivation domain by the retinoblastoma tumor suppressor', *Genes & Development*. Cold Spring Harbor Laboratory Press, 16(24), p. 3199–3212.

Lee, J. O., Russo, A. A. and Pavletich, N. P. (1998) 'Structure of the retinoblastoma tumour-suppressor pocket domain bound to a peptide from HPV E7.', *Nature*, 391(6670), p. 859–65.

Lee, S., Cheng, H., King, K. E., Wang, W., He, Y., Hussain, A., Lo, J., Harberd, N. P. and Peng, J. (2002) 'Gibberellin regulates Arabidopsis seed germination via RGL2, a GAI/RGA-like gene whose expression is up-regulated following imbibition', *Genes & Development*. Cold Spring Harbor Laboratory Press, 16(5), p. 646–658.

Lewis, D. R., Negi, S., Sukumar, P. and Muday, G. K. (2011) 'Ethylene inhibits lateral root development, increases IAA transport and expression of PIN3 and PIN7 auxin efflux carriers', *Development*, 138(16), p. 3485 LP-3495.

Li, S., Zhao, Y., Zhao, Z., Wu, X., Sun, L., Liu, Q. and Wu, Y. (2016) 'Crystal Structure of the GRAS Domain of SCARECROW-LIKE7 in Oryza sativa', *The Plant Cell*. American Society of Plant Biologists, 28(5), p. 1025–1034.

Lim, S., Park, J., Lee, N., Jeong, J., Toh, S., Watanabe, A., Kim, J., Kang, H., Kim, D. H., Kawakami, N. and Choi, G. (2013) 'ABA-INSENSITIVE3, ABA-INSENSITIVE5, and DELLAs Interact to Activate the Expression of SOMNUS and Other High-Temperature-Inducible Genes in Imbibed Seeds in Arabidopsis', *The Plant Cell* , 25(12), p. 4863–4878.

Liu, C., Xu, Z. and Chua, N. H. (1993) 'Auxin Polar Transport Is Essential for the Establishment of

Bilateral Symmetry during Early Plant Embryogenesis.', *The Plant Cell* , 5(6), p. 621–630.

Locascio, A., Blázquez, M. a and Alabadí, D. (2013) 'Genomic analysis of DELLA protein activity.', *Plant & cell physiology*, 54(8), p. 1229–37.

Long, Y., Stahl, Y., Weidtkamp-Peters, S., Postma, M., Zhou, W., Goedhart, J., Sánchez-Pérez, M.-I., Gadella, T. W. J., Simon, R., Scheres, B. and Blilou, I. (2017) 'In vivo FRET–FLIM reveals cell-type-specific protein interactions in Arabidopsis roots', *Nature*. Macmillan Publishers Limited, part of Springer Nature. All rights reserved., 548(7665), p. 97–102.

Lor, V. S. and Olszewski, N. E. (2015) 'GA signalling and cross-talk with other signalling pathways', *Essays in Biochemistry*, 58, p. 49–60.

de Lucas, M., Davière, J.-M., Rodríguez-Falcón, M., Pontin, M., Iglesias-Pedraz, J. M., Lorrain, S., Fankhauser, C., Blázquez, M. A., Titarenko, E. and Prat, S. (2008) 'A molecular framework for light and gibberellin control of cell elongation.', *Nature*, 451(7177), p. 480–4.

Magyar, Z. (2008) 'Keeping the Balance Between Proliferation and Differentiation by the E2F Transcriptional Regulatory Network is Central to Plant Growth and Development', in Bögre, L. and Beemster, G. (eds) *Plant Growth Signaling*. Berlin, Heidelberg: Springer Berlin Heidelberg, p. 89–105.

Magyar, Z., Atanassova, A., De Veylder, L., Rombauts, S. and Inzé, D. (2000) 'Characterization of two distinct DP-related genes from Arabidopsis thaliana1', *FEBS Letters*, 486(1), p. 79–87.

Magyar, Z., Horváth, B., Khan, S., Mohammed, B., Henriques, R., De Veylder, L., Bakó, L., Scheres, B. and Bögre, L. (2012) 'Arabidopsis E2FA stimulates proliferation and endocycle separately through RBR-bound and RBR-free complexes.', *The EMBO journal*, 31(6), p. 1480–93.

Magyar, Z., De Veylder, L., Atanassova, A., Bakó, L., Inzé, D. and Bögre, L. (2005) 'The Role of the Arabidopsis E2FB Transcription Factor in Regulating Auxin-Dependent Cell Division', *The Plant Cell* , 17(9), p. 2527–2541.

Marín-de la Rosa, N., Pfeiffer, A., Hill, K., Locascio, A., Bhalerao, R. P., Miskolczi, P., Grønlund, A. L., Wanchoo-Kohli, A., Thomas, S. G., Bennett, M. J., Lohmann, J. U., Blázquez, M. A. and Alabadi, D. (2015) 'Genome Wide Binding Site Analysis Reveals Transcriptional Coactivation of Cytokinin-Responsive Genes by DELLA Proteins', *PLoS Genet*. Public Library of Science, 11(7), p. e1005337.

Martí-Renom, M. A., Stuart, A. C., Fiser, A., Sánchez, R., Melo, F. and Šali, A. (2000) 'Comparative Protein Structure Modeling of Genes and Genomes', *Annual Review of Biophysics and Biomolecular Structure*. Annual Reviews, 29(1), p. 291–325.

Martín-Trillo, M. and Cubas, P. (2010) 'TCP genes: a family snapshot ten years later', *Trends in Plant Science*, 15(1), p. 31–39.

Masia, F., Glen, A., Stephens, P., Borri, P. and Langbein, W. (2013) 'Quantitative Chemical Imaging and Unsupervised Analysis Using Hyperspectral Coherent Anti-Stokes Raman Scattering Microscopy', *Analytical Chemistry*. American Chemical Society, 85(22), p. 10820–10828.

McGinnis, K. M., Thomas, S. G., Soule, J. D., Strader, L. C., Zale, J. M., Sun, T. and Steber, C. M. (2003) 'The Arabidopsis SLEEPY1 Gene Encodes a Putative F-Box Subunit of an SCF E3 Ubiquitin Ligase', *The Plant Cell*. American Society of Plant Biologists, 15(5), p. 1120–1130.

Menges, M. and Murray, J. A. H. (2002) 'Synchronous Arabidopsis suspension cultures for analysis of cell-cycle gene activity', *Plant Journal*.

Menges, M., Pavesi, G., Morandini, P., Bögre, L. and Murray, J. A. H. (2007) 'Genomic Organization and Evolutionary Conservation of Plant D-Type Cyclins', *Plant Physiology* , 145(4), p. 1558–1576.

Morgan, D. (2006) *The Cell Cycle: Principles of Control*. London: OUP Oxford.

Mundy, J., Nielsen, H. B. and Brodersen, P. (2006) 'Crosstalk.', *Trends in plant science*, 11(2), p. 63–4.

Murase, K., Hirano, Y., Sun, T. and Hakoshima, T. (2008) 'Gibberellin-induced DELLA recognition by the gibberellin receptor GID1.', *Nature*, 456(7221), p. 459–63.

Murray, A. W. (2004) 'Recycling the Cell Cycle', *Cell*. Elsevier, 116(2), p. 221–234.

Murray, J. (1997) *The retinoblastoma protein is in plants!* 2nd edn. Trends Plant Sci.

Nakagami, H., Sekine, M., Murakami, H. and Shinmyo, A. (1999) 'Tobacco retinoblastoma-related protein phosphorylated by a distinct cyclin-dependent kinase complex with Cdc2/cyclin D in vitro.', *The Plant journal : for cell and molecular biology*, 18(3), p. 243–52.

Nakajima, M., Shimada, A., Takashi, Y., Kim, Y.-C., Park, S.-H., Ueguchi-Tanaka, M., Suzuki, H., Katoh, E., Iuchi, S., Kobayashi, M., Maeda, T., Matsuoka, M. and Yamaguchi, I. (2006) 'Identification and characterization of Arabidopsis gibberellin receptors.', *The Plant journal : for cell and molecular biology*, 46(5), p. 880–9.

Nieuwland, J., Menges, M. and Murray, J. A. H. (2007) 'The Plant Cyclins', in *Annual Plant Reviews Volume 32: Cell Cycle Control and Plant Development*. Blackwell Publishing Ltd, p. 31–61.

Novak, B., Csikasz-Nagy, A., Gyorffy, B., Nasmyth, K. and Tyson, J. J. (1998) 'Model scenarios for evolution of the eukaryotic cell cycle', *Philosophical Transactions of the Royal Society of London. Series B: Biological Sciences*, 353(1378), p. 2063 LP-2076.

Nowack, M. K., Harashima, H., Dissmeyer, N., Zhao, X., Bouyer, D., Weimer, A. K., De Winter, F., Yang, F. and Schnittger, A. (2012) 'Genetic Framework of Cyclin-Dependent Kinase Function in Arabidopsis', *Developmental Cell*.

Nugent, J. H., Alfa, C. E., Young, T. and Hyams, J. S. (1991) 'Conserved structural motifs in cyclins identified by sequence analysis', *Journal of Cell Science*, 99(3), p. 669–674.

O'Leary, N. A. *et al.* (2016) 'Reference sequence (RefSeq) database at NCBI: current status, taxonomic expansion, and functional annotation', *Nucleic Acids Research*, 44(D1), p. D733–D745.

Oakenfull, E. A., Riou-Khamlichi, C. and Murray, A. H. (2002) 'Plant D–type cyclins and the control of G1 progression', *Philosophical Transactions of the Royal Society of London B: Biological Sciences*, 357(1422), p. 749–760.

Overvoorde, P., Fukaki, H. and Beeckman, T. (2010) 'Auxin Control of Root Development', *Cold Spring Harbor Perspectives in Biology*. Cold Spring Harbor Laboratory Press, 2(6), p. a001537.

Paquette, A. J. and Benfey, P. N. (2005) 'Maturation of the ground tissue of the root is regulated by gibberellin and SCARECROW and requires SHORT-ROOT.', *Plant physiology*, 138(2), p. 636–40.

Park, J.-A., Ahn, J.-W., Kim, Y.-K., Kim, S. J., Kim, J.-K., Kim, W. T. and Pai, H.-S. (2005) 'Retinoblastoma protein regulates cell proliferation, differentiation, and endoreduplication in plants', *The Plant Journal*. Blackwell Science Ltd, 42(2), p. 153–163.

Park, J., Nguyen, K. T., Park, E., Jeon, J.-S. and Choi, G. (2013) 'DELLA proteins and their interacting RING Finger proteins repress gibberellin responses by binding to the promoters of a subset of gibberellin-responsive genes in Arabidopsis.', *The Plant cell*. United States, 25(3), p. 927–943.

Pearce, S., Saville, R., Vaughan, S. P., Chandler, P. M., Wilhelm, E. P., Sparks, C. a, Al-Kaff, N., Korolev, A., Boulton, M. I., Phillips, A. L., Hedden, P., Nicholson, P. and Thomas, S. G. (2011)

'Molecular characterization of Rht-1 dwarfing genes in hexaploid wheat.', *Plant physiology*, 157(4), p. 1820–31.

Peng, J., Carol, P., Richards, D. E., King, K. E., Cowling, R. J., Murphy, G. P. and Harberd, N. P. (1997) 'The Arabidopsis GAI gene defines a signaling pathway that negatively regulates gibberellin responses ', *Genes & Development*, 11(23), p. 3194–3205.

Peng, J. and Harberd, N. P. (1993) 'Derivative Alleles of the Arabidopsis Gibberellin-Insensitive (gai) Mutation Confer a Wild-Type Phenotype.', *The Plant Cell* , 5(3), p. 351–360.

Peng, J., Richards, D. E., Hartley, N. M., Murphy, G. P., Devos, K. M., Flintham, J. E., Beales, J., Fish, L. J., Worland, a J., Pelica, F., Sudhakar, D., Christou, P., Snape, J. W., Gale, M. D. and Harberd, N. P. (1999) '"Green revolution" genes encode mutant gibberellin response modulators.', *Nature*, 400(6741), p. 256–61.

Peres, A., Churchman, M. L., Hariharan, S., Himanen, K., Verkest, A., Vandepoele, K., Magyar, Z., Hatzfeld, Y., Van Der Schueren, E., Beemster, G. T. S., Frankard, V., Larkin, J. C., Inzé, D. and De Veylder, L. (2007) 'Novel Plant-specific Cyclin-dependent Kinase Inhibitors Induced by Biotic and Abiotic Stresses', *Journal of Biological Chemistry* , 282(35), p. 25588–25596.

Phillips, G. J. (2001) 'Green fluorescent protein – a bright idea for the study of bacterial protein localization', *FEMS Microbiology Letters*, 204(1), p. 9–18.

Pitts, R. J., Cernac, A. and Estelle, M. (1998) 'Auxin and ethylene promote root hair elongation in Arabidopsis.', *The Plant journal : for cell and molecular biology*. England, 16(5), p. 553–560.

Plackett, A. R. G., Ferguson, A. C., Powers, S. J., Wanchoo-Kohli, A., Phillips, A. L., Wilson, Z. A., Hedden, P. and Thomas, S. G. (2014) 'DELLA activity is required for successful pollen development in the Columbia ecotype of Arabidopsis.', *The New phytologist*, 201(3), p. 825–36.

Pound, M. P., French, A. P., Atkinson, J., Wells, D. M., Bennett, M. J. and Pridmore, T. P. (2013) 'RootNav: Navigating images of complex root architectures', *Plant Physiology*.

Pysh, L. D., Wysocka-Diller, J. W., Camilleri, C., Bouchez, D. and Benfey, P. N. (1999) 'The GRAS gene family in Arabidopsis: sequence characterization and basic expression analysis of the SCARECROW-LIKE genes.', *The Plant journal : for cell and molecular biology*, 18(1), p. 111–9.

Ramirez-Parra, E., Fründt, C. and Gutierrez, C. (2003) 'A genome-wide identification of E2F-regulated genes in Arabidopsis', *The Plant Journal*. Blackwell Science Ltd, 33(4), p. 801–811.

Ramirez-Parra, E., López-Matas, M. A., Fründt, C. and Gutierrez, C. (2004) 'Role of an Atypical E2F Transcription Factor in the Control of Arabidopsis Cell Growth and Differentiation', *The Plant Cell* , 16(9), p. 2350–2363.

Rasmussen, A., Mason, M. G., De Cuyper, C., Brewer, P. B., Herold, S., Agusti, J., Geelen, D., Greb, T., Goormachtig, S., Beeckman, T. and Beveridge, C. A. (2012) 'Strigolactones suppress adventitious rooting in Arabidopsis and pea.', *Plant physiology*. United States, 158(4), p. 1976–1987.

Redman, J. C., Haas, B. J., Tanimoto, G. and Town, C. D. (2004) 'Development and evaluation of an Arabidopsis whole genome Affymetrix probe array', *The Plant Journal*. Blackwell Science, Ltd, 38(3), p. 545–561.

Reitz, M. U., Gifford, M. L. and Schäfer, P. (2015) 'Hormone activities and the cell cycle machinery in immunity-triggered growth inhibition.', *Journal of experimental botany*, 66(8), p. 2187–97.

Resentini, F., Felipo-Benavent, A., Colombo, L., Blázquez, M. A., Alabadí, D. and Masiero, S. (2015) 'TCP14 and TCP15 Mediate the Promotion of Seed Germination by Gibberellins in Arabidopsis thaliana', *Molecular Plant*. Elsevier, 8(3), p. 482–485.

Richards, D. E., Peng, J. and Harberd, N. P. (2000) 'Plant GRAS and metazoan STATs: one family?', *BioEssays : news and reviews in molecular, cellular and developmental biology*. United States, 22(6), p. 573–577.

Ruyter-Spira, C., Kohlen, W., Charnikhova, T., van Zeijl, A., van Bezouwen, L., de Ruijter, N., Cardoso, C., Lopez-Raez, J. A., Matusova, R., Bours, R., Verstappen, F. and Bouwmeester, H. (2011) 'Physiological Effects of the Synthetic Strigolactone Analog GR24 on Root System Architecture in Arabidopsis: Another Belowground Role for Strigolactones?', *Plant Physiology*. American Society of Plant Biologists, 155(2), p. 721–734.

Růžička, K., Ljung, K., Vanneste, S., Podhorská, R., Beeckman, T., Friml, J. and Benková, E. (2007) 'Ethylene Regulates Root Growth through Effects on Auxin Biosynthesis and Transport-Dependent Auxin Distribution', *The Plant Cell*, 19(7), p. 2197 LP-2212.

Rymen, B., Coppens, F., Dhondt, S., Fiorani, F. and Beemster, G. T. S. (2010) 'Kinematic Analysis of Cell Division and Expansion', in Hennig, L. and Köhler, C. (eds) *Plant Developmental Biology: Methods and Protocols*. Totowa, NJ: Humana Press, p. 203–227.

Sabatini, S., Heidstra, R., Wildwater, M. and Scheres, B. (2003) 'SCARECROW is involved in positioning the stem cell niche in the Arabidopsis root meristem.', *Genes & development*, 17(3), p. 354–8.

Santner, A. and Estelle, M. (2009) 'Recent advances and emerging trends in plant hormone signalling.', *Nature*. Macmillan Publishers Limited. All rights reserved, 459(7250), p. 1071–8.

Sanz, L., Dewitte, W., Forzani, C., Patell, F., Nieuwland, J., Wen, B., Quelhas, P., De Jager, S., Titmus, C., Campilho, A., Ren, H., Estelle, M., Wang, H. and Murray, J. A. H. (2011) 'The Arabidopsis D-Type Cyclin CYCD2;1 and the Inhibitor ICK2/KRP2 Modulate Auxin-Induced Lateral Root Formation', *The Plant Cell*. American Society of Plant Biologists, 23(2), p. 641–660.

Sasaki, A., Itoh, H., Gomi, K., Ueguchi-Tanaka, M., Ishiyama, K., Kobayashi, M., Jeong, D.-H., An, G., Kitano, H., Ashikari, M. and Matsuoka, M. (2003) 'Accumulation of phosphorylated repressor for gibberellin signaling in an F-box mutant.', *Science (New York, N.Y.)*, 299(5614), p. 1896–8.

Schindelin, J., Arganda-Carreras, I., Frise, E., Kaynig, V., Longair, M., Pietzsch, T., Preibisch, S., Rueden, C., Saalfeld, S., Schmid, B., Tinevez, J.-Y., White, D. J., Hartenstein, V., Eliceiri, K., Tomancak, P. and Cardona, A. (2012) 'Fiji: an open-source platform for biological-image analysis', *Nat Meth*. Nature Publishing Group, a division of Macmillan Publishers Limited. All Rights Reserved., 9(7), p. 676–682.

Scofield, S., Jones, A. and Murray, J. A. H. (2014) 'The plant cell cycle in context', *Journal of Experimental Botany*, 65(10), p. 2557–2562.

Serrano-Mislata, A., Bencivenga, S., Bush, M., Schiessl, K., Boden, S. and Sablowski, R. (2017) 'DELLA genes restrict inflorescence meristem function independently of plant height', *Nature Plants*, 3(9), p. 749–754.

Sessions, A. *et al.* (2002) 'A High-Throughput Arabidopsis Reverse Genetics System', *The Plant Cell*, 14(12), p. 2985.

Shani, E., Weinstain, R., Zhang, Y., Castillejo, C., Kaiserli, E. and Chory, J. (2013) 'Gibberellins accumulate in the elongating endodermal cells of Arabidopsis root', p. 1–6.

Shimada, A., Ueguchi-Tanaka, M., Nakatsu, T., Nakajima, M., Naoe, Y., Ohmiya, H., Kato, H. and Matsuoka, M. (2008) 'Structural basis for gibberellin recognition by its receptor GID1.', *Nature*, 456(7221), p. 520–3.

Shimomura, O., Johnson, F. H. and Saiga, Y. (1962) 'Extraction, purification and properties of aequorin, a bioluminescent protein from the luminous hydromedusan, Aequorea.', *Journal of Cellular and Comparative Physiology*, 59(3), p. 223–239.

Silverstone, A. L., Jung, H.-S., Dill, A., Kawaide, H., Kamiya, Y. and Sun, T. (2001) 'Repressing a Repressor: Gibberellin-Induced Rapid Reduction of the RGA Protein in Arabidopsis ', *The Plant Cell* , 13(7), p. 1555–1566.

Silverstone, A. L., Mak, P. Y. A., Martinez, E. C. and Sun, T. (1997) 'The New Rga Locus Encodes a Negative Regulator of Gibberellin Response in Arabidopsis Thaliana', *Genetics*, 146(3), p. 1087–1099.

Silverstone, a L., Ciampaglio, C. N. and Sun, T. (1998) 'The Arabidopsis RGA gene encodes a transcriptional regulator repressing the gibberellin signal transduction pathway.', *The Plant cell*, 10(2), p. 155–69.

Singh, M., Krajewski, M., Mikolajka, A. and Holak, T. A. (2005) 'Molecular determinants for the complex formation between the retinoblastoma protein and LXCXE sequences', *Journal of Biological Chemistry*.

Sliwinska, E., Bassel, G. W. and Bewley, J. D. (2009) 'Germination of Arabidopsis thaliana seeds is not completed as a result of elongation of the radicle but of the adjacent transition zone and lower hypocotyl', *Journal of Experimental Botany*, 60(12), p. 3587–3594.

Slovak, R., Göschl, C., Seren, Ü. and Busch, W. (2015) 'Genome-Wide Association Mapping in Plants Exemplifi ed', *Plant Functional Genomics: Methods and Protocols*, 1284, p. 343–357.

Slovak, R., Göschl, C., Su, X., Shimotani, K., Shiina, T. and Busch, W. (2014) 'A Scalable Open-Source Pipeline for Large-Scale Root Phenotyping of Arabidopsis', *The Plant Cell Online*.

Song, X.-M., Liu, T.-K., Duan, W.-K., Ma, Q.-H., Ren, J., Wang, Z., Li, Y. and Hou, X.-L. (2014) 'Genome-wide analysis of the GRAS gene family in Chinese cabbage (Brassica rapa ssp. pekinensis)', *Genomics*. Academic Press, 103(1), p. 135–146.

Sozzani, R., Maggio, C., Varotto, S., Canova, S., Bergounioux, C., Albani, D. and Cella, R. (2006) 'Interplay between Arabidopsis Activating Factors E2Fb and E2Fa in Cell Cycle Progression and Development', *Plant Physiology* , 140(4), p. 1355–1366.

Stern, B. and Nurse, P. (1996) 'A quantitative model for the cdc2 control of S phase and mitosis in fission yeast.', *Trends in genetics : TIG*. England, 12(9), p. 345–350.

Strader, L. C., Chen, G. L. and Bartel, B. (2010) 'Ethylene directs auxin to control root cell expansion', *The Plant journal : for cell and molecular biology*, 64(5), p. 874–884.

Street, I. H., Aman, S., Zubo, Y., Ramzan, A., Wang, X., Shakeel, S. N., Kieber, J. J. and Schaller, G. E. (2015) 'Ethylene Inhibits Cell Proliferation of the Arabidopsis Root Meristem', *Plant Physiology*, 169(1), p. 338 LP-350.

Sun, T. (2010) 'Gibberellin-GID1-DELLA: a pivotal regulatory module for plant growth and development.', *Plant physiology*, 154(2), p. 567–70.

Sun, T. P. and Kamiya, Y. (1994) 'The Arabidopsis GA1 locus encodes the cyclase ent-kaurene synthetase A of gibberellin biosynthesis.', *The Plant Cell* , 6(10), p. 1509–1518.

Takatsuka, H. and Umeda, M. (2014) 'Hormonal control of cell division and elongation along differentiation trajectories in roots.', *Journal of experimental botany*, 65(10), p. 2633–2643.

Torres Acosta, J. A., Fowke, L. C. and Wang, H. (2011) 'Analyses of phylogeny, evolution, conserved

sequences and genome-wide expression of the ICK/KRP family of plant CDK inhibitors', *Annals of Botany*. Oxford University Press, 107(7), p. 1141–1157.

Tyler, L., Thomas, S. G., Hu, J., Dill, A., Alonso, J. M. and Ecker, J. R. (2004) 'DELLA Proteins and Gibberellin-Regulated Seed Germination and Floral Development', 135(June), p. 1008–1019.

Ubeda-Tomás, S., Federici, F., Casimiro, I., Beemster, G. T. S., Bhalerao, R., Swarup, R., Doerner, P., Haseloff, J. and Bennett, M. J. (2009) 'Gibberellin signaling in the endodermis controls Arabidopsis root meristem size.', *Current biology : CB*, 19(14), p. 1194–9.

Ubeda-Tomás, S., Swarup, R., Coates, J., Swarup, K., Laplaze, L., Beemster, G. T. S., Hedden, P., Bhalerao, R. and Bennett, M. J. (2008) 'Root growth in Arabidopsis requires gibberellin/DELLA signalling in the endodermis.', *Nature cell biology*. Nature Publishing Group, 10(5), p. 625–8.

Ueguchi-Tanaka, M., Ashikari, M., Nakajima, M., Itoh, H., Katoh, E., Kobayashi, M., Chow, T., Hsing, Y. C., Kitano, H., Yamaguchi, I. and Matsuoka, M. (2005) 'GIBBERELLIN INSENSITIVE DWARF1 encodes a soluble receptor for gibberellin.', *Nature*, 437(7059), p. 693–8.

Ueguchi-Tanaka, M., Nakajima, M., Katoh, E., Ohmiya, H., Asano, K., Saji, S., Hongyu, X., Ashikari, M., Kitano, H., Yamaguchi, I. and Matsuoka, M. (2007) 'Molecular Interactions of a Soluble Gibberellin Receptor, GID1, with a Rice DELLA Protein, SLR1, and Gibberellin', *The Plant Cell* , 19(7), p. 2140–2155.

Umen, J. G. and Goodenough, U. W. (2001) 'Control of cell division by a retinoblastoma protein homolog in Chlamydomonas.', *Genes & development*, 15(13), p. 1652–61.

Vandepoele, K., Raes, J., De Veylder, L., Rouzé, P., Rombauts, S. and Inzé, D. (2002) 'Genome-Wide Analysis of Core Cell Cycle Genes in Arabidopsis', *The Plant Cell* , 14(4), p. 903–916.

Verkest, A., Manes, C.-L. de O., Vercruysse, S., Maes, S., Van Der Schueren, E., Beeckman, T., Genschik, P., Kuiper, M., Inzé, D. and De Veylder, L. (2005) 'The Cyclin-Dependent Kinase Inhibitor KRP2 Controls the Onset of the Endoreduplication Cycle during Arabidopsis Leaf Development through Inhibition of Mitotic CDKA;1 Kinase Complexes', *The Plant Cell*. American Society of Plant Biologists, 17(6), p. 1723–1736.

De Veylder, L., Beeckman, T., Beemster, G. T. S., de Almeida Engler, J., Ormenese, S., Maes, S., Naudts, M., Van Der Schueren, E., Jacqmard, A., Engler, G. and Inzé, D. (2002) 'Control of proliferation, endoreduplication and differentiation by the Arabidopsis E2Fa–DPa transcription factor', *The EMBO Journal*, 21(6), p. 1360–1368.

De Veylder, L., Beeckman, T., Beemster, G. T. S., Krols, L., Terras, F., Landrieu, I., Van Der Schueren, E., Maes, S., Naudts, M. and Inzé, D. (2001) 'Functional Analysis of Cyclin-Dependent Kinase Inhibitors of Arabidopsis', *The Plant Cell* , 13(7), p. 1653–1668.

De Veylder, L., Beeckman, T. and Inzé, D. (2007) 'The ins and outs of the plant cell cycle.', *Nature reviews. Molecular cell biology*, 8(8), p. 655–65.

Walker, J. D., Oppenheimer, D. G., Concienne, J. and Larkin, J. C. (2000) 'SIAMESE, a gene controlling the endoreduplication cell cycle in Arabidopsis thaliana trichomes', *Development*, 127(18), p. 3931 LP-3940.

Wang, G., Kong, H., Sun, Y., Zhang, X., Zhang, W., Altman, N., dePamphilis, C. W. and Ma, H. (2004) 'Genome-Wide Analysis of the Cyclin Family in Arabidopsis and Comparative Phylogenetic Analysis of Plant Cyclin-Like Proteins', *Plant Physiology*, 135(2), p. 1084 LP-1099.

Wang, H., Fowke, L. C. and Crosby, W. L. (1997) 'A plant cyclin-dependent kinase inhibitor gene', *Nature*, 386(6624), p. 451–452.

Wang, H., Qi, Q., Schorr, P., Cutler, A. J., Crosby, W. L. and Fowke, L. C. (1998) 'ICK1, a cyclin-dependent protein kinase inhibitor fromArabidopsis thalianainteracts with both Cdc2a and CycD3, and its expression is induced by abscisic acid', *The Plant Journal*. Blackwell Science Ltd, 15(4), p. 501–510.

Weinberg, R. A. (1995) 'The retinoblastoma protein and cell cycle control', *Cell*, 81(3), p. 323–330.

Weiss, D. and Ori, N. (2007) 'Mechanisms of Cross Talk between Gibberellin and Other Hormones', *Plant Physiology* , 144(3), p. 1240–1246.

Wen, C.-K. and Chang, C. (2002) 'Arabidopsis RGL1 Encodes a Negative Regulator of Gibberellin Responses', *The Plant Cell* , 14(1), p. 87–100.

Wildwater, M., Campilho, A., Perez-Perez, J. M., Heidstra, R., Blilou, I., Korthout, H., Chatterjee, J., Mariconti, L., Gruissem, W. and Scheres, B. (2006) 'The RETINOBLASTOMA-RELATED Gene Regulates Stem Cell Maintenance in Arabidopsis Roots', *Cell*. Elsevier, 123(7), p. 1337–1349.

Willige, B. C., Ghosh, S., Nill, C., Zourelidou, M., Dohmann, E. M. N., Maier, A. and Schwechheimer, C. (2007) 'The DELLA domain of GA INSENSITIVE mediates the interaction with the GA INSENSITIVE DWARF1A gibberellin receptor of Arabidopsis.', *The Plant cell*, 19(4), p. 1209–20.

Winkler, R. G. and Freeling, M. (1994) 'Physiological genetics of the dominant gibberellin-nonresponsive maize dwarfs, Dwarf8 and Dwarf9', *Planta*, 193(3), p. 341–348.

Winter, D., Vinegar, B., Nahal, H., Ammar, R., Wilson, G. V and Provart, N. J. (2007) 'An "Electronic Fluorescent Pictograph" browser for exploring and analyzing large-scale biological data sets.', *PloS one*. Public Library of Science, 2(8), p. e718.

Xie, Q., Sanz-Burgos, A. P., Hannon, G. J. and Gutiérrez, C. (1996) 'Plant cells contain a novel member of the retinoblastoma family of growth regulatory proteins.', *The EMBO journal*, 15(18), p. 4900–8.

Yabuta T., S. Y. (1938) 'On the crystal of gibberellin, a substance to promote plant growth.', *J. Agric. Chem. Soc. Japan*, (14), p. 1526.

Yamaguchi, N., Winter, C. M., Wu, M.-F., Kanno, Y., Yamaguchi, A., Seo, M. and Wagner, D. (2014) 'Gibberellin Acts Positively Then Negatively to Control Onset of Flower Formation in Arabidopsis', *Science*, 344(6184), p. 638–641.

Yamaguchi, S. (2008) 'Gibberellin metabolism and its regulation.', *Annual review of plant biology*, 59, p. 225–51.

Yoshida, H., Hirano, K., Sato, T., Mitsuda, N., Nomoto, M., Maeo, K., Koketsu, E., Mitani, R., Kawamura, M., Ishiguro, S., Tada, Y., Ohme-Takagi, M., Matsuoka, M. and Ueguchi-Tanaka, M. (2014) 'DELLA protein functions as a transcriptional activator through the DNA binding of the INDETERMINATE DOMAIN family proteins', *Proceedings of the National Academy of Sciences of the United States of America*. National Academy of Sciences, 111(21), p. 7861–7866.

Zentella, R., Zhang, Z.-L., Park, M., Thomas, S. G., Endo, A., Murase, K., Fleet, C. M., Jikumaru, Y., Nambara, E., Kamiya, Y. and Sun, T.-P. (2007) 'Global analysis of della direct targets in early gibberellin signaling in Arabidopsis.', *The Plant cell*, 19(10), p. 3037–57.

Zhang, H., Han, W., De Smet, I., Talboys, P., Loya, R., Hassan, A., Rong, H., Jürgens, G., Paul Knox, J. and Wang, M.-H. (2010) 'ABA promotes quiescence of the quiescent centre and suppresses stem cell differentiation in the Arabidopsis primary root meristem', *The Plant Journal*. Blackwell Publishing Ltd, 64(5), p. 764–774.

Zhou, Y., Wang, H., Gilmer, S., Whitwill, S. and Fowke, L. C. (2003) 'Effects of co-expressing the

plant CDK inhibitor ICK1 and D-type cyclin genes on plant growth, cell size and ploidy in Arabidopsis thaliana', *Planta*. Springer, 216(4), p. 604–613.

Appendix

Appendix

3.1.1 *GAI*, *RGA* and *RBR* transcripts are differentially expressed in the root

As well as reporting on the differential accumulation patterns of *GAI*, *RGA* and *RBR* at the protein level, microarray data also revealed differential expression of these genes at the transcript level. The eFP browser outcome for absolute *GAI* expression initially showed very low levels throughout all root zones. I noted that the absolute maximum threshold value, as calculated by the eFP browser, was high at 4026.33. Since barely any expression pattern could be visualised with this threshold, I lowered it to 600 to examine GAI levels above or below this level. The highest region of *GAI* expression was localised to the meristematic zone, followed by a region of the maturation zone, just prior to the region of lateral root primordia formation (Appendix Figure 3.1Ai). Consistent with the GAI-GFP pattern observed in my time-course analysis, absolute *GAI* expression was generally highest in the cortical cell layer of the root meristem and at the basal end i.e. closer to the root tip (Appendix Figure 3.1Ai). Interestingly, there were also high expression levels in tissues contained within the central stele of this region, such as phloem pole pericycle cells and phloem companion cells. The relative expression picturegraph for *GAI* also reflects this type of expression pattern and is more apparent (Appendix Figure 3.1Aii). Overall, high *GAI* expression was found in the meristematic zone and the maturation zone, which was localised mainly to the cortical cell layer and tissues that comprise the vasculature of the central stele. Regions of negative relative expression were within the elongation zone and a particular region of the maturation zone where lateral root primordia begin to form.

Similar to *GAI*, the eFP browser outcome for absolute *RGA* transcript levels throughout most root zones was generally low (Appendix Figure 3.1Bi). Therefore, the threshold level was also lowered to allow better visualisation for the distribution of absolute *RGA* expression in the root. In contrast to *GAI*, the region of highest *RGA* expression was localised to the beginning of the elongation zone, followed by the meristematic zone and a specific region of the maturation zone, prior to the region of lateral root primordia formation (Appendix Figure 3.1Bi). These findings were generally consistent with the observations made from the time-course analysis that demonstrated little variation of RGA-GFP accumulation between the meristematic and elongation zone (Figure 3.4ii). However, transcript levels for *RGA* do appear to vary slightly between these regions, specifically at the transition zone where *RGA* levels decrease, prior to a subsequent increase in the elongation zone (Appendix Figure 3.1Bi). Furthermore, *RGA* was found to be differentially expressed in a tissue-specific manner, which was less clear at the protein level. *RGA* transcript levels were generally highest in the cortical cell layer and in the phloem companion cells contained within the vasculature throughout most regions of the

Appendix Figure 3.1 Differential expression of *GAI*, *RGA* and *RBR* transcript levels in the root

High-resolution spatio-temporal maps of (i) *GAI* (AT1G14920), (ii) *RGA* (AT2G01570) and (iii) *RBR* (AT3G12280) expression in the root, respectively. For each gene, two pictographs are portrayed as:

(A) Absolute expression
(B) Relative expression.

Images were generated using the eFP browser, based on microarray results from from Brady et al. 2007. Regions of high absolute expression are coloured from red to orange (red being highest), whilst regions of low expression are coloured in yellow. Similarly, regions of high relative expression are coloured red. Regions of negative relative expression are coloured in blue/green.

A (i)


Vasculature
Pericyle
Endodermis
Cortex
Epidermis
Xylem pole pericycle
Phloem pole pericycle
Phloem companion
Proto & metaphloem
Phloem companion
Procambium
Xylem
Old 7-12
Young 1-6
Proto & Meta Phloem
Lateral Root Primordium
MATURATION ZONE
ELONGATION ZONE
MERISTEMATIC ZONE
12
11
10
9
8
7
6
5
4
3
2
1
Columella
Absolute
> 600.0
540.0
480.0
420.0
360.0
300.0
240.0
180.0
120.0
60.0
0.0
Masked

B (i)

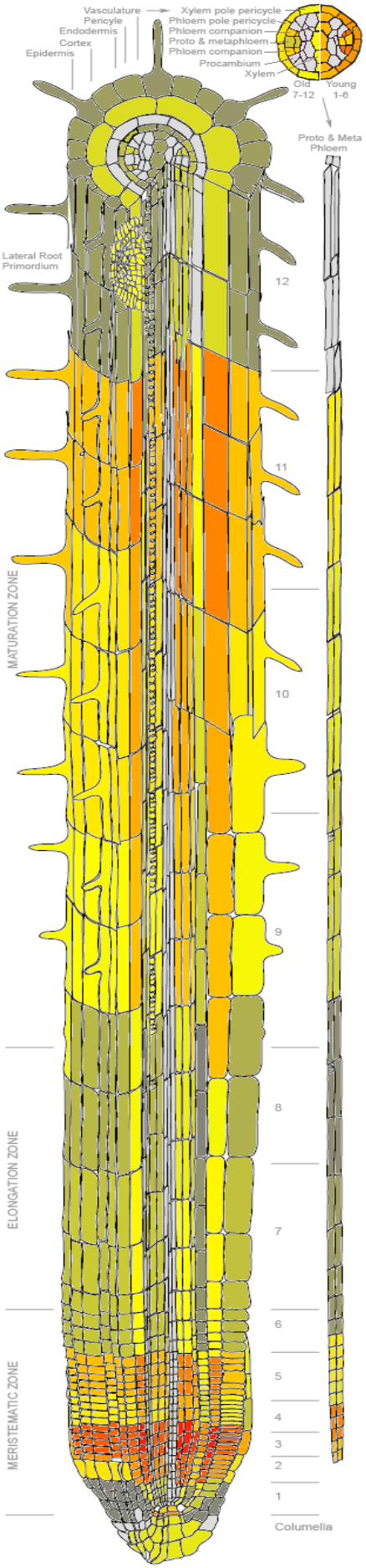
Vasculature
Pericyle
Endodermis
Cortex
Epidermis
Xylem pole pericycle
Phloem pole pericycle
Phloem companion
Proto & metaphloem
Phloem companion
Procambium
Xylem
Old 7-12
Young 1-6
Proto & Meta Phloem
Lateral Root Primordium
MATURATION ZONE
ELONGATION ZONE
MERISTEMATIC ZONE
12
11
10
9
8
7
6
5
4
3
2
1
Columella
Log2 Ratio
3.58 (11.9-Fold)
2.86
2.14
1.43
0.71
-0.01
-0.72
-1.44
-2.15
-2.87
-3.58
Masked

A (ii)

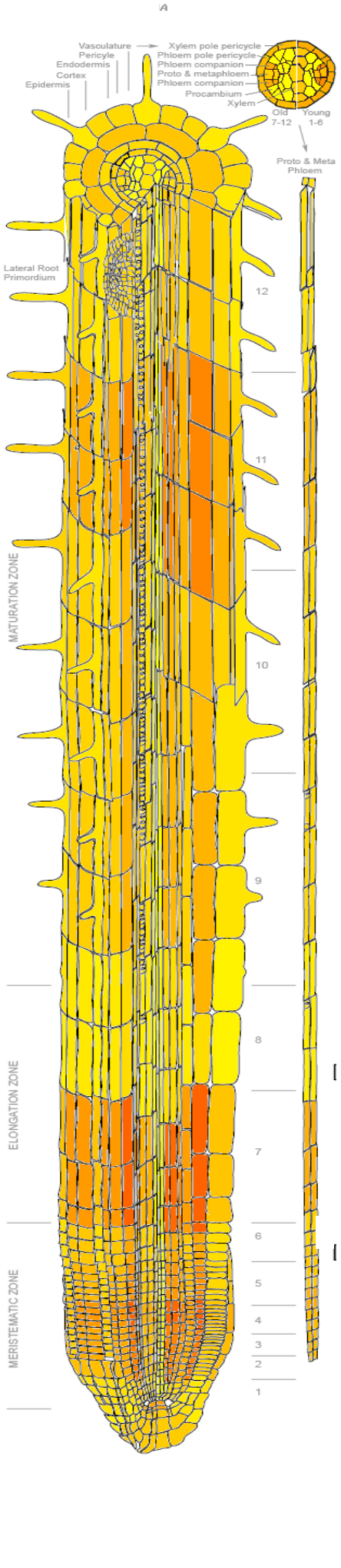
Vasculature
Pericyle
Endodermis
Cortex
Epidermis
Xylem pole pericycle
Phloem pole pericycle
Phloem companion
Proto & metaphloem
Phloem companion
Procambium
Xylem
Old 7-12
Young 1-6
Proto & Meta Phloem
Lateral Root Primordium
MATURATION ZONE
ELONGATION ZONE
MERISTEMATIC ZONE
12
11
10
9
8
7
6
5
4
3
2
1
Absolute
> 600.0
540.0
480.0
420.0
360.0
300.0
240.0
180.0
120.0
60.0
0.0
Masked

B (ii)


Vasculature
Pericyle
Endodermis
Cortex
Epidermis
Xylem pole pericycle
Phloem pole pericycle
Phloem companion
Proto & metaphloem
Phloem companion
Procambium
Xylem
Old 7-12
Young 1-6
Proto & Meta Phloem
Lateral Root Primordium
MATURATION ZONE
ELONGATION ZONE
MERISTEMATIC ZONE
12
11
10
9
8
7
6
5
4
3
2
1
Columella
Log2 Ratio
2.15 (4.4-Fold)
1.72
1.29
0.86
0.43
0.0
-0.43
-0.86
-1.29
-1.72
-2.15
Masked

A (iii)

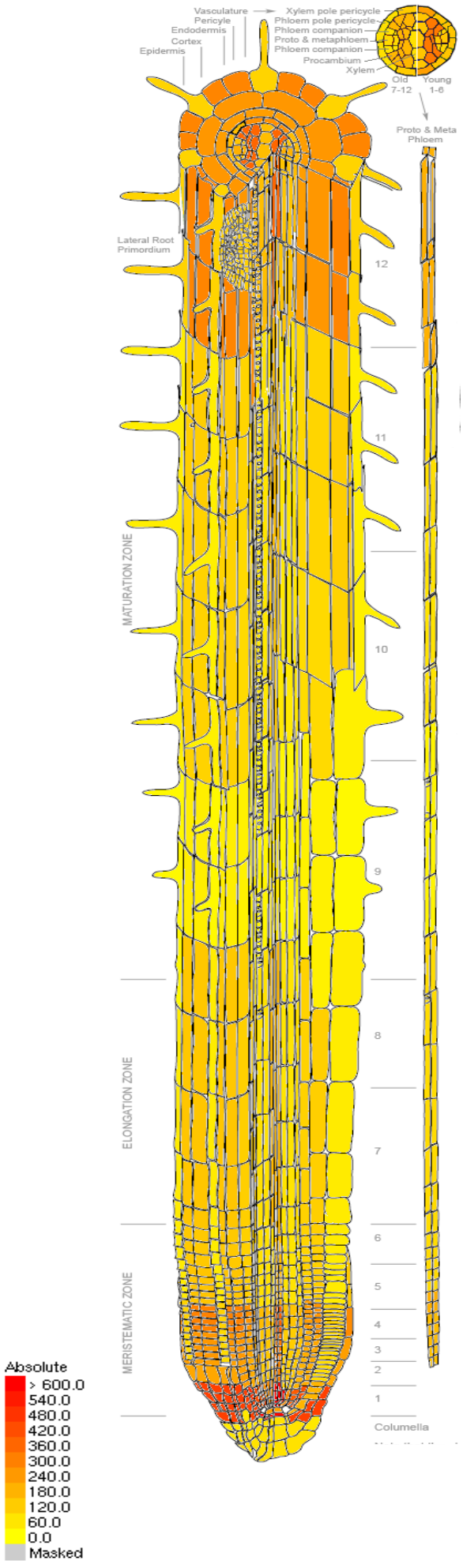
Vasculature
Pericyle
Endodermis
Cortex
Epidermis
Xylem pole pericycle
Phloem pole pericycle
Phloem companion
Proto & metaphloem
Phloem companion
Procambium
Xylem
Old 7-12
Young 1-6
Proto & Meta Phloem
Lateral Root Primordium
MATURATION ZONE
ELONGATION ZONE
MERISTEMATIC ZONE
12
11
10
9
8
7
6
5
4
3
2
1
Columella
Absolute
> 600.0
540.0
480.0
420.0
360.0
300.0
240.0
180.0
120.0
60.0
0.0
Masked

B (iii)

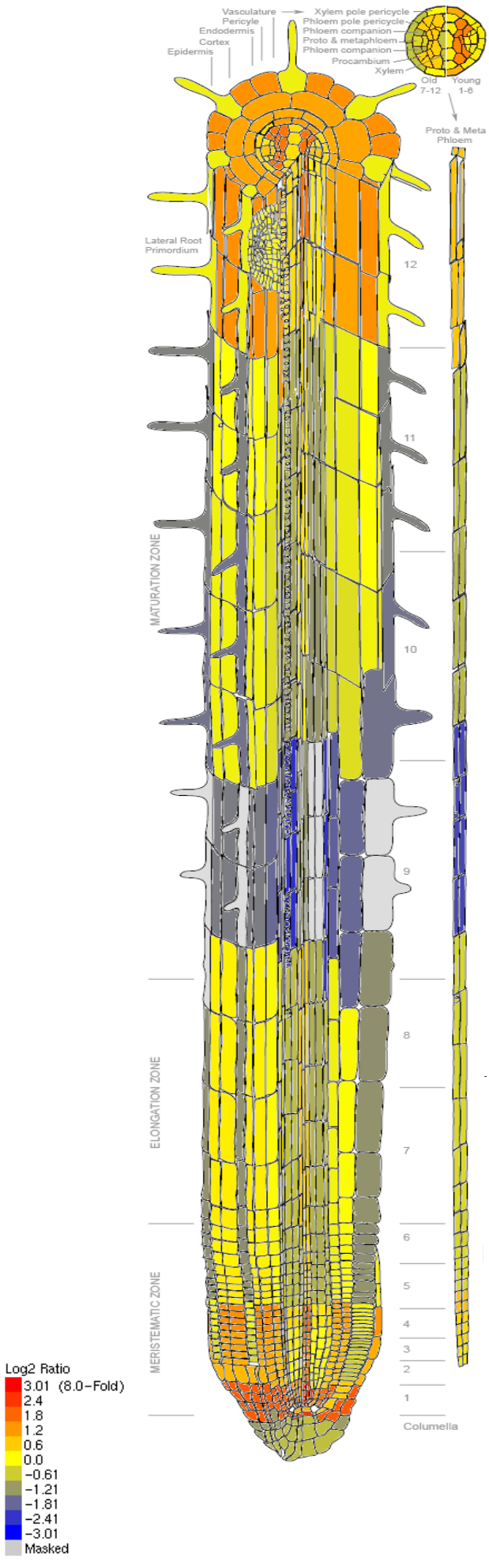
Vasculature
Pericyle
Endodermis
Cortex
Epidermis
Xylem pole pericycle
Phloem pole pericycle
Phloem companion
Proto & metaphloem
Phloem companion
Procambium
Xylem
Old 7-12
Young 1-6
Proto & Meta Phloem
Lateral Root Primordium
MATURATION ZONE
ELONGATION ZONE
MERISTEMATIC ZONE
12
11
10
9
8
7
6
5
4
3
2
1
Columella
Log2 Ratio
3.01 (8.0-Fold)
2.4
1.8
1.2
0.6
0.0
-0.61
-1.21
-1.81
-2.41
-3.01
Masked

primary root, including the meristematic, elongation and maturation zone. There was one particular region in the elongation zone, just after the region of highest expression, where all cells had low *RGA* expression levels and this was also not seen at the protein level, although the whole of the root was not completely imaged during the time-course experiment. This type of expression pattern was reflected and more apparent when examining the relative expression of *RGA*. Clearly, the elongation zone was the region of highest relative expression, followed by the meristematic and the maturation zone (Appendix Figure 3.1Bii). In the meristem, the highest region of relative expression was in the cortical cell layer and the central region of the proximal meristem. Regions of negative relative expression were localised to cells in and around the stem cell niche situated at the root tip, the elongation zone just after the region of highest expression and in elongating cells of the maturation zone where root primordia begin to form, particularly in root hair cells (Appendix Figure 3.1Bii).

The Arabidopsis eFP browser outcome for absolute expression of *RBR* in the root was generally consistent with observations made from my time-course analysis. For example, the region of highest RBR expression was found mostly in the meristematic zone and increased closer to the root tip (Figure 3.1Aiii). Highest RBR expression in this region was concentrated around the stem cell niche particularly in endodermal and cortical cells, as well as procambium cells within the vasculature.

Interestingly, there was a previously unidentified region of high *RBR* expression within the maturation zone where lateral root primordia begin to form. This contrasts with the eFP outcomes for expression levels of *GAI* and *RGA* where very low absolute values and negative relative values were found in this region for both genes. Absolute *RBR* expression levels throughout this region were highest in non-root hair cells of the epidermis, cells within the cortex, endodermis, pericycle and tissues that constitute the vasculature. Conversely, *RBR* levels in epidermal root hair cells of this region were low. In fact, these cell types tended to have very low RBR expression levels throughout all regions of the root. The relative expression picturegraph of RBR in the root exemplified this type of expression pattern (Appendix Figure 3.6b). This observation is similar to that of the expression pattern found for *RGA*, but not for *GAI*. Furthermore, there was also region of negative relative expression at the beginning of the maturation zone, which was less visible in the picturegraph for absolute RBR expression (Appendix Figure 3.1Biii).

3.1.2 Comparative analysis of *GAI* and *RGA* with *RBR* transcript levels reveals differential regions of expression in the root

Another feature of the eFP browser is to allow the user to compare the transcriptional expression of one gene with reference to another. This is useful for determining regions where one gene is expressed more abundantly in relation to the other. As a result, I decided to use this browser to

Appendix Figure 3.2: Comparative transcriptional expression of *GAI* and *RGA* with *RBR* in the root

High-resolution spatio-temporal maps of (i) *GAI* (AT1G14920) and (ii) *RGA* (AT2G01570) relative to *RBR* (AT3G12280) expression in the root. For each gene comparison, the relative expression values are portrayed as a pictograph. Images were generated using the eFP browser, based on microarray results from from Brady et al. 2007. Regions of high *GAI/RGA* expression relative to *RBR* are coloured red. Regions of high *RBR* expression relative to *GAI/RGA* are coloured in blue.

(i)


Vasculature
Pericyle
Endodermis
Cortex
Epidermis
Xylem pole pericycle
Phloem pole pericycle
Phloem companion
Proto & metaphloem
Phloem companion
Procambium
Xylem
Old 7-12
Young 1-6
Proto & Meta Phloem
Lateral Root Primordium
MATURATION ZONE
ELONGATION ZONE
MERISTEMATIC ZONE
12
11
10
9
8
7
6
5
4
3
2
1
Columella
Log2 Ratio
3.39 (10.4-Fold)
2.71
2.03
1.35
0.67
0.0
-0.68
-1.36
-2.04
-2.72
-3.39
Masked

(ii)


Vasculature
Pericyle
Endodermis
Cortex
Epidermis
Xylem pole pericycle
Phloem pole pericycle
Phloem companion
Proto & metaphloem
Phloem companion
Procambium
Xylem
Old 7-12
Young 1-6
Proto & Meta Phloem
Lateral Root Primordium
MATURATION ZONE
ELONGATION ZONE
MERISTEMATIC ZONE
12
11
10
9
8
7
6
5
4
3
2
1
Columella
Log2 Ratio
2.93 (7.6-Fold)
2.34
1.75
1.17
0.58
0.0
-0.59
-1.18
-1.76
-2.35
-2.93
Masked

compare the expression patterns of *GAI* and *RGA* relative to that of *RBR* to determine these regions. In the case of *GAI* relative to *RBR*, the highest regions of *GAI* expression were located in the meristematic region and throughout the maturation zone, apart from the region where lateral root primordia form (Appendix Figure 3.2i). In the meristematic region, highest *GAI* expression was localised to the cortical and epidermal cell layers and phloem companion cells within the vasculature. This type of expression pattern was also found in the maturation zone. Interestingly, the cells that form root hairs had higher *GAI* expression than non-root hair cells, which was consistent between the regions of the meristematic and maturation zones. This finding is reflective of the expression pattern of *RBR* alone because cells that form root hairs tended to have lower expression values throughout all regions of the root, whereas *GAI* expression didn't vary between these cell types. Regions of high *RBR* expression relative to *GAI* were located in cells in and around the stem cell niche of the meristematic zone and the maturation zone where root primordia begin to form (Appendix Figure 3.2i). This observation is consistent with the fact that *RBR* expression alone was highest in these regions, whereas *GAI* expression levels were found to be very low and were higher in the proximal region of the meristem.

The expression pattern of *RGA* compared with *RBR* appear to be similar to that of *GAI* compared with *RBR*, although *RGA* expression is lower in the meristematic zone when compared to *GAI* (Appendix Figure 3.2ii). The region of highest *RGA* expression is situated at the beginning of the maturation zone in the epidermal, cortical, endodermal cell layers and phloem cells contained within the vasculature (Appendix Figure 3.2ii). Unlike in the case of *GAI* expression, there was also a region of high *RGA* expression relative to *RBR* at the beginning of the elongation zone, particularly in phloem companion cells of the vasculature (Appendix Figure 3.2ii). This was also reflected in the expression pattern of *RGA* alone where the highest absolute and relative transcriptional values were specific to this region (Appendix Figure 3.1iii). Similar to that of *GAI*, the expression of *RGA* relative to *RBR* was higher in root hair cells of the epidermal cell layer throughout most regions of the root (Appendix Figure 3.2ii). Furthermore, regions of high *RBR* expression relative to *RGA* were located in cells in and around the stem cell niche of the meristematic zone and the maturation zone where root primordia begin to form.

Appendix Figure 4.1 Residual plots for assessing the fit of the statistical model

(A) Root growth of WT, *rga-28* and *gai-td1* seedlings
(B) Root growth of WT, *ga1-t*, *rga-28* and *gai-td1* seedlings

A

Residual plots - Root Growth WT, *gai-td1* and *rga-28*

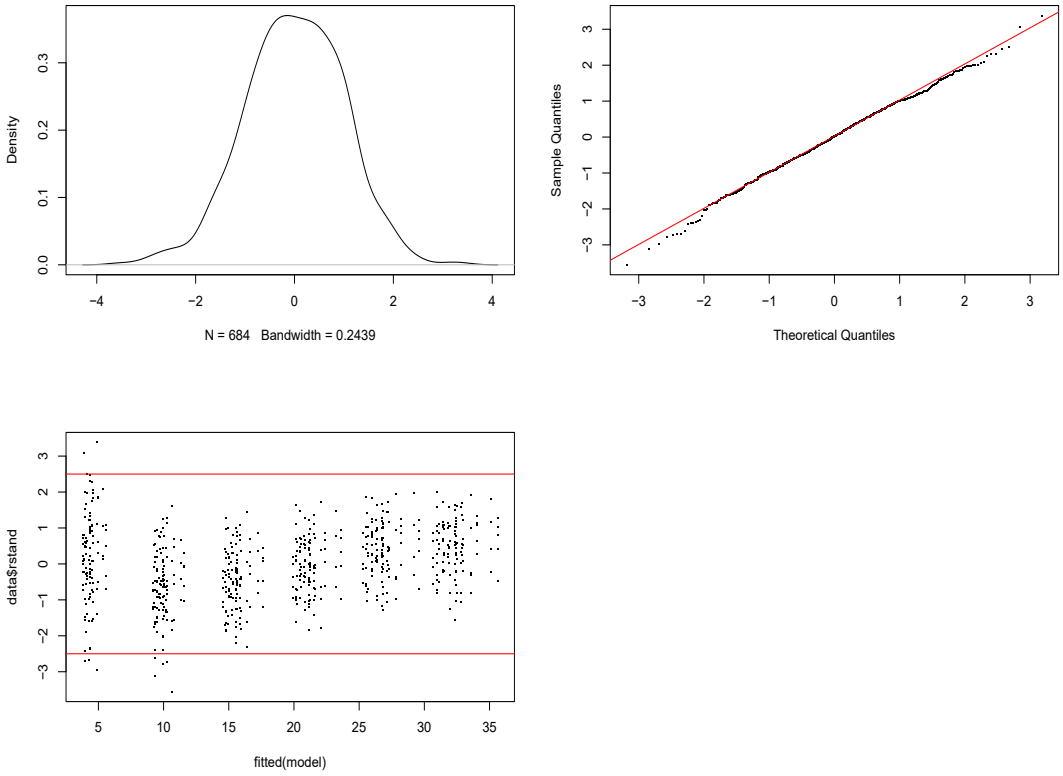

B

Residual plots - Root Growth WT, *ga1-t*, *gai-td1* and *rga-28*

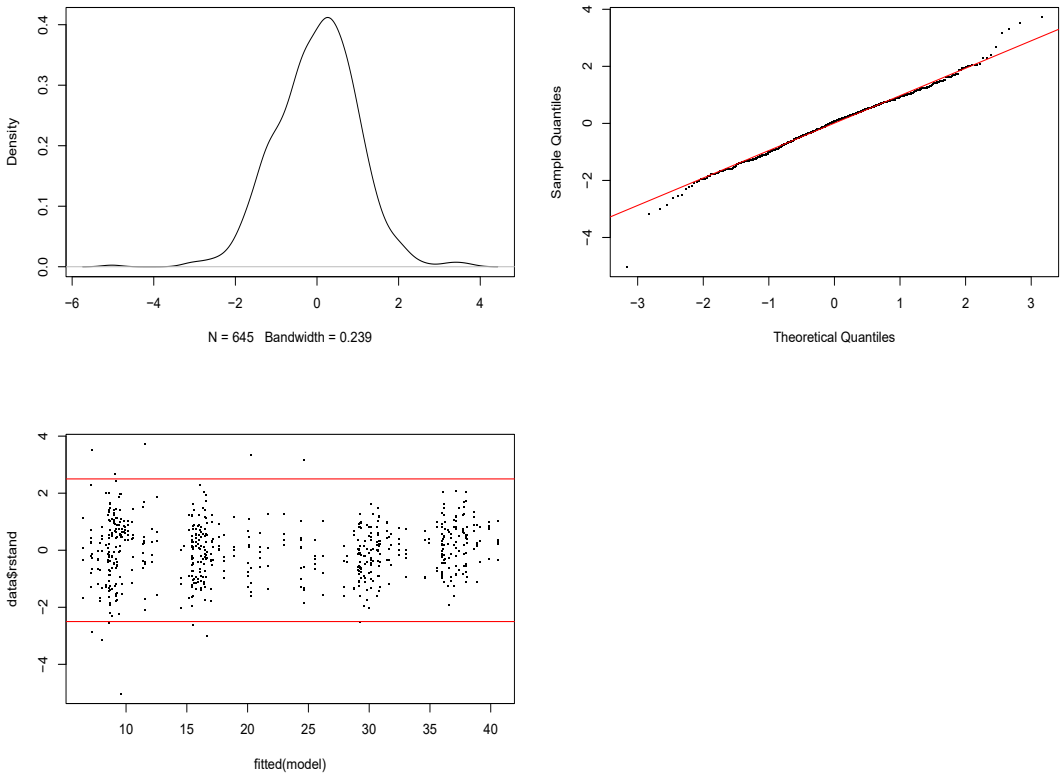

Appendix Figure 4.2 Residual plots for assessing the fit of the statistical model for analysis of WT, *ga1-t*, *ga1-t rga-28* and *ga1-t gai-td1* seedlings for the following dependent variable

(A) Root growth
(B) Meristem length
(C) Cortical cell number
(D) Cell production rate

A

Residual plots - Root growth

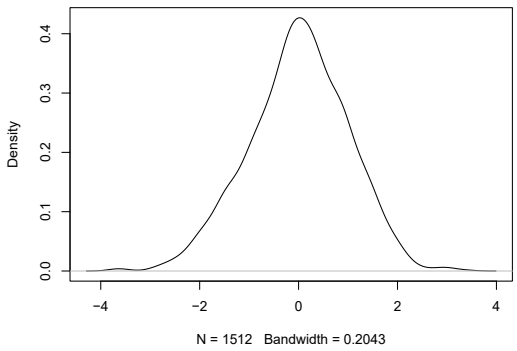

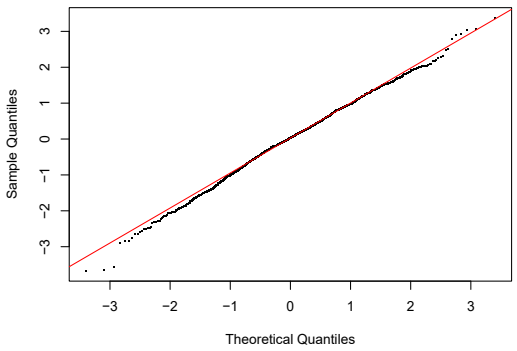

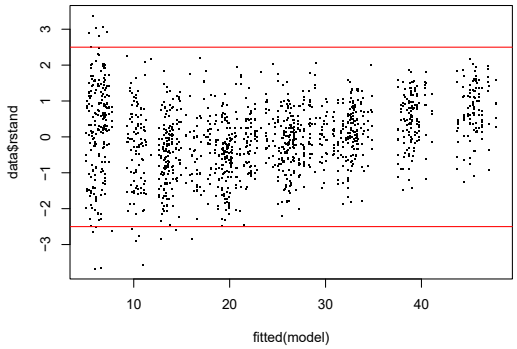

B

Residual plots - Meristem Length

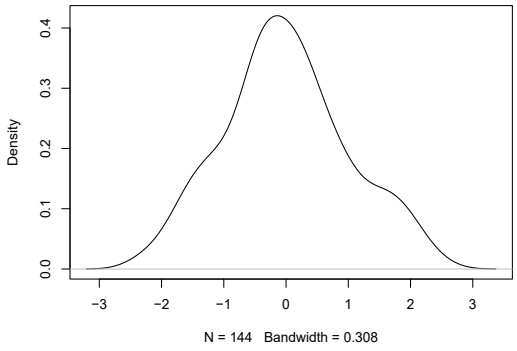

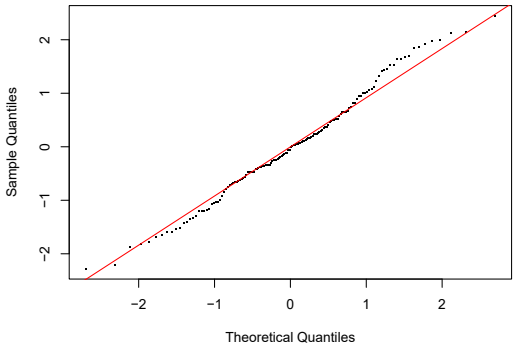

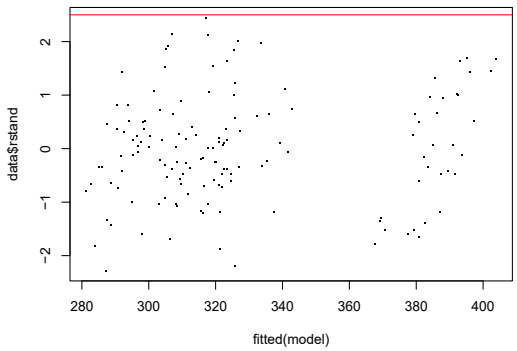

C

Residual plots - Cortical Cell Number

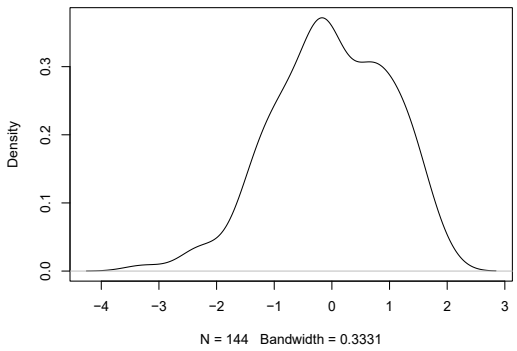

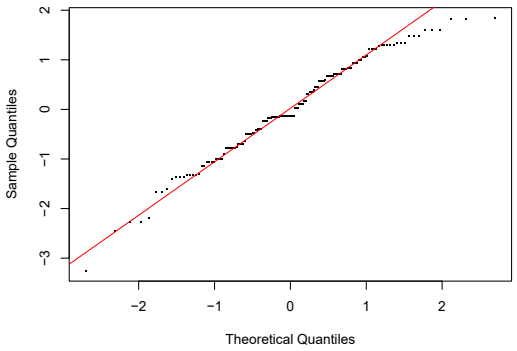

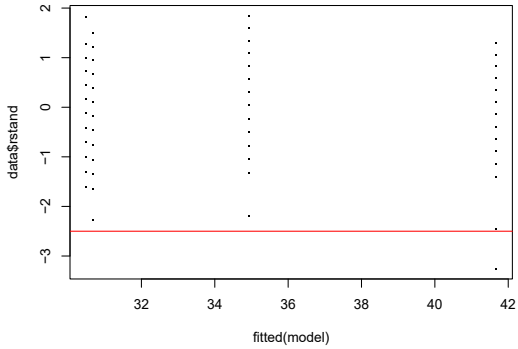

D

Residual plots - Cell Production Rate

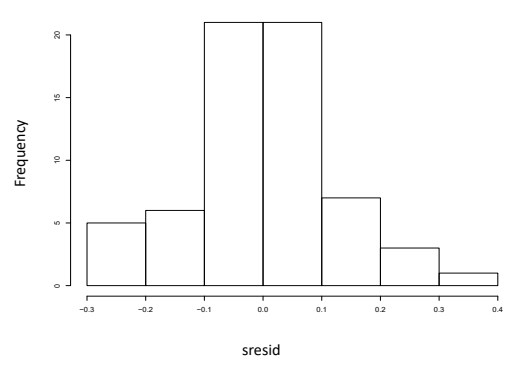

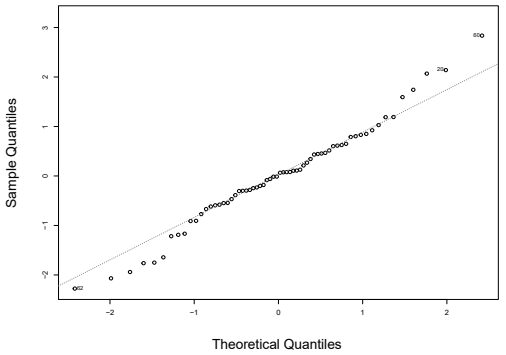

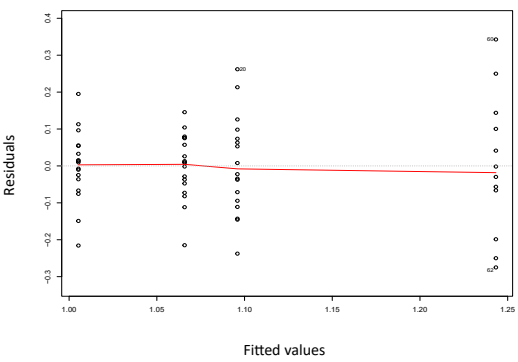

Appendix Figure 4.3 Residual plots for assessing the fit of the statistical model for analysis of WT, *gai-td1*, *rga-28*, pRBR::RBR-GFP, pRBR::RBR-GFP *gai-td1* and pRBR::RBR-GFP rga-28 seedlings for the following dependent variables

(A) Root growth between all genotypes under the control treatment
(B) Root growth between genotypes under GA treatment
(C) Root growth between genotypes under PAC treatment
(D) Root growth of WT seedlings between treatments
(E) Root growth of *gai-td1* seedlings between treatments
(F) Root growth of *rga-28* seedlings between treatments
(G) Root growth of pRBR::RBR-GFP seedlings between treatments
(H) Root growth of pRBR::RBR-GFP *gai-td1* seedlings between treatments
(I) Root growth of pRBR::RBR-GFP *rga-28* seedlings between treatments

A

Residual plots - C

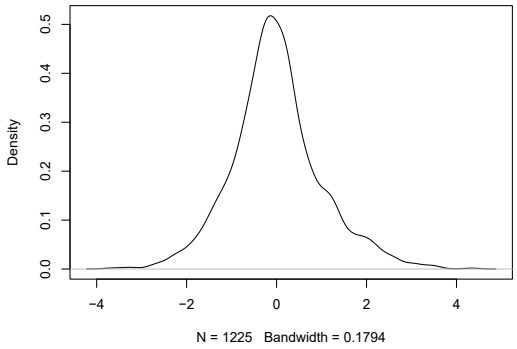

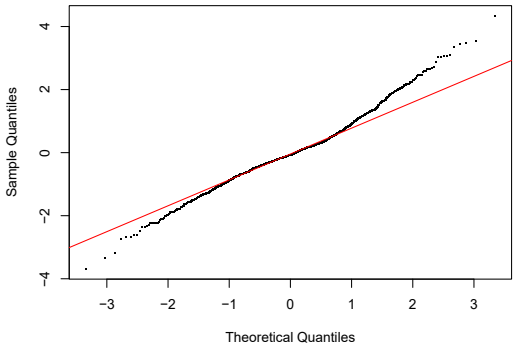

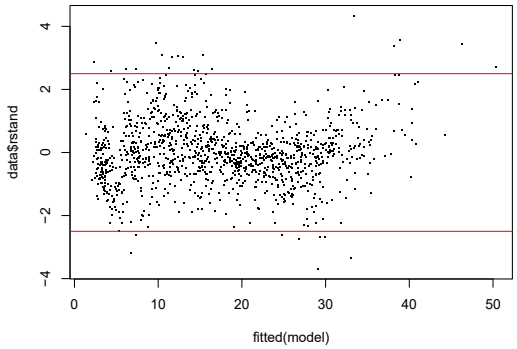

B

Residual plots - GA

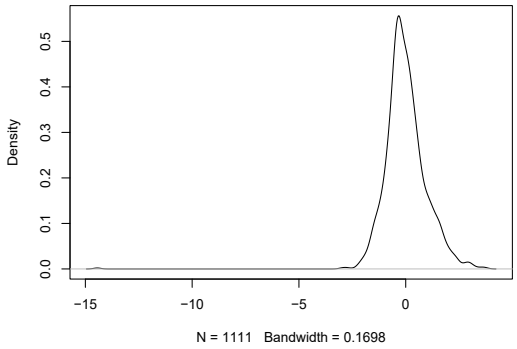

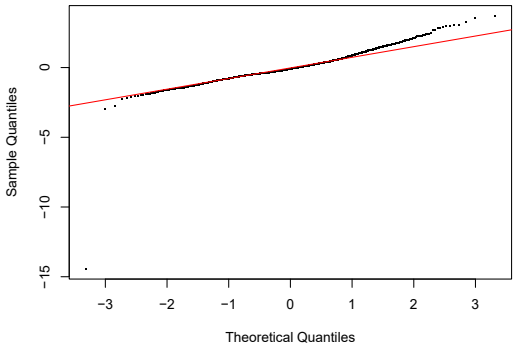

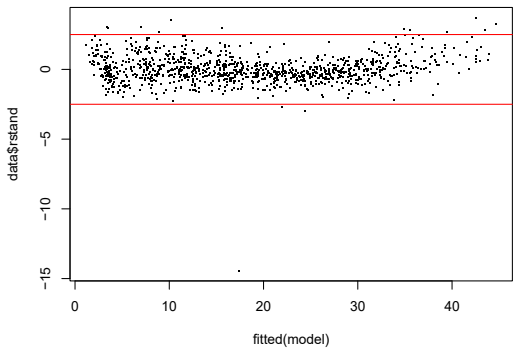

C

Residual plots - PAC

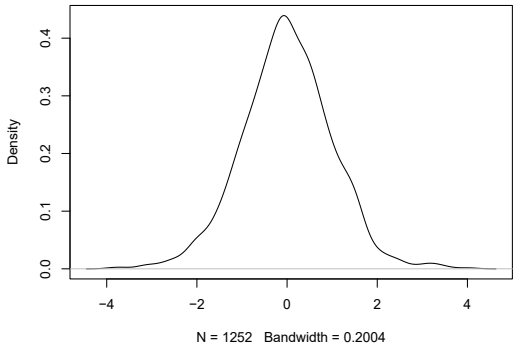

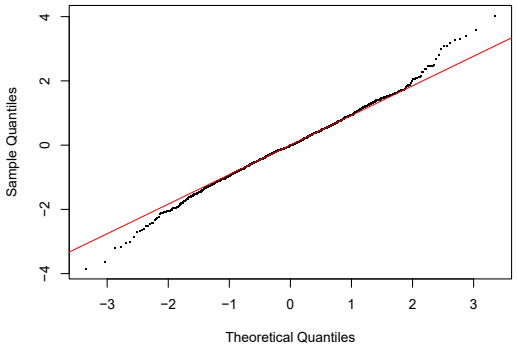

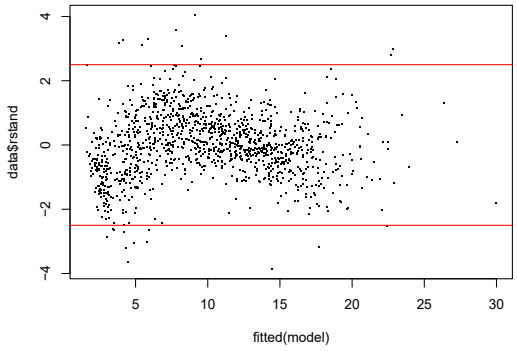

D

Residual plots - WT

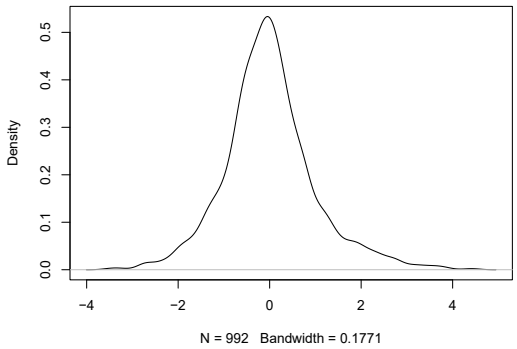

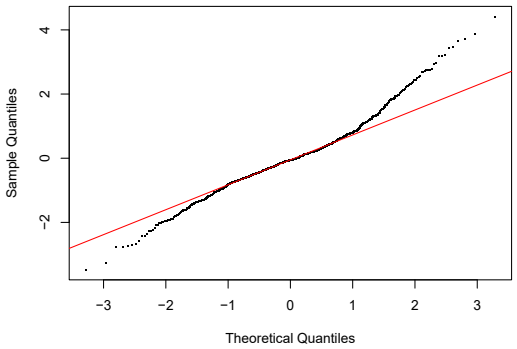

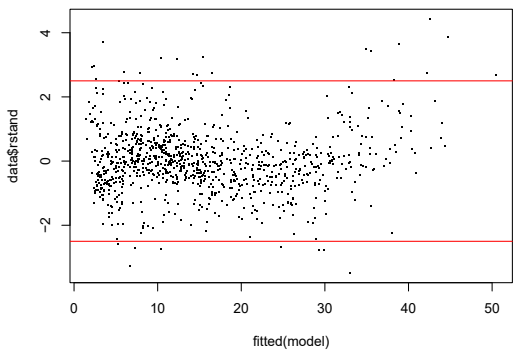

E

Residual plots - *gai-td1*

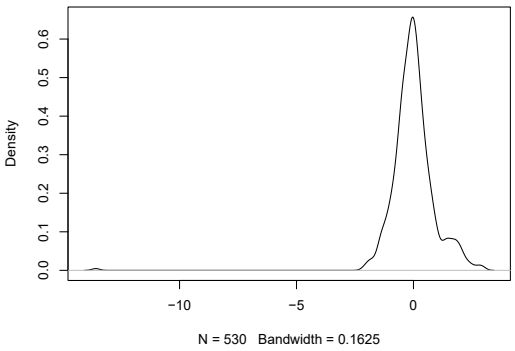

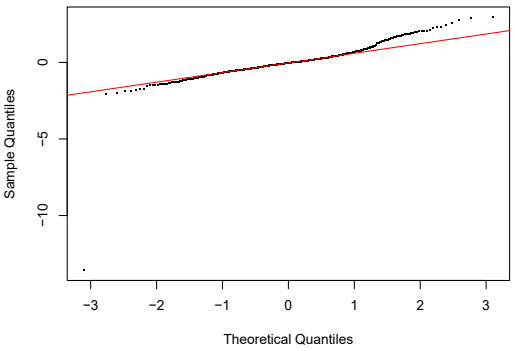

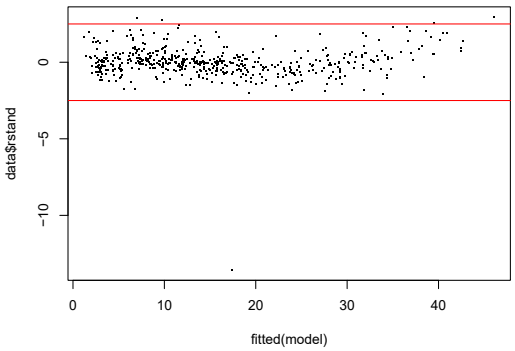

F

Residual plots - *rga-28*

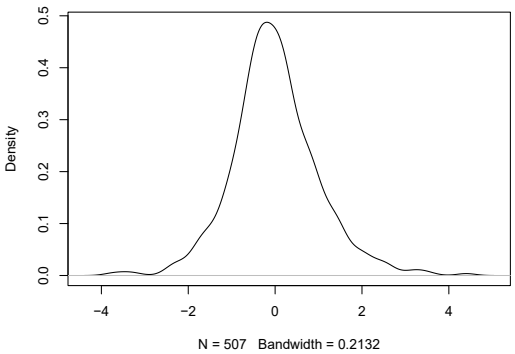

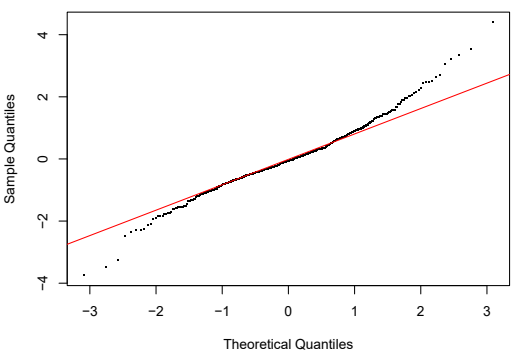

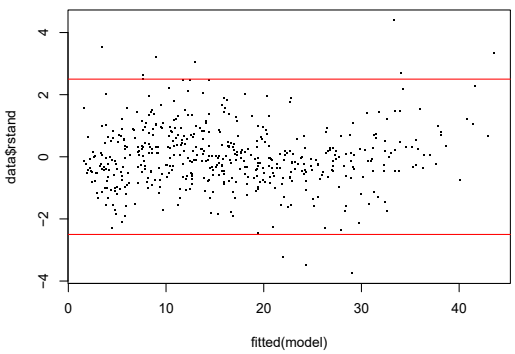

G

Residual plots - RBR-GFP

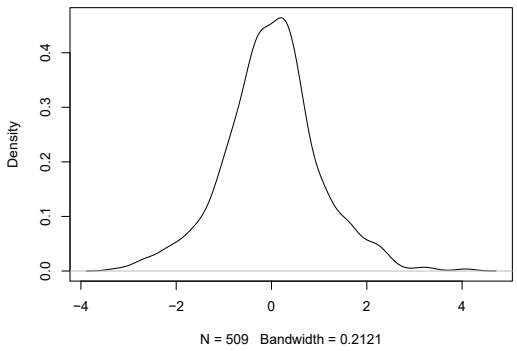

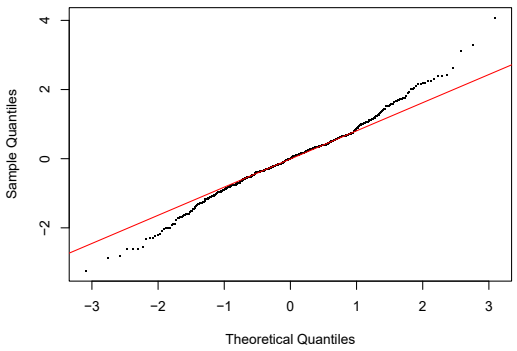

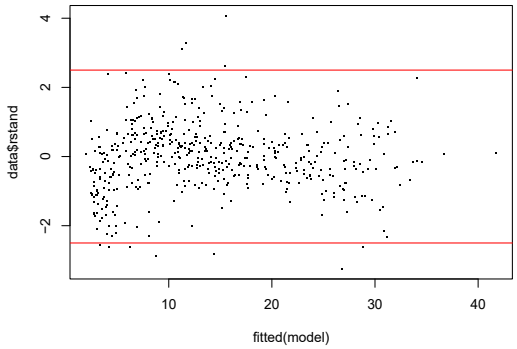

H

Residual plots - RBR-GFP *gai-td1*

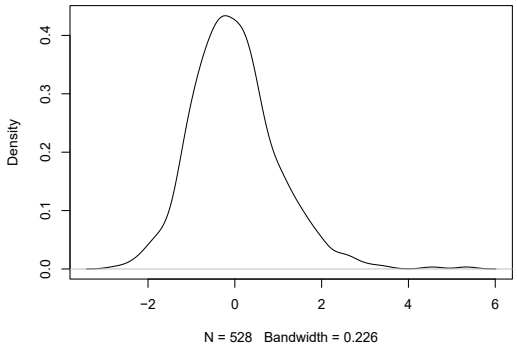

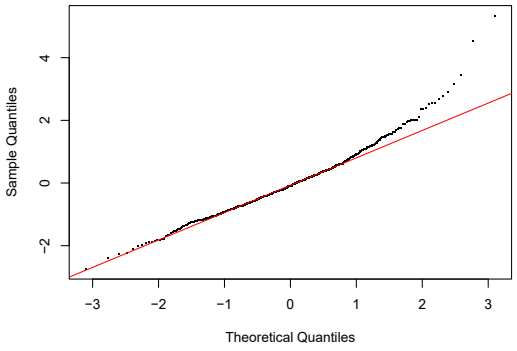

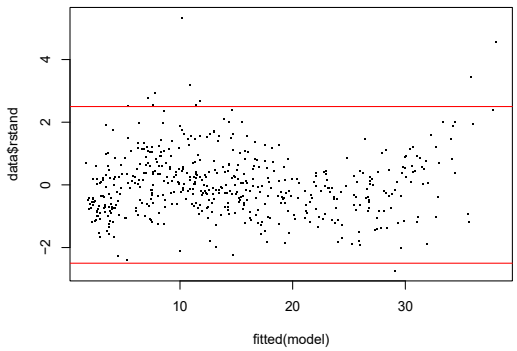

I

Residual plots - RBR-GFP *rga-28*

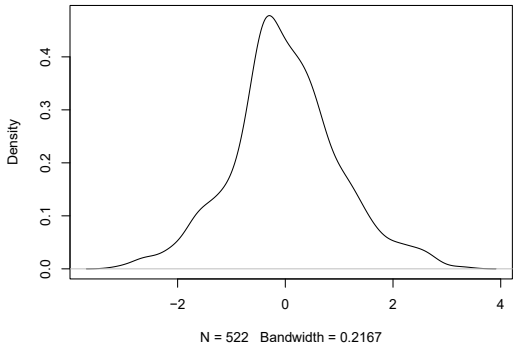

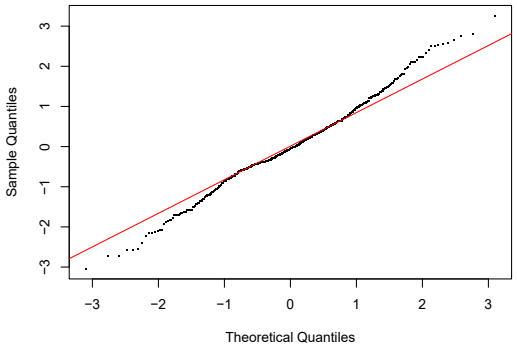

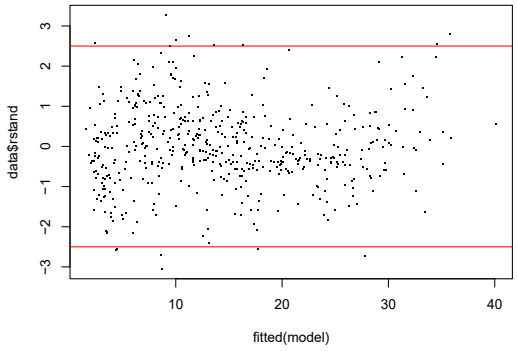

Appendix Figure 4.4 Residual plots for assessing the fit of the statistical model for analysis of WT, 35S::KRP2-GFP, 35S::KRP2-GFP *gai-td1* and 35S::KRP2-GFP *rga-28* seedlings for the following dependent variables

(A) Root growth between genotypes under control treatment
(B) Root growth between genotypes under GA treatment
(C) Root growth between genotypes under PAC treatment
(D) Root growth for WT seedlings between treatments
(E) Root growth for 35S::KRP2-GFP seedlings between treatments
(F) Root growth for 35S::KRP2-GFP *gai-td1* seedlings between treatments
(G) Root growth for 35S::KRP2-GFP *rga-28* seedlings between treatments

A

Residual plots - C

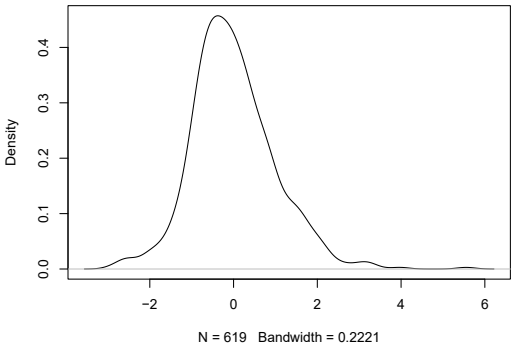

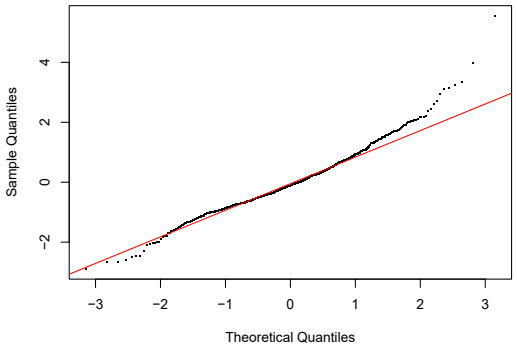

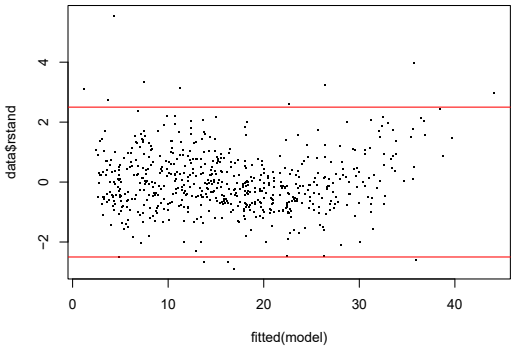

B

Residual plots - GA

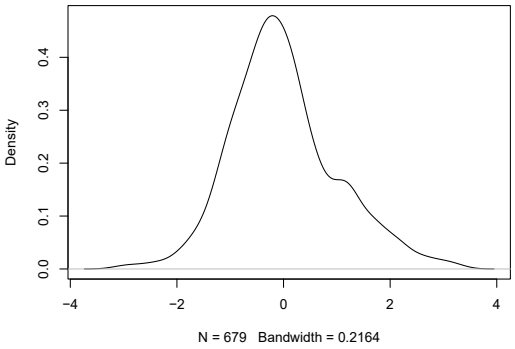

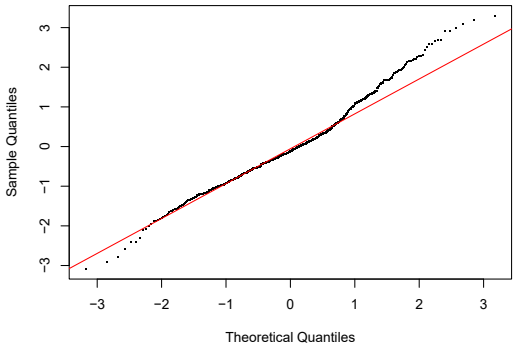

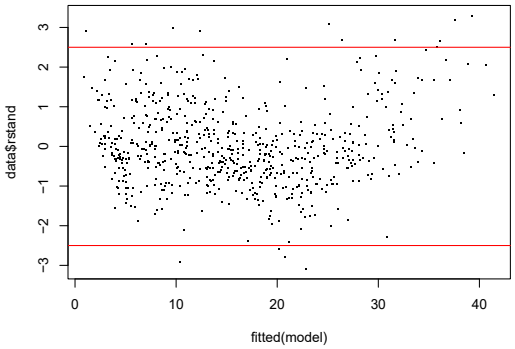

C

Residual plots - PAC

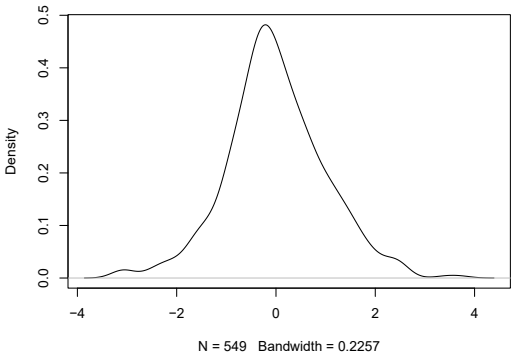

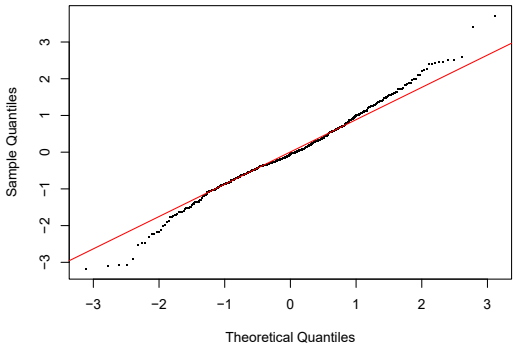

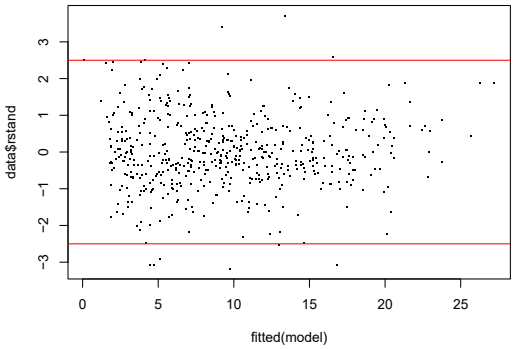

D

Residual plots - WT

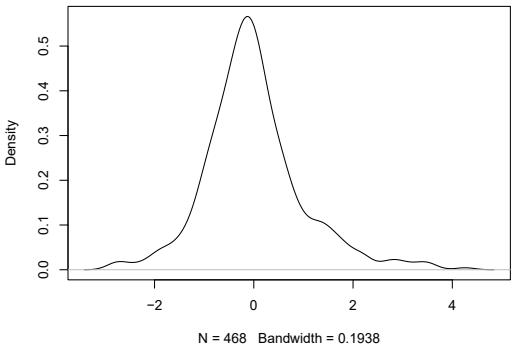

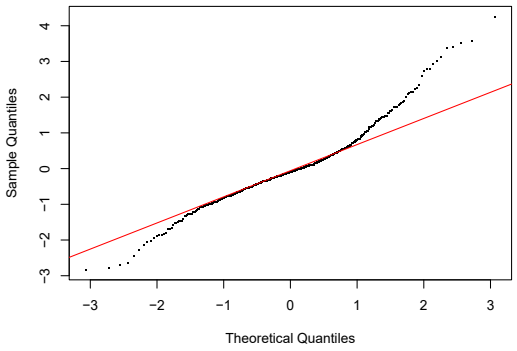

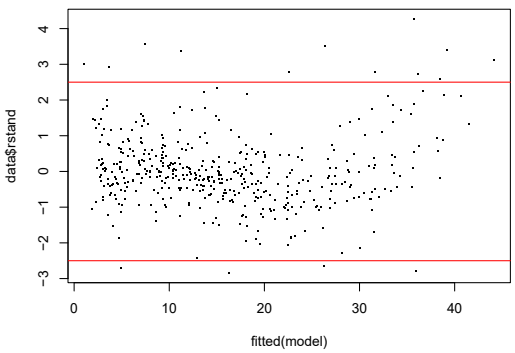

E

Residual plots - 35SKRP2-GFP

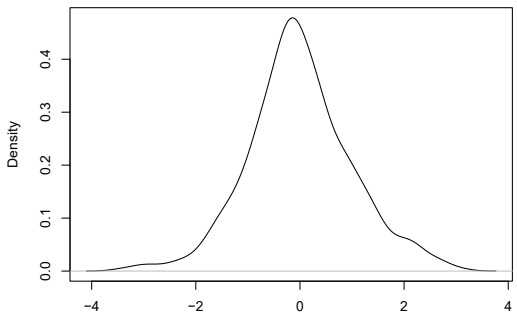

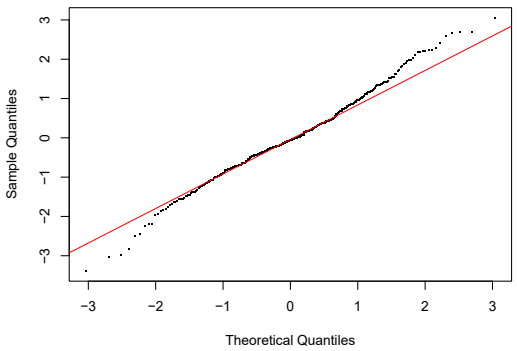

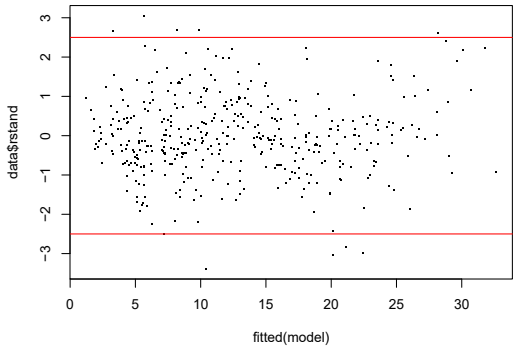

F

Residual plots - 35SKRP2-GFP *gai-td1*

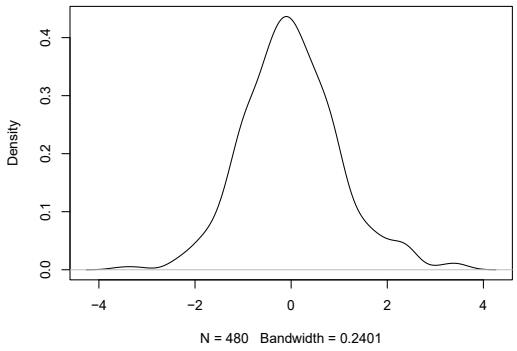

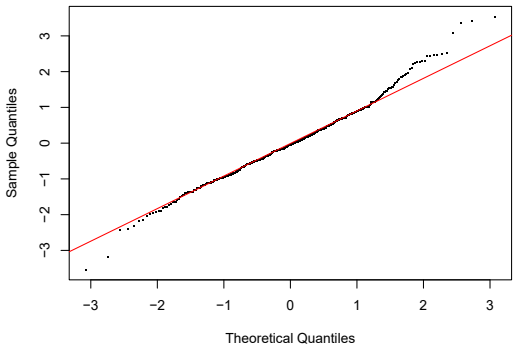

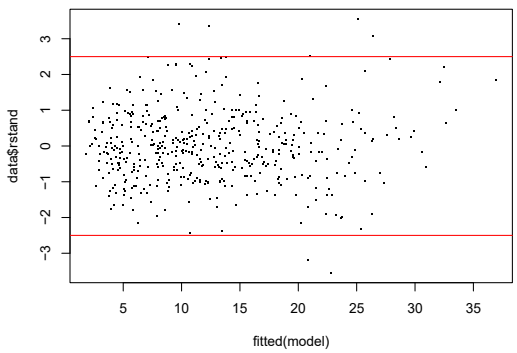

G

Residual plots - 35SKRP2-GFP *rga-28*

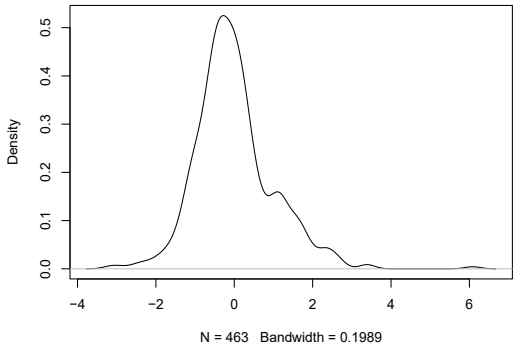

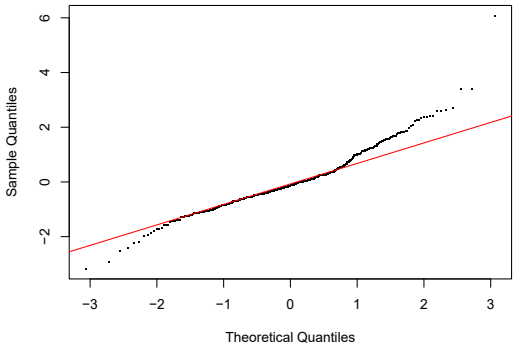

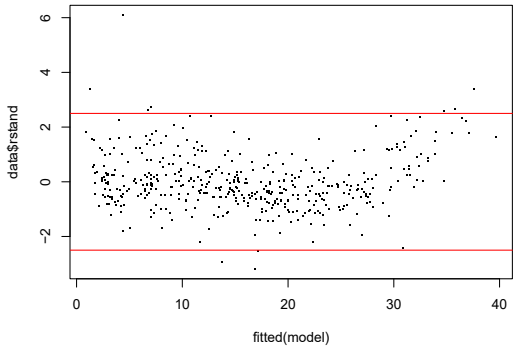

Appendix Figure 4.5 Residual plots for assessing the fit of the statistical model for analysis of the repeated experiment for WT, 35S::KRP2-GFP, 35S::KRP2-GFP *gai-td1* and 35S::KRP2-GFP *rga-28* seedlings for the following dependent variables

(A) Root growth between genotypes under control treatment
(B) Root growth between genotypes under GA treatment
(C) Root growth between genotypes under PAC treatment
(D) Root growth for 35S::KRP2-GFP seedlings between treatments
(E) Root growth for 35S::KRP2-GFP *gai-td1* seedlings between treatments
(F) Root growth for 35S::KRP2-GFP *rga-28* seedlings between treatments

Root growth for WT seedlings between treatments was the same as Appendix 4.3D

A

Residual plots - C

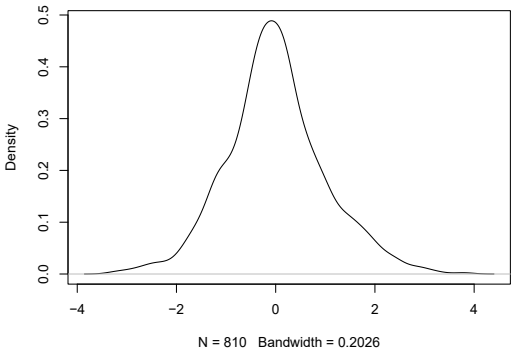

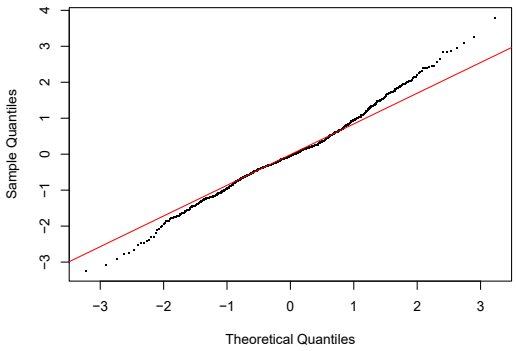

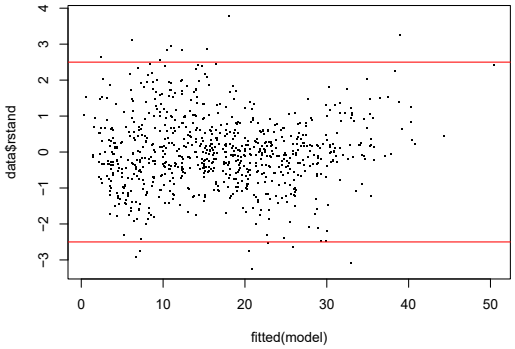

B

Residual plots - GA

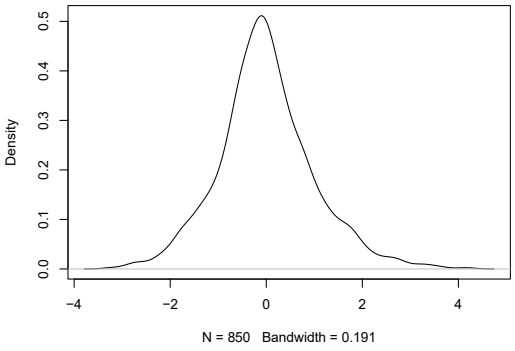

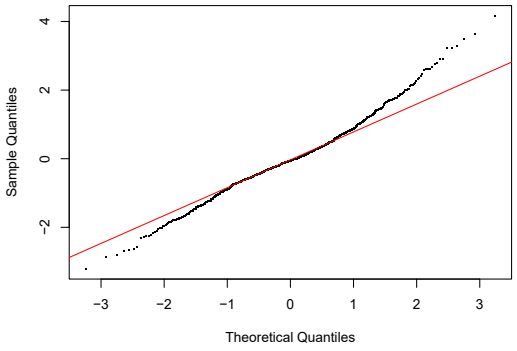

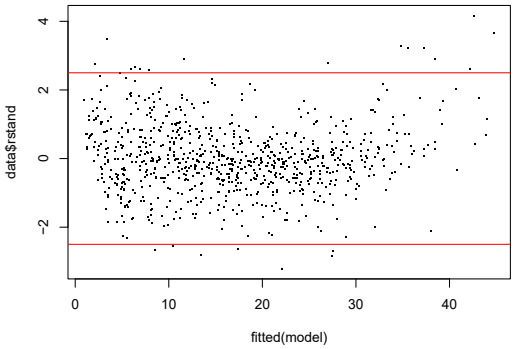

C

Residual plots - PAC

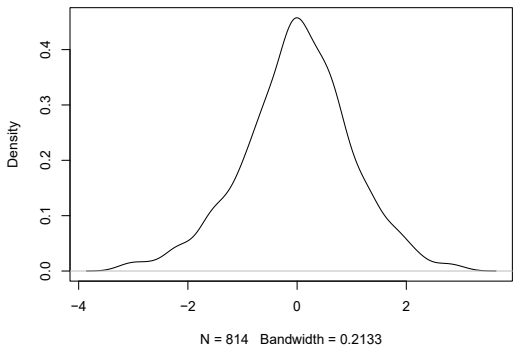

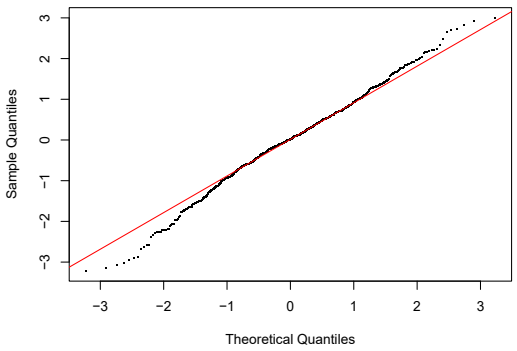

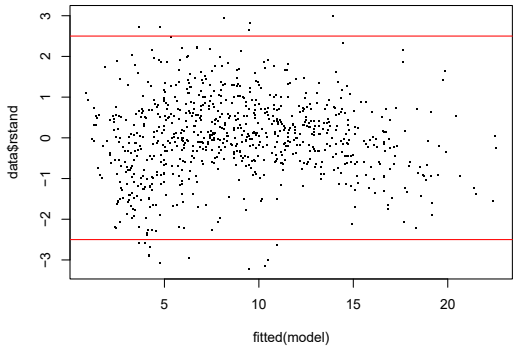

D

Residual plots - 35SKRP2-GFP

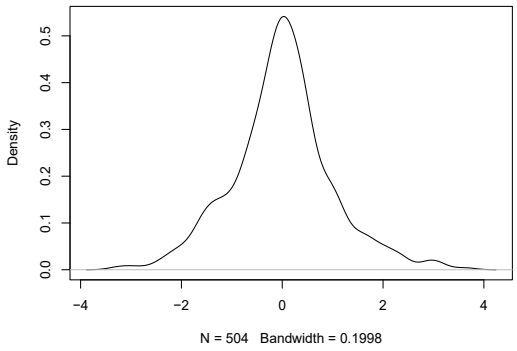

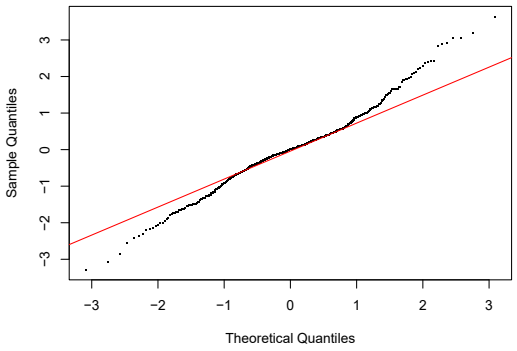

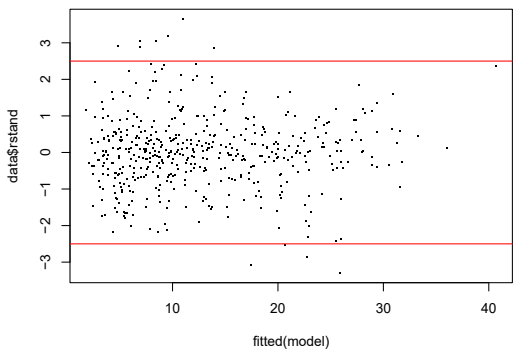

E

Residual plots - 35SKRP2-GFP *gai-td1*

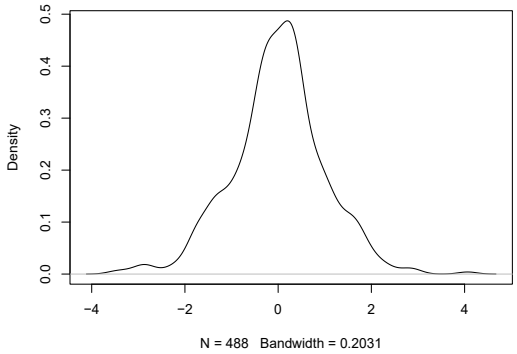

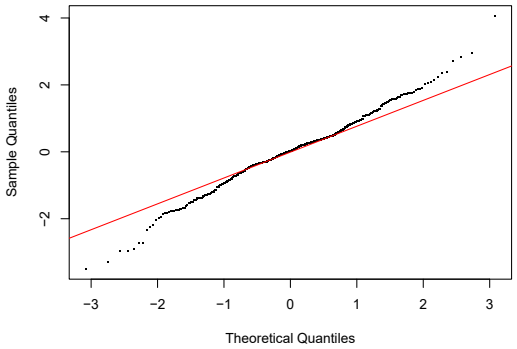

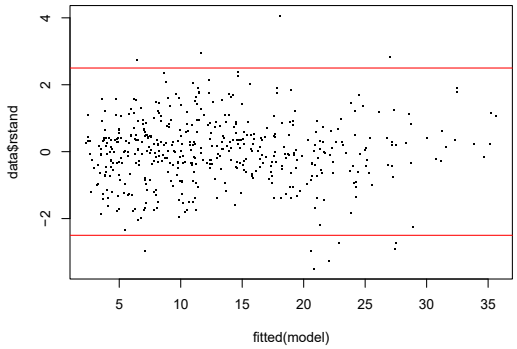

F

Residual plots - 35SKRP2-GFP *rga-28*

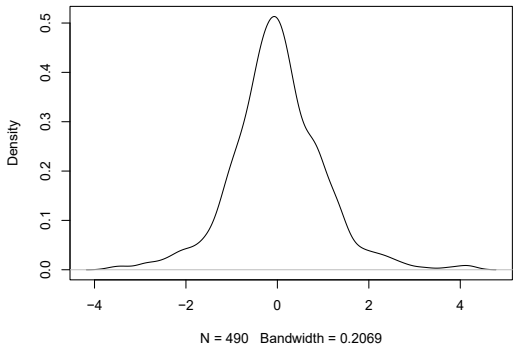

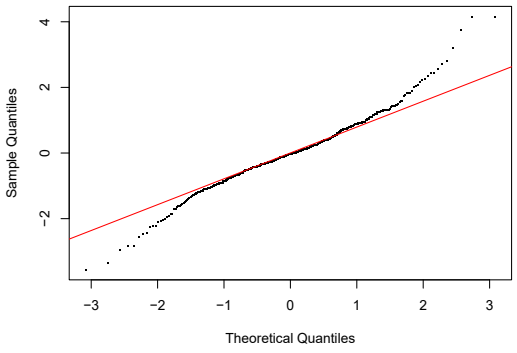

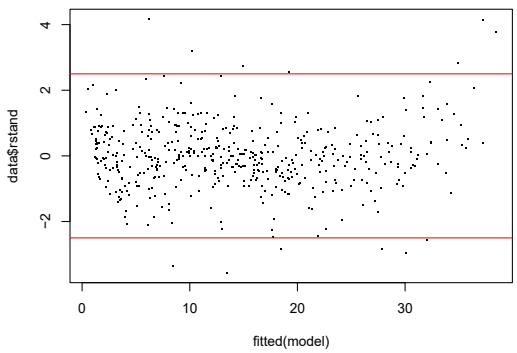

Appendix 4.6 Biological replicate of root lengths over time (2-9 DAS) for 35S::KRP2-GFP crosses

Root growth rates for C treatment

Genotype	Root growth rate mm/day	Standard Error	Degrees of freedom	t-value	p-value
WT	4.06	0.093	1	43.26	<0.001
35S::KRP2-GFP	2.96	0.141	1	20.99	<0.001
35S::KRP2-GFP *gai-td1*	2.9	0.135	1	21.47	<0.001
35S::KRP2-GFP *rga-28*	4.04	0.132	1	30.557	<0.001

Root growth rates for GA treatment

Genotype	Root growth rate mm/day	Standard Error	Degrees of freedom	t-value	p-value
WT	4.44	0.087	1	51.18	<0.001
35S::KRP2-GFP	3.06	0.12	1	25.52	<0.001
35S::KRP2-GFP *gai-td1*	2.94	0.123	1	23.99	<0.001
35S::KRP2-GFP *rga-28*	4.29	0.124	1	34.63	<0.001

Root growth rates for PAC treatment

Genotype	Root growth rate mm/day	Standard Error	Degrees of freedom	t-value	p-value
WT	1.84	0.044	1	42.21	<0.001
35S::KRP2-GFP	1.29	0.063	1	20.34	<0.001
35S::KRP2-GFP *gai-td1*	1.47	0.065	1	22.67	<0.001
35S::KRP2-GFP *rga-28*	2.52	0.065	1	39.05	<0.001